The Effects of Nuclear Weapons

Compiled and edited by
Samuel Glasstone *and* Philip J. Dolan

Third Edition

Prepared and published by the
UNITED STATES DEPARTMENT OF DEFENSE
and the
UNITED STATES DEPARTMENT OF ENERGY

1977

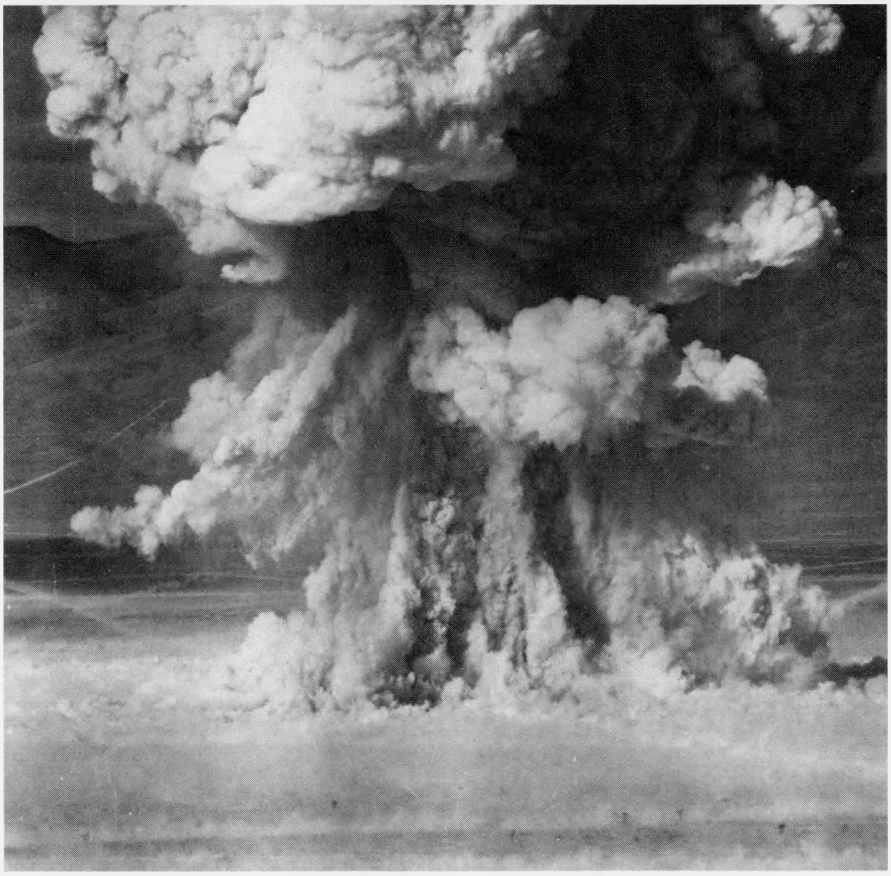

Figure 2.18b. Formation of dirt cloud in surface burst.

cause of the intense heat, some of the rock, soil, and other material in the area is vaporized and taken into the fireball. Additional material is melted, either completely or on its surface, and the strong afterwinds cause large amounts of dirt, dust, and other particles to be sucked up as the fireball rises (Fig. 2.18b).

2.19 An important difference between a surface burst and an air burst is, consequently, that in the surface burst the radioactive cloud is much more heavily loaded with debris. This consists of particles ranging in size from the very small ones produced by condensation as the fireball cools to the much larger debris particles which have been raised by the afterwinds. The exact composition of the cloud will, of course, depend on the nature of the surface materials and the extent of their contact with the fireball.

2.20 For a surface burst associated with a moderate amount of debris, such as has been the case in several test explosions in which the weapons were detonated near the ground, the rate of

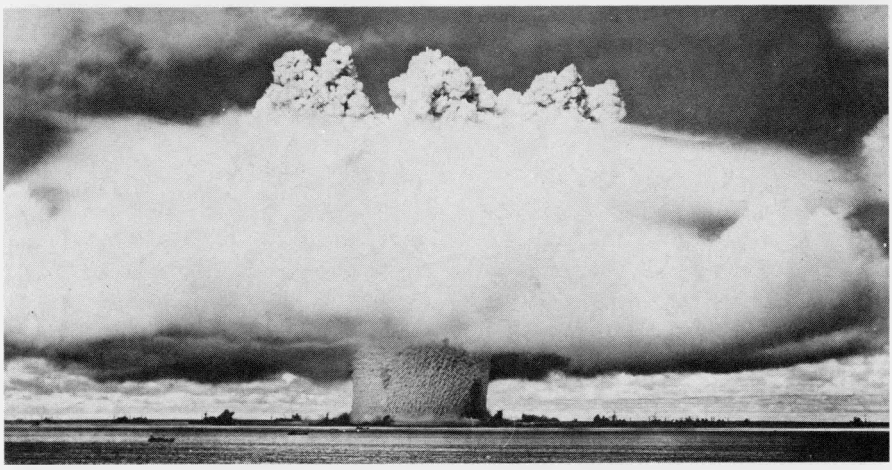

Figure 2.67b. Formation of the hollow column in a shallow underwater explosion; the top is surrounded by a late stage of the condensation cloud.

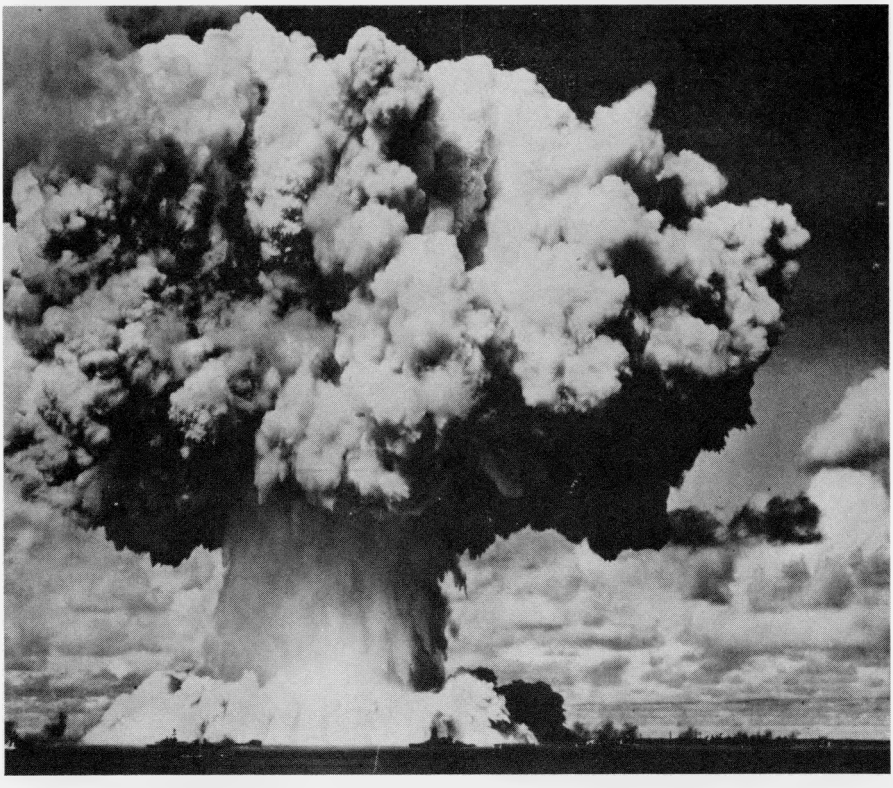

Figure 2.68. The radioactive cloud and first stages of the base surge following a shallow underwater burst. Water is beginning to fall back from the column into the lagoon.

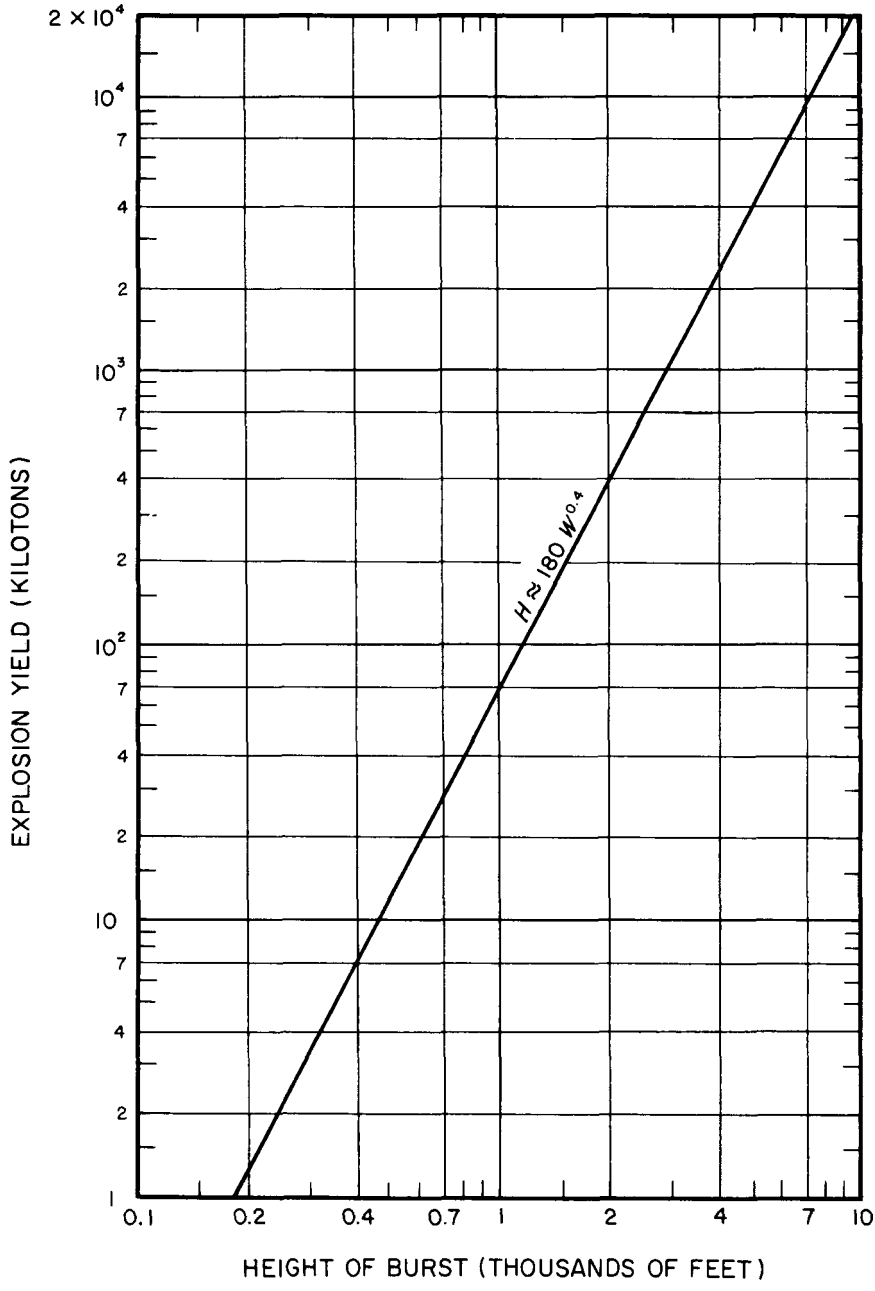

Figure 2.128. Approximate maximum height of burst for appreciable local fallout.

Reinhold Publishing Corp., 1955, Vol. II, p. 395.

BRODE, H. L., "Review of Nuclear Weapons Effects," *Ann Rev. Nuclear Science*, **18**, 153 (1968).

CHRISTOFILOS, N. C., "The Argus Experiment," *J. Geophys. Res.*, **64**, 869 (1959).

FOLEY, N. M., and M. A. RUDERMAN, "Stratospheric Nitric Oxide Production from Past Nuclear Explosions and Its Relevance to Projected SST Pollution," Institute for Defense Analyses, August 1972, Paper P–894, IDA Log. No. HQ 72–14452.

GILMORE, F. R., "The Production of Nitrogen Oxides by Low Altitude Nuclear Explosions," Institute for Defense Analyses, July 1974, Paper P–986, IDA Log. No. HQ 73–15738.

GLASSTONE, S., "Public Safety and Underground Nuclear Detonations," U.S. Atomic Energy Commission, June 1971, TID–25708.

HESS, W. N., Ed., "Collected Papers on the Artificial Radiation Belt from the July 9, 1962 Nuclear Detonation," *J. Geophys. Res.*, **68**, 605 *et seq.* (1963).

*HOERLIN, H., "United States High-Altitude Test Experiences," University of California, Los Alamos Scientific Laboratory, October 1976, LA–6405.

*JOHNSON, G. W., and C. E. VIOLET, "Phenomenology of Contained Nuclear Explosions," University of California, Lawrence Radiation Laboratory, Livermore, December 1958, UCRL 5124 Rev. 1.

*JOHNSON, G. W., *et al.*, "Underground Nuclear Detonations," University of California, Lawrence Radiation Laboratory, Livermore, July 1959, UCRL 5626.

MATSUSHITA, S., "On Artificial Geomagnetic and Ionospheric Storms Associated with High Altitude Explosions," *J. Geophys. Res.*, **64**, 1149 (1959).

NELSON, D. B., "EMP Impact on U.S. Defense," *Survive, 2*, No. 6, 2 (1969).

*"Proceedings of the Third Plowshare Symposium, Engineering with Nuclear Explosives," April 1966, University of California, Lawrence Radiation Laboratory, Livermore, TID–695.

"Proceedings of the Symposium on Engineering with Nuclear Explosives," Las Vegas, Nevada, January 1970, American Nuclear Society and U.S. Atomic Energy Commission, CONF–700101, Vols. 1 and 2.

"Proceedings for the Symposium on Public Health Aspects of Peaceful Uses of Nuclear Explosives," Las Vegas, Nevada, April 1969, Southwestern Radiological Health Laboratory, SWRHL–82.

"Proceedings of the Special Session on Nuclear Excavation," *Nuclear Applications and Technology*, **7**, 188 *et seq.* (1969).

SNAY, H. G., and R. C. TIPTON, "Charts for the Parameters of Migrating Explosion Bubbles," U.S. Naval Ordnance Laboratory, 1962, NOLTR 62–184.

STEIGER, W. R., and S. MATSUSHITA, "Photographs of the High Altitude Nuclear Explosion TEAK," *J. Geophys. Res.*, **65**, 545 (1960).

STRANGE, J. N., and L. MILLER, "Blast Phenomena from Explosions and an Air-Water Interface," U.S. Army Engineer Waterways Experiment Station, 1966, Report 1, Misc. Paper 1–814.

TELLER, E., *et al.*, "The Constructive Uses of Nuclear Explosives," McGraw-Hill Book Company, 1968.

VAN DORN, W. G., B. LE MÉHAUTÉ, and L. HWANG, "Handbook of Explosion-Generated Water Waves, Vol. I—State of the Art," Tetra Tech, Inc., Pasadena, California, October 1968, Report No. TC–130.

*These documents may be purchased from the National Technical Information Center, U.S. Department of Commerce, Springfield, Virginia, 22161.

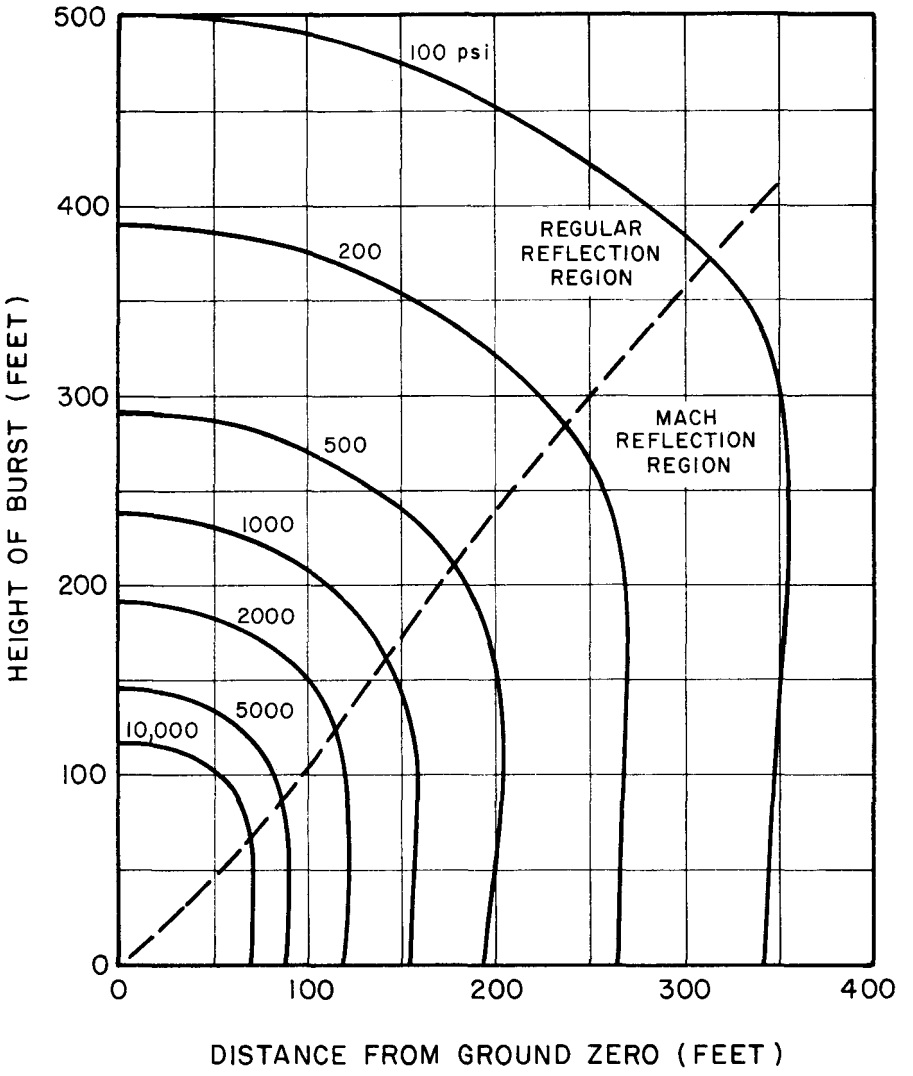

Figure 3.73a. Peak overpressures on the ground for a 1-kiloton burst (high-pressure range).

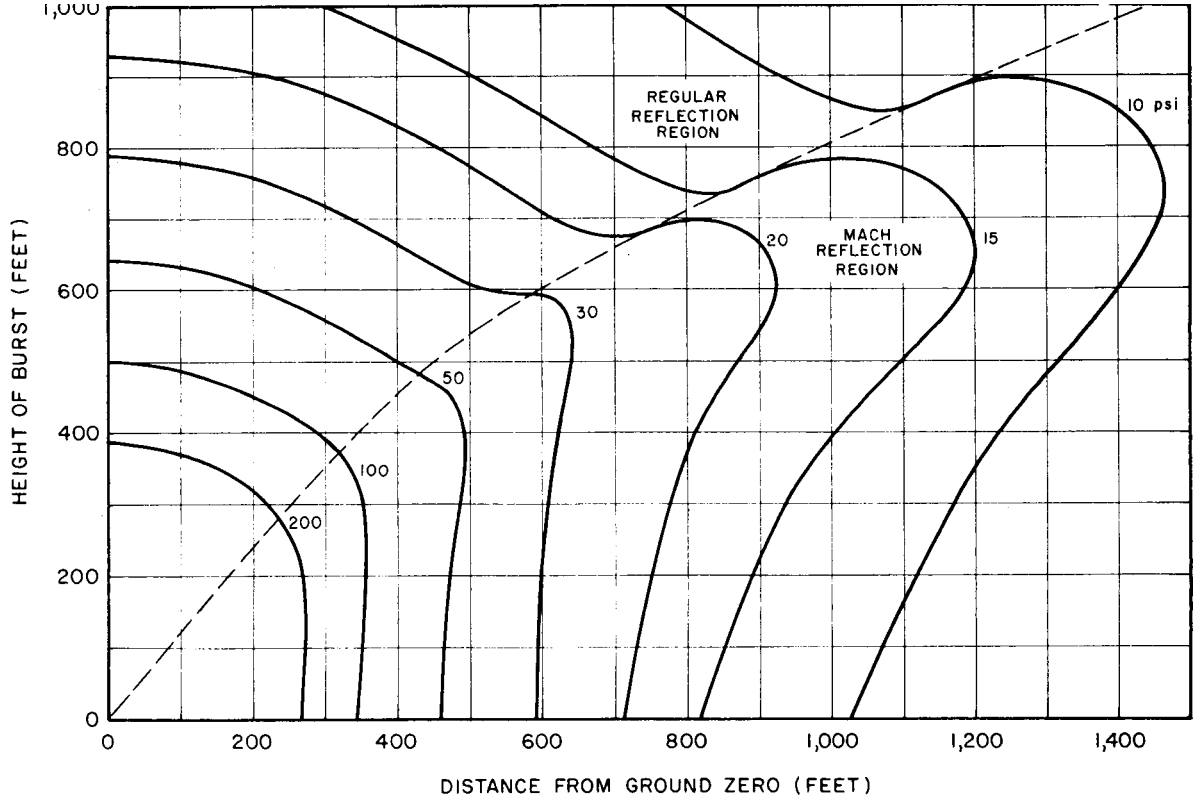

Figure 3.73b. Peak overpressures on the ground for a 1-kiloton burst (intermediate-pressure range).

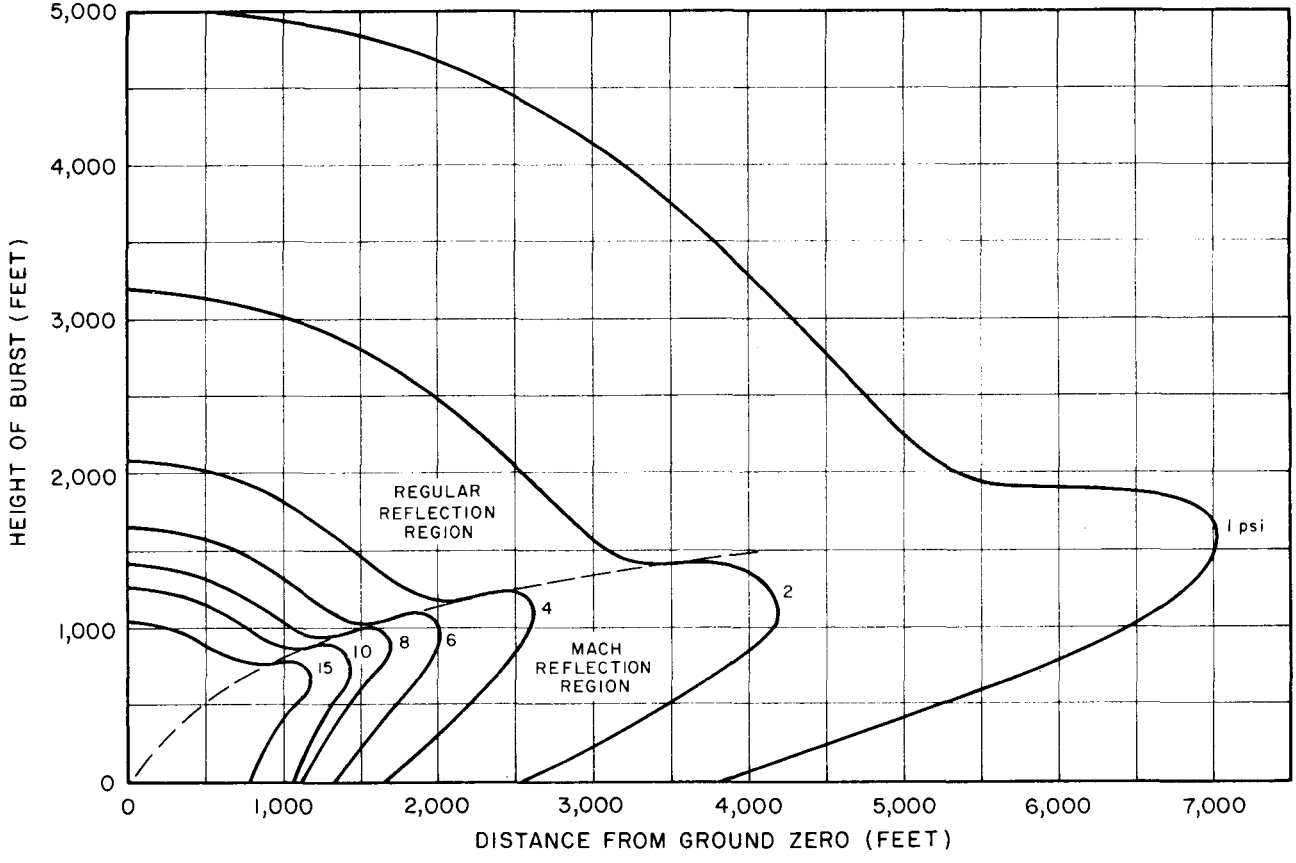

Figure 3.73c. Peak overpressures on the ground for 1-kiloton burst (low-pressure range).

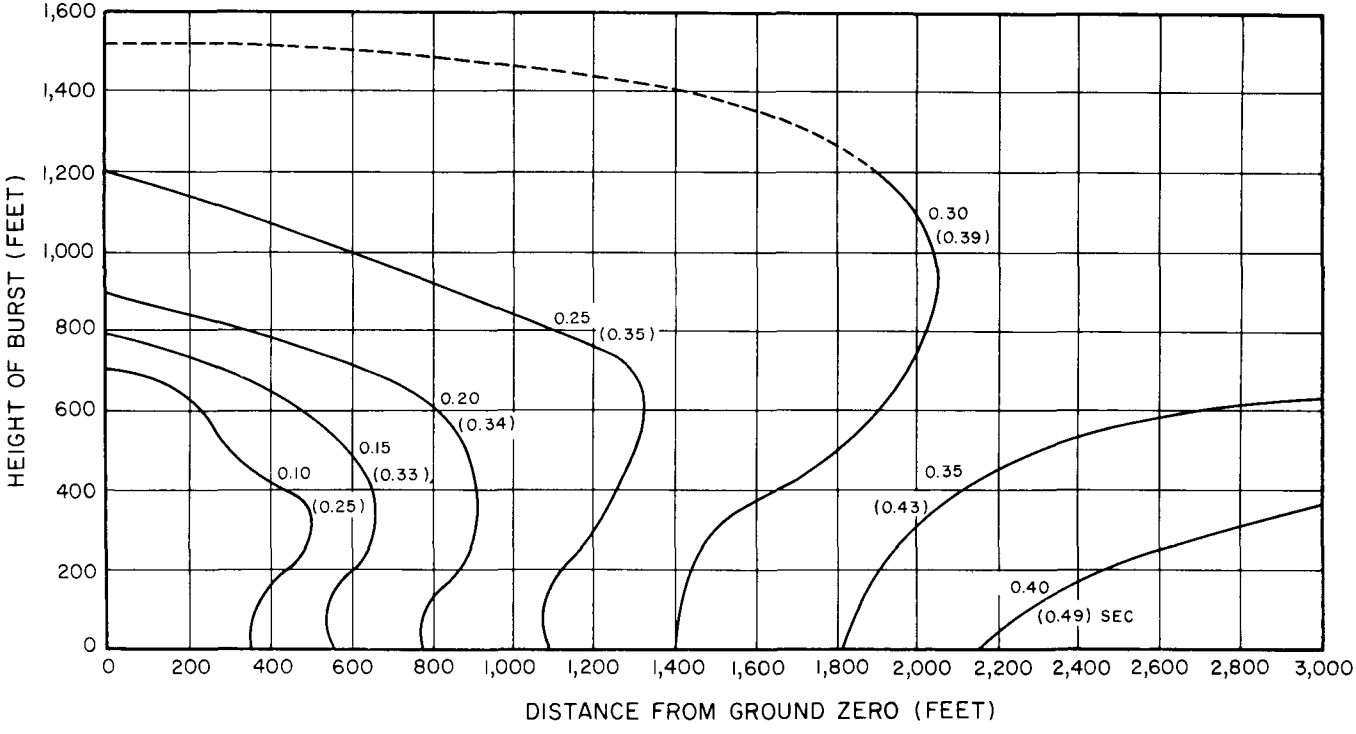

Figure 3.76. Positive phase duration on the ground of overpressure and dynamic pressure (in parentheses) for 1-kiloton burst.

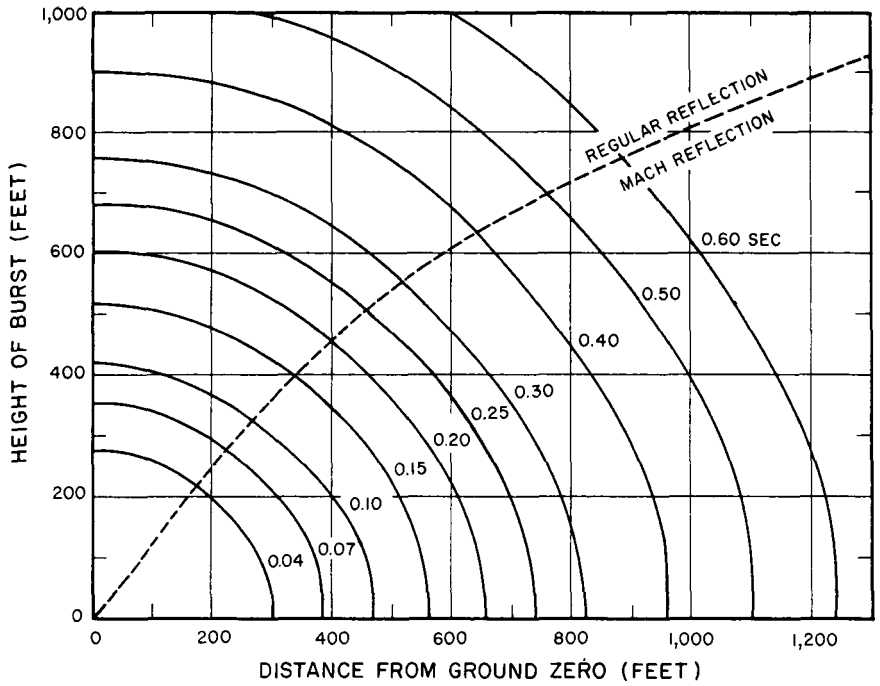

Figure 3.77a. Arrival times on the ground of blast wave for 1-kiloton burst (early times).

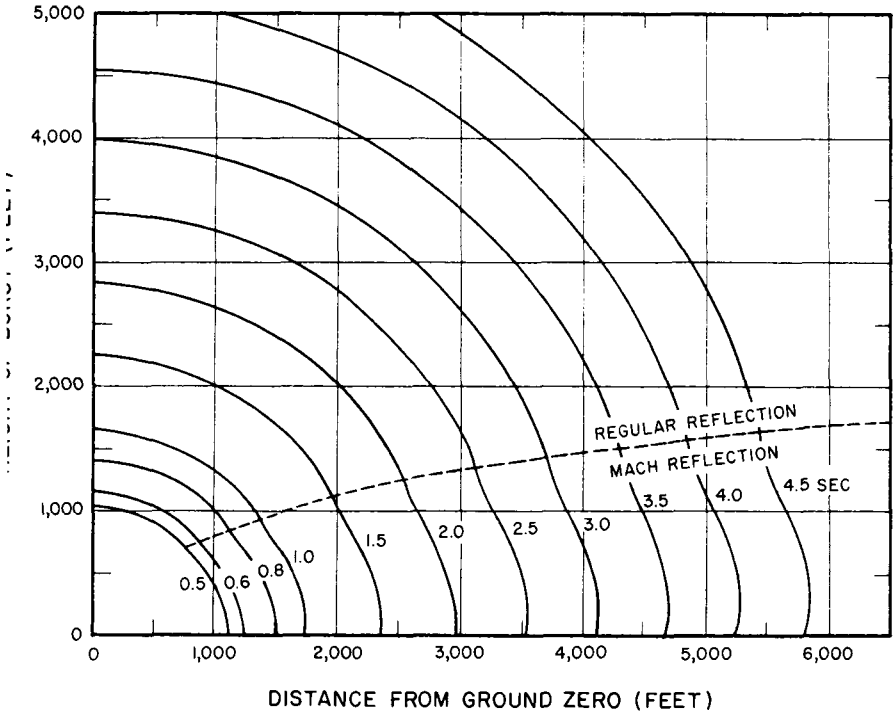

Figure 3.77b. Arrival times on the ground of blast wave for 1-kiloton burst (late times).

(Text continued from page 107.)

THE PRECURSOR

3.79 The foregoing results have referred to blast wave conditions near the surfaces that are ideal or nearly ideal (§ 3.47), so that the Rankine-Hugoniot equations are applicable. When the surface is nonideal, there may be mechanical or thermal effects (or both) on the blast wave. Some of the phenomena associated with mechanical effects were mentioned in § 3.48. As a consequence of thermal nonideal behavior, the overpressure and dynamic pressure patterns can be distorted. Severe thermal effects are associated with the formation of a precursor (§ 3.49) which produces significant changes in the parameters of the blast wave.

3.80 When a nuclear weapon is detonated over a thermally nonideal (heat-absorbing) surface, radiation from the fireball produces a hot layer of air, referred to as a "thermal layer," near the surface. This layer, which often includes smoke, dust, and other particulate matter, forms before the arrival of the blast wave from an air burst. It is thus referred to as the preshock thermal layer. Interaction of the blast wave with the hot air layer may affect the reflection process to a considerable extent. For appropriate combinations of explosion energy yield, burst height, and heat-absorbing surfaces, an auxiliary (or secondary) blast wave, the precursor, will form and will move ahead of the main incident wave for some distance. It is called precursor because it precedes the main blast wave.

3.81 After the precursor forms, the main shock front usually no longer extends to the ground; if it does, the lower portion is so weakened and distorted that it is not easily recognized. Between the ground and the bottom edge of the main shock wave is a gap, probably not sharply defined, through which the energy that feeds the precursor may flow. Ahead of the main shock front, the blast energy in the precursor is free not only to follow the rapidly moving shock front in the thermal layer, but also to propagate upward into the undisturbed air ahead of the main shock front. This diverging flow pattern within the precursor tends to weaken it, while the energy which is continually fed into the precursor from the main blast wave tends to strengthen the precursor shock front. The foregoing description of what happens within a precursor explains some of the characteristics shown in Fig. 3.81. Only that portion of the precursor shock front that is in the preshock thermal layer travels faster than the main shock front; the energy diverging upward, out of this layer, causes the upper portion to lose some of its forward speed. The interaction of the precursor and the main shock front indicates that the main shock is continually overtaking this upward-traveling energy. Dust, which may billow to heights of more than 100 feet, shows the upward flow of air in the precursor.

3.82 Considerable modification of the usual blast wave characteristics may occur within the precursor region. The overpressure wave form shows a rounded leading edge and a slow rise to its peak amplitude. In highly disturbed waveforms, the pressure jump at the leading edge may be completely absent. (An example of a measured overpressure waveform in the precursor region is

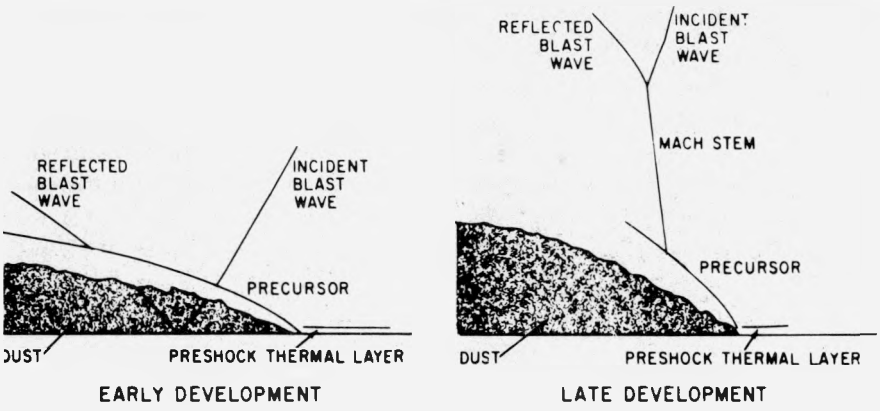

Figure 3.81. Precursor characteristics.

given in Fig. 4.67a.) Dynamic pressure waveforms often have high-frequency oscillations that indicate severe turbulence. Peak amplitudes of the precursor waveforms show that the overpressure has a lower peak value and the dynamic pressure a higher peak value than over a surface that did not permit a precursor to form. The higher peak value of the dynamic pressure is primarily attributable to the increased density of the moving medium as a result of the dust loading in the air. Furthermore, the normal Rankine-Hugoniot relations at the shock front no longer apply.

3.83 Examples of surfaces which are considered thermally nearly ideal (unlikely to produce significant precursor effects) and thermally nonideal (expected to produce a precursor for suitable combinations of burst height and ground distance) are given in Table 3.83. Under many conditions, e.g., for scaled heights of burst in excess of 800 feet or at large ground distances (where the peak overpressure is less than about 6 psi), precursors are not expected to occur regardless of yield and type of surface. Thermal effects on the blast wave are also expected to be small for contact surface bursts; consequently, it is believed that in many situations, especially in urban areas, nearly ideal blast wave conditions would prevail.

3.84 For this reason, the curves for various air blast parameters presented earlier, which apply to nearly ideal surface conditions, are considered to be

Table 3.83

EXAMPLES OF THERMALLY NEARLY IDEAL AND THERMALLY NONIDEAL SURFACES

Thermally Nearly Ideal (precursor unlikely)	Thermally Nonideal (precursor may occur for low air bursts)
Water	Desert sand
Ground covered by white smoke	Coral
Heat-reflecting concrete	Asphalt
Ice	Surface with thick low vegetation
Packed snow	Surface covered by dark smoke
Moist soil with sparse vegetation	Most agricultural areas
Commercial and industrial areas	Dry soil with sparse vegetation

most representative for general use. It should be noted, however, that blast phenomena and damage observed in the precursor region for low air bursts at the Nevada Test Site may have resulted from nonideal behavior of the surface. Under such conditions, the overpressure waveform may be irregular and may show a slow rise to a peak value somewhat less than that expected for nearly ideal conditions (§ 3.82). Consequently, the peak value of reflected pressure on the front face of an object struck by the blast wave may not exceed the peak value of the incident pressure by more than a factor of two instead of the much higher theoretical factor for an ideal shock front as given by equation (3.56.2).

3.85 Similarly, the dynamic pressure waveform will probably be irregular (§ 3.82), but the peak value may be several times that computed from the peak overpressure by the Rankine-Hugoniot relations. Damage to and displacement of targets which are affected by dynamic pressure may thus be considerably greater in the nonideal precursor region for a given value of peak overpressure than under nearly ideal conditions.

BIBLIOGRAPHY

*BANISTER, J. R., and L. J. VORTMAN, "Effects of a Precursor Shock Wave on Blast Loading of a Structure," Sandia Corporation, Albuquerque, New Mexico, October 1960, WT-1472.

*BETHE, H. A., *et al.*, "Blast Wave," University of California, Los Alamos Scientific Laboratory, March 1958, LA-2000.

BRINKLEY, S. R., JR., and J. G. KIRKWOOD, "Theory of the Propagation of Shock Waves," *Phys. Rev.*, **71**, 606 (1947); **72**, 1109 (1947).

BRODE, H. L., "Numerical Solution of Spherical Blast Waves," *J. Appl. Phys.* **26**, 766 (1955).

BRODE, H. L., "Review of Nuclear Weapons Effects," *Ann. Rev. Nuclear Science*, **18**, 153 (1968).

BRODE, H. L., "Height of Burst Effects at High Overpressures," Rand Corporation, Santa Monica, California, July 1970, RM-6301-DASA, DASA 2506.

COURANT, R., and K. O. FRIEDRICHS, "Supersonic Flow and Shock Waves," Interscience Publishers, Inc., 1948.

GOLDSTINE, H. H., and J. VON NEUMANN, "Blast Wave Calculations," *Comm. on Pure and Appl. Math.* **8**, 327 (1955).

LETHO, D. L. and R. A. LARSON, "Long Range Propagation of Spherical Shockwaves from Explosions in Air," U.S. Naval Ordnance Laboratory, July 1969, NOLTR 69-88.

LIEPMANN, H. W., and A. E. PUCKETT, "Aerodynamics of a Compressible Fluid," John Wiley and Sons, Inc., 1947.

PENNEY, W. G., D. E. J. SAMUELS, and G. C. SCORGIE, "The Nuclear Explosive Yields at Hiroshima and Nagasaki," *Phil. Trans. Roy. Soc., A* **266**, 357 (1970).

REED, J. W., "Airblast from Plowshare Projects," in Proceedings for the Symposium on Public Health Aspects of Peaceful Uses of Nuclear Explosives, Southwestern Radiological Health Laboratory, April 1969, SWRHL-82, p. 309.

TAYLOR, G. I., "The Formation of a Blast Wave by a Very Intense Explosion," *Proc. Roy. Soc., A* **201**, 159, 175 (1950).

*U.S. Standard Atmosphere, U.S. Government Printing Office, Washington, D.C., 1962, Supplements, 1966.

*These documents may be purchased from the National Technical Information Service, U.S. Department of Commerce, Arlington, Virginia 22161.

blast wave enters and tends to equalize the interior and exterior pressures. In fact, a structure may be designed to have certain parts frangible to lessen damage to all other portions of the structure. Thus, the response of certain elements in such cases influences the blast loading on the structure as a whole. In general, the movement of a structural element is not considered to influence the blast loading on that element itself. However, an exception to this rule arises in the case of an aircraft in flight when struck by a blast wave.

BLAST LOADING–TIME CURVES

4.38 The procedures whereby curves showing the air blast loading as a function of time may be derived are given below. The methods presented are for the following five relatively simple shapes: (1) closed box-like structure; (2) partially open box-like structure; (3) open frame structure; (4) cylindrical structure; and (5) semicircular arched structure. These methods can be altered somewhat for objects having similar characteristics. For very irregularly shaped structures, however, the procedures described may provide no more than a rough estimate of the blast loading to be expected.

4.39 As a general rule, the loading analysis of a diffraction-type structure is extended only until the positive phase overpressure falls to zero at the surface under consideration. Although the dynamic pressure persists after this time, the value is so small that the drag force can be neglected. However, for drag-type structures, the analysis is continued until the dynamic pressure is zero. During the negative overpressure phase, both overpressure and dynamic pressure are too small to have any significant effect on structures (§ 3.11 *et seq.*).

4.40 The blast wave characteristics which need to be known for the loading analysis and their symbols are summarized in Table 4.40. The locations in Chapter III where the data may be obtained, at a specified distance from ground zero for an explosion of given energy yield and height of burst, are also indicated.

4.41 A closed box-like structure may be represented simply by a parallelepiped, as in Fig. 4.41, having a length L, height H, and breadth B. Structures

Table 4.40

BLAST WAVE CHARACTERISTICS FOR DETERMINATION OF LOADING

Property	Symbol	Source
Peak overpressure	p	Figs. 3.73a, b, and c
Time variation of overpressure	$p(t)$	Fig. 3.57
Peak dynamic pressure	q	Fig. 3.75
Time variation of dynamic pressure	$q(t)$	Fig. 3.58
Reflected overpressure	p_r	Fig. 3.78b
Duration of positive phase of overpressure	t_p^+	Fig. 3.76
Duration of positive phase of dynamic pressure	t_q^+	Fig. 3.76
Blast front (shock) velocity	U	Fig. 3.55

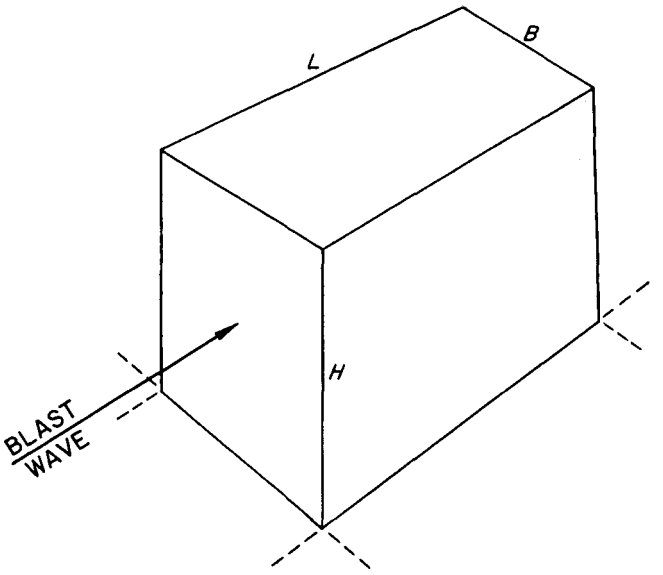

Figure 4.41. Representation of closed box-like structure.

with a flat roof and walls of approximately the same blast resistance as the frame will fall into this category. The walls have either no openings (doors and windows), or a small number of such openings up to about 5 percent of the total area. The pressures on the interior of the structure then remain near the ambient value existing before the arrival of the blast wave, while the outside is subjected to blast loading. To simplify the treatment, it will be supposed that one side of the structure faces toward the explosion and is perpendicular to the direction of propagation of the blast wave. This side is called the front face. The loading diagrams are computed below for (*a*) the front face, (*b*) the side and top, and (*c*) the back face. By combining the data for (*a*) and (*c*), the net horizontal loading is obtained in (*d*).

4.42 (*a*) *Average Loading on Front Face.*—The first step is to determine the reflected pressure, p_r; this gives the pressure at the time $t = 0$, when the blast wave front strikes the front face (Fig. 4.42). Next, the time, t_s, is calculated at which the stagnation pressure, p_s, is first attained. It has been found from laboratory studies that, for peak overpressures being considered (50 pounds per square inch or less), t_s can be represented, to a good approximation, by

$$t_s = \frac{3S}{U},$$

where S is equal to H or $B/2$, whichever is less, and U is the blast front (shock) velocity. The drag coefficient for the front face is unity, so that the drag pressure is here equal to the dynamic pressure. The stagnation pressure is thus

$$p_s = p(t_s) + q(t_s),$$

where $p(t_s)$ and $q(t_s)$ are the overpressure and dynamic pressure at the time t_s. The average pressure subsequently decays with time, so that,

$$\text{Pressure at time } t = p(t) + q(t),$$

where t is any time between t_s and t_p^+. The pressure–time curve for the front face can thus be determined, as in Fig. 4.42.

4.43 *(b) Average Loading on Sides and Top.*—Although loading commences immediately after the blast wave strikes the front face, i.e., at $t = 0$, the sides and top are not fully loaded until the wave has traveled the distance L, i.e., at times $t = L/U$. The average pressure, p_a, at this time is considered to be the overpressure plus the drag loading at the distance $L/2$ from the front of the structure, so that

$$p_a = p\left(\frac{L}{2U}\right) + C_d q\left(\frac{L}{2U}\right)$$

The drag coefficient on the sides and top of the structure is approximately -0.4 for the blast pressure range under consideration (§ 4.23). The loading increases from zero at $t = 0$ to the value p_a at the time L/U, as shown in Fig. 4.43. Subsequently, the average pressure at any time t is given by

$$\text{Pressure at time } t = p\left(t - \frac{L}{2U}\right) + C_d q\left(t - \frac{L}{2U}\right),$$

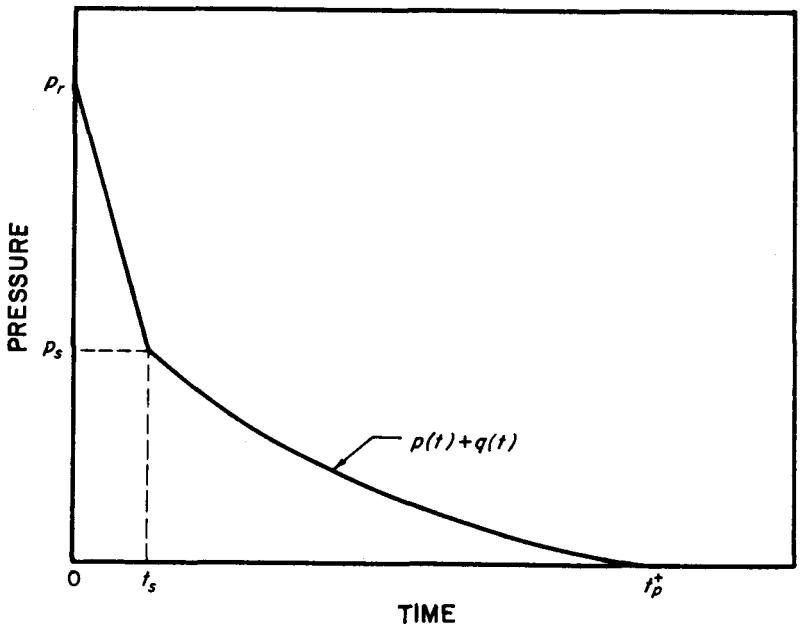

Figure 4.42. Average front face loading of closed box-like structure.

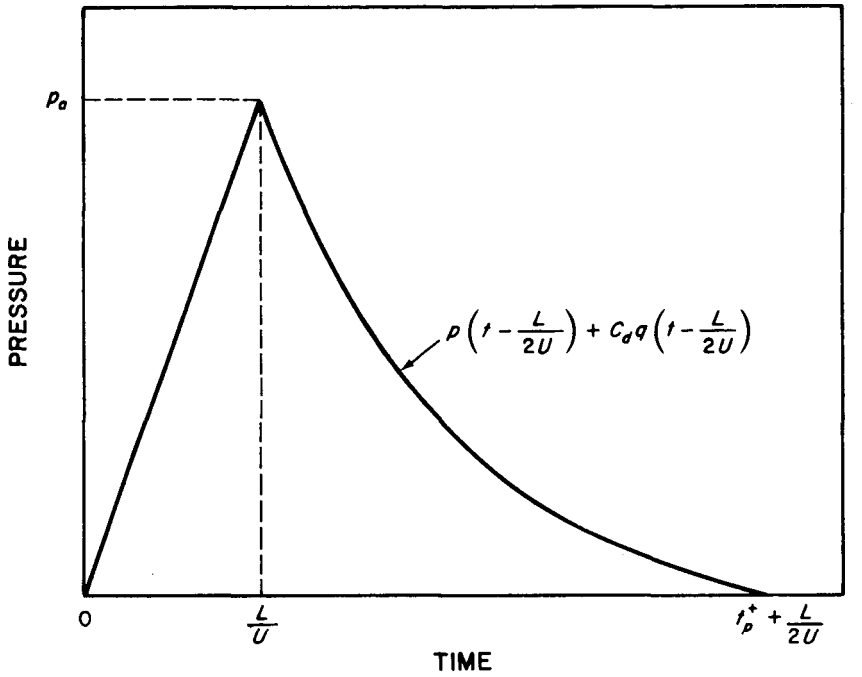

Figure 4.43. Average side and top loading of closed box-like structure.

where t lies between L/U and $t_p^+ + L/2U$, as seen in Fig. 4.43. The overpressure and dynamic pressure, respectively, are the values at the time $t - L/2U$. Hence, the overpressure on the sides and top becomes zero at time $t_p^+ + L/2U$.

4.44 *(c) Average Loading on Back Face.*—The shock front arrives at the back face at time L/U, but it requires an additional time, $4S/U$, for the average pressure to build up to the value p_b (Fig. 4.44), where p_b is given approximately by

$$p_b = p\left(\frac{L+4S}{U}\right) + C_dq\left(\frac{L+4S}{U}\right).$$

Here, as before, S is equal to H or $B/2$ whichever is the smaller. The drag coefficient on the back face is about -0.3 for the postulated blast pressure range. The average pressure at any time t after the attainment of p_b is represented by

Pressure at time t =

$$p\left(t-\frac{L}{U}\right) + C_dq\left(t-\frac{L}{U}\right),$$

where t lies between $(L + 4S)/U$ and $t_p^+ + L/U$, as seen in Fig. 4.44.

4.45 *(d) Net Horizontal Loading.*—The net loading is equal to the front loading minus the back loading. This subtraction is best performed graphically, as shown in Fig. 4.45. The left-hand diagram gives the individual front and back loading curves, as derived from Figs. 4.42 and 4.44, respectively. The difference indicated by the shaded region is then transferred to

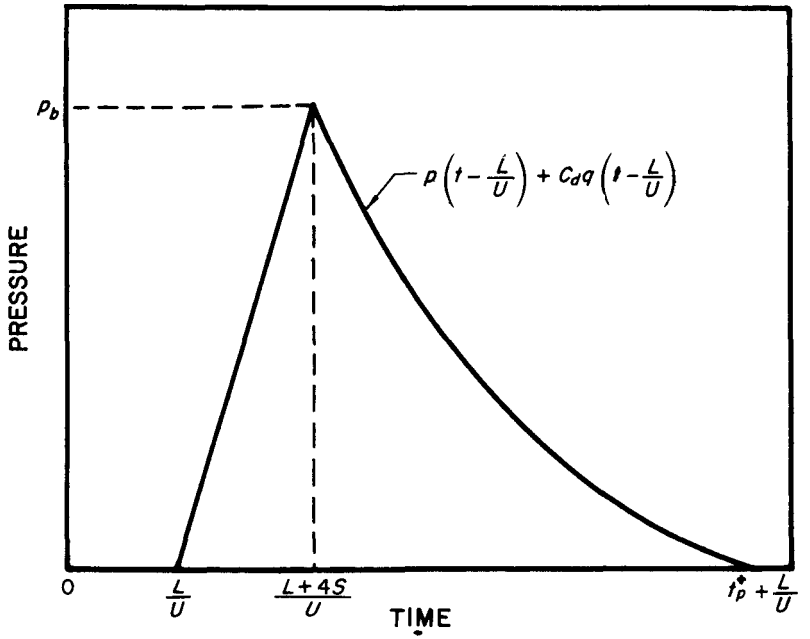

Figure 4.44. Average back face loading of closed box-like structure.

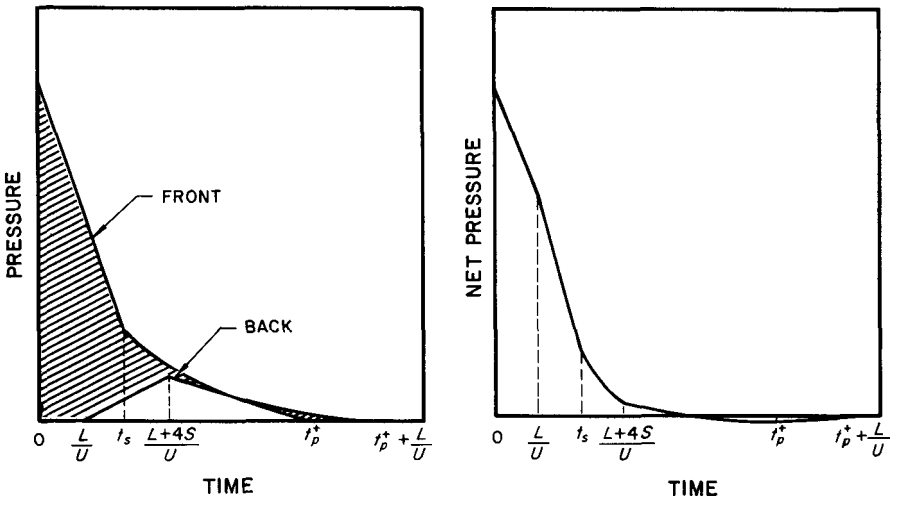

Figure 4.45. Net horizontal loading of closed box-like structure.

the right-hand diagram to give the net pressure. The net loading is necessary for determining the frame response, whereas the wall actions are governed primarily by the loadings on the individual faces.

PARTIALLY OPEN BOX-LIKE STRUCTURES

4.46 A partially open box-like structure is one in which the front and back walls have about 30 percent of openings or window area and no interior partitions to influence the passage of the blast wave. As in the previous case, the loading is derived for *(a)* the front face, *(b)* the sides and roof, *(c)* the back face, and *(d)* the net horizontal loading. Because the blast wave can now enter the inside of the structure, the loading–time curves must be considered for both the exterior and interior of the structure.

4.47 *(a) Average Loading on Front Face.*—The outside loading is computed in the same manner as that used for a closed structure, except that S is replaced by S'. The quantity S' is the average distance (for the entire front face) from the center of a wall section to an open edge of the wall. It represents the average distance which rarefaction waves must travel on the front face to reduce the reflected pressures to the stagnation pressure.

4.48 The pressure on the inside of the front face starts rising at zero time, because the blast wave immediately enters through the openings, but it takes a time $2L/U$ to reach the blast wave overpressure value. Subsequently, the inside pressure at any time t is given by $p(t)$. The dynamic pressures are assumed to be negligible on the interior of the structure. The variations of the in-

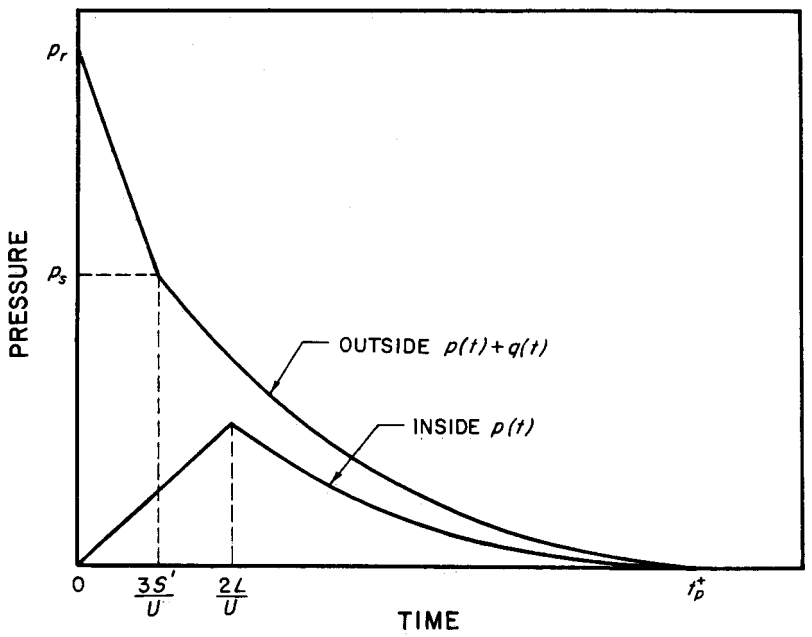

Figure 4.48. Average front face loading of partially open box-like structure.

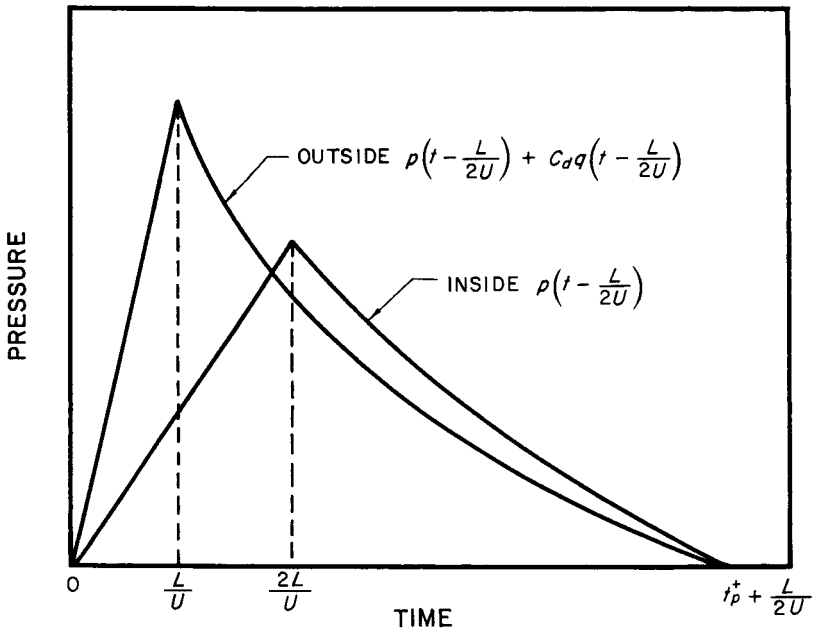

Figure 4.49 Average side and top loading of partially open box-like structure.

side and the outside pressures with time are as represented in Fig. 4.48.

4.49 *(b) Average Loading on Sides and Top.*— The outside pressures are obtained as for a closed structure (§ 4.43), but the inside pressures, as for the front face, require a time $2L/U$ to attain the overpressure in the blast wave. Here also, the dynamic pressures on the interior are neglected, and side wall openings are ignored because their effect on the loading is uncertain. The loading curves are depicted in Fig. 4.49.

4.50 *(c) Average Loading on Back Face.*—The outside pressures are the same as for a closed structure, with the exception that S is replaced by S', as described above. The inside pressure, reflected from the inside of the back face, reaches the same value as the blast overpressure at a time L/U and then decays as $p(t - L/U)$; as before, the dynamic pressure is regarded as being negligible (Fig. 4.50).

4.51 *(d) Net Horizontal Loading.*—The net horizontal loading is equal to the net front loading, i.e., outside minus inside, minus the net back face loading.

OPEN FRAME STRUCTURE

4.52 A structure in which small separate elements are exposed to a blast wave, e.g., a truss bridge, may be regarded as an open frame structure. Steel-frame office buildings with a majority of the wall area of glass, and industrial buildings with asbestos, light steel, or aluminum panels quickly become open frame structures after the initial impact of the blast wave.

4.53 It is difficult to determine the magnitude of the loading that the frang-

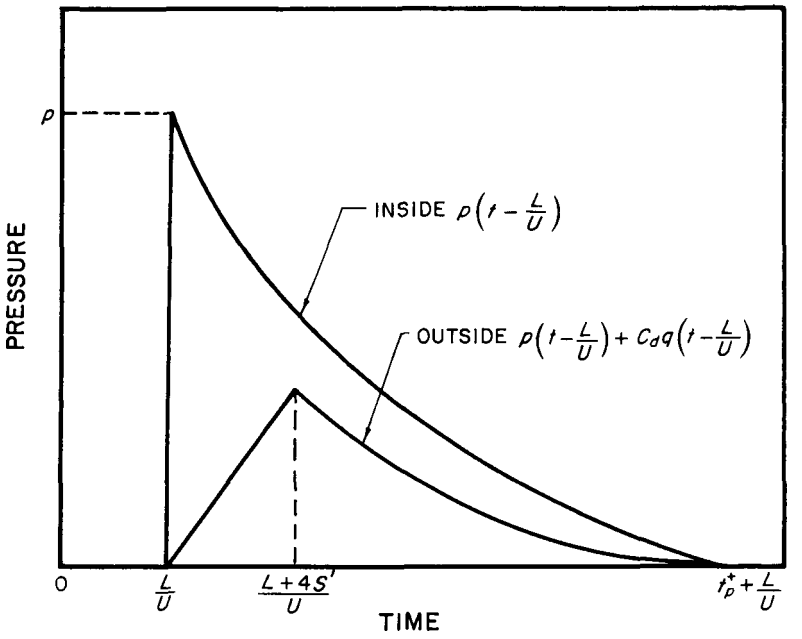

Figure 4.50. Average back face loading of partially open box-like structure.

ible wall material transmits to the frame before failing. For glass, the load transmitted is assumed to be negligible if the loading is sufficient to fracture the glass. For asbestos, transite, corrugated steel, or aluminum paneling, an approximate value of the load transmitted to the frame is an impulse of 0.04 pound-second per square inch. Depending on the span lengths and panel strength, the panels are not likely to fail when the peak overpressure is less than about 2 pounds per square inch. In this event, the full blast load is transmitted to the frame.

4.54 Another difficulty in the treatment of open frame structures arises in the computations of the overpressure loading on each individual member during the diffraction process. Because this process occurs at different times for various members and is affected by shielding of one member by adjacent members, the problem must be simplified. A recommended simplification is to treat the loading as an impulse, the value of which is obtained in the following manner. The overpressure loading impulse is determined for an average member treated as a closed structure and this is multiplied by the number of members. The resulting impulse is considered as being delivered at the time the shock front first strikes the structure, or it can be separated into two impulses for front and back faces where the majority of the elements are located, as shown below in Fig. 4.56.

4.55 The major portion of the loading on an open frame structure consists of the drag loading. For an individual member in the open, the drag coefficient for I-beams, channels, angles, and for members with rectangular cross section

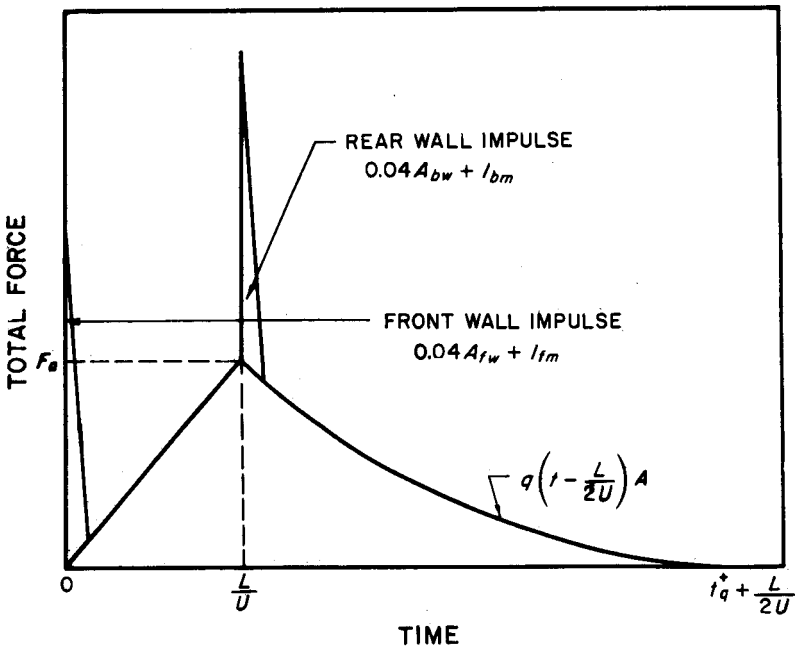

Figure 4.56. Net horizontal loading of an open frame structure.

is approximately 1.5. However, because in a frame the various members shield one another to some extent from the full blast loading, the average drag coefficient when the whole frame is considered is reduced to 1.0. The force F, i.e., pressure multiplied by area, on an individual member is thus given by

$$F(\text{member}) = C_d q(t) A_i,$$

where C_d is 1.5 and A_i is the member area projected perpendicular to the direction of blast propagation. For the loading on the frame, however, the force is

$$F(\text{frame}) = C_d q(t) \Sigma A_i,$$

where C_d is 1.0 and ΣA_i is the sum of the projected areas of all the members. The result may thus be written in the form

$$F(\text{frame}) = q(t)A,$$

where $A = \Sigma A_i$.

4.56 The loading (force) versus time for a frame of length L, having major areas in the planes of the front and rear faces, is shown in Fig. 4.56. The symbols A_{fw} and A_{bw} represent the areas of the front and back faces, respectively, which transmit loads before failure, and I_{fm} and I_{bm} are the overpressure loading impulses on front and back members, respectively. Although drag loading commences immediately after the blast wave strikes the front face, i.e., at $t = 0$, the back face is not fully loaded until the wave has traveled the distance L, i.e., at time $t = L/U$. The

average drag loading, q_a, on the entire structure at this time is considered to be that which would occur at the distance $L/2$ from the front of the structure, so that

$$q_a = C_d q\left(\frac{L}{2U}\right),$$

and the average force on the frame, F_a (frame), is

$$F_a \text{ (frame)} = q\left(\frac{L}{2U}\right)A,$$

where C_d is 1.0, as above. After this time, the average drag force on the frame at any time t is given by

$$F_a \text{ (frame) at time } t = q\left(t - \frac{L}{2U}\right)A,$$

where t lies between L/U and $t_q^+ + L/2U$, as seen in Fig. 4.56.

CYLINDRICAL STRUCTURE

4.57 The following treatment is applicable to structures with a circular cross section, such as telephone poles and smokestacks, for which the diameters are small compared to the lengths. The discussion presented here provides methods for determining average pressures on projected areas of cylindrical structures with the direction of propagation of the blast perpendicular to the axis of the cylinder. A more detailed method for determining the pressure–time curves for points on cylinders is provided in the discussion of the loading on arched structures in § 4.62 *et seq.* The general situation for a blast wave approaching a cylindrical structure is represented in section in Fig. 4.57.

4.58 *(a) Average Loading on Front Surface.*—When an ideal blast wave impinges on a flat surface of a structure, the pressure rises instantaneously to the reflected value and then it soon drops to the stagnation pressure (§ 4.25). On the curved surface of a cylinder the interaction of the blast wave with the front face is much more complex in detail. However, in terms of the average pressure, the load appears as a force that increases with time from zero when the blast front arrives to a maximum when the blast wave has propagated one radius. This occurs at a time $D/2U$, where D is the diameter of the cylinder. For the blast

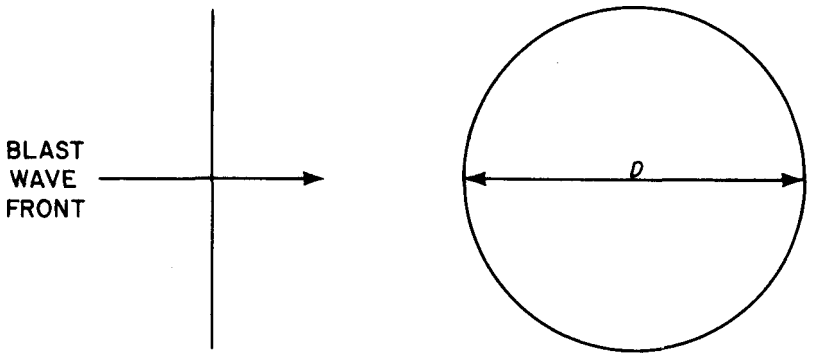

Figure 4.57. Representation of a cylindrical structure.

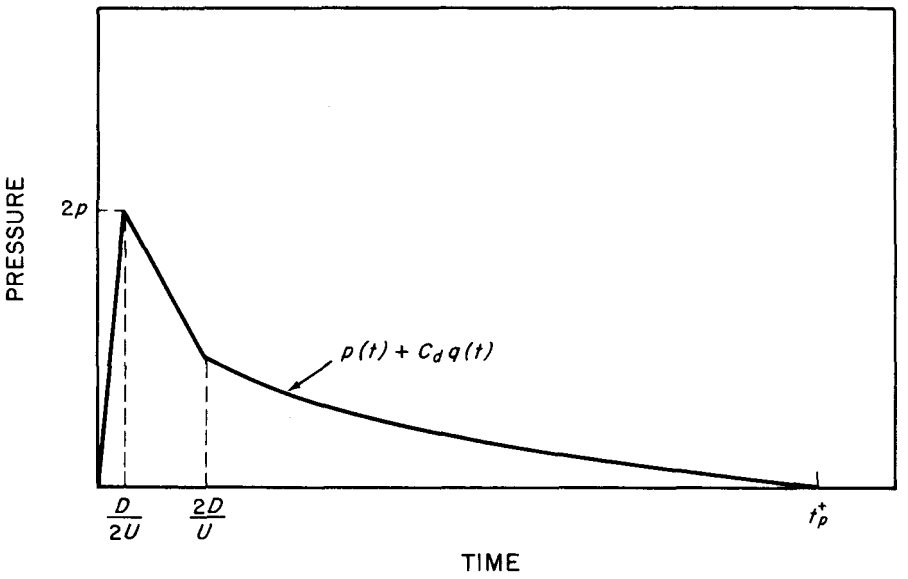

Figure 4.58. Average pressure variation on the front face of a cylinder.

pressure range being considered, the maximum average pressure reaches a value of about $2p$ as depicted in Fig. 4.58. The load on the front surface then decays in an approximately linear manner to the value it would have at about time $t = 2D/U$. Subsequently, the average pressure decreases as shown. The drag coefficient for the front surface of the cylinder is 0.8.

4.59 *(b) Average Loading on the Sides.*—Loading of the sides commences immediately after the blast wave strikes the front surface but, as with the closed box discussed in § 4.41 *et seq.*, the sides are not fully loaded until the wave has traveled the distance D, i.e., at time $t = D/U$. The average pressure on the sides at this time is indicated by p_{s1}, given approximately by

$$p_{s1} = p\left(\frac{D}{U}\right)$$

Complex vortex formation then causes the average pressure to drop to a minimum, p_{s2}, at the time $t = 3D/2U$; the value of p_{s2} is about half the maximum overpressure at this time, i.e.,

$$p_{s2} \approx \frac{1}{2}\, p\left(\frac{3D}{2U}\right).$$

The average pressure on the side then rises until time $9D/2U$ and subsequently decays as shown in Fig. 4.59. The drag coefficient for the side face is 0.9.

4.60 *(c) Average Loading on Back Surface.*—The blast wave begins to affect the back surface of the cylinder at time $D/2U$ and the average pressure gradually builds up to p_{b1} (Fig. 4.60) at a time of about $4D/U$. The value of p_{b1} is given by

$$p_{b1} = \frac{1}{2}p\left(\frac{4D}{U}\right)$$

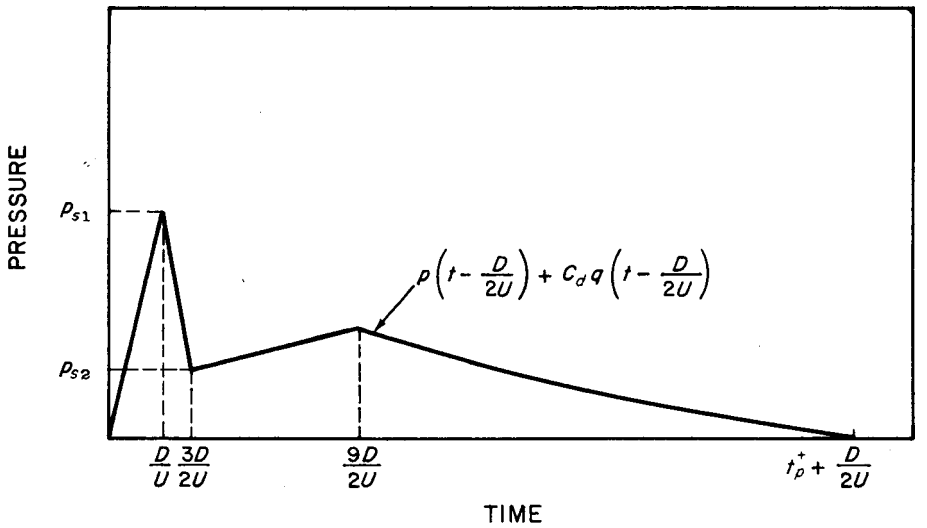

Figure 4.59. Average pressure variation on the side face of a cylinder.

The average pressure continues to rise until it reaches a maximum, p_{b2}, at a time of about $20D/U$, where

$$p_{b2} = p\left(\frac{20D}{U}\right) + C_d q\left(\frac{20D}{U}\right)$$

The average pressure at any time t after the maximum is represented by

$$\text{Pressure at time } t = p\left(t - \frac{D}{2U}\right) + C_d q\left(t - \frac{D}{2U}\right)$$

where t lies between $20D/U$ and $t_p^+ + D/2U$. The drag coefficient for the back surface is -0.2.

4.61 The preceding discussion has been concerned with average values of the loads on the various surfaces of a cylinder, whereas the actual pressures vary continuously from point to point. Consequently, the net horizontal loading cannot be determined accurately by the simple process of subtracting the back loading from the front loading. A rough approximation of the net load may be obtained by procedures similar to those described for a closed box-like structure (§ 4.45), but a better approximation is given by the method referred to in § 4.65 *et seq.*

ARCHED STRUCTURES

4.62 The following treatment is applicable to arched structures, such as ground huts, and, as a rough approximation, to dome shaped or spherical structures. The discussion presented here is for a semicylindrical structure with the direction of propagation of the blast perpendicular to the axis of the cylinder. The results can be applied to a cylindrical structure, such as discussed above, since it consists of two such semicylinders with identical loadings on

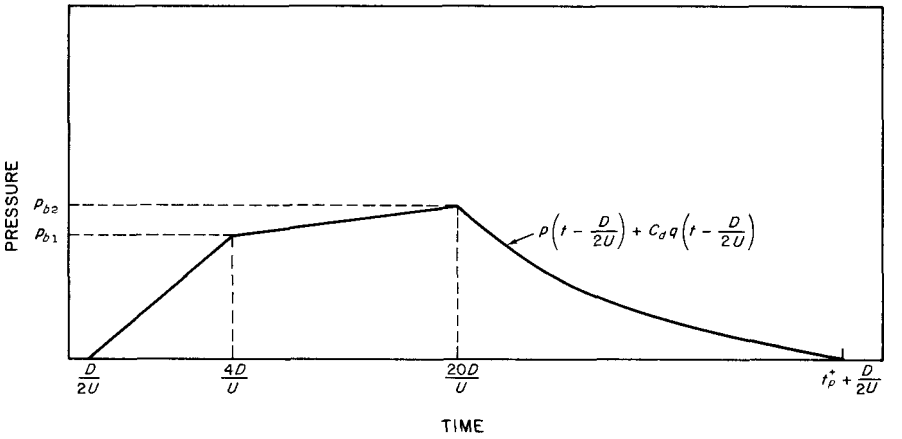

Figure 4.60. Average pressure variation on the back face of a cylinder.

each half. Whereas the preceding treatment referred to the average loads on the various faces of the cylinder (§ 4.57 *et seq.*), the present discussion describes the loads at each point. The general situation is depicted in Fig. 4.62; H is the height of the arch (or the radius of the cylinder) and z represents any point on the surface. The angle between the horizontal (or springing line) and the line joining z to the center of curvature of the semicircle is indicated by α; and X, equal to $H(1 - \cos \alpha)$, is the horizontal distance, in the direction of propagation of the blast wave, between the bottom of the arch and the arbitrary point z.

4.63 When an ideal blast wave impinges on a curved surface, vortex formation occurs just after reflection, so that there may be a temporary sharp pressure drop before the stagnation pressure is reached. A generalized representation of the variation of the pressure with time at any point, z, is shown in Fig. 4.63. The blast wave

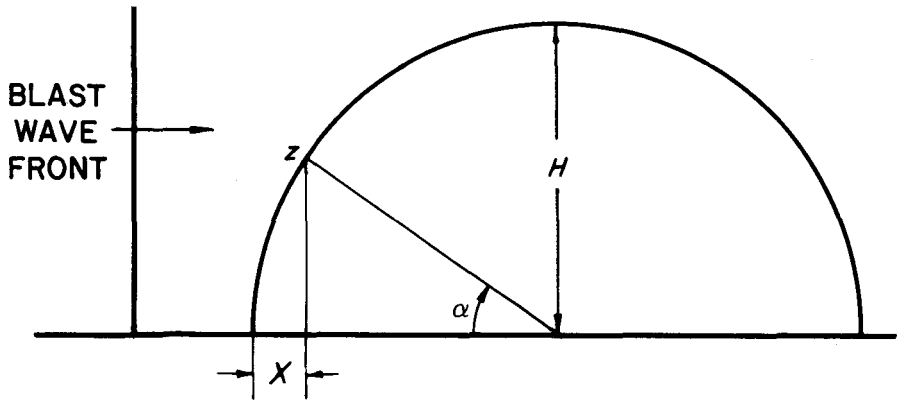

Figure 4.62. Representation of a typical semicircular arched structure.

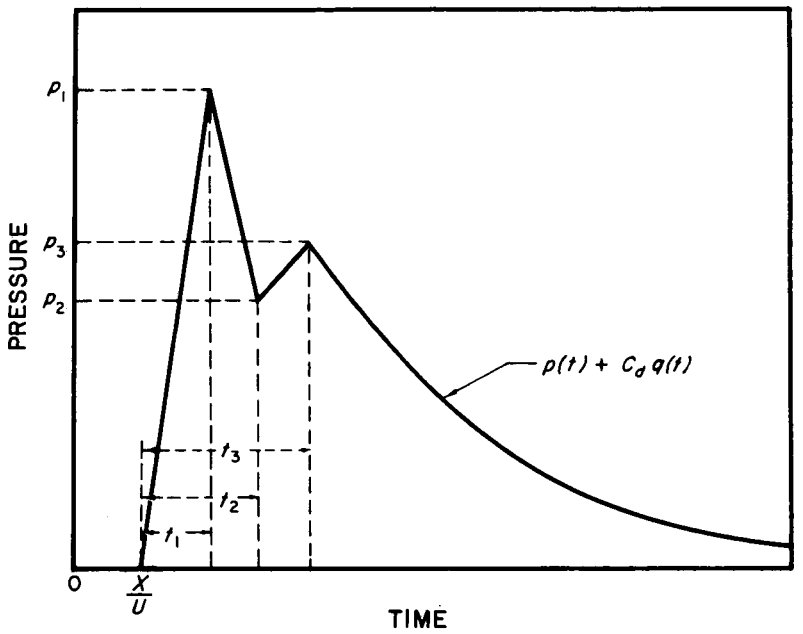

Figure 4.63. Typical pressure variation at a point on an arched structure subjected to a blast wave.

front strikes the base of the arch at time $t = 0$ and the time of arrival at the point z, regardless of whether it is on the front or back half, is X/U. The overpressure then rises sharply, in the time interval t_1, to the reflected value, p_1, so that t_1 is the rise time. Vortex formation causes the pressure to drop to p_2, and this is followed by an increase to p_3, the stagnation pressure; subsequently, the pressure, which is equal to $p(t) + C_d q(t)$, where C_d is the appropriate drag coefficient, decays in the normal manner.

4.64 The dependence of the pressures p_1 and p_2 and the drag coefficient C_d on the angle α is represented in Fig. 4.64; the pressure values are expressed as the ratios to p_r, where p_r is the ideal reflected pressure for a flat surface. When α is zero, i.e., at the base of the arch, p_1 is identical with p_r, but for larger angles it is less. The rise time t and the time intervals t_2 and t_3, corresponding to vortex formation and attainment of the stagnation pressure, respectively, after the blast wave reaches the base of the arch, are also given in Fig. 4.64, in terms of the time unit H/U. The rise time is seen to be zero for the front half of the arch, i.e., for α between 0° and 90°, but it is finite and increases with α on the back half, i.e., for a α between 90° and 180°. The times t_2 and t_3 are independent of the angle α.

4.65 Since the procedures described above give the loads normal to the surface at any arbitrary point z, the net horizontal loading is not determined by the simple process of subtracting the back loading from that on the front. To obtain the net horizontal loading, it is necessary to sum the horizontal compo-

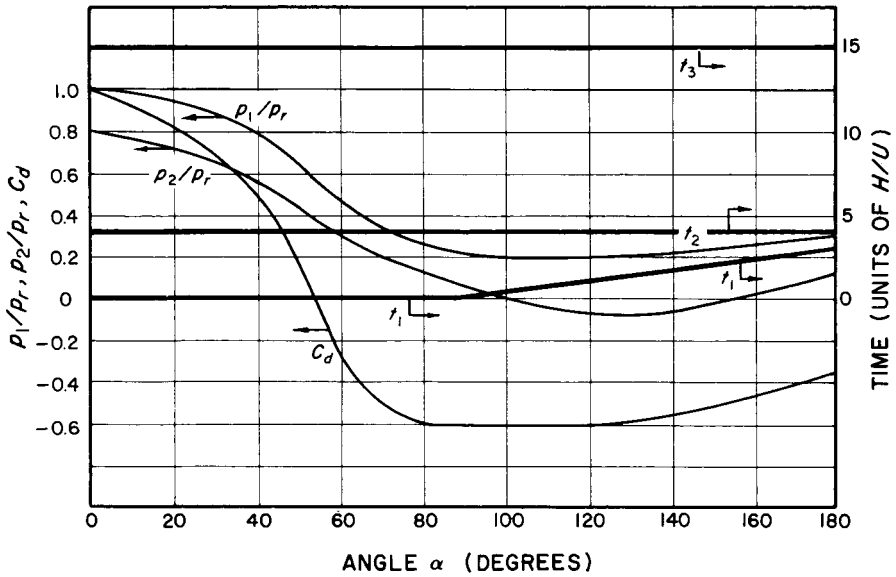

Figure 4.64. Variation of pressure ratios, drag coefficient, and time intervals for an arched structure.

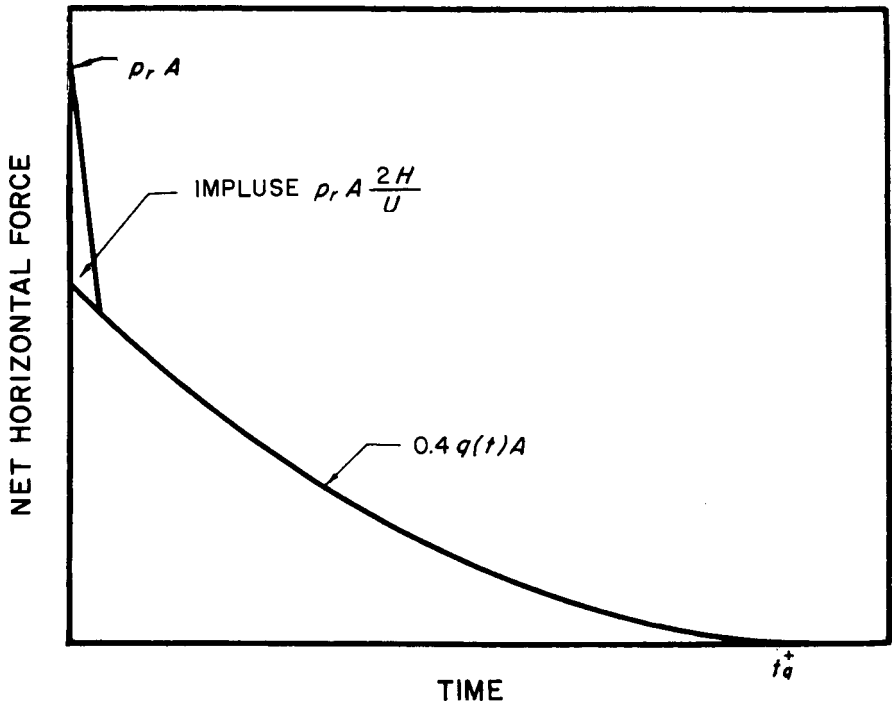

Figure 4.66. Approximate equivalent net horizontal force loading on semicylindrical structure.

nents of the loads over the two areas and then subtract them. In practice, an approximation may be used to obtain the required result in such cases where the net horizontal loading is considered to be important. It may be pointed out that, in certain instances, especially for large structures, it is the local loading, rather than the net loading, which is the significant criterion of damage.

4.66 In the approximate procedure for determining the net loading, the overpressure loading during the diffraction stage is considered to be equivalent to an initial impulse equal to $p_r A(2H/U)$, where A is the projected area normal to the direction of the blast propagation. It will be noted that $2H/U$ is the time taken for the blast front to traverse the structure. The net drag coefficient for a single cylinder is about 0.4 in the blast pressure range of interest (§ 4.23). Hence, in addition to the initial impulse, the remainder of the net horizontal loading may be represented by the force $0.4\, q(t)A$, as seen in Fig. 4.66, which applies to a single structure. When a frame is made up of a number of circular elements, the methods used are similar to those for an open frame structure (§ 4.55) with C_d equal to 0.2.

NONIDEAL BLAST WAVE LOADING

4.67 The preceding discussions have dealt with loading caused by blast waves reflected from nearly ideal ground surfaces (§ 3.47). In practice, however, the wave form will not always be ideal. In particular, if a precursor wave is formed (§ 3.79 *et seq.*), the loadings may depart radically from

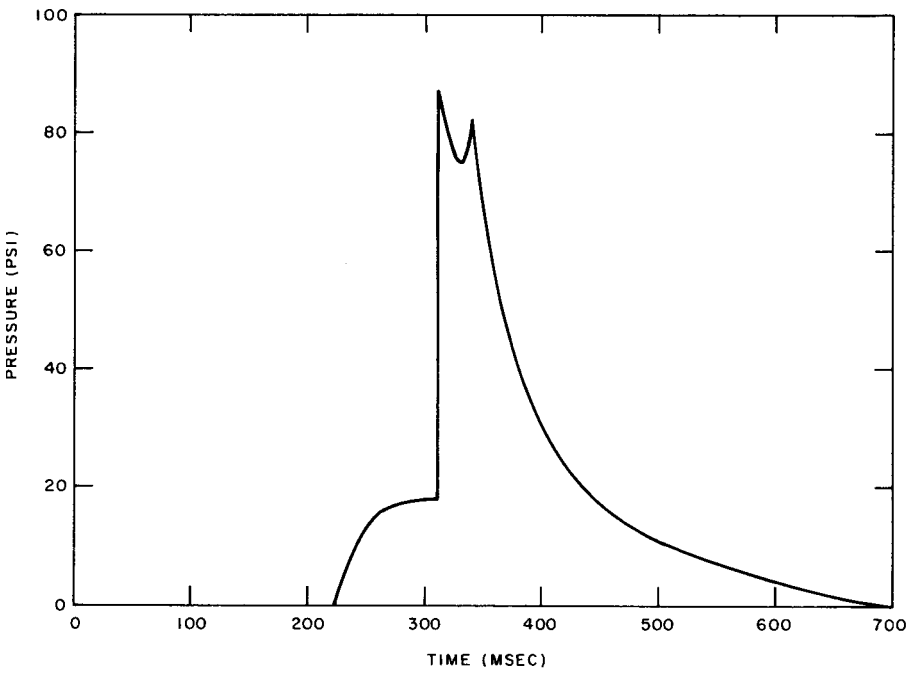

Figure 4.67a. Nonideal incident air blast (shock) wave.

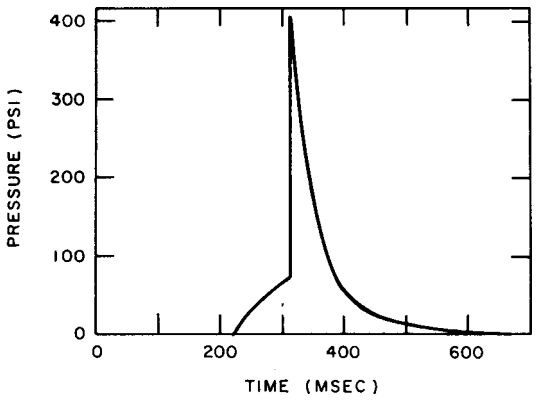

b.

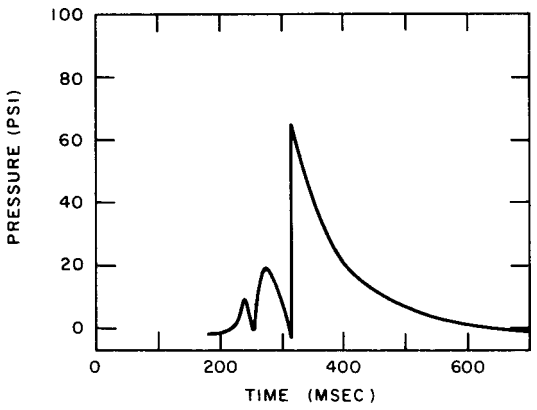

c.

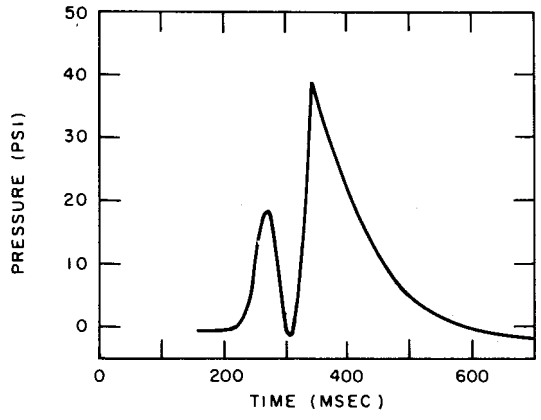

d.

Figure 4.67b, c, d. Loading pattern on the front, top, and back, respectively, on a rectangular block from nonideal blast wave.

those described above. Although it is beyond the scope of the present treatment to provide a detailed discussion of nonideal loading, one qualitative example is given here. Figure 4.67a shows a nonideal incident air blast (shock) wave and Figs. 4.67b, c, and d give the loading patterns on the front, top, and back, respectively, of a rectangular block as observed at a nuclear weapon test. Comparison of Figs. 4.67b, c, and d with the corresponding Figs. 4.42, 4.43, and 4.44 indicates the departures from ideal loadings that may be encountered in certain circumstances. The net loading on this structure was significantly less than it would have been under ideal conditions, but this would not necessarily always be the case.

BIBLIOGRAPHY

*AMERICAN SOCIETY OF CIVIL ENGINEERS, "Design of Structures to Resist Nuclear Weapons Effects," ASCE Manual of Engineering Practice No. 42, 1961.

*ARMOUR RESEARCH FOUNDATION, "A Simple Method of Evaluating Blast Effects on Buildings," Armour Research Foundation, Chicago, Illinois, 1954.

*BANISTER, J. R., and L. J. VORTMAN, "Effect of a Precursor Shock Wave on Blast Loading of a Structure," Sandia Corporation, Albuquerque, New Mexico, October 1960, WT-1472.

JACOBSEN, L. S. and R. S. AYRE, "Engineering Vibrations," McGraw-Hill Book Co., Inc., New York, 1958.

KAPLAN, K. and C. WIEHLE, "Air Blast Loading in the High Shock Strength Region," URS Corporation, Burlingame, California, 1965, URS 633-3 (DASA 1460-1), Part II.

*MITCHELL, J. H., "Nuclear Explosion Effects on Structures and Protective Construction—A Selected Bibliography," U.S. Atomic Energy Commission, April 1961, TID-3092.

PICKERING, E. E., and J. L. BOCKHOLT, "Probabilistic Air Blast Failure Criteria for Urban Structures," Stanford Research Institute, Menlo Park, California, November 1971.

WILLOUGHBY, A. B., *et al.*, "A Study of Loading, Structural Response, and Debris Characteristics of Wall Panels," URS Research Co., Burlingame, California, July 1969.

WILTON, C., *et al.*, "Final Report Summary, Structural Response and Loading of Wall Panels," URS Research Co., Burlingame, California, July 1971.

*These documents may be purchased from the National Technical Information Service, U.S. Department of Commerce, Springfield, Virginia 22161.

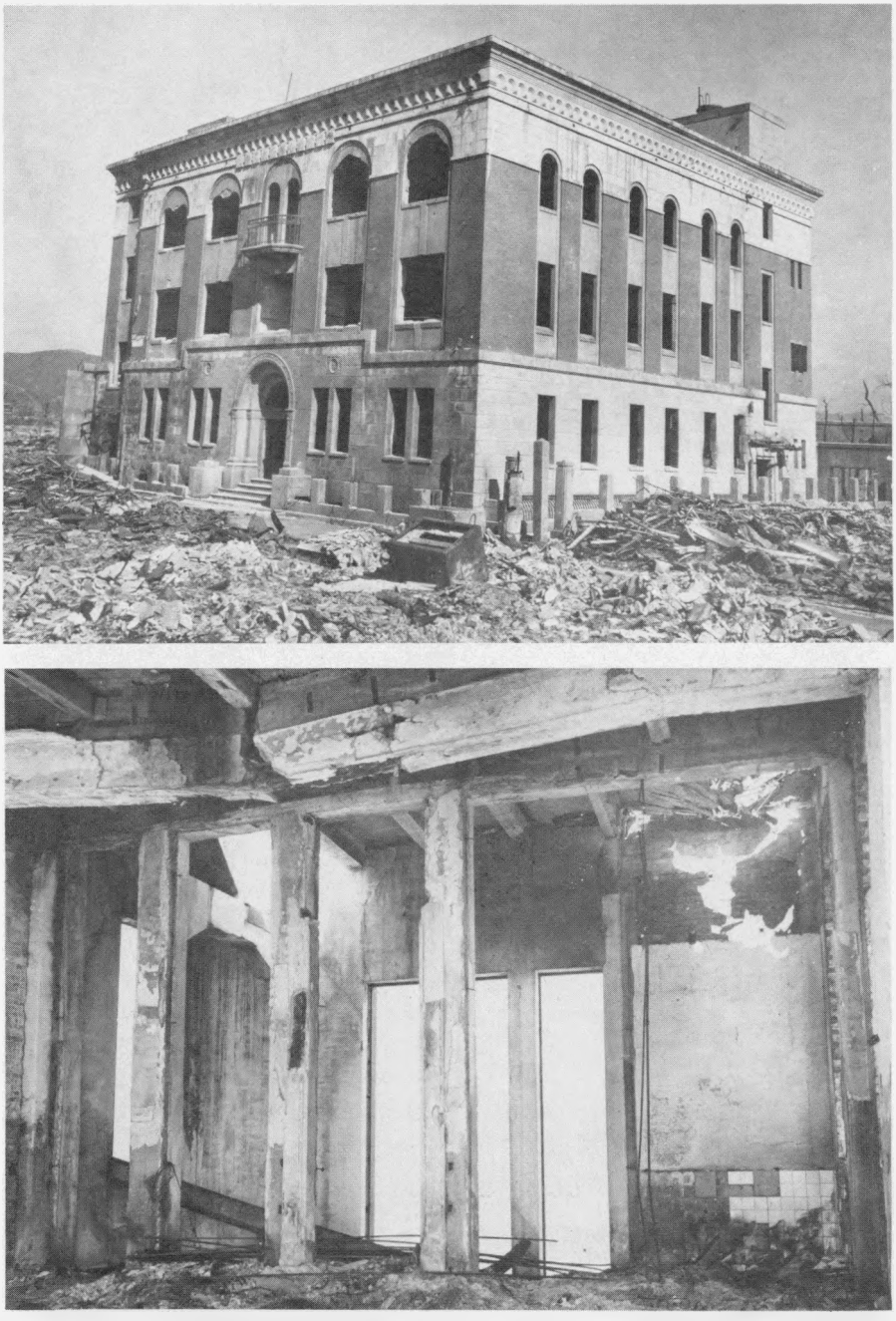

Figure 5.20a. Upper photo: Reinforced-concrete, aseimic structure; window fire shutters were blown in by blast and the interior gutted by fire (0.12 mile from ground zero at Hiroshima). Lower photo: Burned out interior of similar structure.

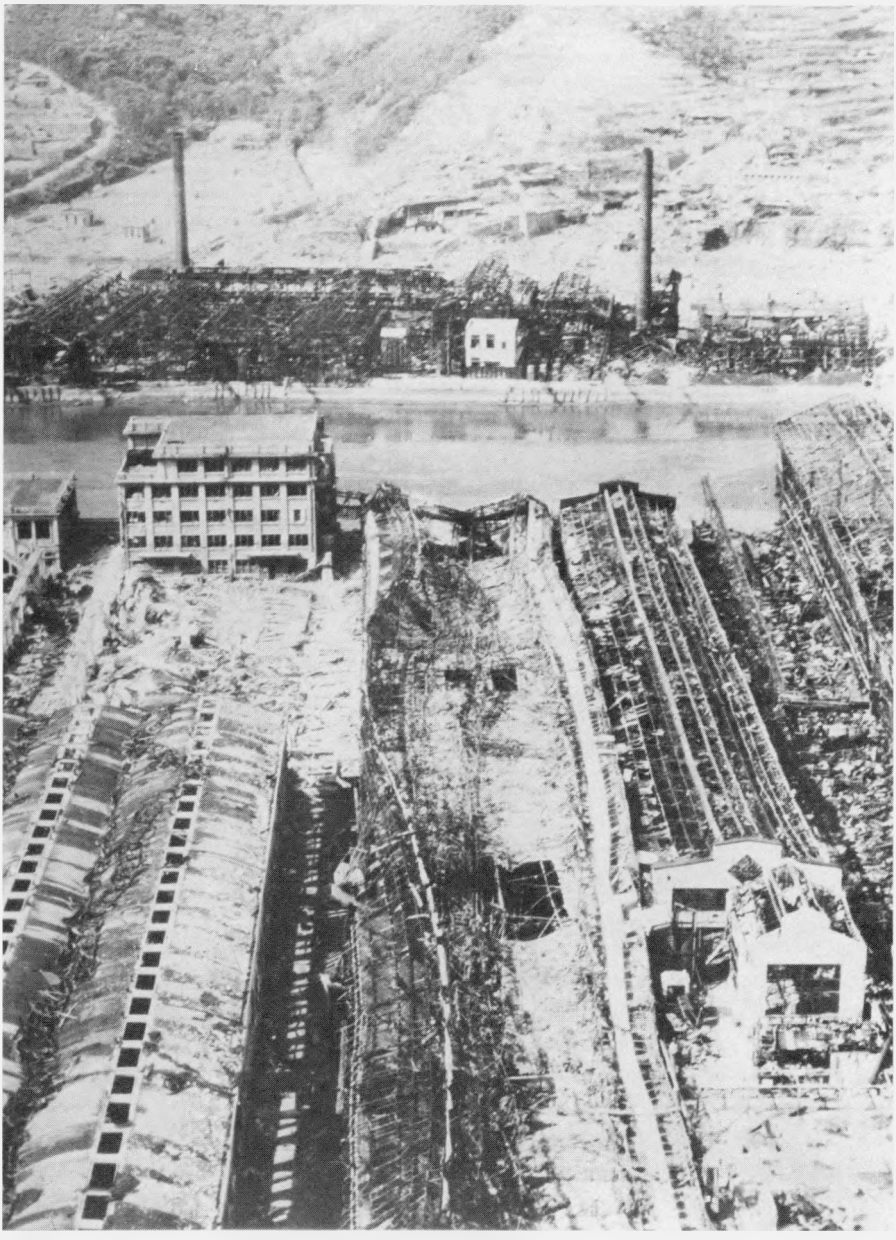

Figure 5.25. At left and back of center is a multistory, steel-frame building (0.85 mile from gound zero at Nagasaki).

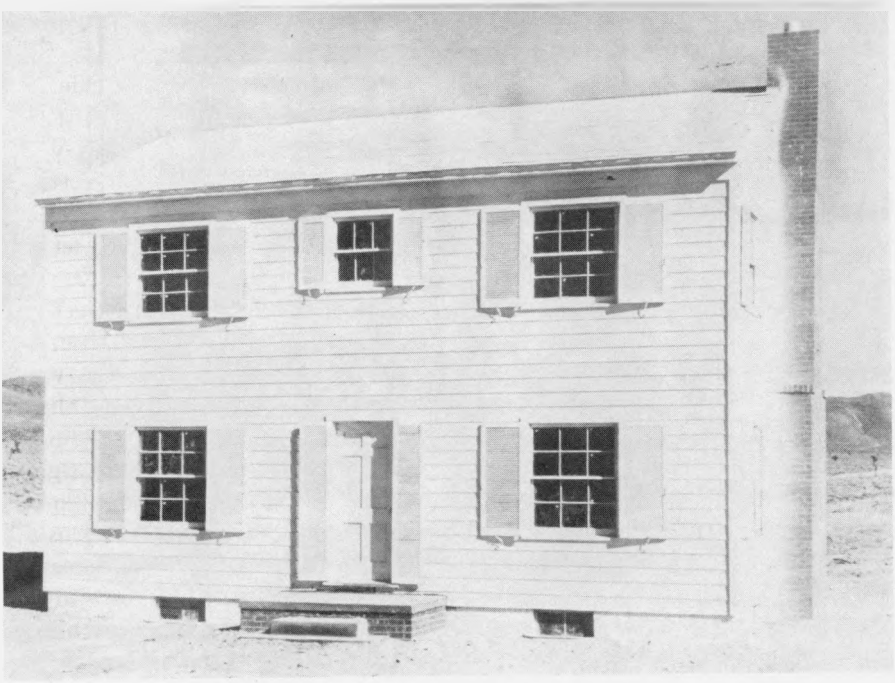

Figure 5.55. Wood-frame house before a nuclear explosion, Nevada Test Site.

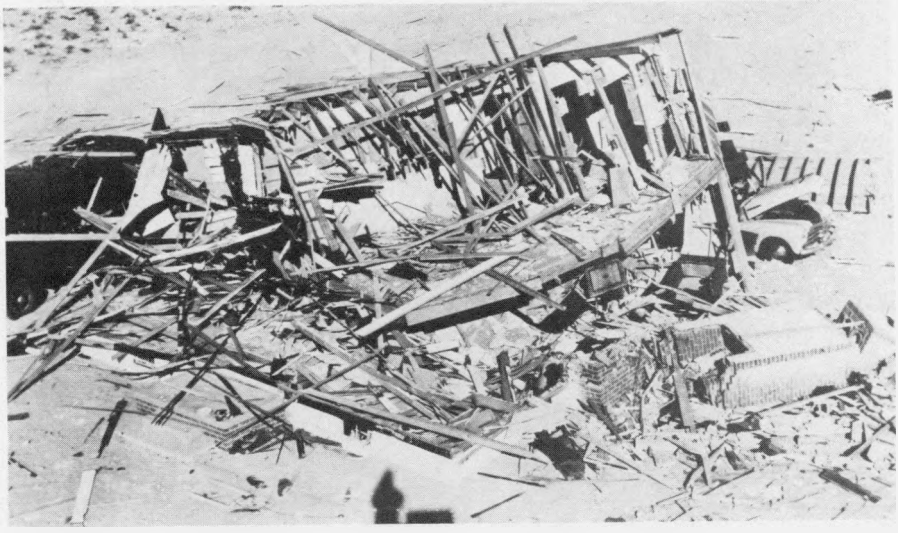

Figure 5.57. Wood-frame house after a nuclear explosion (5 psi peak overpressure).

Figure 5.66. Unreinforced brick house before a nuclear explosion, Nevada Test Site.

Figure 5.67. Unreinforced brick house after a nuclear explosion (5 psi peak overpressure).

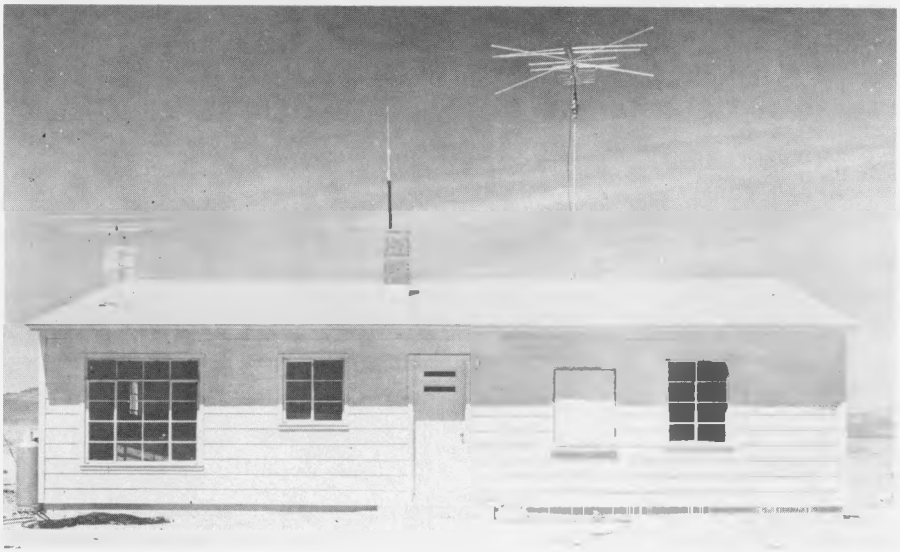

Figure 5.69. Rambler-type house before a nuclear explosion, Nevada Test Site. (Note blast door over bathroom window at right.)

5.70 When exposed to an incident peak overpressure of about 5 pounds per square inch, one of these houses was demolished beyond repair. However, the bathroom shelter was not damaged at all. Although the latch bolt on the blast shutter failed, leaving the shutter unfastened, the window was still intact. The roof was blown off and the rafters were split and broken. The side walls at gable ends were blown outward, and fell to the ground. A portion of the front wall remained standing, although it was leaning away from the direction of the explosion (Fig. 5.70).

5.71 The other house of the same type, subjected to a peak overpressure of 1.7 pounds per square inch, did not suffer too badly and it could easily have been made habitable. Windows were broken, doors blown off their hinges, and plaster-board walls and ceilings were badly damaged. The main structural damage was a broken midspan rafter beam and distortion of the frame. In addition, the porch roof was lifted 6 inches off its supports.

ONE-STORY, PRECAST CONCRETE HOUSE: 1955 TEST

5.72 Another residential type of construction tested in Nevada in 1955 was a single-story house made of precast, lightweight (expanded shale aggregate) concrete wall and partition panels, joined by welded matching steel lugs. Similar roof panels were anchored to the walls by special countersunk and grouted connections. The walls were supported on concrete piers and a concrete floor slab, poured in place on a tamped fill after the walls were erected. The floor was anchored securely to the walls by means of perimeter reinforcing rods held by hook bolts screwed into

Figure 5.70. Rambler-type house after a nuclear explosion (5 psi peak overpressure).

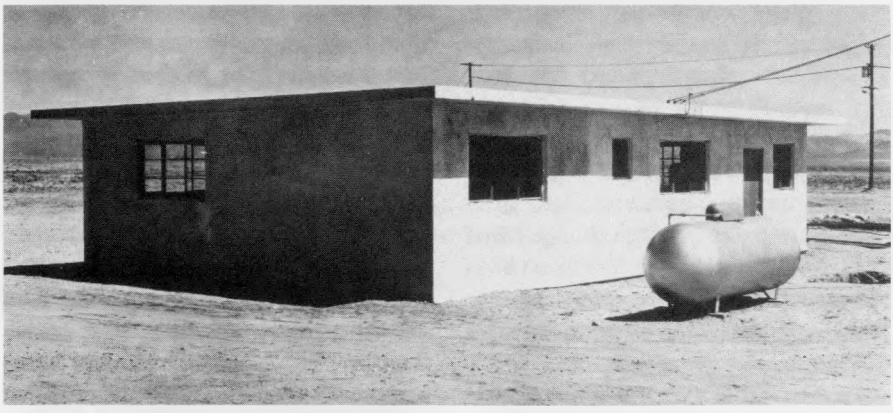

Figure 5.72. Reinforced precast concrete house before a nuclear explosion, Nevada Test Site.

inserts in the wall panels. The overall design was such as to comply with the California code for earthquake-resistant construction (Fig. 5.72).

5.73 This house stood up well, even at a peak overpressure of 5 pounds per square inch. By replacement of demolished or badly damaged doors and windows, it could have been made available for occupancy (Fig. 5.73).

5.74 There was some indication that the roof slabs at the front of the house were lifted slightly from their supports, but this was not sufficient to break any connections. Some of the walls were cracked slightly and others showed indications of minor movement. In certain areas the concrete around the slab connections was spalled, so that the connectors were exposed. The steel

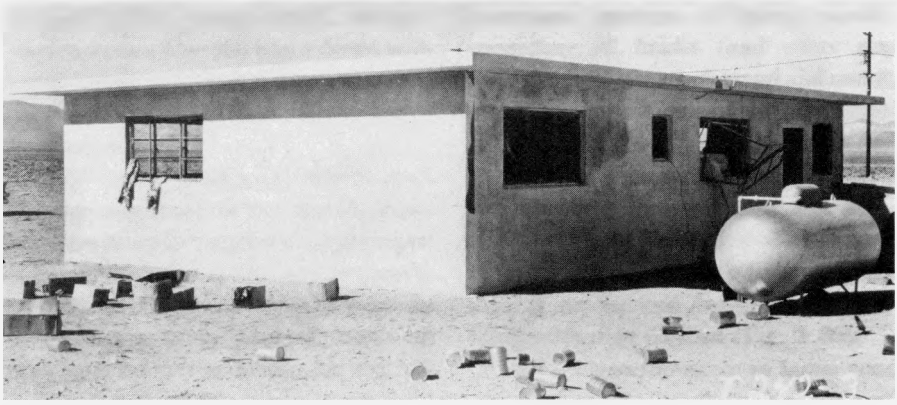

Figure 5.73. Reinforced precast concrete house after a nuclear explosion (5 psi peak overpressure). The LP-gas tank, sheltered by the house, is essentially undamaged.

window-sash was somewhat distorted, but it remained in place.

5.75 At a peak overpressure of 1.7 pounds per square inch, the precast concrete-slab house suffered relatively minor damage. Glass was broken extensively, and doors were blown off their hinges and demolished, as in other houses exposed to the same air pressure. But, apart from this and distortion of the steel window-sash, the only important damage was spalling of the concrete at the lug connections, i.e., where the sash projected into the concrete.

ONE-STORY, REINFORCED-MASONRY HOUSE: 1955 TEST

5.76 The last type of house subjected to test in 1955 was also of earthquake-resistant design. The floor was a concrete slab, poured in place at grade. The walls and partitions were built of lightweight (expanded shale aggregate) 8-inch masonry blocks, reinforced with vertical steel rods anchored into the floor slab. The walls were also reinforced with horizontal steel rods at two levels, and openings were spanned by reinforced lintel courses. The roof was made of precast, lightweight concrete slabs, similar to those used in the precast concrete houses described above (Fig. 5.76).

5.77 At a peak overpressure of about 5 pounds per square inch, windows were destroyed and doors blown in the demolished. The steel window-sash was distorted, but nearly all remained in place. The house suffered only minor structural damage and could have been made habitable at relatively small cost (Fig. 5.77).

5.78 There was some evidence that the roof slabs had been moved, but not sufficiently to break any connections. The masonry wall under the large window (see Fig. 5.77) was pushed in about 4 inches on the concrete floor slab; this appeared to be due to the omission of dowels between the walls and the floor beneath window openings. Some cracks developed in the wall above the same window, probably as a result of improper installation of the reinforced lintel course and the substitution of a pipe

Figure 5.76. Reinforced masonry-block house before a nuclear explosion, Nevada Test Site.

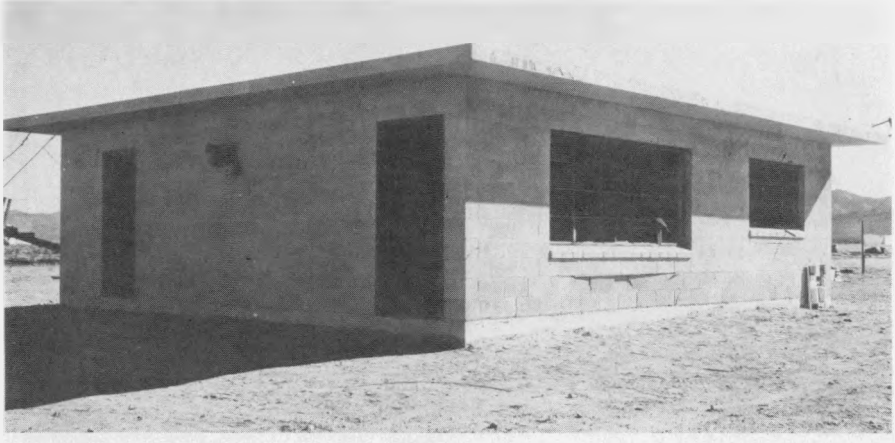

Figure 5.77. Reinforced masonry-block house after a nuclear explosion (5 psi peak overpressure).

column in the center span of the window.

5.79 A house of the same type exposed to the blast at a peak overpressure of 1.7 pounds per square inch suffered little more than the usual destruction of doors and windows. The steel window-sash remained in place but was distorted, and some spalling of the concrete around lug connections was noted. On the whole, the damage to the house was of a minor character and it could readily have been repaired.

TRAILER-COACH MOBILE HOMES: 1955 TEST

5.80 Sixteen trailer-coaches of various makes, intended for use as mobile homes, were subjected to blast in the 1955 test in Nevada. Nine were located where the peak blast overpressure was 1.7 pounds per square inch, and the other seven where the peak overpressure was about 1 pound per square inch. They were parked at various angles with respect to the direction of travel of the blast wave.

5.81 At the higher overpressure two of the mobile homes were tipped over by the explosion. One of these was originally broadside to the blast, whereas the second, at an angle of about 45°, was of much lighter weight. All the others at both locations remained standing. On the whole, the damage sustained was not of a serious character.

5.82 From the exterior, many of the mobile homes showed some dents in walls or roof, and a certain amount of distortion. There were, however, relatively few ruptures. Most windows were broken, but there was little or no glass in the interior, especially in those coaches having screens fitted on the inside. Where there were no screens or venetian blinds, and particularly where there were large picture windows, glass was found inside.

5.83 The interiors of the mobile homes were usually in a state of disorder due to ruptured panels, broken and upset furniture, and cupboards, cabinets, and wardrobes which had been torn loose and damaged. Stoves, refrigerators, and heaters were not displaced, and the floors were apparently unharmed. The plumbing was, in general, still operable after the explosion. Consequently, by rearranging the displaced furniture, repairing cabinets, improvising window coverings, and cleaning up the debris, all trailer-coaches could have been made habitable for emergency use.

5.84 At the 1 pound per square inch overpressure location some windows were broken, but no major damage was sustained. The principal repairs required to make the mobile homes available for occupancy would be window replacement or improvised window covering.

TRANSPORTATION

LIGHT LAND TRANSPORTATION EQUIPMENT

5.85 In Japan, trolley-car equipment was heavily damaged by both blast and fire, although the poles were frequently left standing. Buses and automobiles generally were rendered inoperable by blast and fire as well as by damage caused by flying debris. However, the damage decreased rapidly with distance. An American made automobile was badly damaged and burned at 3,000 feet (0.57 mile) from ground zero, but a similar vehicle at 6,000 feet (1.14 miles) suffered only minor damage.

5.86 Automobiles and buses have been exposed to several of the nuclear test explosions in Nevada, where the conditions, especially as regards dam-

Figure 5.87a. Damage to automobile originally located behind wood-frame house (5 psi peak overpressure); the front of this car can be seen in Figure 5.57. Although badly damaged, the car could still be driven after the explosion.

Figure 5.87b. Typical public bus damaged by a nuclear explosion, Nevada Test Site; this bus, like the one in the left background, was overturned, coming to rest as shown after a displacement of 50 feet.

age by fire and missiles, were somewhat different from those in Japan. In the descriptions that follow, distance is related to peak overpressure. In most cases, however, it was not primarily overpressure, but drag forces, which produced the damage. In addition, allowance must be made for the effect of the blast wave precursor (§ 3.79 *et seq.*). Hence, the damage radii cannot be determined from overpressure alone.

5.87 Some illustrations of the effects of a nuclear explosion on motorized vehicles are shown in Figs. 5.87a and b. At a peak overpressure of 5 pounds per square inch motor vehicles were badly battered, with their tops and sides pushed in, windows broken, and hoods blown open. But the engines were still operable and the vehicles could be driven away after the explosion. Even at higher blast pressures, when the overall damage was greater, the motors appeared to be intact.

5.88 During the 1955 tests in Nevada, studies were made to determine the extent to which various emergency vehicles and their equipment would be available for use immediately following a nuclear attack. The vehicles included a rescue truck, gas and electric utility service or repair trucks, telephone service trucks, and fire pumpers and ladder trucks. One vehicle was exposed to a peak overpressure of about 30 pounds per square inch, two at 5 pounds per square inch, two at 1.7 pounds per square inch, and six at about 1 pound per square inch. It should be emphasized, however, that, for vehicles in general, overpressure is not usually the sole or even the primary damage mechanism.

5.89 The rescue truck at the 30 pounds per square inch location was completely destroyed, and only one wheel and part of the axle were found after the blast. At 5 pounds per square inch peak overpressure a truck, with an earth-boring machine bolted to the bed, was broadside to the blast. This truck was overturned and somewhat damaged, but still operable (Fig. 5.89). The earth-boring machine was knocked loose and was on its side leaking gasoline and water. At the same location, shown to the left of the overturned truck in Fig. 5.89, was a heavy-duty electric utility truck, facing head-on to the blast. It had the windshield shattered, both doors and cab dished in, the hood partly blown off, and one tool-compartment door dished. There was, however, no damage to tools or equipment and the truck was driven away without any repairs being required.

5.90 At the 1.7 pounds per square inch location, a light-duty electric utility truck and a fire department 75-foot aerial ladder truck sustained minor exterior damage, such as broken windows and dished-in panels. There was no damage to equipment in either case, and both vehicles would have been available for immediate use after an attack. Two telephone trucks, two gas utility trucks, a fire department pumper, and a Jeep firetruck, exposed to a peak overpressure of 1 pound per square inch, were largely unharmed.

5.91 It may be concluded that vehicles designed for disaster and emergency operation are substantially constructed, so that they can withstand a peak overpressure of about 5 pounds per square inch and the associated dynamic pressure and still be capable of operation. Tools and equipment are protected

Figure 5.89. Truck broadside to the blast wave (5 psi peak overpressure) overturned; electric utility truck in background head-on to blast was damaged but remained standing.

from the blast by the design of the truck body or when housed in compartments with strong doors.

RAILROAD EQUIPMENT

5.92 Railroad equipment suffered blast damage in Japan and also in tests in Nevada. Like motor vehicles, these targets are primarily drag sensitive and damage cannot be directly related to overpressure. At a peak overpressure of 2 pounds per square inch from a kiloton-range weapon, an empty wooden boxcar may be expected to receive relatively minor damage. At 4 pounds per square inch overpressure, the damage to a loaded wooden boxcar would be more severe (Fig. 5.92a). At a peak overpressure of 6 pounds per square inch the body of an empty wooden boxcar, weighing about 20 tons, was lifted off the trucks, i.e., the wheels, axles, etc., carrying the body, and landed about 6 feet away. The trucks themselves were pulled off the rails, apparently by the brake rods connecting them to the car body. A similar boxcar, at the same location, loaded with 30 tons of sandbags remained upright (Fig. 5.92b). Although the sides were badly damaged and the roof demolished, the car was capable of being moved on its own wheels. At 7.5 pounds per square inch peak overpressure, a loaded boxcar of the same type was overturned, and at 9 pounds per square inch it was completely demolished.

5.93 A Diesel locomotive weighing 46 tons was exposed to a peak over-

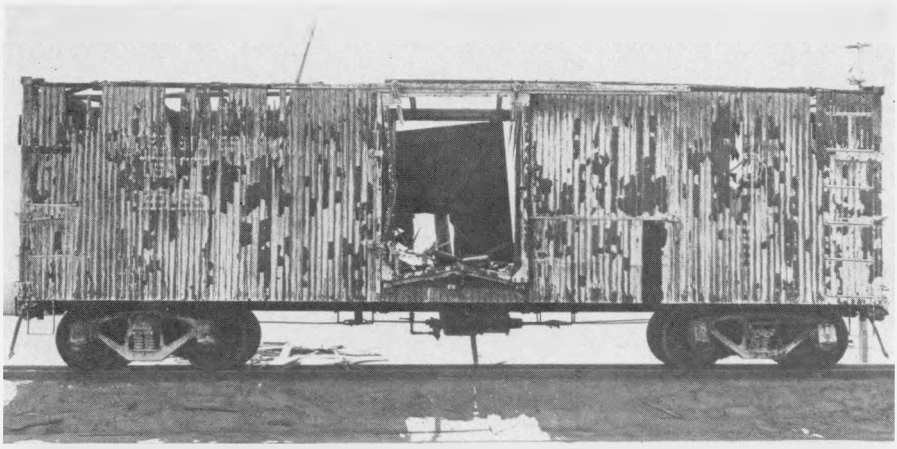

Figure 5.92a. Loaded wooden boxcar after a nuclear explosion (4 psi peak overpressure).

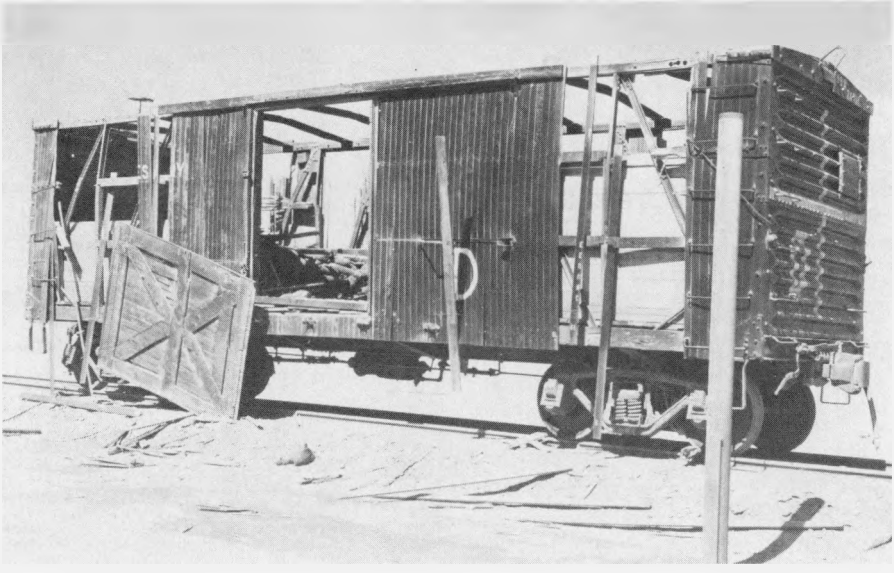

Figure 5.92b. Loaded wooden boxcar after a nuclear explosion (6 psi peak overpressure).

pressure of 6 pounds per square inch while the engine was running. It continued to operate normally after the blast, in spite of damage to windows and compartment doors and panels. There was no damage to the railroad track at this point.

AIRCRAFT

5.94 Aircraft are damaged by blast effects at levels of peak overpressure as low as 1 to 2 pounds per square inch. Complete destruction or damage beyond economical repair may be expected at peak overpressures of 4 to 10 pounds per square inch. Within this range, the peak overpressure appears to be the main criterion of damage. However, tests indicate that, at a given overpressure, damage to an aircraft oriented with the nose toward the burst will be less than damage to one with the tail or a side directed toward the explosion.

5.95 Damage to an aircraft exposed with its left side to the blast at a peak overpressure of 3.6 pounds per square inch is shown in Fig. 5.95a. The fuselage of this aircraft failed completely just aft of the wing. The skin of the fuselage, stabilizers, and engine cowling was severely buckled. Figure 5.95b shows damage to an aircraft oriented with its tail toward the burst and exposed to 2.4 pounds per square inch peak overpressure. Skin was dished in on the vertical stabilizer, horizontal stabilizers, wing surface above the flaps, and outboard wing sections. Vertical stabilizer bulkheads and the fuselage frame near the cockpit were buckled.

SHIPPING

5.96 Damage to ships from an air or surface burst is due primarily to the air blast, since little pressure is transmitted through the water. At closer ranges, air blast can cause hull rupture resulting in flooding and sinking. Such rupture appears likely to begin near the waterline on the side facing the burst. Since the main hull generally is stronger than the superstructure, structures and equipment exposed above the waterline may be damaged at ranges well beyond that at which hull rupture might occur. Masts, spars, radar antennas, stacks, electrical equipment, and other light objects are especially sensitive to air blast. Damage to masts and stacks is apparent in Fig. 5.96; the ship was approximately 0.47 mile from surface zero at the ABLE test (about 20-kiloton air burst) at Bikini in 1946. Air blast may also roll and possibly capsize the ship; this effect would be most pronounced for the air blast wave from a large weapon striking the ship broadside.

5.97 Blast pressures penetrating through openings of ventilation systems and stack-uptake systems can cause damage to interior equipment and compartments, and also to boilers. Damage to the latter may result in immobilization of the ship. The distortion of weather bulkheads may render useless interior equipment mounted on or near them. Similarly, the suddenly applied blast loading induces rapid motion of the structures which may cause shock damage to interior equipment. Equipment in the superstructure is most susceptible to this type of damage, although shock motions may be felt throughout the ship.

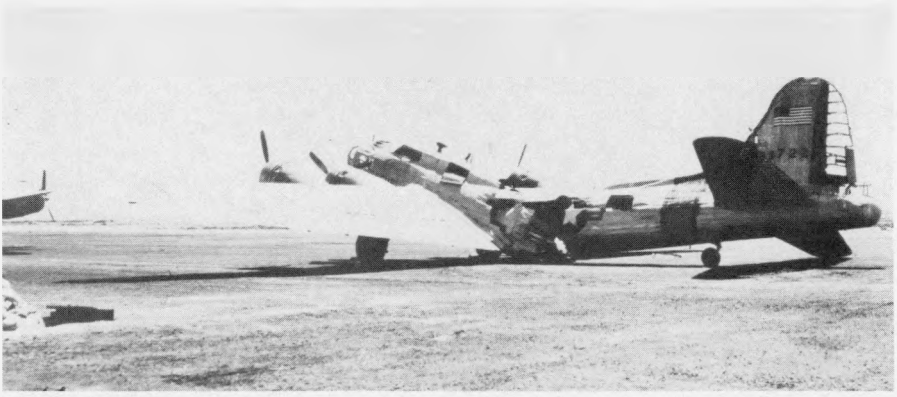

Figure 5.95a. Aircraft after side exposed to a nuclear explosion (3.6 psi peak overpressure).

Figure 5.95b. Aircraft after tail exposed to a nuclear explosion (2.4 psi peak overpressure).

UTILITIES

ELECTRICAL DISTRIBUTION SYSTEMS

5.98 Because of the extensive damage caused by the nuclear explosions to the cities in Japan, the electrical distribution systems suffered severely. Utility poles were destroyed by blast or fire, and overhead lines were heavily damaged at distances up to 9,000 feet (1.7 miles) from ground zero (Fig. 5.98).

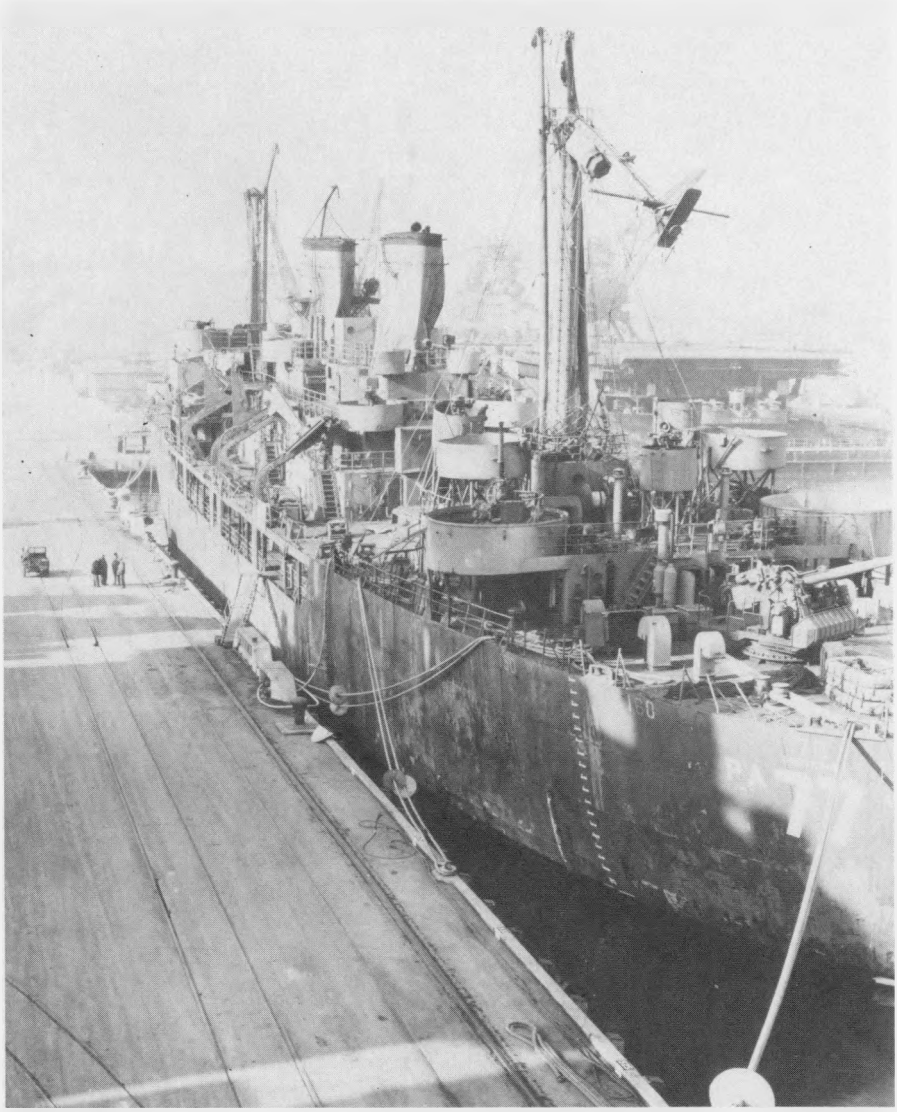

Figure 5.96. The U.S.S. Crittenden after ABLE test; damage resulting was generally serious (0.47 mile from surface zero).

Underground electrical circuits were, however, little affected. Switchgear and transformers were not damaged so much directly by blast as by secondary effects, such as collapse of the structure in which they were located or by debris. Motors and generators were damaged by fire.

5.99 A fairly extensive study of the effects of a nuclear explosion on electric utilities was made in the Nevada tests in 1955. Among the purposes of these tests

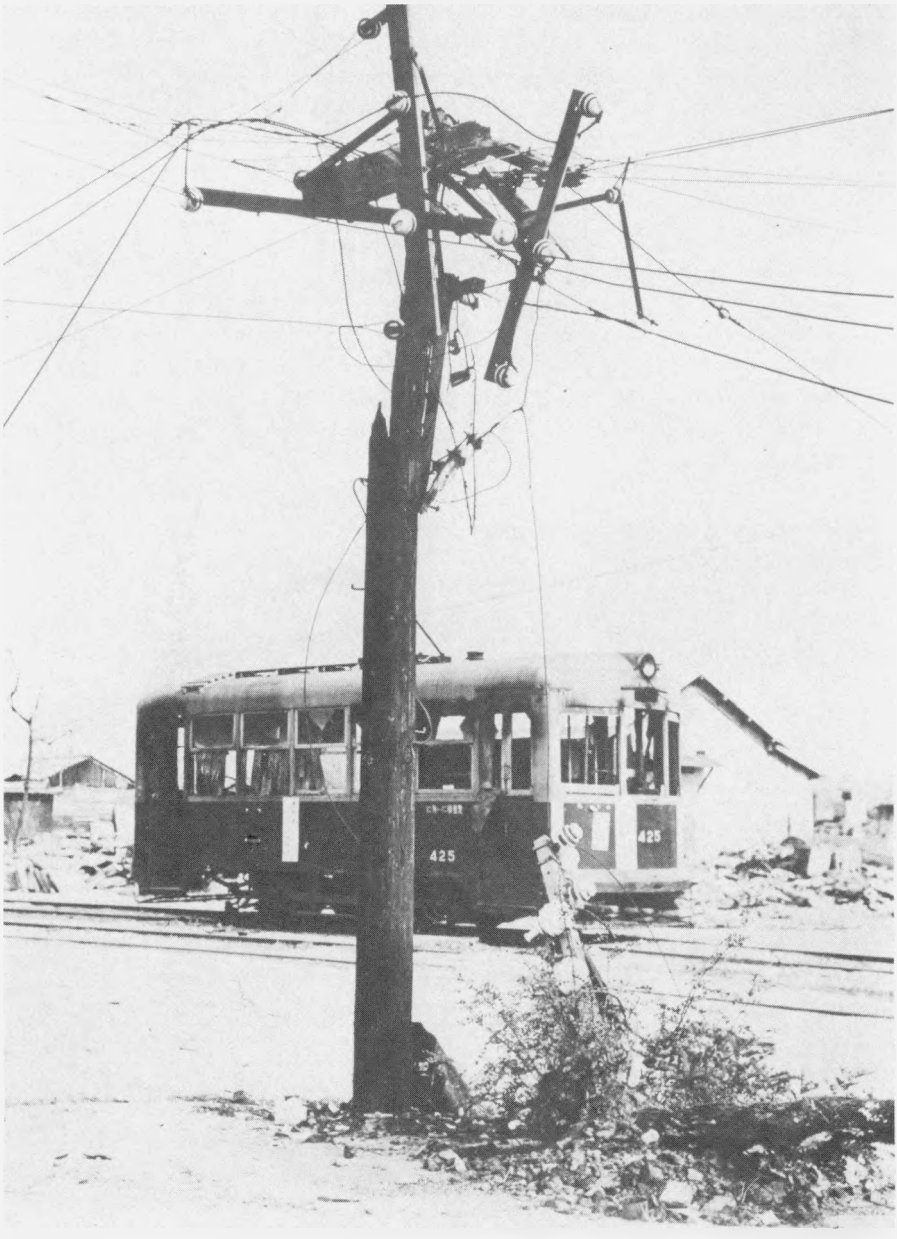

Figure 5.98. Damage to utility pole (0.80 mile from ground zero at Hiroshima).

were the following: (1) to determine the blast pressure at which standard electrical equipment might be expected to suffer little or no damage; (2) to study the extent and character of the damage that might be sustained in a nuclear

attack; and (3) to determine the nature of the repairs that would be needed to restore electrical service in those areas where homes and factories would survive sufficiently to permit their use after some repair. With these objectives in mind, two identical power systems were erected; one to be subjected to a peak overpressure of about 5 and a dynamic pressure of 0.6 pounds per square inch and the other to 1.7 and 0.1 pounds per square inch, respectively. It will be recalled that, at the lower overpressure, typical American residences would not be damaged beyond the possibility of further use.

5.100 Each power system consisted of a high-voltage (69-kV) transmission line on steel towers connected to a conventional, outdoor transformer substation. From this proceeded typical overhead distribution lines on 15 wood poles; the latter were each 45 feet long and were set 6 feet in the ground. Service drops from the overhead lines supplied electricity to equipment placed in some of the houses used in the tests described earlier. These installations were typical of those serving an urban community. In addition, the 69-kV transmission line, the 69-kV switch rack with oil circuit-breakers, and power transformer represented equipment of the kind that might supply electricity to large industrial plants.

5.101 At a peak overpressure of 5 and a dynamic pressure of 0.6 pounds per square inch the power system suffered to some extent, but it was not seriously harmed. The type of damage appeared, on the whole, to be similar to that caused by severe wind storms. In addition to the direct effect of blast, some destruction was due to missiles.

5.102 The only damage suffered by the high-voltage transmission line was the collapse of the suspension tower, bringing down the distribution line with it (Fig. 5.102a). It may be noted that the dead-end tower, which was much stronger and heavier, and another suspension tower of somewhat stronger design were only slightly affected (Fig. 5.102b). In some parts of the United States, the suspension towers are of similar heavy construction. Structures of this type are sensitive to drag forces which are related to dynamic pressure and positive phase duration, so that the overpressure is not the important criterion of damage.

5.103 The transformer substation survived the blast with relatively minor damage to the essential components. The metal cubicle, which housed the meters, batteries, and relays, suffered badly, but this substation and its contents were not essential to the emergency operation of the power system. The 4-kV regulators had been shifted on the concrete pad, resulting in separation of the electrical connections to the bus. The glass cells of the batteries were broken and most of the plates were beyond repair. But relays, meters, and other instruments were undamaged, except for broken glass. The substation as a whole was in sufficiently sound condition to permit operation on a nonautomatic (manual) basis. By replacing the batteries, automatic operation could have been restored.

5.104 Of the 15 wood poles used to carry the lines from the substation to the houses, four were blown down completely and broken, and two others were extensively damaged. The collapse of the poles was attributed partly to the

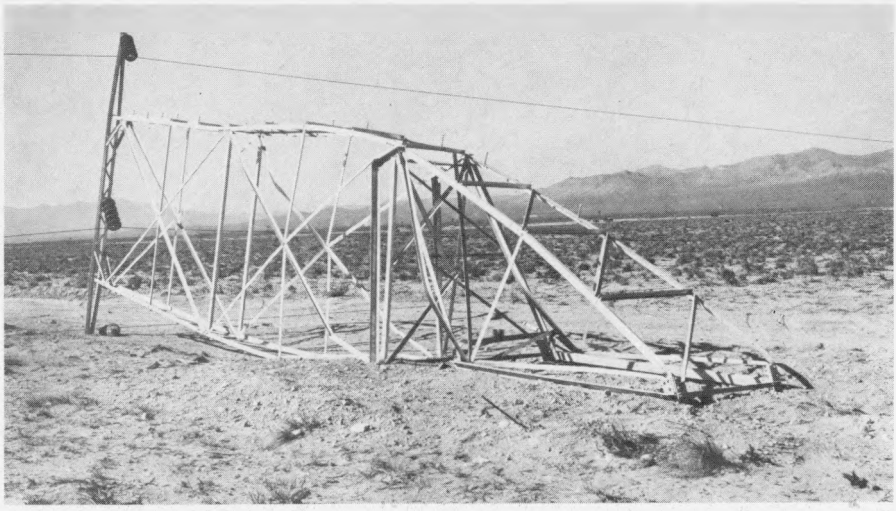

Figure 5.102a. Collapsed suspension tower (5 psi peak overpressure, 0.6 psi dynamic pressure from 30-kiloton explosion), Nevada Test Site.

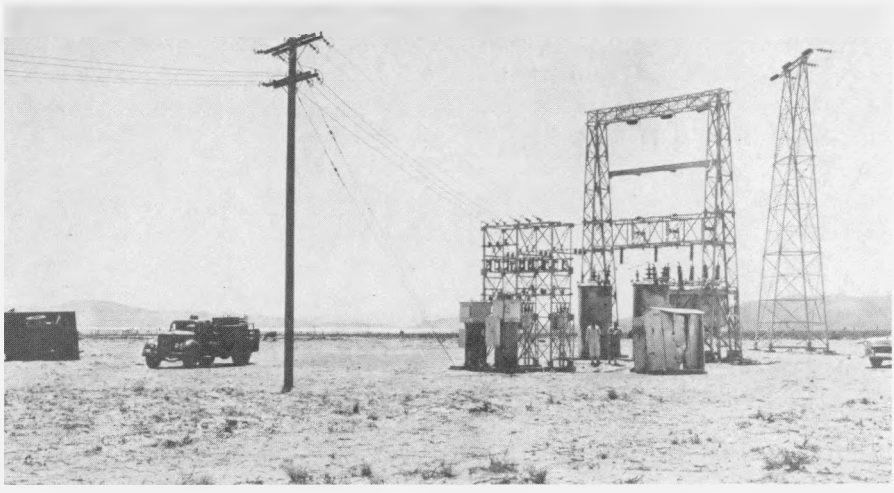

Figure 5.102b. Dead-end tower, suspension tower, and transformers (5 psi peak overpressure, 0.6 psi dynamic pressure from 30-kiloton explosion), Nevada Test Site. The trucks at the left of the photograph are those in Figure 5.89.

weight and resistance of the aerial cable (Fig. 5.104). Other damage was believed to be caused by missiles.

5.105 Several distributor transformers had fallen from the poles and secondary wires and service drops were down (Fig. 5.105). Nevertheless the transformers, pot heads, arresters, cutouts, primary conductors of both aluminum and copper, and the aerial cables

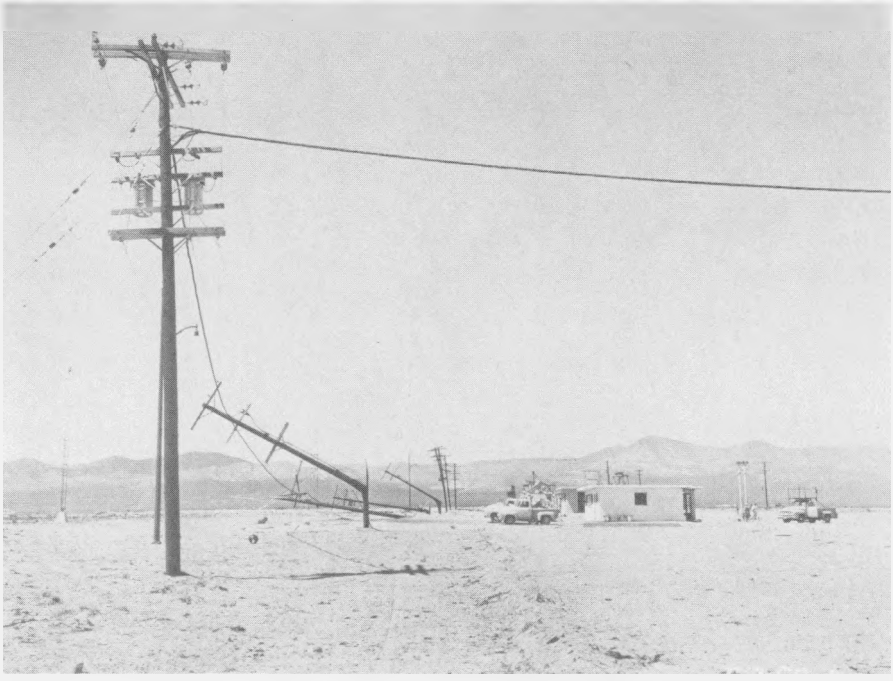

Figure 5.104. Collapse of utility poles on line (5 psi peak overpressure, 0.6 psi dynamic pressure from 30-kiloton explosion), Nevada Test Site.

were unharmed. Although the pole line would have required some rebuilding, the general damage was such that it could have been repaired within a day or so with materials normally carried in stock by electric utility companies.

GAS, WATER, AND SEWERAGE SYSTEMS

5.106 The public utility system in Nagasaki was similar to that of a somewhat smaller town in the United States, except that open sewers were used. The most significant damage was suffered by the water supply system, so that it became almost impossible to extinguish fires. Except for a special case, described below, loss of water pressure resulted from breakage of pipes inside and at entrances to buildings or on structures, rather than from the disruption of underground mains (Figs. 5.106a and b). The exceptional case was one in which the 12-inch cast iron water pipes were 3 feet below grade in a filled-in area. A number of depressions, up to 1 foot in depth, were produced in the fill, and these caused failure of the underground pipes, presumably due to unequal displacements.

5.107 There was no appreciable damage to reservoirs and water-treatment plants in Japan. As is generally the case, these were located outside the cities, and so were at too great a distance from the explosions to be damaged in any way.

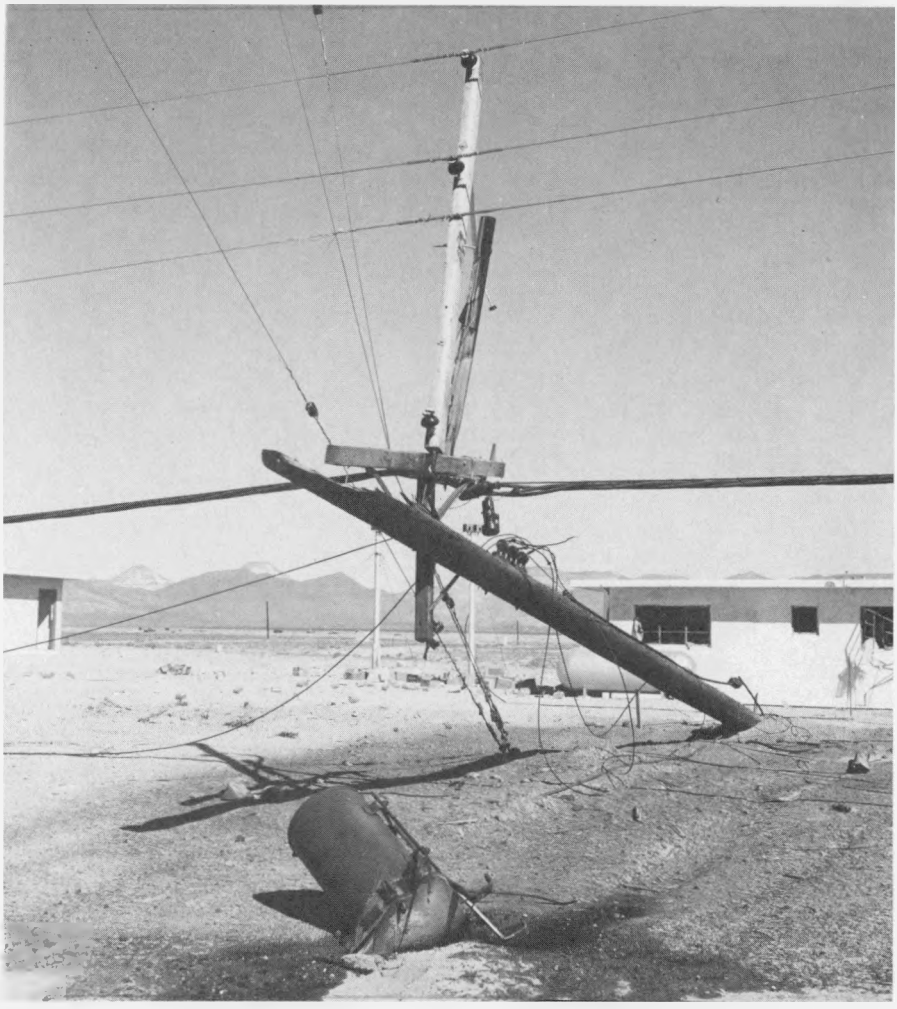

Figure 5.105. Transformer fallen from collapsed utility pole (5 psi peak overpressure), Nevada Test Site.

5.108 Gas holders suffered heavily from blast up to 6,000 feet (1.1 miles) from ground zero and the escaping gas was ignited, but there was no explosion. Underground gas mains appear to have been little affected by the blast.

NATURAL AND MANUFACTURED GAS INSTALLATIONS

5.109 One of the objectives of the tests made in Nevada in 1955 was to determine the extent to which natural and manufactured gas utility installations might be disrupted by a nuclear explosion. The test was intended, in particular, to provide information concerning the effect of blast on critical underground units of a typical gas distribution system.

Figure 5.106a. Four-inch gate valve in water main broken by debris from brick wall (0.23 mile from ground zero at Hiroshima).

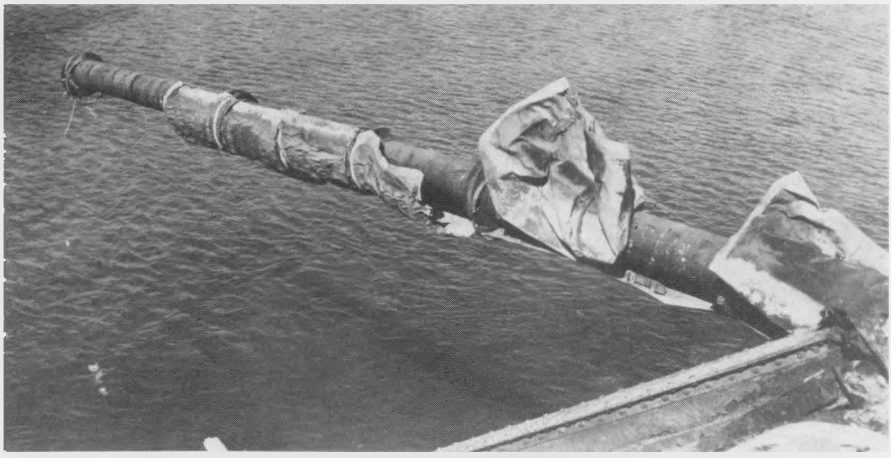

Figure 5.106b. Broken portion of 16-inch water main carried on bridge (0.23 mile from ground zero at Hiroshima).

5.110 The installations tested were of two kinds, each in duplicate. The first represented a typical underground gas-transmission and distribution main of 6-inch steel and cast iron pipe, at a depth of 3 feet, with its associated ser-

vice pipes and attachments. Valve pits of either brick or concrete blocks contained 6-inch valves with piping and protective casings. A street regulator-vault held a 6-inch, low-pressure, pilot-loaded regulator, attached to steel piping projecting through the walls. One of these underground systems was installed where the blast overpressure was about 30 pounds per square inch and the other at 5 pounds per square inch. No domestic or ordinary industrial structures at the surface would have survived the higher of these pressures.

5.111 The second type of installation consisted of typical service lines of steel, copper, and plastic materials connected to 20-foot lengths of 6-inch steel main. Each service pipe rose out of the ground at the side of a house, and was joined to a pressure regulator and meter. The pipe then entered the wall of the house about 2 feet above floor level. The copper and plastic services terminated inside the wall, so that they would be subject to strain if the house moved on its foundation. The steel service line similarly terminated inside the wall, but it was also attached outside to piping that ran around the back of the house at ground level to connect to the house piping. This latter connection was made with flexible seamless bronze tubing, passing through a sleeve in the wall of the building. Typical domestic gas appliances, some attached to the interior piping, were located in several houses. Duplicate installations were located at peak overpressures of 5 and 1.7 pounds per square inch, respectively.

5.112 Neither of the underground installations was greatly affected by the blast. At the 30 pounds per square inch peak overpressure location a 1½-inch pipe pressure-test riser was bent to the ground, and the valve handle, stem, and bonnet had blown off. At the same place two 4-inch ventilating pipes of the street regulator-vaults were sheared off just below ground level. A few minor leaks developed in jute and lead caulked cast iron bell and spigot joints because of ground motion, presumably due to ground shock induced by air blast. Otherwise the blast effects were negligible.

5.113 At the peak overpressure of 1.7 pounds per square inch, where the houses did not suffer severe damage, (§ 5.59), the service piping both inside and outside the houses was unharmed, as also were pressure regulators and meters. In the two-story, brick house at 5 pounds per square inch peak overpressure, which was demolished beyond repair (§ 5.57), the piping in the basement was displaced and bent as a result of the collapse of the first floor. The meter also became detached from the fittings and fell to the ground, but the meter itself and the regulator were undamaged and still operable. All other service piping and equipment were essentially intact.

5.114 Domestic gas appliances, such as refrigerators, ranges, room heaters, clothes dryers, and water heaters suffered to a moderate extent only. There was some displacement of the appliances and connections which was related to the damage suffered by the house. However, even in the collapsed two-story, brick house (§ 5.67), the upset refrigerator and range were probably still usable, although largely buried in debris. The general conclusion is, therefore, that domestic gas (and also electric) appliances would be operable

in all houses that did not suffer major structural damage.

LIQUID PETROLEUM (LP) GAS INSTALLATIONS

5.115 Various LP-gas installations have been exposed to air blast from nuclear tests in Nevada to determine the effects of typical gas containers and supply systems such as are found at suburban and farm homes and at storage, industrial, and utility plants. In addition, it was of interest to see what reliance might be placed upon LP-gas as an emergency fuel after a nuclear attack.

5.116 Two kinds of typical home (or small commercial) LP-gas installations were tested: (1) a system consisting of two replaceable ICC-approved cylinders each of 100-pound capacity; and (2) a 500-gallon bulk storage type system filled from a tank truck. Some of these installations were in the open and others were attached, in the usual manner, by means of either copper tubing or steel pipe service line, to the houses exposed to peak overpressures of 5 and 1.7 pounds per square inch. Others were located where the peak overpressures were about 25 and 10 pounds per square inch. In these cases, piping from the gas containers passed through a concrete wall simulating the wall of a house.

5.117 In addition to the foregoing, a complete bulk storage plant was erected at a point where the peak overpressure was 5 pounds per square inch. This consisted of an 18,000-gallon tank (containing 15,400 gallons of propane), pump compressor, cylinder-filling building, cylinder dock, and all necessary valves, fittings, hose, accessories, and interconnecting piping.

5.118 The dual-cylinder installation, exposed to 25 pounds per square inch peak overpressure, suffered most; the regulators were torn loose from their mountings and the cylinders displaced. One cylinder came to rest about 2,000 feet from its original position; it was badly dented, but was still usable. At both 25 and 10 pounds per square inch peak overpressure the components, although often separated, could generally be salvaged and used again. The cylinder installations at 5 pounds per square inch peak overpressure were mostly damaged by missiles and falling debris from the houses to which they were attached. The component parts, except for the copper tubing, suffered little and were usable. At 1.7 pounds per square inch, there was neither damage to nor dislocation of LP-gas cylinders. Of those tested, only one cylinder developed a leak, and this was a small puncture resulting from impact with a sharp object.

5.119 The 500-gallon bulk gas tanks also proved very durable and experienced little damage. The tank closest to the explosion was bounced end-over-end for a distance of some 700 feet; nevertheless, it suffered only superficially and its strength and serviceability were not impaired. The filler valve was damaged, but the internal check valve prevented escape of the contents. The tank exposed at 10 pounds per square inch peak overpressure was moved about 5 feet, but it sustained little or no damage. All the other tanks, at 5 or 1.7 pounds per square inch, including those at houses piped for service, were unmoved and undamaged (Fig. 5.73).

5.120 The equipment of the

Figure 5.120. Upper photo: LP-gas bulk storage and filling plant before a nuclear explosion. Lower photo: The plant after the explosion (5 psi peak overpressure).

18,000-gallon bulk storage and filling plant received only superficial damage from the blast at 5 pounds per square inch peak overpressure. The cylinder-filling building was completely demolished; the scale used for weighing the cylinders was wrecked, and a filling line was broken at the point where it entered the building (Fig. 5.120). The major operating services of the plant would, however, not be affected because the transfer facilities were outside and undamaged. All valves and nearly all piping in the plant were intact and there was no leakage of gas. The plant could have been readily put back into operation if power, from electricity or a gasoline engine, were restored. If not, liquid propane in the storage tank could have been made available by taking advantage of gravity flow in conjunction with the inherent pressure of the gas in the tank.

5.121 The general conclusion to be drawn from the tests is that standard LP-gas equipment is very rugged, except for copper tubing connections. Disruption of the service as a result of a

nuclear attack would probably be localized and perhaps negligible, so that LP-gas might prove to be a very useful emergency fuel. Where LP-gas is used mainly for domestic purposes, it appears that the gas supply would not be affected under such conditions that the house remains habitable.

MISCELLANEOUS TARGETS

COMMUNICATIONS EQUIPMENT

5.122 The importance of having communications equipment in operating condition after a nuclear attack is evident and so a variety of such equipment has been tested in Nevada. Among the items exposed to air blast were mobile radio-communication systems and units, a standard broadcasting transmitter, antenna towers, home radio and television receivers, telephone equipment (including a small telephone exchange), public address sound systems, and sirens. Some of these were located where the peak overpressure was 5 pounds per square inch, and in most cases there were duplicates at 1.7 pounds per square inch. The damage at the latter location was of such a minor character that it need not be considered here.

5.123 At the higher overpressure region, where typical houses were damaged beyond repair, the communications equipment proved to be very resistant to blast. This equipment is drag sensitive and so the peak overpressure does not determine the extent of damage. Standard broadcast and television receivers, and mobile radio base stations were found to be in working condition, even though they were covered with debris and had, in some cases, been damaged by missiles, or by being thrown or dropped several feet. No vacuum or picture tubes were broken. The only mobile radio station to be seriously affected was one in an automobile which was completely crushed by a falling chimney.

5.124 A guyed 150-foot antenna tower was unharmed, but an unguyed 120-foot tower, of lighter construction, close by, broke off at a height of about 40 feet and fell to the ground (Fig. 5.124). This represented the only serious damage to any of the equipment tested.

5.125 The base station antennas, which were on the towers, appeared to withstand blast reasonably well, although those attached to the unguyed tower, referred to above, suffered when the tower collapsed. As would have been expected from their lighter construction, television antennas for home receivers were more easily damaged. Several were bent both by the blast and the collapse of the houses upon which they were mounted. Since the houses were generally damaged beyond repair at a peak overpressure of 5 pounds per square inch, the failure of the television antennas is not of great significance.

5.126 Some items, such as power lines and telephone service equipment, were frequently attached to utility-line poles. When the poles failed, as they did in some cases (§ 5.104), the communi-

Figure 5.124. Unguyed lightweight 120-foot antenna tower (5 psi peak overpressure, 0.6 psi dynamic pressure from 30-kiloton explosion), Nevada Test Site.

cations systems suffered accordingly. Although the equipment operated satisfactorily after repairs were made to the wire line, it appears that the power supply represents a weak link in the communications chain.

BRIDGES

5.127 There were a number of different kinds of bridges exposed to the nuclear explosions in Hiroshima and Nagasaki. Those of wood were burned in most cases, but steel-girder bridges suffered relatively little destruction (Figs. 5.127a and b). One bridge, only 270 feet from ground zero, i.e., about 2,100 feet from the burst point, which was of a girder type with a reinforced-concrete deck, showed no sign of any structural damage. It had, apparently, been deflected downward by the blast force and had rebounded, causing only a slight net displacement. Other bridges,

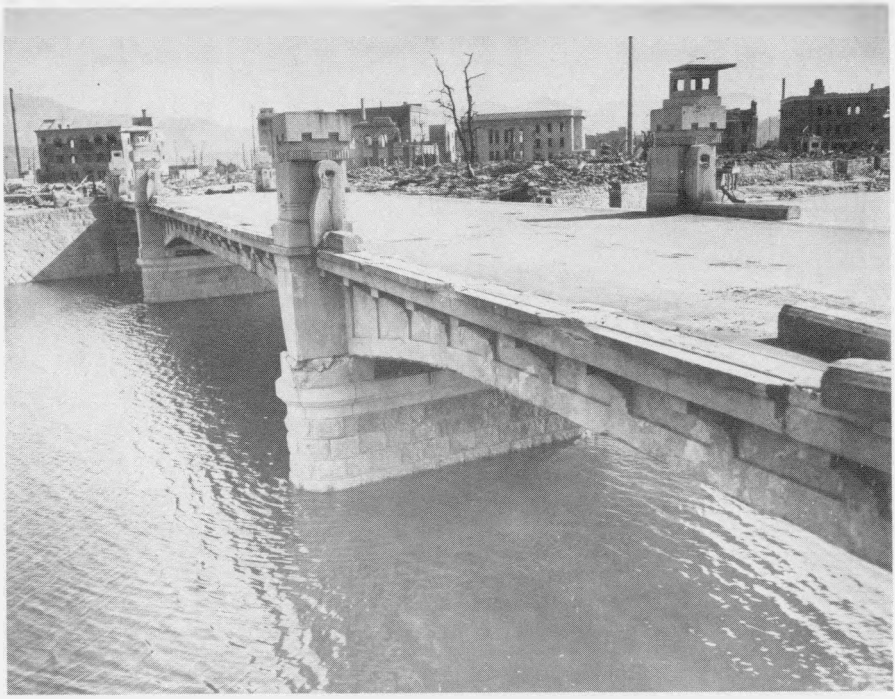

Figure 5.127a. Bridge with deck of reinforced concrete on steel-plate girders; outer girder had concrete facing (270 feet from ground zero at Hiroshima). The railing was blown down but the deck received little damage so that traffic continued.

at greater distances from ground zero, suffered more lateral shifting. A reinforced-concrete deck was lifted from the supporting steel girder of one bridge, apparently as a result of reflection of the blast wave from the surface of the water below.

HEAVY-DUTY MACHINE TOOLS

5.128 The vulnerability of heavy-duty machine tools and their components to air blast from a nuclear explosion was studied at the Nevada Test Site to supplement the information from Nagasaki (§ 5.33). A number of machine tools were anchored on a reinforced-concrete slab in such a manner as to duplicate good industrial practice. Two engine lathes (weighing approximately 7,000 and 12,000 pounds, respectively), and two horizontal milling machines (7,000 and 10,000 pounds, respectively) were exposed to a peak overpressure of 10 pounds per square inch. A concrete-block wall, 8 inches thick and 64 inches high, was constructed immediately in front of the machines, i.e., between the machines and ground zero (Fig. 5.128). The purpose of this wall was to simulate the exterior wall of the average industrial plant and to provide debris and missiles.

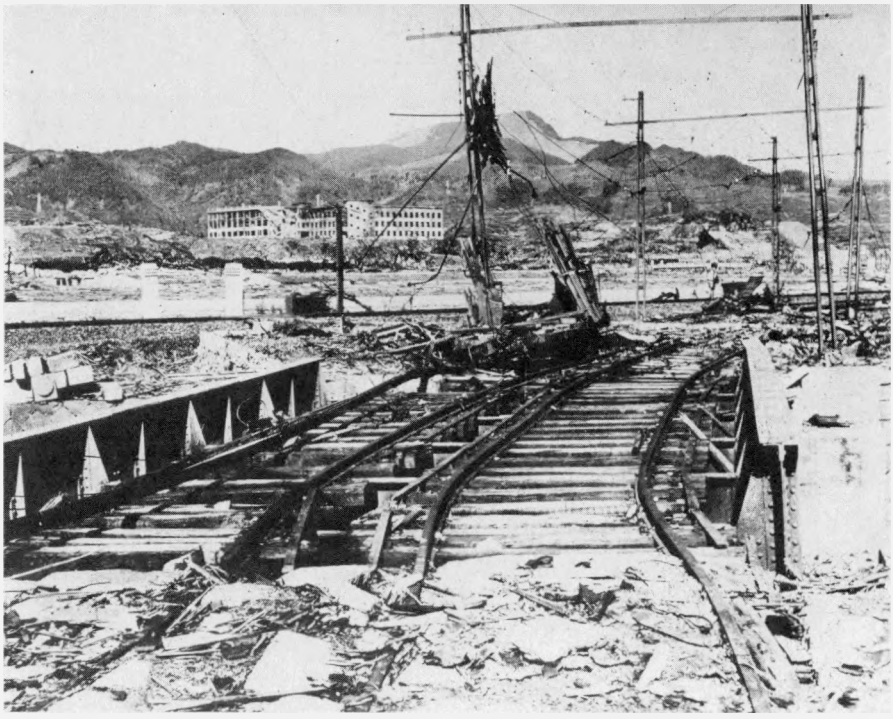

Figure 5.127b. A steel-plate girder, double-track railway bridge (0.16 mile from ground zero at Nagasaki). The plate girders were moved about 3 feet by the blast; the railroad track was bent out of shape and trolley cars were demolished, but the poles were left standing.

5.129 Of the four machines, the three lighter ones were moved from their foundations and damaged quite badly (Fig. 5.129a). The fourth, weighing 12,000 pounds, which was considered as the only one to be actually of the heavy-duty type, survived (Fig. 5.129b). From the observations it was concluded that a properly anchored machine tool of the true heavy-duty type would be able to withstand peak overpressures of 10 pounds per square inch or more without substantial damage.

5.130 In addition to the direct effects of blast, considerable destruction was caused by debris and missiles, much of which resulted from the expected complete demolition of the concrete-block wall. Delicate mechanisms and appendages, which are usually on the exterior and unprotected, suffered especially severely. Gears and gear cases were damaged, hand valves and control levers were broken off, and drive belts were broken. It appears, however, that most of the missile damage could be easily repaired if replacement parts were available, since major dismantling would not be required.

5.131 Behind the two-story brick house in the peak overpressure region of 5 pounds per square inch (§ 5.67), a

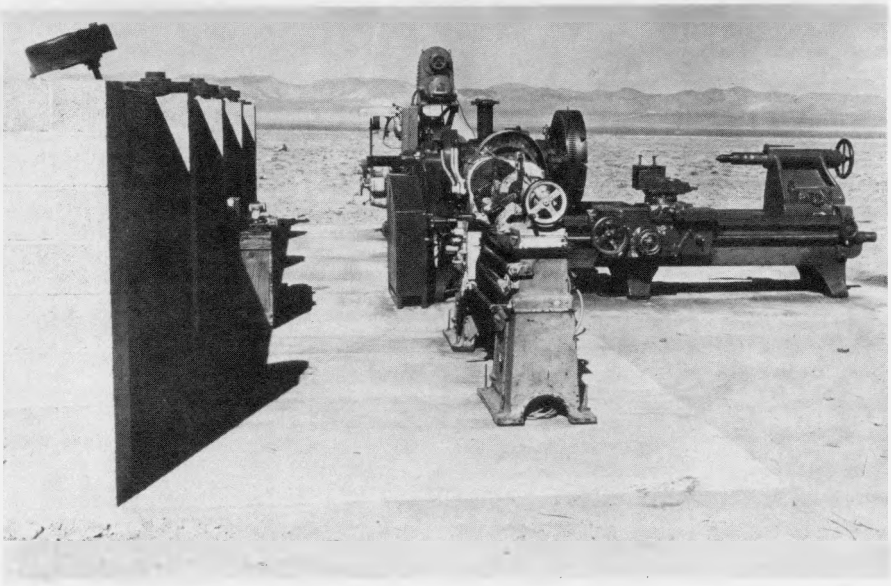

Figure 5.128. Machine tools behind masonry wall before a nuclear explosion, Nevada Test Site.

200-ton capacity hydraulic press weighing some 49,000 pounds was erected. The location was chosen as being the best to simulate actual factory conditions. This unusually tall (19 feet high) and slim piece of equipment showed little evidence of blast damage, even though the brick house was demolished. It was probable that the house provided some shielding from the blast wave. Moreover, at the existing blast pressure, missiles did not have high velocities. Such minor damage as was suffered by the machine was probably due to debris falling from the house.

5.132 At the 3-pounds per square inch peak overpressure location, there were two light, industrial buildings of standard type. In each of these was placed a vertical milling machine weighing about 3,000 pounds, a 50-gallon capacity, stainless-steel, pressure vessel weighing roughly 4,100 pounds, and a steel steam oven approximately 2½ feet wide, 5 feet high, and 9 feet long. Both buildings suffered extensively from blast, but the equipment experienced little or no operational damage. In one case, the collapsing structure fell on and broke off an exposed part of the milling machine.

5.133 The damage sustained by machine tools in the Nevada tests was probably less than that suffered in Japan at the same blast pressures (§ 5.33). Certain destructive factors, present in the latter case, were absent in the tests. First, the conditions were such that there was no damage by fire; and, second, there was no exposure to the elements after the explosion. In addition, the total amount of debris and missiles produced in the tests was probably less than in the industrial buildings in Japan.

Figure 5.129a. Machine tools after a nuclear explosion (10 psi peak overpressure).

Figure 5.129b. Heavy-duty lathe after a nuclear explosion (10 psi peak overpressure).

ANALYSIS OF DAMAGE FROM AIR BLAST

INTRODUCTION

5.134 The remainder of this chapter is concerned with descriptions of air-blast damage criteria for various types of targets and with the development of damage–distance relationships for predicting the distances at which damage may be expected from nuclear explosions of different energy yields. The nature of any target complex, such as a city, is such, however, that exact predictions are not possible. Nevertheless, by application of proper judgment to the available information, results of practical value can be obtained. The conclusions given here are considered to be applicable to average situations that might be encountered in an actual target complex.

5.135 Damage to structures and objects is generally classified in three categories: severe, moderate, and light. In several of the cases discussed below, the specific nature of each type of damage is described, but the following broad definitions are a useful guide.

Severe Damage

A degree of damage that precludes further use of the structure or object for its intended purpose without essentially complete reconstruction. For a structure or building, collapse is generally implied.

Moderate Damage

A degree of damage to principal members that precludes effective use of the structure or object for its intended purpose unless major repairs are made.

Light Damage

A degree of damage to buildings resulting in broken windows, slight damage to roofing and siding, blowing down of light interior partitions, and slight cracking of curtain walls in buildings. Minor repairs are sufficient to permit use of the structure or object for its intended purpose.

5.136 For a number of types of targets, the distances out to which different degrees of damage may be expected from nuclear explosions of various yields have been represented by diagrams, such as Figs. 5.140 and 5.146. These are based on observations made in Japan and at various nuclear tests, on experiments conducted in shock tubes in laboratories and with high-explosives in field tests, and on theoretical analyses of the loading and response of structures (see Chapter IV). As a result of these studies, it is possible to make reasonably accurate predictions of the response of interior as well as exterior wall panels and complete structures to the air-blast wave. These predictions, however, must take into account constructional details of each individual structure. Moreover, observations made during laboratory tests have indicated a large scatter in failure loadings as a result of statistical variations among wall and material properties. The data in Figs. 5.140 and 5.146 are intended, however,

to provide only gross estimates for the categories of structures given in Tables 5.139a and b. The response of a particular structure may thus deviate from that shown for its class in the figures.

5.137 For structures that are damaged primarily by diffraction loading (§ 4.03), the peak overpressure is the important factor in determining the response to blast. In some instances, where detailed analyses have not been performed, peak overpressures are given for various kinds of damage. Approximate damage–distance relationships can then be derived by using peak overpressure–distance curves and scaling laws from Chapter III. For equal scaled heights of burst, as defined in § 3.62, the range for a specified damage to a diffraction-sensitive structure increases in proportion to the cube root, and the damage area in proportion to the two-thirds power, of the energy of the explosion. This means, for example, that a thousand-fold increase in the energy will increase the range for a particular kind of diffraction-type damage by a factor of roughly ten; the area over which the damage occurs will be increased by a factor of about a hundred, for a given scaled burst height.

5.138 Where the response depends mainly on drag (or wind) loading, the peak overpressure is no longer a useful criterion of damage. The response of a drag-sensitive structure is determined by the length of the blast wave positive phase as well as by the peak dynamic pressure (§ 4.12 *et seq.*). The greater the energy of the weapon, the farther will be the distance from the explosion at which the peak dynamic pressure has a specific value and the longer will be the duration of the positive phase. Since there is increased drag damage with increased duration at a given pressure, the same damage will extend to lower dynamic pressure levels. Structures which are sensitive to drag loading will therefore be damaged over a range that is larger than is given by the cube root rule for diffraction-type structures. In other words, as the result of a thousand-fold increase in the energy of the explosion, the range for a specified damage to a drag-sensitive structure will be increased by a factor of more than ten, and the area by more than a hundred.

ABOVE-GROUND BUILDINGS AND BRIDGES

5.139 The detailed nature of the damage in the severe, moderate, and light categories to above-ground structures of various types are given in Tables 5.139a and b. For convenience, the information is divided into two groups. Table 5.139a is concerned with structures of the type that are primarily affected by the blast wave during the diffraction phase, whereas the structures in Table 5.139b are drag sensitive.

5.140 The ranges for severe and moderate damage to the structures in Tables 5.139a and b are presented in Fig. 5.140, based on actual observations and theoretical analysis. The numbers (1 to 21) in the figure identify the target types as given in the first column of the tables. The data refer to air bursts with the height of burst chosen so as to maximize the radius of damage for the particular target being considered and is not necessarily the same for different targets. For a surface burst, the respective ranges are to be multiplied by three-fourths. An example illustrating the use of the diagram is given.

(Text continued on page 220.)

Table 5.139a

DAMAGE CRITERIA FOR STRUCTURES PRIMARILY AFFECTED BY DIFFRACTION LOADING

Structural Type	Description of Structure	Description of Damage		
		Severe	Moderate	Light
1	Multistory reinforced concrete building with reinforced concrete walls, blast resistant design for 30 psi Mach region pressure from 1 MT, no windows.	Walls shattered, severe frame distortion, incipient collapse.	Walls breached or on the point of being so, frame distorted, entranceways damaged, doors blown in or jammed, extensive spalling of concrete.	Some cracking of concrete walls and frame.
2	Multistory reinforced concrete building with concrete walls, small window area, three to eight stories.	Walls shattered, severe frame distortion, incipient collapse.	Exterior walls severely cracked. Interior partitions severely cracked or blown down. Structural frame permanently distorted, extensive spalling of concrete.	Windows and doors blown in, interior partitions cracked.
3	Multistory wall-bearing building, brick apartment house type, up to three stories.	Collapse of bearing walls, resulting in total collapse of structure.	Exterior walls severely cracked, interior partitions severely cracked or blown down.	Windows and doors blown in, interior partitions cracked.
4	Multistory wall-bearing building, monumental type, up to four stories.	Collapse of bearing walls, resulting in collapse of structure supported by these walls. Some bearing walls may be shielded by intervening walls so that part of the structure may receive only moderate damage.	Exterior walls facing blast severely cracked, interior partitions severely cracked with damage toward far end of building possibly less intense.	Windows and doors blown in, interior partitions cracked.
5	Wood frame building, house type, one or two stories.	Frame shattered resulting in almost complete collapse.	Wall framing cracked. Roof severely damaged, interior partitions blown down.	Windows and doors blown in, interior partitions cracked.

Table 5.139b

DAMAGE CRITERIA FOR STRUCTURES PRIMARILY AFFECTED BY DRAG LOADING

Structural Type	Description of Structure	Description of Damage		
		Severe	Moderate	Light
6	Light steel frame industrial building, single story, with up to 5-ton crane capacity; low strength walls which fail quickly.	Severe distortion or collapse of frame.	Minor to major distortion of frame; cranes, if any, not operable until repairs made.	Windows and doors blown in, light siding ripped off.
7	Heavy steel-frame industrial building, single story, with 25 to 50-ton crane capacity; lightweight, low strength walls which fail quickly.	Severe distortion or collapse of frame.	Some distortion to frame; cranes not operable until repairs made.	Windows and doors blown in, light siding ripped off.
8	Heavy steel frame industrial building, single story, with 60 to 100-ton crane capacity; lightweight low strength walls which fail quickly.	Severe distortion or collapse of frame.	Some distortion or frame; cranes not operable until repairs made.	Windows and doors blown in, light siding ripped off.
9	Multistory steel-frame office-type building, 3 to 10 stories. Lightweight low strength walls which fail quickly, earthquake resistant construction.	Severe frame distortion, incipient collapse.	Frame distorted moderately, interior partitions blown down.	Windows and doors blown in, light siding ripped off, interior partitions cracked.
10	Multistory steel-frame office-type building, 3 to 10 stories. Lightweight low strength walls which fail quickly, non-earthquake resistant construction.	Severe frame distortion, incipient collapse.	Frame distorted moderately, interior partitions blown down.	Windows and doors blown in, light siding ripped off, interior partitions cracked.

Table 5.139b (continued)

Structural Type	Description of Structure	Description of Damage		
		Severe	Moderate	Light
11	Multistory reinforced concrete frame office-type building, 3 to 10 stories; lightweight low strength walls which fail quickly, earthquake resistant construction.	Severe frame distortion, incipient collapse.	Frame distorted moderately, interior partitions blown down, some spalling of concrete.	Windows and doors blown in, light siding ripped off, interior partitions cracked.
12	Multistory reinforced concrete frame office type building, 3 to 10 stories; lightweight low strength walls which fail quickly, non-earthquake resistant construction.	Severe frame distortion, incipient collapse.	Frame distorted moderately, interior partitions blown down, some spalling of concrete.	Windows and doors blown in, light siding ripped off, interior partitions cracked.
13	Highway truss bridges, 4-lane, spans 200 to 400 ft; railroad truss bridges, double track ballast floor, spans 200 to 400 ft.	Total failure of lateral bracing or anchorage, collapse of bridge.	Substantial distortion of lateral bracing or slippage on supports, significant reduction in capacity of bridge.	Capacity of bridge not significantly reduced, slight distortion of some bridge components.
14	Highway truss bridges, 2-lane, spans 200 to 400 ft; railroad truss bridges, single track ballast or double track open floors, spans 200 to 400 ft; railroad truss bridges, single track open floor, span 400 ft.	(Ditto)	(Ditto)	(Ditto)
15	Railroad truss bridges, single track open floor, span 200 ft.	(Ditto)	(Ditto)	(Ditto)
16	Highway girder bridges, 4-lane through, span 75 ft.	(Ditto)	(Ditto)	(Ditto)

Table 5.139b (concluded)

Structural Type	Description of Structure	Description of Damage		
		Severe	Moderate	Light
17	Highway girder bridges, 2-lane deck, 2-lane through, 4-lane deck, span 75 ft; railroad girder bridges, double-track deck, open or ballast floor, span 75 ft; railroad girder bridges, single or double track through, ballast floors, span 75 ft.	(Ditto)	(Ditto)	(Ditto)
18	Railroad girder bridges, single track deck, open or ballast floors, span 75 ft; railroad girder bridges, single or double track through, open floors, span 75 ft.	(Ditto)	(Ditto)	(Ditto)
19	Highway girder bridges, 2-lane through, 4-lane deck or through, span 200 ft; railroad girder bridges, double track deck or through, ballast floor, span 200 ft.	(Ditto)	(Ditto)	(Ditto)
20	Highway girder bridges, 2-lane deck, span 200 ft; railroad girder bridges, single track deck or through, ballast floors, span 200 ft; railroad girder bridges, double track deck or through, open floors, span 200 ft.	(Ditto)	(Ditto)	(Ditto)
21	Railroad girder bridges, single track deck or through, open floors, span 200 ft.	(Ditto)	(Ditto)	(Ditto)

The various above-ground structures in Fig. 5.140 are identified (Items 1 through 21) and the different types of damage are described in Tables 5.139a and b. The "fan" from each point indicates the range of yields for which the diagram may be used. For a surface burst multiply the damage distances obtained from the diagram by three-fourths. The results are estimated to be accurate within ±20 percent for the average target conditions specified in § 5.141.

Example

Given: Wood-frame building (Type 5). A 1 MT weapon is burst (*a*) at optimum height, (*b*) at the surface.

Find: The distances from ground zero to which severe and moderate damage extend.

Solution: (*a*) From the point 5 (at the right) draw a straight line to 1 MT (1000 KT) on the severe damage scale and another to 1 MT (1000 KT) on the moderate damage scale. The intersections of these lines with the distance scale give the required solutions for the optimum burst height; thus,

Distance for severe damage = 29,000 feet. *Answer.*

Distance for moderate damage = 33,000 feet. *Answer.*

(*b*) For a surface burst the respective distances are three-fourths those obtained above; hence,

Distance for severe damage = 22,000 feet. *Answer.*

Distance for moderate damage = 25,000 feet. *Answer.*

(The values have been rounded off to two significant figures, since greater precision is not warranted.)

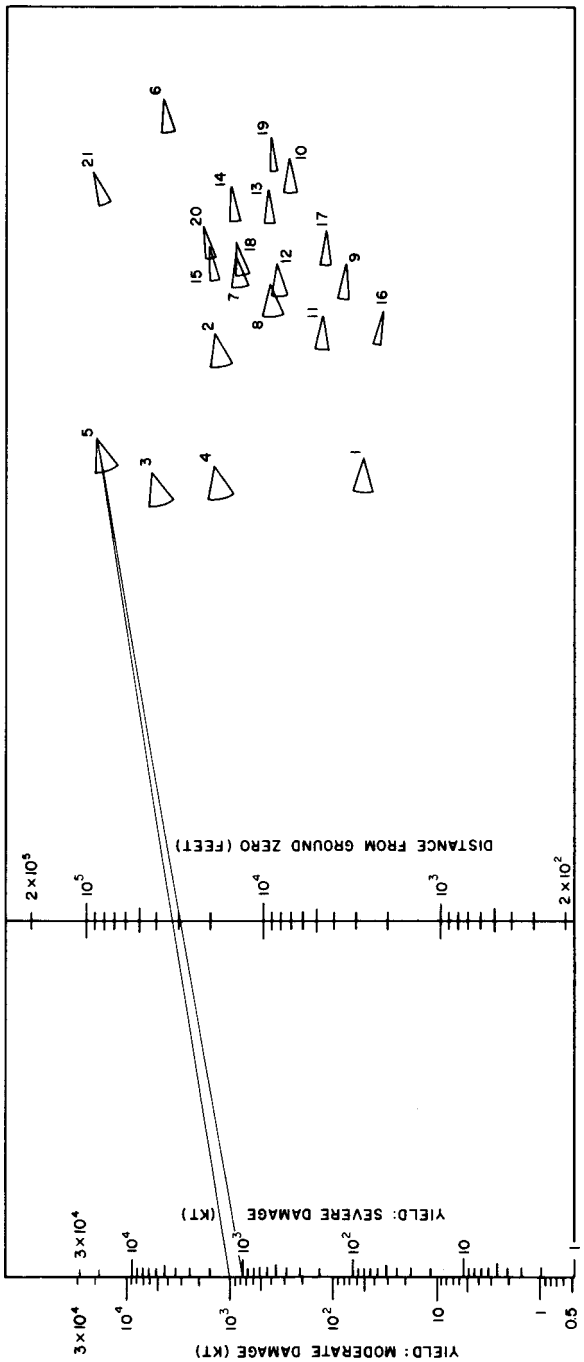

Figure 5.140. Damage-distance relationships for above ground structures.

5.141 The data in Fig. 5.140 are for certain average target conditions. These are that (1) the target is at sea level (no correction is necessary if the target altitude is less than 5,000 feet); (2) the terrain is fairly flat (rugged terrain would provide some local shielding and protection in certain areas and local enhancement of damage in others); and (3) the structures have average characteristics (that is, they are of average size and strength and that orientation of the target with respect to the burst is no problem, i.e., that the ratio of loading to resistance is relatively the same in all directions from the target).

5.142 The "fan" from each point in the figure designating a target type delineates the range of yields over which theoretical analyses have been made. For yields falling within this range, the diagram is estimated to be accurate within ± 20 percent for the average conditions discussed above. The significance of results obtained by applying the diagram to conditions that depart appreciably from the average or to yields outside the limits of the fans must be left to the judgment of the analyst.

5.143 Figure 5.140 gives the distances from ground zero for severe and moderate damage. Light damage to all targets except blast-resistant structures and bridges can be expected at the range at which the overpressure is 1 pound per square inch. For the blast-resistant structure (Type 1) described in Table 5.139a, a peak overpressure of 10 pounds per square inch should be used to estimate the distance for light damage. Light damage to bridges can be expected at the range at which 0.6 pound per square inch dynamic pressure occurs.

5.144 The foregoing results do not take into consideration the possibility of fire. Generally speaking, the direct effects of thermal radiation on the structures and other targets under consideration are inconsequential. However, thermal radiation may initiate fires, and in structures with severe or moderate damage fires may start because of disrupted gas and electric utilities. In some cases, as in Hiroshima (§ 7.71), the individual fires may develop into a mass fire which may exist throughout a city, even beyond the range of significant blast damage. The spread of such a fire depends to a great extent on local weather and other conditions and is therefore difficult to predict. This limitation must be kept in mind when Fig. 5.140 is used to estimate the damage to a particular city or target area.

STRUCTURAL ELEMENTS

5.145 For certain structural elements, with short periods of vibration (up to about 0.05 second) and small plastic deformation at failure, the conditions for failure can be expressed as a peak overpressure without considering the duration of the blast wave. The failure conditions for elements of this type are given in Table 5.145. Some of these elements fail in a brittle fashion, and thus there is only a small difference between the pressures that cause no damage and those that produce complete failure. Other elements may fail in a moderately ductile manner, but still with little difference between the pressures for light damage and complete failure. The pressures are side-on blast overpressures for panels that face

Table 5.145

CONDITIONS OF FAILURE OF OVERPRESSURE-SENSITIVE ELEMENTS

Structural element	Failure	Approximate side-on peak overpressure (psi)
Glass windows, large and small.	Shattering usually, occasional frame failure.	0.5– 1.0
Corrugated asbestos siding.	Shattering.	1.0– 2.0
Corrugated steel or aluminum paneling.	Connection failure followed by buckling.	1.0– 2.0
Brick wall panel, 8 in. or 12 in. thick (not reinforced).	Shearing and flexure failures.	3.0–10.0
Wood siding panels, standard house construction.	Usually failure occurs at the main connections allowing a whole panel to be blown in.	1.0– 2.0
Concrete or cinder-block wall panels, 8 in. or 12 in. thick (not reinforced).	Shattering of the wall.	1.5– 5.5

ground zero. For panels that are oriented so that there are no reflected pressures thereon, the side-on pressures must be doubled. The fraction of the area of a panel wall that contains windows will influence the overpressure required to damage the panel. Such damage is a function of the net load, which may be reduced considerably if the windows fail early. This allows the pressure to become equalized on the two sides of the wall before panel failure occurs.

DRAG-SENSITIVE TARGETS

5.146 A diagram of damage–distance relationships for various targets which are largely affected by drag forces is given in Fig. 5.146. The conditions under which it is applicable and the limits of accuracy are similar to those in § 5.141 and § 5.142, respectively; the possibility of fire mentioned in § 5.144 must also be kept in mind. The targets (Items 1 to 13) in the figure are enumerated on the page facing Fig. 5.146 and the different types of damage are described in the following paragraphs.

Transportation Equipment

5.147 The damage criteria for various types of land transportation equipment, including civilian motor-driven vehicles and earth-moving equipment, and railroad rolling stock are given in Table 5.147a. The various types of damage to merchant shipping from air blast are described in Table 5.147b.

(Text continued on page 225.)

The drag-sensitive targets in Fig. 5.146 are identified as follows:

1. Truck mounted engineering equipment (unprotected).
2. Earth moving engineering equipment (unprotected).
3. Transportation vehicles.
4. Unloaded railroad cars.
5. Loaded boxcars, flatcars, full tank cars, and gondola cars (side-on orientation).
6. Locomotives (side-on orientation).
7. Telephone lines (radial).
8. Telephone lines (transverse).
9. Unimproved coniferous forest stand.
10. Average deciduous forest stand.
11. Loaded boxcars, flatcars, full tank cars, and gondola cars (end-on orientation).
12. Locomotives (end-on orientation).
13. Merchant shipping.

Subscript "m" refers to moderate damage and subscript "s" refers to severe damage.

For a surface burst multiply the distance by three-fourths for Items 1 through 8 and by one-half for Items 9 and 10. For Items 11 through 13, the distances are the same for a surface burst as for the optimum burst height. Estimated accuracy ± 20 percent for average targets.

Example

Given: A transportation type vehicle (Item 3). A 10 KT weapon is burst at (*a*) the optimum height, (*b*) at the surface.

Find: The distances from ground zero to which severe and moderate damage extend.

Solution: (*a*) Draw straight lines from the points 3_s and 3_m, at the right, to 10 KT on the yield scale at the left. The intersections of these lines with the distance scale give the solutions for severe and moderate damage, respectively, for the optimum burst height; thus,

Distance for severe damage = 1,400 feet. *Answer.*

Distance for moderate damage = 1,600 feet. *Answer.*

(*b*) For a surface burst the distances in this case are three-fourths those obtained above; thus,

Distance for severe damage = 1,000 feet. *Answer.*

Distance for moderate damage = 1,200 feet. *Answer.*

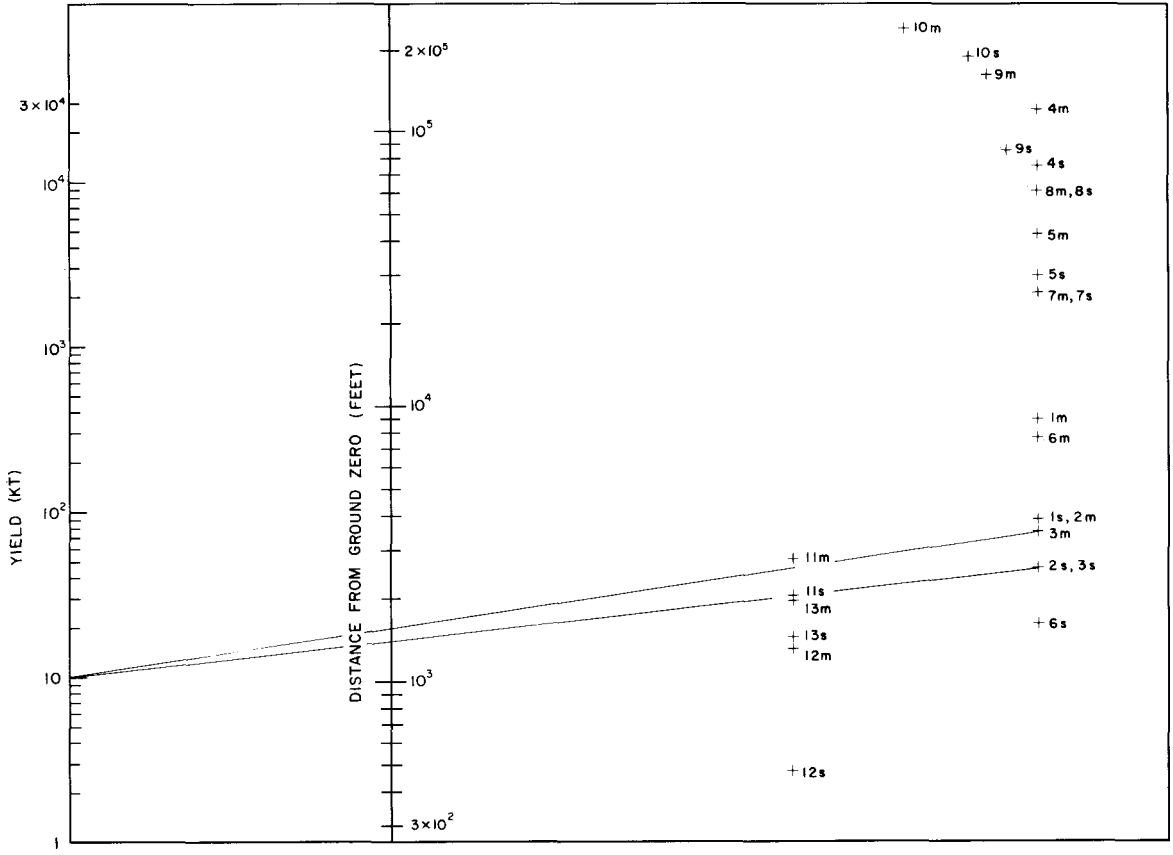

Figure 5.146. Damage–distance relationships for drag-sensitive targets.

Table 5.147a

DAMAGE CRITERIA FOR LAND TRANSPORTATION EQUIPMENT

Description of equipment	Damage	Nature of damage
Motor equipment (cars and trucks).	Severe	Gross distortion of frame, large displacements, outside appurtenances (doors and hoods) torn off, need rebuilding before use.
	Moderate	Turned over and displaced, badly dented, frames sprung, need major repairs.
	Light	Glass broken, dents in body, possibly turned over, immediately usable.
Railroad rolling stock (box, flat, tank, and gondola cars).	Severe	Car blown from track and badly smashed, extensive distortion, some parts usable.
	Moderate	Doors demolished, body damaged, frame distorted, could possibly roll to repair shop.
	Light	Some door and body damage, car can continue in use.
Railroad locomotives (Diesel or steam).	Severe	Overturned, parts blown off, sprung and twisted, major overhaul required.
	Moderate	Probably overturned, can be towed to repair shop after being righted, need major repairs.
	Light	Glass breakage and minor damage to parts, immediately usable.
Construction equipment (bulldozers and graders).	Severe	Extensive distortion of frame and crushing of sheet metal, extensive damage to caterpillar tracks and wheels.
	Moderate	Some frame distortion, overturning, track and wheel damage.
	Light	Slight damage to cabs and housing, glass breakage.

Table 5.147b

DAMAGE CRITERIA FOR SHIPPING FROM AIR BLAST

Damage type	Nature of damage
Severe	The ship is either sunk, capsized, or damaged to the extent of requiring rebuilding.
Moderate	The ship is immobilized and requires extensive repairs, especially to shock-sensitive components or their foundations, e.g., propulsive machinery, boilers, and interior equipment.
Light	The ship may still be able to operate, although there will be damage to electronic, electrical, and mechanical equipment.

Communication and Power Lines

5.148 Damage to telephone, telegraph, and utility power lines is generally either severe or light. Such damage depends on whether the poles supporting the lines are damaged or not. If the poles are blown down, damage to the lines will be severe and extensive repairs will be required. On the other hand, if the poles remain standing, the lines will suffer only light damage and will need little repair. In general, lines extending radially from ground zero are less susceptible to damage than are those running at right angles to this direction.

Forests

5.149 The detailed characteristics of the damage to forest stands resulting from a nuclear explosion will depend on a variety of conditions, e.g., deciduous or coniferous trees, degree of foliation of the trees, natural or planted stands, and favorable or unfavorable growing conditions. A general classification of forest damage, applicable in most cases, is given in Table 5.149. Trees are primarily sensitive to the drag forces from a blast wave and so it is of interest that the damage in an explosion is similar to that resulting from a strong, steady wind; the velocities of such winds that would produce comparable damage are included in the table.

5.150 The damage–distance results derived from Fig. 5.146 apply in particular to unimproved coniferous forests which have developed under unfavorable growing conditions and to most deciduous forests in the temperate zone when foliation is present. Improved coniferous forests, with trees of uniform height and a smaller average tree density per acre, are more resistant to blast than are unimproved forests which have grown under unfavorable conditions. A forest of defoliated deciduous trees is also somewhat more blast resistant than is implied by the data in Fig. 5.146.

Table 5.149

DAMAGE CRITERIA FOR FORESTS

Damage type	Nature of damage	Equivalent steady wind velocity (miles per hour)
Severe	Up to 90 percent of trees blown down; remainder denuded of branches and leaves. (Area impassable to vehicles and very difficult on foot.)	130–140
Moderate	About 30 percent of trees blown down; remainder have some branches and leaves blown off. (Area passable to vehicles only after extensive clearing.)	90–100
Light	Only applies to deciduous forest stands. Very few trees blown down; some leaves and branches blown off. (Area passable to vehicles.)	60–80

PARKED AIRCRAFT

5.151 Aircraft are relatively vulnerable to air blast effects associated with nuclear detonations. The forces developed by peak overpressures of 1 to 2 pounds per square inch are sufficient to dish in panels and buckle stiffeners and stringers. At higher overpressures, the drag forces due to wind (dynamic) pressure tend to rotate, translate, overturn, or lift a parked aircraft, so that damage may then result from collision with other aircraft, structures, or the ground. Aircraft are also very susceptible to damage from flying debris carried by the blast wave.

5.152 Several factors influence the degree of damage that may be expected for an aircraft of a given type at a specified range from a nuclear detonation. Aircraft that are parked with the nose pointed toward the burst will suffer less damage than those with the tail or either side directed toward the oncoming blast wave (§ 5.94). Shielding of one aircraft by another or by structures or terrain features may reduce damage, especially that caused by flying debris. Standard tiedown of aircraft, as used when high winds are expected, will also minimize the extent of damage at ranges where destruction might otherwise occur.

5.153 The various damage categories for parked transport airplanes, light liaison airplanes, and helicopters are outlined in Table 5.153 together with the approximate peak overpressures at which the damage may be expected to occur. The aircraft are considered to be parked in the open at random orientation with respect to the point of burst. The

Table 5.153

DAMAGE CRITERIA FOR PARKED AIRCRAFT

Damage type	Nature of damage		Overpressure (psi)
Severe	Major (or depot level) maintenance required to restore aircraft to operational status.	Transport airplanes	3
		Light liaison craft	2
		Helicopters	3
Moderate	Field maintenance required to restore aircraft to operational status.	Transport airplanes	2
		Light liaison craft	1
		Helicopters	1.5
Light	Flight of the aircraft not prevented, although performance may be restricted.	Transport airplanes	1.0
		Light liaison craft	0.75
		Helicopters	1.0

data in the table are based on tests in which aircraft were exposed to detonations with yields in the kiloton range. For megaton yields, the longer duration of the positive phase of the blast wave may result in some increase in damage over that estimated from small-yield explosions at the same overpressure level. This increase is likely to be significant at pressures producing severe damage, but will probably be less important for moderate and light damage conditions.

5.154 Aircraft with exposed ignitable materials may, under certain conditions, be damaged by thermal radiation at distances beyond those at which equivalent damage would result from blast effects. The vulnerability to thermal radiation may be decreased by protecting ignitable materials from exposure to direct radiation or by painting them with protective (light colored) coatings which reflect, rather than absorb, most of the thermal radiation (see Chapter VII).

POL STORAGE TANKS

5.155 The chief cause of failure of POL (petroleum, oil, lubricant) storage tanks exposed to the blast wave appears to be the lifting of the tank from its foundation. This results in plastic deformation and yielding of the joint between the side and bottom so that leakage can occur. Severe damage is regarded as that damage which is associated with loss of the contents of the tank by leakage. Furthermore, the leakage can lead to secondary effects, such as the development of fires. If failure by lifting does not occur, it is expected that there will be little, if any, loss of liquid from the tank as a consequence of sloshing. There is apparently no clear-cut overall structural collapse which initially limits the usefulness of the tank. Peak overpressures required for severe damage to POL tanks of diameter D may be obtained from Figs. 5.155a and b. Figure 5.155a is applicable to nuclear explosions with energy yields from 1 to 500 kilotons and Fig. 5.155b to yields over 500 kilotons. For yields less than 1 kiloton, the peak overpressure for severe damage may be taken to be 1 pound per square inch.

LIGHTWEIGHT, EARTH COVERED AND BURIED STRUCTURES

5.156 Air blast is the controlling factor for damage to lightweight earth covered structures and shallow buried underground structures. The earth cover provides surface structures with substantial protection against air blast and also some protection against flying debris. The depth of earth cover above the structure would usually be determined by the degree of protection from nuclear radiation required at the design overpressure or dynamic pressure (see Chapter VIII).

5.157 The usual method of providing earth cover for surface or "cut-and-cover" semiburied structures is to build an earth mound over the portion of the structure that is above the normal ground level. If the slope of the earth cover is chosen properly, the blast reflection factor is reduced and the aerodynamic shape of the structure is improved. This results in a considerable reduction in the applied translational forces. An additional benefit of the earth cover is the stiffening or resistance to

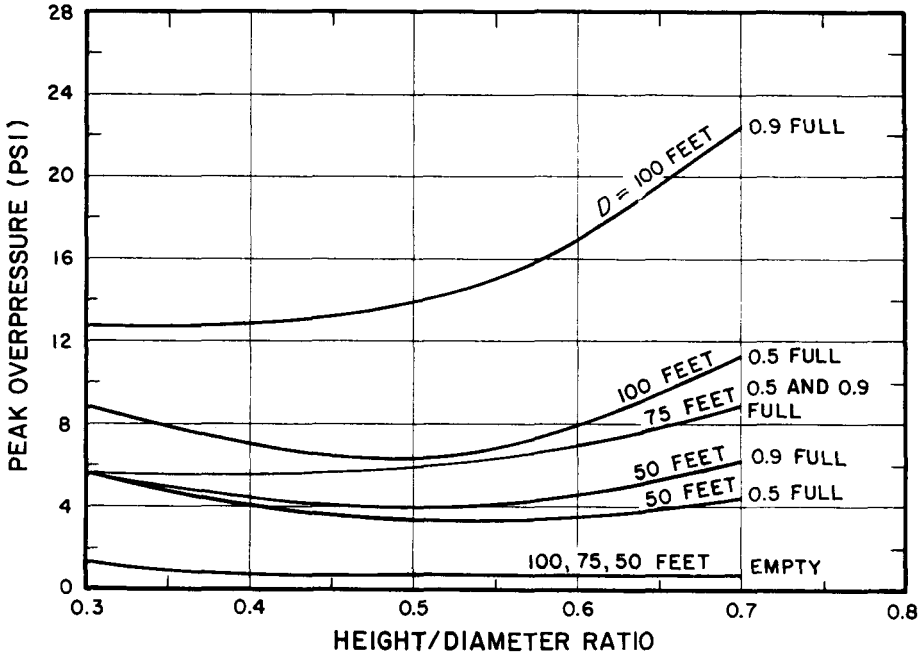

Figure 5.155a. Peak overpressures for severe blast damage to floating- or conical-roof tanks of diameter D for explosions from 1 to 500 kilotons.

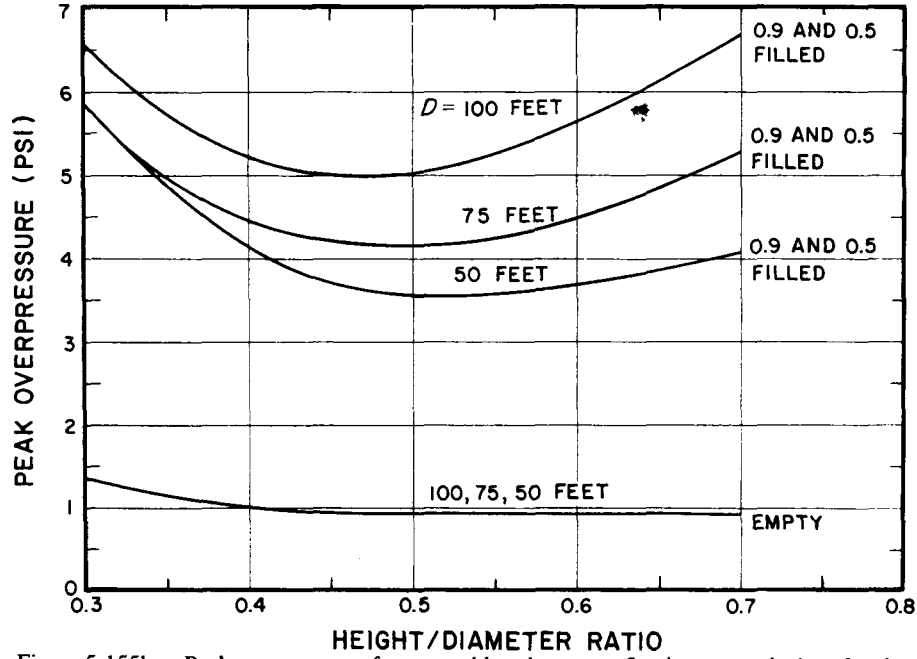

Figure 5.155b. Peak overpressures for severe blast damage to floating- or conical-roof tanks of diameter D from explosions of 500 kilotons or more.

deformation that the earth provides to flexible structures by the buttressing action of the soil.

5.158 For lightweight, shallow buried underground structures the top of the earth cover is at least flush with the original grade but the depth of cover is not more than 6 percent of the span. Such structures are not sufficiently deep for the ratio of the depth of burial to the span to be large enough to obtain the benefits described in § 5.161. The soil provides little attenuation of the air blast pressure applied to the top surface of a shallow buried underground structure. Observations made at full-scale nuclear tests indicate that there is apparently no increase in pressure on the structure as a result of ground shock reflection at the interface between the earth and the top of the structure.

5.159 The lateral blast pressures exerted on the vertical faces of a shallow buried structure have been found to be as low as 15 percent of the blast pressure on the roof in dry, well-compacted, silty soils. For most soils, however, this lateral blast pressure is likely to be somewhat higher and may approach 100 percent of the roof blast pressure in porous saturated soil. The pressures on the bottom of a buried structure, in which the bottom slab is a structural unit integral with the walls, may range from 75 to 100 percent of the pressure exerted on the roof.

5.160 The damage that might be suffered by a shallow buried structure

Table 5.160

DAMAGE CRITERIA FOR SHALLOW BURIED STRUCTURES

Type of structure	Damage type	Peak overpressure (psi)	Nature of damage
Light, corrugated steel arch, surface structure (10-gage corrugated steel with a span of 20–25 ft), central angle of 180°; 5 ft of earth cover at the crown.*	Severe	45– 60	Collapse
	Moderate	50– 50	Large deformations of end walls and arch, also major entrance door damage.
	Light	30– 40	Damage to ventilation and entrance door.
Buried concrete arch 8-in. thick with a 16 ft span and central angle of 180°; 4 ft of earth cover at the crown.	Severe	220–280	Collapse.
	Moderate	100–220	Large deformations with considerable cracking and spalling.
	Light	120–160	Cracking of panels, possible entrance door damage.

*For arched structures reinforced with ribs, the collapse pressure is higher depending on the number of ribs.

will depend on a number of variables, including the structural characteristics, the nature of the soil, the depth of burial, and the downward pressure, i.e., the peak overpressure and direction of the blast wave. In Table 5.160 are given the limiting values of the peak overpressure required to cause various degrees of damage to two types of shallow buried structures. The range of pressures is intended to allow for differences in structural design, soil conditions, shape of earth mound, and orientation with respect to the blast wave.

5.161 Underground structures, buried at such a depth that the ratio of the burial depth to the span approaches (or exceeds) a value of 3.0, will obtain some benefit from the attenuation with depth of the pressure induced by air blast, and from the arching of the load from more deformable areas to less deformable ones. Limited experience at nuclear tests suggests that the arching action of the soil effectively reduces the loading on flexible structures.

BIBLIOGRAPHY

JACOBSEN, L. S. and R. S. AYRE, "Engineering Vibrations," McGraw-Hill Book Co., Inc., 1958.

*JOHNSTON, B. G., "Damage to Commercial and Industrial Buildings Exposed to Nuclear Effects," Federal Civil Defense Administration, February 1956, WT-1189.

*MITCHELL, J. H., "Nuclear Explosion Effects on Structures and Protective Construction—A Selected Bibliography," U.S. Atomic Energy Commission, April 1961, TID-3092.

NEWMARK, N. M., "An Engineering Approach to Blast Resistant Design," *Trans. Amer. Soc. of Civil Engineers*, **121**, 45 (1956).

NORRIS, C. H., *et al.*, "Structural Design for Dynamic Loads," McGraw-Hill Book Co., Inc., 1959.

PICKERING, E. E., and J. L. BOCKHOLT, "Probabilistic Air Blast Failure Criteria for Urban Structures," Stanford Research Institute, Menlo Park, California, November 1971.

*RANDALL, P. A., "Damage to Conventional and Special Types of Residences Exposed to Nuclear Effects," OCDM, FHA, and HHFA, March 1961, WT-1194.

RODGERS, G. L., "Dynamics of Framed Structures," John Wiley and Sons, Inc., 1959.

*SHAW, E. R. and F. P. MCNEA, "Exposure of Mobile Homes and Emergency Vehicles to Nuclear Explosions," Federal Civil Defense Administration, July 1957, WT-1181.

*SPARKS, L. N., "Nuclear Effects on Machine Tools," U.S. Atomic Energy Commission, December 1956, WT-1184.

*TAYLOR, B. C., "Blast Effects of Atomic Weapons Upon Curtain Walls and Partitions of Masonry and Other Materials," Federal Civil Defense Administration, August 1956, WT-741.

*TUCKER, P. W. and G. R. WEBSTER, "Effects of a Nuclear Explosion on Typical Liquefied Petroleum Gas (LP-Gas) Installations and Facilities," Liquefied Petroleum Gas Association, December 1956, WT-1175.

TUNG, T. P. and N. M. NEWMARK, "A Review of Numerical Integration Methods for Dynamic Response of Structures," University of Illinois Structural Research Series No. 69, 1954.

*WILLIAMSON, R. H., "Effects of a Nuclear Explosion on Commercial Communications Equipment," Federal Civil Defense Administration, May 1955, ITR-1193.

WILLOUGHBY, A. B., *et al.*, "A Study of Loading, Structural Response, and Debris Characteristics of Wall Panels," URS Research Co., Burlingame, California, July 1969.

WILTON, C., *et al.*, "Final Report Summary, Structural Response and Loading of Wall Panels," URS Research Co., Burlingame, California, July 1971.

*These publications may be purchased from the National Technical Information Service, U.S. Department of Commerce, Springfield, Virginia, 22161.

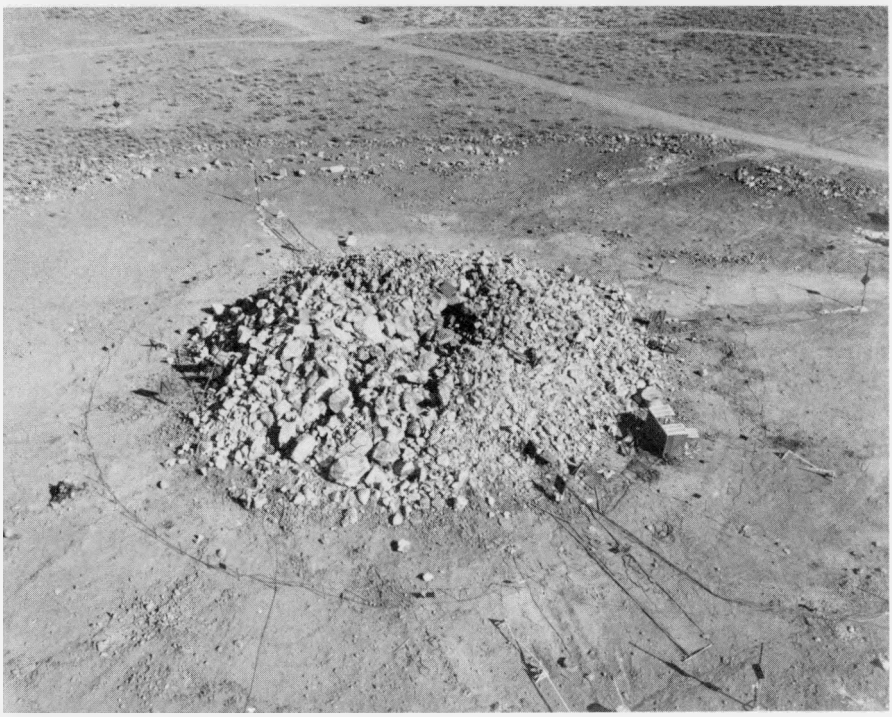

Figure 6.05. SULKY event; mound created by the bulking of rock material in a 0.087-kiloton nuclear detonation at a depth of 90 feet.

cracks of various sizes. Beyond the rupture zone is the "plastic zone" in which the stress level has declined to such an extent that there is no visible rupture, although the soil is permanently deformed and compressed to a higher density. Plastic deformation and distortion of soil around the edges of the crater contribute to the production of the crater lip. The thicknesses of the rupture and plastic zones depend on the nature of the soil, as well as upon the energy yield of the explosion and location of the burst point. If the earth below the burst consists of rock, then there will be a rupture zone but little or no plastic zone.

CRATER DIMENSIONS

6.08 For an explosion above the earth's surface, appreciable formation of a vaporization (depression) crater will commence when the height of burst is less than about a tenth of the maximum fireball radius (§ 2.127). With decreasing distance from the surface, the dimensions of the crater vary in a complex manner, especially as the ground is approached, because of the change in the mechanism of crater formation. In general, however, the depth of the depression increases rapidly with decreasing burst height and the ratio of the depth to radius also increases. The dimensions of the crater increase with the explosion

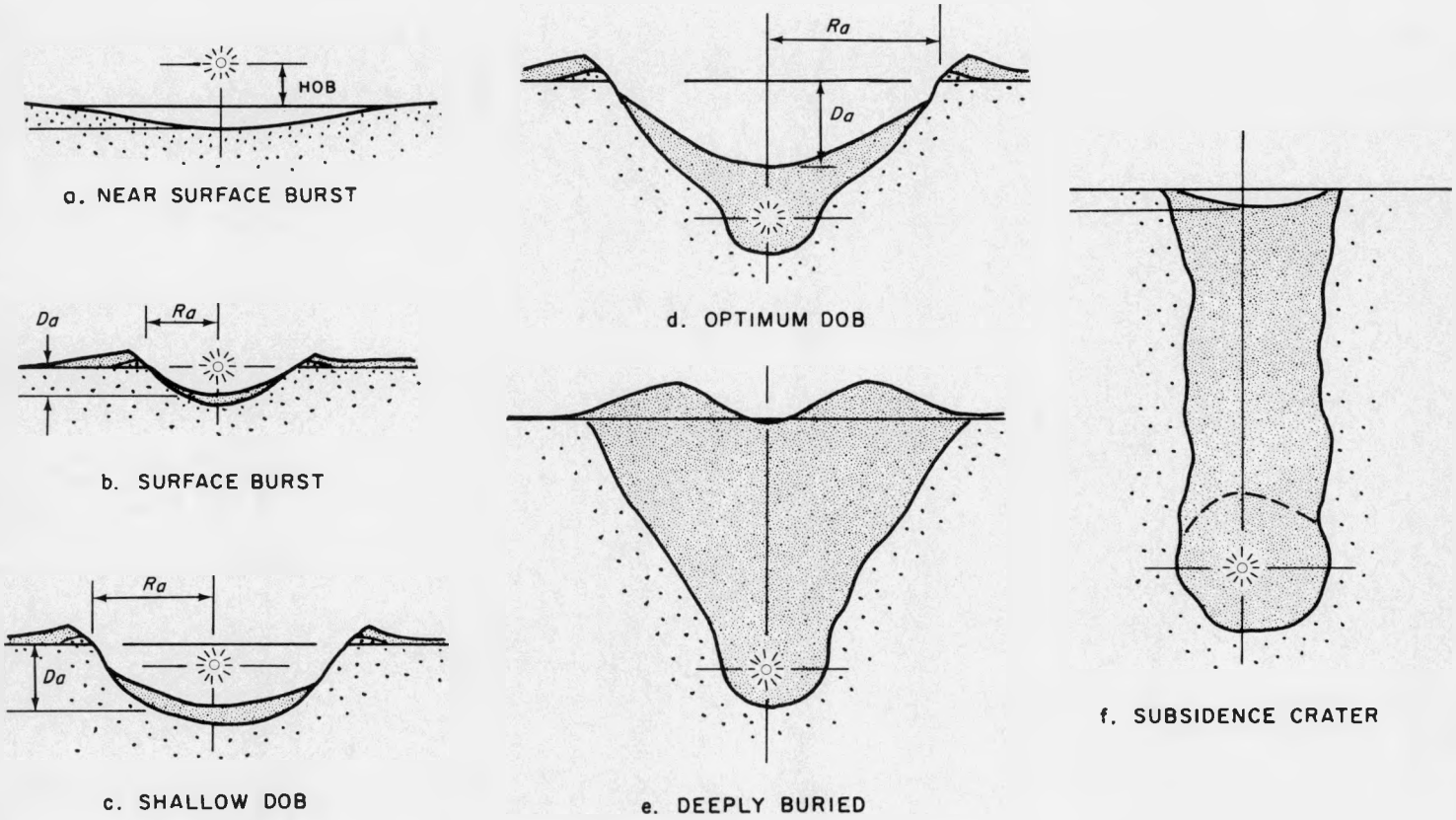

Figure 6.06. Relative crater sizes and shapes resulting from various burst depths; R_a and D_a are the apparent radius and depth, respectively, of the crater (see Figure 6.70).

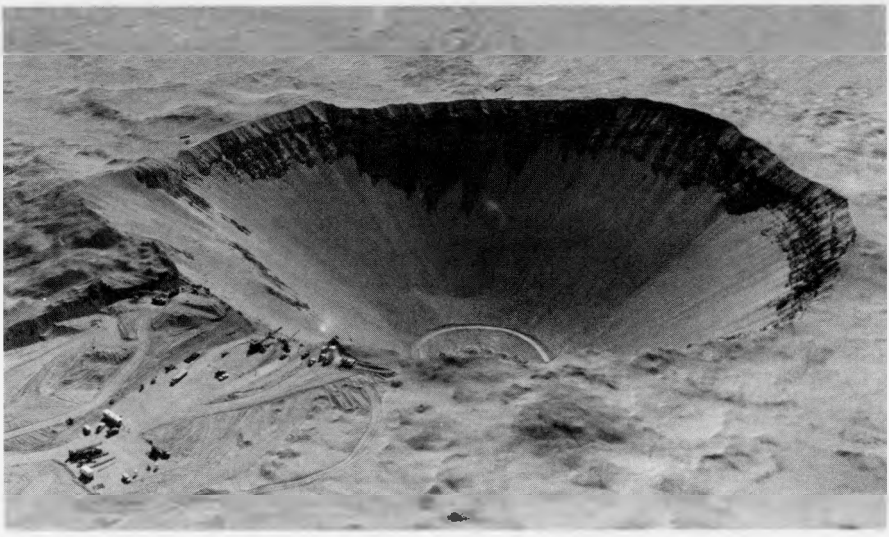

Figure 6.10. SEDAN event; crater formed by a 100-kiloton explosion in alluvial soil at the optimum depth of burst (635 feet) for cratering. The crater radius is 611 feet, the depth 323 feet, and the volume 179 million cubic feet.

yield but the actual values depend on the soil characteristics.

6.09 For contact surface bursts, approximate values of the crater dimensions can be given. For a 1-kiloton nuclear explosion at the surface, the apparent radius of the crater in dry soil or dry soft rock is estimated to be about 60 feet. The radius at the crest of the lip will be 15 feet or so greater. The apparent depth of the crater is expected to be about 30 feet. In hard rock, consisting of granite or sandstone, the dimensions will be somewhat less. The radius will be appreciably greater in soil saturated with water, and so also will be the initial depth, to which structural damage is related. The final depth, however, will be shallower because of "hydraulic fill," i.e., slumping back of wet material and the seepage of water carrying loose soil. All crater dimensions resulting from a surface burst of yield W kilotons are related approximately to those given above for a yield of 1-kiloton by the factor $W^{0.3}$. For example, for a 100-kiloton explosion on the surface of dry soil, the radius of the crater may be expected to be roughly $60 \times (100)^{0.3} = 240$ feet, and the depth about $30 \times (100)^{0.3} = 120$ feet. Further information on crater dimensions will be found in § 6.72 *et seq.*

6.10 As the depth of burial is increased, the radius and depth of the crater also increase until maxima are reached; deeper burial then results in progressively smaller craters. These maximum values of radius and depth for a given yield are termed "optimum" (Fig. 6.06d) and depths of burial for optimum crater radius and for optimum crater depth are roughly equal. A photograph of a crater formed at the optimum burst depth is shown in Fig. 6.10. For a 1-kiloton weapon, the

Figure 6.55. Waves from the BAKER underwater explosion reaching the beach at Bikini, 11 miles from surface zero.

Table 6.57

MAXIMUM HEIGHTS (CREST TO TROUGH) AND ARRIVAL TIMES OF WATER WAVES AT BIKINI BAKER TEST

Distance (yards)	330	660	1,330	2,000	2,700	3,300	4,000
Wave height (feet)	94	47	24	16	13	11	9
Time (seconds)	11	23	48	74	101	127	154

at the Bikini BAKER test. A more generalized treatment of wave heights, which can be adapted to underwater explosions of any specified energy, is given in § 6.119 *et seq.*

6.58 For the conditions that existed in the BAKER test, water wave damage is possible to ships that are moderately near to surface zero. There was evidence for such damage to the carrier U.S.S. Saratoga, anchored in Bikini lagoon almost broadside on to the explosion with its stern 400 yards from surface zero. The "island" structure was

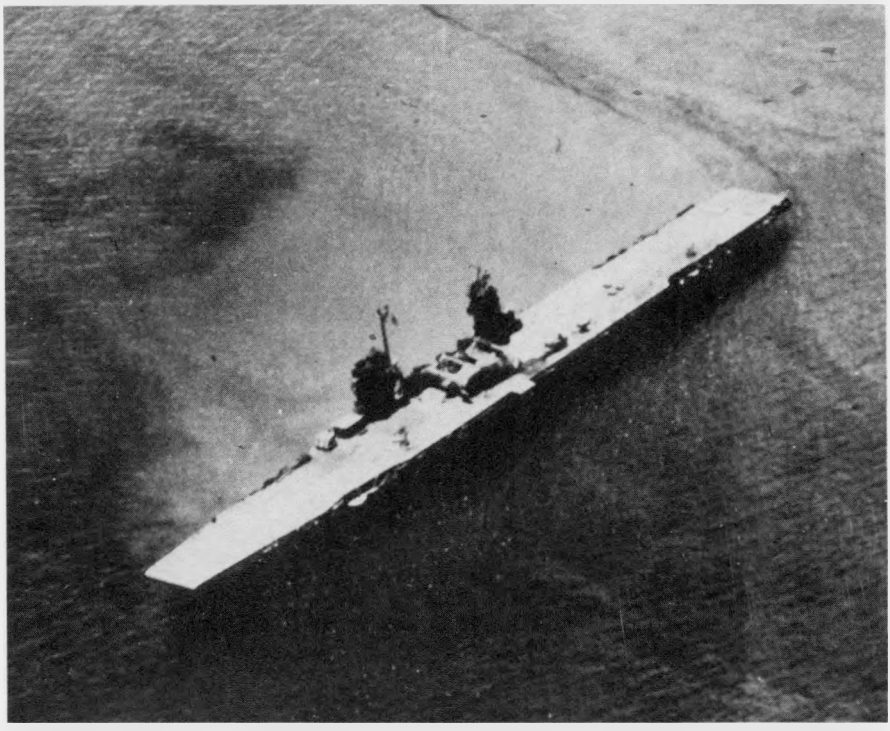

Figure 6.58. The aircraft carrier U.S.S. Saratoga after the BAKER explosion.

not affected by the air blast, but later the central part of the structure was observed to be folded down on the deck of the carrier (Fig. 6.58). Shortly after rising on the first wave crest, when the stern was over 43 feet above its previous position, the Saratoga fell into the succeeding trough. It appears probable that the vessel was then struck by the second wave crest which caused the damage to the island structure.

6.59 Water waves generated by an underwater detonation can cause damage in harbors or near the shoreline, both by the force of the waves and by inundation. The waves will increase in height as they move into shallower water, and inundation, similar to that observed with tidal waves, can occur to an extent depending on the beach slope and wave height and steepness (§ 2.71).

UNDERWATER CRATERING

6.60 For a nuclear explosion in (or even just above) a body of water, a significant crater forms in the bottom material if the gaseous bubble or a cavity in the water (§ 6.52) formed by the explosion makes contact with the bottom. Such an underwater crater is similar to a crater on land formed by an explosion near the ground surface since both are characterized by a dish-shaped depression, wider than it is deep, and surrounded by a lip raised above the undisturbed surface (see Fig. 6.70). For most underwater craters, however, the

observed ratio of crater radius to depth is larger and the lip height is smaller than for craters from comparable bursts in similar materials on land. These differences are caused by water displaced by the explosion washing back over the crater. This flow increases the crater radius by as much as 10 percent and decreases the depth by up to 30 percent. An exception to this general rule occurs when the water layer is so shallow that the lip formed by the initial cratering extends above the surface of the water. Such craters, termed "unwashed craters," approach surface craters in appearance, with higher lips and smaller radius-to-depth ratios than washed craters.

6.61 The Bikini BAKER explosion resulted in a measurable increase in depth of the bottom of the lagoon over an area roughly 2,000 feet across. The greatest apparent change in depth was 32 feet, but this represented the removal of an elevated region rather than an excavation in a previously flat surface. Before the test, samples of sediment collected from the bottom of the lagoon consisted of coarse-grained algal debris mixed with less than 10 percent of sand and mud. Samples taken after the explosion were, however, quite different. Instead of algal debris, layers of mud, up to 10 feet thick, were found on the bottom near the burst point.

UNDERWATER SHOCK DAMAGE: GENERAL CHARACTERISTICS

6.62 The impact of a shock wave on a ship or structure, such as a breakwater or dam, is comparable to a sudden blow. Shocks of this kind have been experienced in connection with underwater detonations of TNT and other chemical explosives. However, because of the smaller yields, the shock damage from such explosions is localized, whereas the shock wave from a high-yield nuclear explosion can engulf an entire ship and cause damage over a large area.

6.63 The effects of an underwater nuclear burst on a ship may be expected to be of two general types. First, there will be the direct effect of the shock on the vessel's hull; and second, the indirect effects resulting from components within the ship being set in motion by the shock. An underwater shock acting on the hull of a ship tends to cause distortion of the hull below the water line and rupture of the shell plating, thus producing leaks as well as severely stressing the ship's framing. The underwater shock also leads to a rapid movement in both horizontal and vertical directions. This motion causes damage by shock to components and equipment within the ship.

6.64 Main feed lines, main steam lines, shafting, and boiler brickwork within the ship are especially sensitive to shock. Because of the effects of inertia, the supporting members or foundations of heavy components, such as engines and boilers, are likely to collapse or become distorted. Lighter or inadequately fastened articles will be thown about with great violence, causing damage to themselves, to bulkheads, and to other equipment. Electronic, fire control, and guided missile equipment is likely to be rendered inoperative, at least temporarily, by shock effects. However, equipment which has been properly designed to be shock resistant will suffer less seriously (cf. § 6.112 *et seq.*). In general, it appears that the

damage to shipboard equipment is dependent on the peak velocity imparted to the particular article by the shock wave.

6.65 The damage to the hull of a ship is related to the energy per unit area of the shock wave, evaluated up to a time corresponding to the surface cutoff time at a characteristic depth. Damage to the gate structure of canal locks and drydock caissons is dependent mainly on the peak pressure of the underwater shock wave. Within the range of very high pressures at the shock front, such structures may be expected to sustain appreciable damage. On the other hand, damage to large, massive subsurface structures, such as harbor installations, is more nearly dependent upon the shock wave impulse. The impulse is dependent upon the duration of the shock wave as well as its pressure (§ 3.59).

UNDERWATER SHOCK: BIKINI EXPERIENCE

6.66 In the shallow, underwater BAKER test, some 70 ships of various types were anchored around the point of burst. From the observations made after the shot, certain general conclusions were drawn, and these will be outlined here. It should be noted, however, that the nature and extent of the damage sustained by a surface vessel from underwater shock will depend upon the depth of the burst, yield, depth of water, range, the ship type, whether it is operating or riding at anchor, and its orientation with respect to the explosion.

6.67 In a shallow underwater burst, boilers and main propulsive machinery suffer heavy damage due to motion caused by the water shock at close-in locations. As the range is increased, auxiliary machinery associated with propulsion of the ship does not suffer as severely, but light interior equipment, especially electronic equipment, is affected to ranges considerably beyond the limit of hull damage. In vessels underway, machinery will probably suffer somewhat more damage than those at anchor.

6.68 Although the major portion of the shock energy from a shallow underwater explosion is propagated through the water, a considerable amount is transmitted through the surface as a shock (or blast) wave in air. Air blast undoubtedly caused some damage to the superstructures of the ships at the Bikini BAKER test, but this was insignificant in comparison to the damage done by the underwater shock. Air blast could also cause some damage to ships by capsizing them. The main effect of the air blast wave, however, would probably be to targets on land, if the explosion occurred not too far from shore. The damage criteria are then the same as for a surface burst over land, at the appropriate overpressures and dynamic pressures.

6.69 As the depth of burst increases, the proportion of the explosion energy going into air blast diminishes, in a manner similar to that in a burst beneath the earth's surface. Consequently, the range for a given overpressure decreases, with the close-in higher pressures decreasing more rapidly than lower pressures at longer ranges.

TECHNICAL ASPECTS OF SURFACE AND UNDERGROUND BURSTS[3]

CRATER DIMENSIONS

6.70 In addition to the rupture and plastic zones (§ 6.07), two other features of a crater may be defined; these are the "apparent crater" and the "true crater." The apparent crater, which has a radius R_a and a depth D_a, as shown in Fig. 6.70, is the depression or hole left in the ground after the explosion. The true crater, on the other hand, extends beyond the apparent crater to the distance at which definite shear has occurred. The volume of the (apparent) crater, assumed to be roughly paraboloid, is given approximately by

$$\text{Volume of crater} \approx \frac{1}{2} \pi R_a^2 D_a.$$

6.71 Values of other crater parameters indicated in Fig. 6.70 can be estimated with respect to the apparent crater radius and the apparent crater depth by the following relations. The radius to the crater lip crest, R_{al}, is

$$R_{al} \approx 1.25 R_a.$$

The height of the lip crest, D_{al}, is

$$D_{al} \approx 1.25 D_a.$$

The height of the apparent lip above the original ground surface, H_{al}, is

$$H_{al} \approx 0.25 D_a.$$

Thus, if R_a and D_a are known, the quantities given above (and others defined in § 6.74 *et seq.*) can be estimated.

6.72 Crater dimensions depend upon the depth of burst (or burial), the explosion energy yield, and the characteristics of the soil. The apparent crater radius and depth, as functions of the depth of burst, are given in Figs. 6.72a and b for a 1-kiloton explosion in four media. For bursts just above the surface, the heights of burst are treated as negative depths of burst. Because of the rapid change in crater dimensions as the depth of bursts passes through zero, the values for a contact surface burst are shown explicitly on the figures. The best empirical fit to crater data indicates that, for a given scaled depth of burst, i.e., actual depth divided by $W^{0.3}$, both the radius and depth vary approximately as $W^{0.3}$, where W is the weapon yield. The procedure for calculating the dimensions of the apparent crater for any specified depth of burst and yield by means of these scaling rules is illustrated in the example facing Fig. 6.72a. The maxima in the curves indicate the so-called optimum depths of burst. It is evident that a change in the moisture content of a soil or rock medium can have a significant influence on the size of a crater; a higher moisture content increases the crater size by increasing the plasticity of a soil medium, weakening a rock medium, and providing a better coupling of the explosive energy to both soil and rock media.

(Text continued on page 255.)

[3]The remaining sections of this chapter may be omitted without loss of continuity.

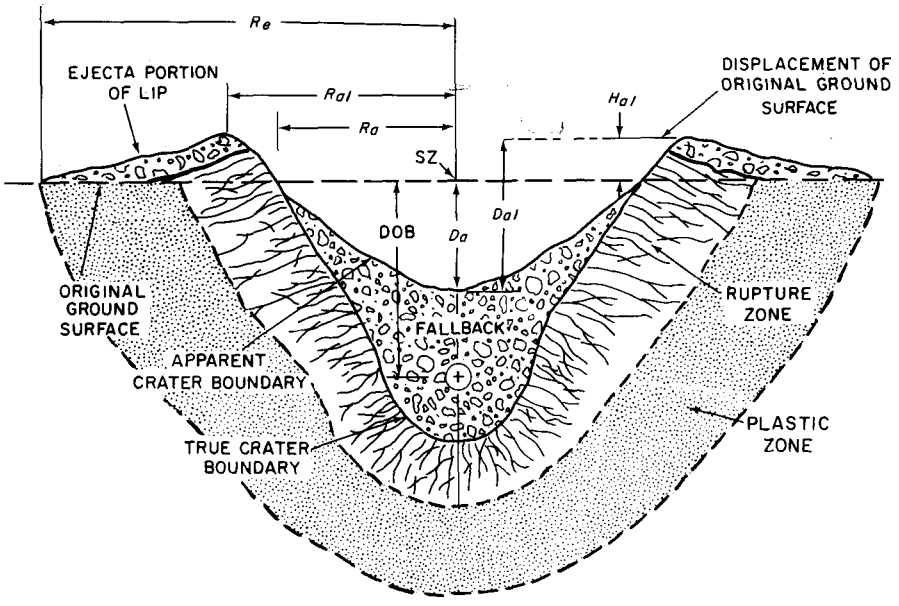

Figure 6.70. Cross section of a crater from a subsurface nuclear detonation.

The curves in Figs. 6.72a and b give the approximate apparent crater radius and depth, respectively, as a function of depth of burst (DOB) in wet hard rock, dry hard rock, wet soil or wet soft rock, and dry soil or dry hard rock. Heights of burst (up to 20 feet) are treated as negative depths of burst.

Scaling. To determine the apparent crater radius and depth for a W KT yield, the actual burst depth is first divided by $W^{0.3}$ to obtain the scaled depth. The radius and depth of a crater for 1 KT at this depth are obtained from Figs. 6.72a and b, respectively, The results are then multiplied by $W^{0.3}$ to obtain the required dimensions.

Example

Given: A 20 KT explosion at a depth of 270 feet in dry hard rock.

Find: Apparent crater radius and depth.

Solution: The scaled burst depth is

$$\text{DOB}/W^{0.3} = 270/20^{0.3}$$
$$= 270/2.46 = 110 \text{ feet.}$$

From Fig. 6.72a the apparent crater radius for a 1 KT explosion at this depth in dry hard rock is 150 feet (curve 4) and from Fig. 6.72b the corresponding crater depth is 87 feet (curve 4). Hence, the apparent crater radius and depth for a 20 KT burst at a depth of 270 feet in dry hard rock are given approximately as follows:

Crater radius (R_a) $\approx 150 \times 20^{0.3} = 150 \times 2.46 = 368$ feet.

Crater depth (D_a) $\approx 87 \times 20^{0.3} = 87 \times 2.46 = 214$ feet. *Answer.*

(With R_a and D_a known, other crater (and lip) dimensions can be obtained from the approximate relations in §§ 6.71, 6.74, and 6.75.)

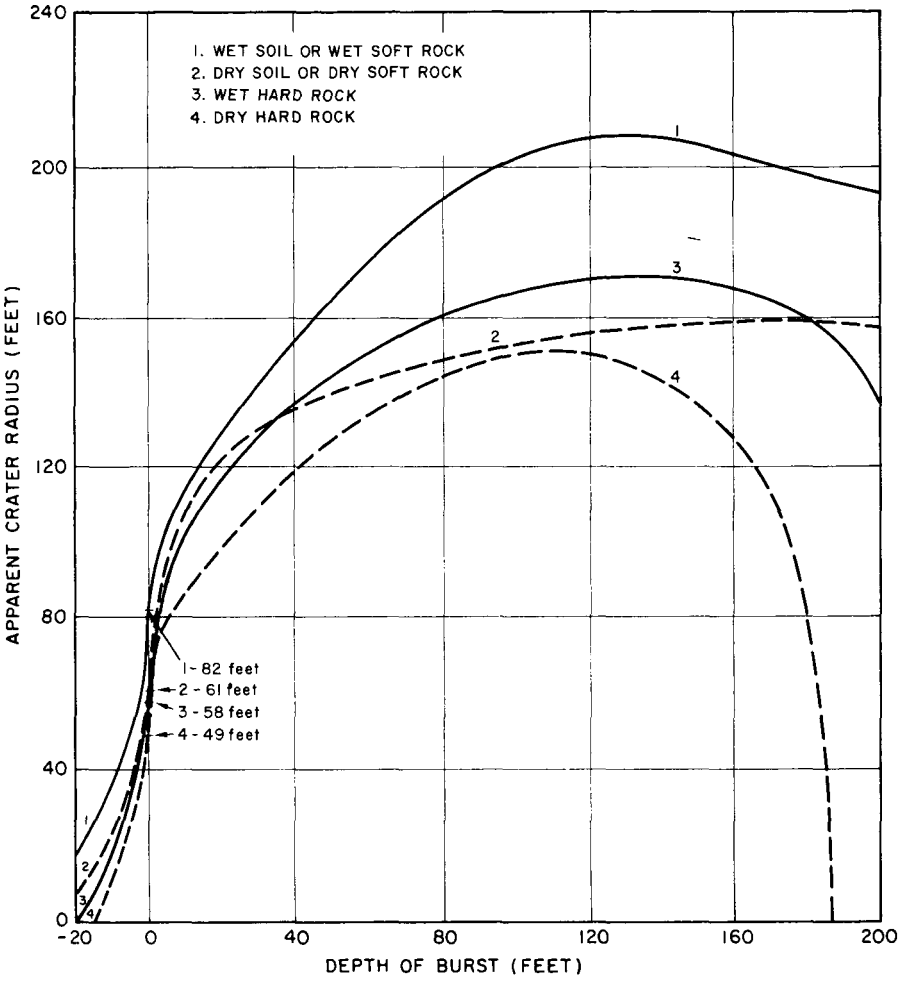

Figure 6.72a. Apparent crater radius as a function of depth of burst for a 1-kiloton explosion in (or above) various media.

CRATER EJECTA

6.73 Crater ejecta consist of soil or rock debris that is thrown beyond the boundaries of the apparent crater. Together with the fallback, which lies between the true and apparent crater boundaries, ejecta comprise all material completely disassociated from the parent medium by the explosion. The ejecta field is divided into two zones: (1) the crater lip including the continuous ejecta surrounding the apparent crater (Fig. 6.70), and (2) the discontinuous ejecta, comprising the discrete missiles that fall beyond the limit of the continuous ejecta.

6.74 The amount and extent of the continuous ejecta in the crater lip are

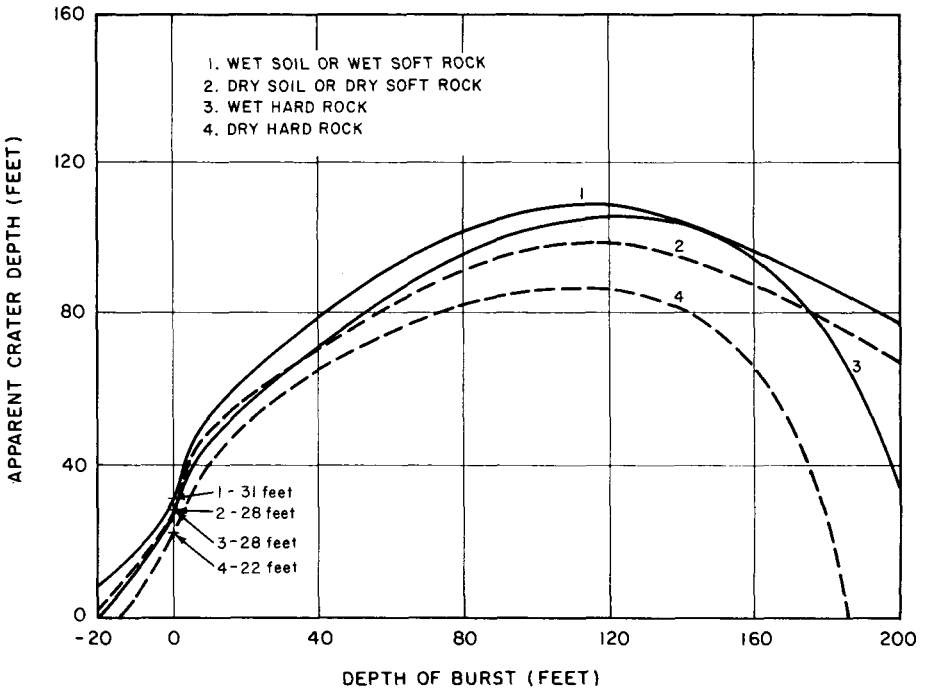

Figure 6.72b. Apparent crater depth as a function of depth of burst for a 1-kiloton explosion in (or above) various media.

determined primarily by the explosion yield and the location of the burst point, although the characteristics of the medium have some effect. The radial limit of the continuous ejecta, which is the outer edge of the lip, will usually vary from two to three times the apparent crater radius. In most cases, a satisfactory approximation to the radius of the continuous ejecta, R_e (Fig. 6.70), is

$$R_e \approx 2.15\ R_a.$$

6.75 The depth of the ejecta decreases rapidly in an exponential manner as the distance from surface zero increases. In general, about 80 to 90 percent of the entire ejecta volume is deposited within the area of the continuous ejecta. Analysis of data for craters formed by nuclear bursts in soil indicates that ejecta mass represents approximately 55 percent of the apparent crater mass (the remainder being found in fallback, compaction, and the dust cloud which is blown away). For an explosion of given yield, the ejecta mass increases significantly with the depth of burst until the optimum depth is reached. Ejecta thickness can be estimated for soil in terms of the apparent radius and diameter; thus:

$$t_e \approx 0.9\ D_a \left(\frac{R_a}{R}\right)^{3.86}, \text{ for } R > 1.8\ R_a, \tag{6.75.1}$$

where t_e is the ejecta thickness and R is the distance from surface zero to the point of interest. In equation (6.75.1), it is assumed that the ejecta mass density is approximately equal to the original in-situ density of the medium, which

underwater structures, since they can be expected to have short characteristic times.

6.124 For large, rigid underwater structures, where the duration of the shock wave is short in comparison with the characteristic times of the structure, the impulse of the shock wave will be significant in determining the damage. It should be remembered, in this connection, that the magnitude of the impulse and damage will be greatly decreased if the negative reflected wave from the air–water surface reaches the target and causes cutoff soon after the arrival of the primary shock wave.

6.125 If the large underwater structure can accept a substantial amount of permanent (plastic) deformation as a result of impact with the shock front, it appears that the damage depends essentially on the energy of the shock wave. If the structure is near the surface, the cutoff effect will decrease the amount of shock energy available for causing damage.

BIBLIOGRAPHY

BARASH, R. M., and J. A. GOERTNER, "Refraction of Underwater Explosion Shock Waves: Pressure Histories Measured at Caustics in a Flooded Quarry," U.S. Naval Ordnance Laboratory, April 1967, NOLTR-67-9.

CARLSON, R. H., and W. A. ROBERTS, "Project SEDAN, Mass Distribution and Throwout Studies," The Boeing Company, Seattle, Washington, August 1963, PNE-217E.

CIRCEO, L. J., and M. D. NORDYKE, "Nuclear Cratering Experience at the Pacific Proving Grounds," University of California, Lawrence Radiation Laboratory, November 1964, UCRL-12172.

COLE, R. H., "Underwater Explosions," Dover Publications, Inc., 1965. (Reprint of 1948 edition, Princeton University Press.)

DAVIS, L. K., "MINE SHAFT Series, Events MINE UNDER and MINE ORE, Subtask, N121, Crater Investigations," U.S. Army Engineer Waterways Experiment Station, March 1970, Technical Report N-70-8.

ENGDAHL, E. R., "Seismic Effects of the MILROW and CANNIKIN Nuclear Explosions," *Bull. Seismol. Soc. America*, **62**, 1411 (1972).

FITCHETT, D. J., "MIDDLE COURSE I Cratering Series," U.S. Army Engineer Nuclear Cratering Group, June 1971, Technical Report 35.

FRANDSEN, A. D., "Project CABRIOLET, Engineering Properties Investigations of the CABRIOLET Crater," U.S. Army Engineer Nuclear Cratering Group, March 1970, PNE-957.

*GLASSTONE, S., "Public Safety and Underground Nuclear Detonations," U.S. Atomic Energy Commission, June 1971, TID-25708.

HEALY, J. H., and P. A. MARSHALL, "Nuclear Explosions and Distant Earthquakes: A Search for Correlations," *Science*, **169**, 176 (1970).

KOT, C. A., "Hydra Program: Theoretical Study of Bubble Behavior in Underwater Explosions," U.S. Naval Radiological Defense Laboratory, April 1964, USNRDL-TR-747.

MALME, C. I., J. R. CARBONELL, and I. DYER, "Mechanisms in the Generation of Airblast by Underwater Explosions," U.S. Naval Ordnance Laboratory, September 1966, Bolt, Beranek and Newman Report No. 1434, NOLTR-66-88.

NEWMARK, N. M., and W. J. HALL, "Preliminary Design Methods for Underground Protective Structures," University of Illinois, June 1962, AFSWC-TDR-62-6.

NEWMARK, N. M., "Notes on Shock Isolation Concepts," Vibration and Civil Engineering Proceedings of Symposium of British National Section International Association for Earthquake Engineering, p. 71, Butterworths, London, 1966.

PHILLIPS, D. E., and T. B. HEATHCOTE, "Underwater Explosion Tests of Two Steam Producing Explosives, I. Small Charge Tests," U.S. Naval Ordnance Laboratory, May 1966, NOLTR-66-79.

*"Proceedings of the Second Plowshare Symposium," Part I, Phenomenology of Underground Nuclear Explosions," University of California, Lawrence Radiation Laboratory, Livermore, May 1959, UCRL-5677.

*"Proceedings of the Third Plowshare Symposium, Engineering with Nuclear Explosives," April 1964, University of California, Lawrence Radiation Laboratory, Livermore, TID-7695.

*"Proceedings of the Symposium on Engineering with Nuclear Explosives," Las Vegas, Nevada, January 1970, American Nuclear Society and U.S. Atomic Energy Commission, CONF-700101, Vols, 1 and 2.

what diffuse, rather than a direct, transmission of the thermal radiation.

EFFECT OF ATMOSPHERIC CONDITIONS

7.11 The decrease in energy of thermal radiation due to scattering by particles in the air depends upon the atmospheric conditions, such as the concentration and size of the particles, and also upon the wavelength of the radiation. This means that radiations of different wavelengths, namely, ultraviolet, visible, and infrared, will suffer energy attenuation to different extents. For most practical purposes, however, it is more convenient and reasonably satisfactory, although less precise, to postulate a mean attenuation averaged over all the wavelengths present in the thermal radiation.

7.12 The extent to which the atmosphere attenuates thermal energy and limits visibility depends largely on the scattering of radiation. Therefore, the state of the atmosphere as far as scattering is concerned can be represented by what is known as the daylight "visibility range" or, in brief, as the "visibility." This is defined as the horizontal distance at which a large dark object on the horizon has just enough contrast with the surrounding sky to be discernible in daylight. The international code for correlating the visibility with the condition of the atmosphere is given in Table 7.12.

7.13 At first thought, it would be expected that the decrease of thermal radiation energy with increasing distance from the explosion would be greater when the visibility is low than when it is high. But, for the reason given below, it has been found that, at distances less than about half the visibility, the degree of attenuation of the thermal radiation is relatively insensitive to atmospheric conditions if at least moderately clear (10 miles or more) visibility prevails. At greater distances, however, a larger proportion of the radiant energy is indeed lost as the atmospheric visibility decreases. As a rough approximation, the amount of thermal energy received at a given distance from a nuclear explosion may be assumed to be independent of the visibility. This leads to overestimates at distances greater than about half the

Table 7.12

VISIBILITY AND CONDITION OF THE ATMOSPHERE

Atmospheric Condition	Visibility	
	Kilometers	Miles
Exceptionally clear	280	170
Very clear	50	31
Clear	20	12
Light haze	10	6
Haze	4	2.5
Thin fog	2	1.2
Light to thick fog	1 or less	0.6 or less

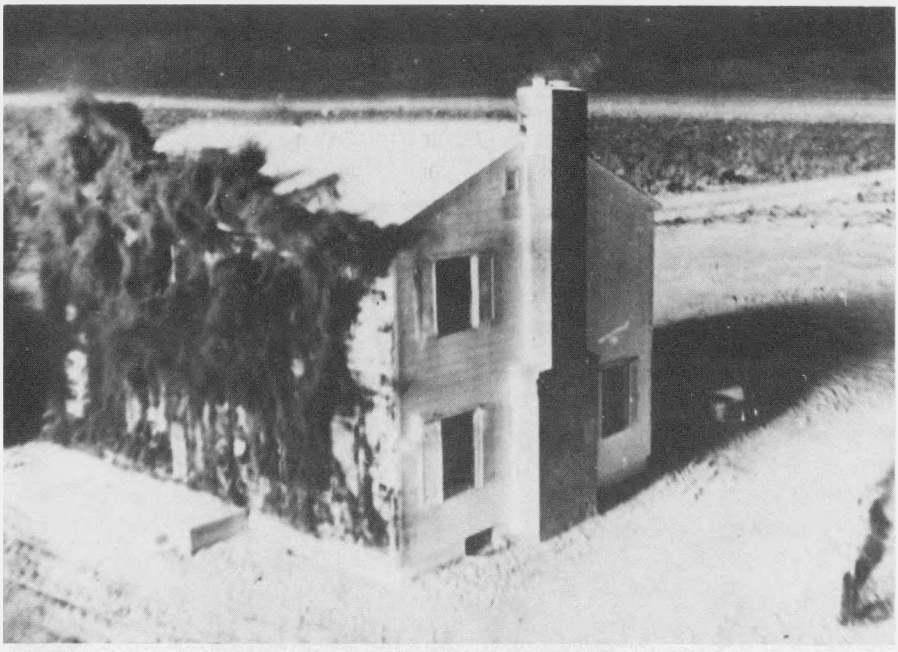

Figure 7.28a. Thermal effects on wood-frame house 1 second after explosion (about 25 cal/cm^2).

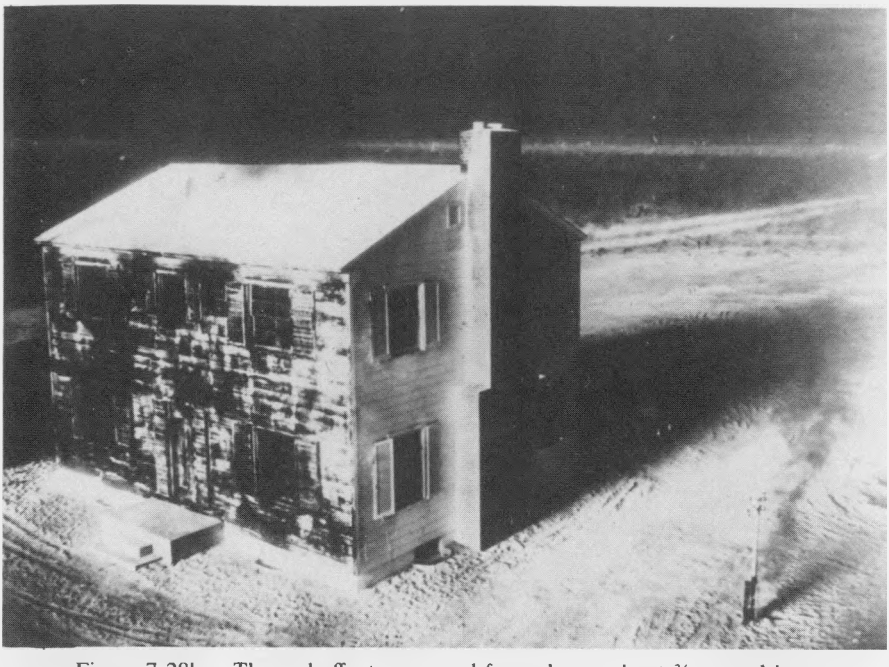

Figure 7.28b. Thermal effects on wood-frame house about ¾ second later.

Table 7.35

APPROXIMATE RADIANT EXPOSURES FOR IGNITION OF FABRICS FOR LOW AIR BURSTS

Material	Weight (oz/yd^2)	Color	Effect on Material	Radiant Exposure* (cal/cm^2) 35 kilotons	1.4 megatons	20 megatons
CLOTHING FABRICS						
Cotton	8	White	Ignites	32	48	85
		Khaki	Tears on flexing	17	27	34
		Khaki	Ignites	20	30	39
		Olive	Tears on flexing	9	14	21
		Olive	Ignites	14	19	21
		Dark blue	Tears on flexing	11	14	17
		Dark blue	Ignites	14	19	21
Cotton corduroy	8	Brown	Ignites	11	16	22
Cotton denim, new	10	Blue	Ignites	12	27	44
Cotton shirting	3	Khaki	Ignites	14	21	28
Cotton-nylon mixture	5	Olive	Tears on flexing	8	15	17
		Olive	Ignites	12	28	53
Wool	8	White	Tears on flexing	14	25	38
		Khaki	Tears on flexing	14	24	34
		Olive	Tears on flexing	9	13	19
		Dark blue	Tears on flexing	8	12	18
	20	Dark blue	Tears on flexing	14	20	26
Rainwear (double neoprene-coated nylon twill)	9	Olive	Begins to melt	5	9	13
		Olive	Tears on flexing	8	14	22
DRAPERY FABRICS						
Rayon gabardine	6	Black	Ignites	9	20	26
Rayon-acetate drapery	5	Wine	Ignites	9	22	28
Rayon gabardine	7	Gold	Ignites	**	24†	28†
Rayon twill lining	3	Black	Ignites	7	17	25
Rayon twill lining	3	Beige	Ignites	13	20	28
Acetate-shantung	3	Black	Ignites	10†	22†	35†
Cotton heavy draperies	13	Dark colors	Ignites	15	18	34
TENT FABRICS						
Canvas (cotton)	12	White	Ignites	13	28	51
Canvas	12	Olive drab	Ignites	12	18	28
OTHER FABRICS						
Cotton chenille bedspread		Light blue	Ignites	**	11†	15†
Cotton venetian blind tape, dirty		White	Ignites	10	18	22
Cotton venetian blind tape		White	Ignites	13†	27†	31†
Cotton muslin window shade	8	Green	Ignites	7	13	19

*Radiant exposures for the indicated responses (except where marked †) are estimated to be valid to ±25% under standard laboratory conditions. Under typical field conditions the values are estimated to be valid within ±50% with a greater likelihood of higher rather than lower values. For materials marked †, ignition levels are estimated to be valid within ±50% under laboratory conditions and within ±100% under field conditions.

**Data not available or appropriate scaling not known.

Table 7.40

APPROXIMATE RADIANT EXPOSURES FOR IGNITION OF VARIOUS MATERIALS FOR LOW AIR BURSTS

Material	Weight (oz/yd²)	Color	Effect on Material	Radiant Exposure* (cal/cm²) 35 kilotons	1.4 megatons	20 megatons
HOUSEHOLD TINDER MATERIALS						
Newspaper, shredded	2		Ignites	4	6	11
Newspaper, dark picture area	2		Ignites	5	7	12
Newspaper, printed text area	2		Ignites	6	8	15
Crepe paper	1	Green	Ignites	6	9	16
Kraft paper	3	Tan	Ignites	10	13	20
Bristol board, 3 ply	10	Dark	Ignites	16	20	40
Kraft paper carton, used (flat side)	16	Brown	Ignites	16	20	40
New bond typing paper	2	White	Ignites	24†	30†	50†
Cotton rags		Black	Ignites	10	15	20
Rayon rags		Black	Ignites	9	14	21
Cotton string scrubbing mop (used)		Gray	Ignites	10†	15†	21†
Cotton string scrubbing mop (weathered)		Cream	Ignites	10†	19†	26†
Paper book matches, blue head exposed			Ignites	11†	14†	20†
Excelsior, ponderosa pine	2 lb/ft³	Light yellow	Ignites	**	23†	23†
OUTDOOR TINDER MATERIALS***						
Dry rotted wood punk (fir)			Ignites	4†	6†	8†
Deciduous leaves (beech)			Ignites	4	6	8
Fine grass (cheat)			Ignites	5	8	10
Coarse grass (sedge)			Ignites	6	9	11
Pine needles, brown (ponderosa)			Ignites	10	16	21
CONSTRUCTION MATERIALS						
Roll roofing, mineral surface			Ignites	**	>34	>116
Roll roofing, smooth surface			Ignites	**	30	77
Plywood, douglas fir			Flaming during exposure	9	16	20
Rubber, pale latex			Ignites	50	80	110
Rubber, black			Ignites	10	20	25
OTHER MATERIALS						
Aluminum aircraft skin (0.020 in. thick) coated with 0.002 in. of standard white aircraft paint			Blisters	15	30	40
Cotton canvas sandbags, dry filled			Failure	10	18	32
Coral sand			Explodes (popcorning)	15	27	47
Siliceous sand			Explodes (popcorning)	11	19	35

*Radiant exposures for the indicated responses (except where marked †) are estimated to be valid to ±25% under standard laboratory conditions. Under typical field conditions, the values are estimated to be valid within ±50% with a greater likelihood of higher rather than lower values. For materials marked †, ignition levels are estimated to be valid within ±50% under laboratory conditions and within ±100% under field conditions.

**Data not available or appropriate scaling not known.

***Radiant exposures for ignition of these substances are highly dependent on the moisture content.

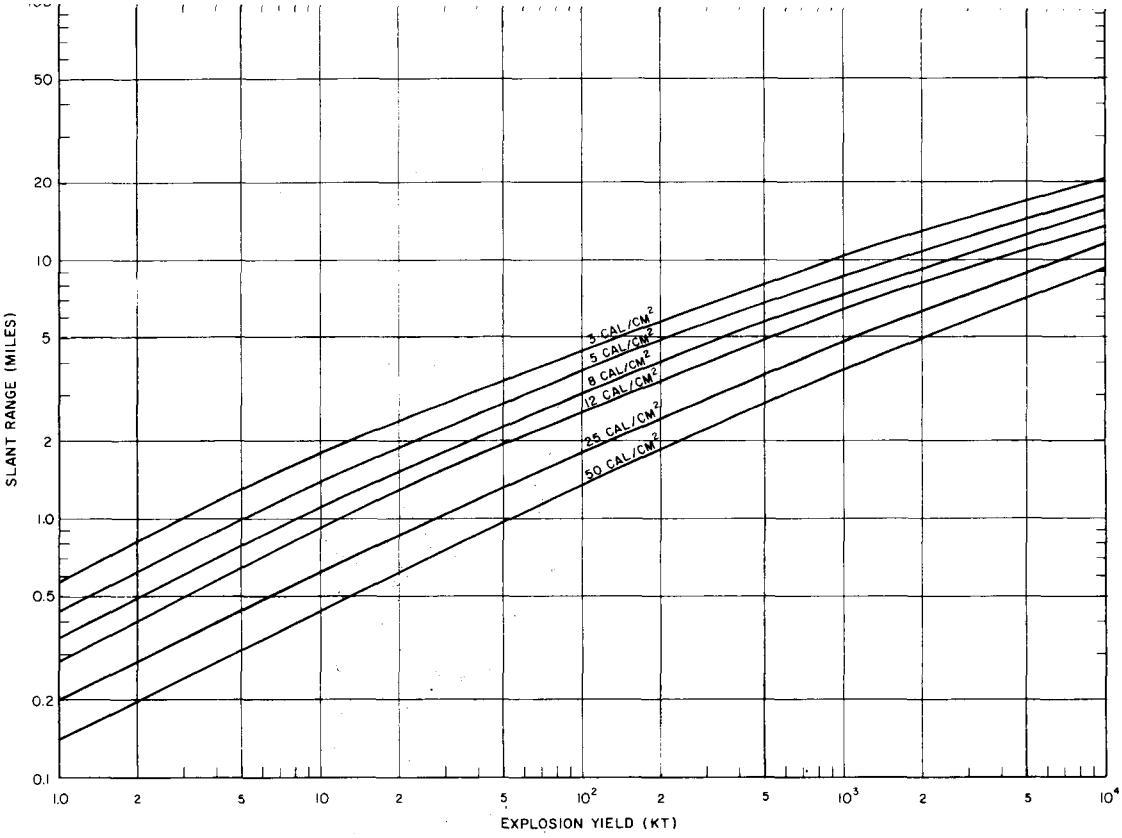

Figure 7.42. Slant ranges for specified radiant exposures on the ground as a function of energy yield of air bursts at altitudes up to 15,000 feet for a 12–mile visibility.

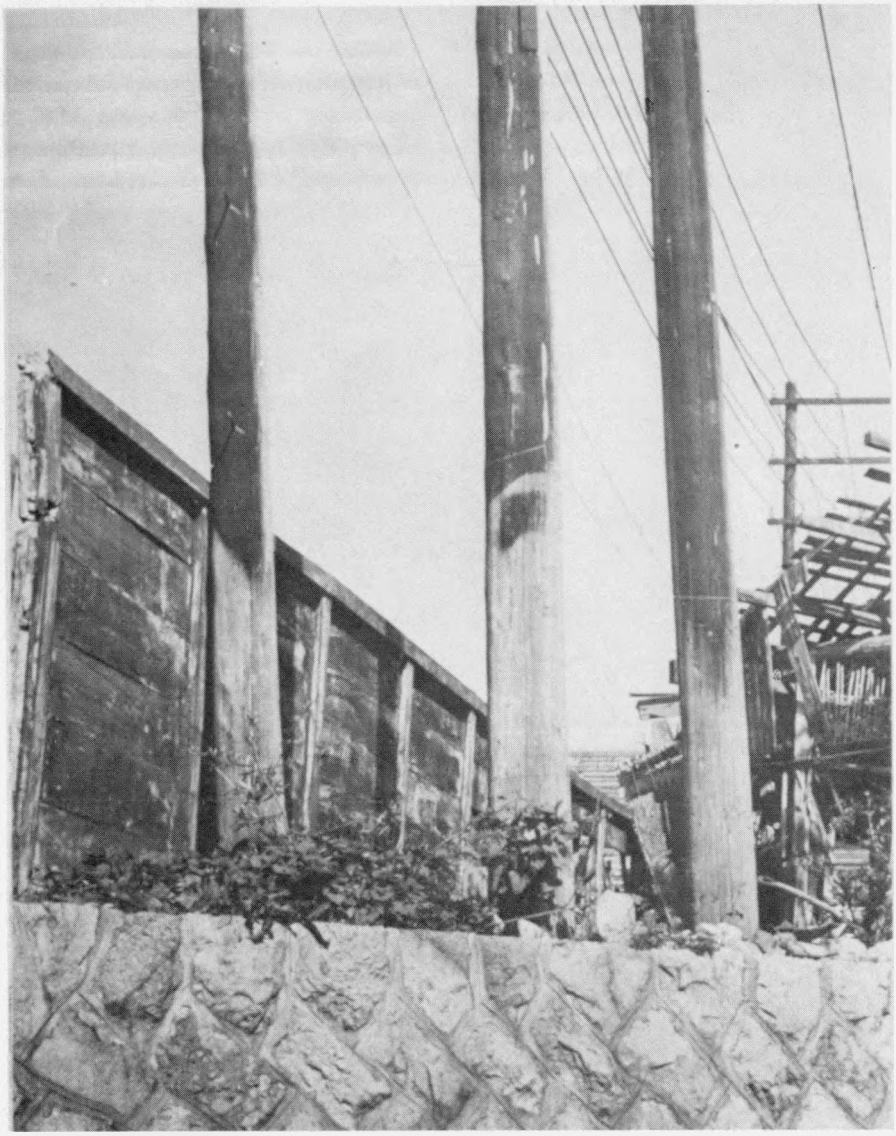

Figure 7.44b. Flash burns on wooden poles (1.17 miles from ground zero at Nagasaki, 5 to 6 cal/cm^2). The uncharred portions were protected from thermal radiation by a fence.

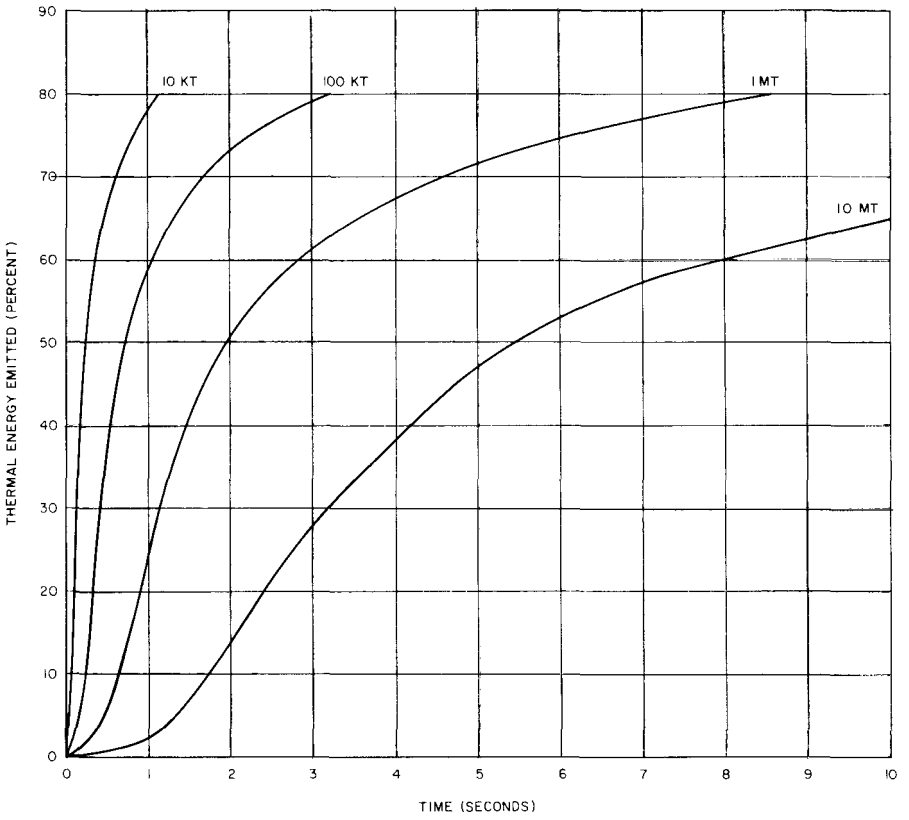

Figure 7.87. Percentage of thermal energy emitted as a function of time for air bursts of various yields.

THERMAL RADIATION IN HIGH-ALTITUDE EXPLOSIONS

7.89 The results described above are applicable to detonations at altitudes below about 100,000 feet (19 miles) where the density of the air is still appreciable. At higher altitudes, the fireball phenomena change, as described in Chapter II, and so also do the thermal pulse characteristics, such as shape and length, and the thermal partition. With increasing altitude, there is a tendency for the relative duration of the first pulse, i.e., up to the first temperature minimum (§§ 2.39, 2.125), to increase and for the minimum to be less marked. Up to an altitude of about 100,000 feet, these changes are small and so also are those in the second thermal pulse. The normalized plot (Fig. 7.84) is thus a satisfactory representation in this altitude range. However, between 100,000 and 130,000 feet (25 miles), the pulse shape changes drastically. The first minimum observed at lower altitudes disappears and essentially all the thermal radiation is emitted as a single pulse (§ 2.132). The thermal emission rises to a maximum in an extremely short time

and then declines steadily, at first rapidly and later more slowly. For an explosion in the megaton range at an altitude of 250,000 feet (about 47 miles), the duration of the thermal pulse is less than a second compared with a few seconds for a similar burst below 100,000 feet (cf. Fig. 7.87). Scaling of the pulse length with respect to the explosion yield at high altitudes is very complex and depends on a variety of factors. However, the duration of the thermal pulse is probably not strongly dependent on the total yield. At altitudes above roughly 270,000 feet (51 miles), the pulse length increases because of the larger mass and lower temperature of the radiating region (§ 7.91).

7.90 At high altitudes shock waves form much less readily in the thinner air and consequently the fireball is able to radiate thermal energy that would, at lower altitudes, have been transformed to hydrodynamic energy of the blast wave. Furthermore, the thinner air allows the primary thermal radiation (X rays) from the explosion to travel much farther than at lower levels. Some of this radiation travels so far from the source that it makes no contribution to the energy in the fireball. Between about 100,000 and 160,000 feet (30 miles), the first factor is dominant and the proportion of energy in the blast wave decreases; consequently, the thermal energy increases. In this altitude range the thermal partition, f, is about 0.6, compared with 0.40 to 0.45 at 100,000 feet (Table 7.88). Above 160,000 feet, however, the second factor, i.e., escape of thermal X rays, becomes increasingly important; the thermal partition decreases to about 0.25 at 200,000 feet (38 miles) and remains at this value up to roughly 260,000 feet (49 miles). At still higher altitudes there is a change in the fireball behavior (§ 2.135) and the thermal partition decreases very rapidly with increasing altitude of the explosion.

7.91 At heights of burst above about 270,000 feet, only the primary X rays traveling downward are absorbed and the energy deposition leads to the formation of the incandescent X-ray pancake described in Chapter II. This heated region then reradiates its energy at longer wavelengths over a period of several seconds. The altitude and dimensions of the pancake depend to some extent on the explosion yield but, as stated in § 2.134, reasonable average values are 30,000 feet for the thickness, 270,000 feet for the mean altitude, and the height of burst minus 270,000 feet for the radius at this altitude. The altitude and thickness of the reradiating region are essentially independent of the height of burst above 270,000 feet, but the mean radius increases with the burst height. The shape of the region thus approaches a thick disk (or frustum) centered at about 270,000 feet altitude.

7.92 Not more than one-fourth of the X-ray energy from the explosion is absorbed in the low-density air of the reradiating region, and only a small fraction, which decreases with increasing height of burst, is reradiated as secondary radiation. Consequently, only a few percent of the weapon energy is emitted as thermal radiation capable of causing damage at the earth's surface. In fact, for bursts at altitudes exceeding some 330,000 feet (63 miles), the thermal radiation from a nuclear explosion even in the megaton range is essentially ineffective so far as skin burns, ignition,

etc., are concerned. However, the early-time debris, which separates from the X-ray pancake (§ 2.135), is at a fairly high temperature and it emits a very short pulse of thermal energy that can cause eye injury to individuals looking directly at the explosion (§ 12.79 *et seq.*).

RADIANT EXPOSURE–DISTANCE RELATIONSHIPS

AIR BURSTS

7.93 The following procedure is used to calculate the dependence of the radiant exposure of a target (§ 7.35) upon its distance from an air burst of specified yield. As seen earlier in this chapter, such information, which is given in Fig. 7.42, combined with the data in Tables 7.35 and 7.40, permits estimates to be made of the probable ranges for various thermal radiation effects.

7.94 If there is no atmospheric attenuation, then at a distance D from the explosion the thermal radiation energy, E_{tot} may be regarded as being spread uniformly over the surface of a sphere of area $4\pi D^2$. If the radiating fireball is treated as a point source, the energy received per unit area of the sphere would be $E_{tot}/4\pi D^2$. If attenuation were due only to absorption in a uniform atmosphere, e.g., for an air burst, this quantity would be multiplied by the factor $e^{-\kappa D}$, where κ is an absorption coefficient averaged over the whole spectrum of wavelengths. Hence in these circumstances, using the symbol Q to represent the radiant exposure, i.e., the energy received per unit area normal to the direction of propagation, at a distance D from the explosion, it follows that

$$Q = \frac{E_{tot}}{4\pi D^2} e^{-\kappa D}. \qquad (7.94.1)$$

7.95 When scattering of the radiation occurs, in addition to absorption, the coefficient κ changes with distance and other variables. The simple exponential attenuation factor in equation (7.94.1) is then no longer adequate. A more useful (empirical) formulation is

$$Q = \frac{E_{tot}\tau}{4\pi D^2}, \qquad (7.95.1)$$

where the transmittance, τ, i.e., the fraction of the radiation (direct and scattered) which is transmitted, is a complex function of the visibility (scattering), absorption, and distance.[5]

7.96 Since $E_{tot} = fW$, equation (7.95.1) for the radiant exposure from an air burst of yield W can be expressed as

$$Q = \frac{fW\tau}{4\pi D^2}. \qquad (7.96.1)$$

[5] Scattered radiation does not cause permanent damage to the retina of the eye. Hence, to determine the effective radiant exposure in this connection equation (7.94.1) should be used; κ is about 0.03 km^{-1} for a visibility of 80 km (50 miles), 0.1 km^{-1} for 40 km (25 miles) and 0.2 km^{-1} for 20 km (12.4 miles). Scattered radiation can, however, contribute to flashblindness, resulting from the dazzling effect of bright light (§ 12.83).

By utilizing the fact that 1 kiloton of TNT is equivalent to 10^{12} calories, equation (7.96.1) for an air burst becomes

$$Q \text{ (cal/cm}^2) = \frac{10^{12} f W \tau}{4\pi D^2}, \qquad (7.96.2)$$

where D is in centimeters and W is in kilotons. If the distance, D, from the explosion to the target, i.e., the slant range, is expressed in kilofeet or miles, equation (7.96.2) reduces approximately to

$$D \text{ in kilofeet: } Q \text{ (cal/cm}^2) \approx \frac{85.6\, f W \tau}{D^2} \qquad (7.96.3)$$

$$D \text{ in miles: } Q \text{ (cal/cm}^2) \approx \frac{3.07\, f W \tau}{D^2}. \qquad (7.96.4)$$

7.97 In nuclear weapons tests, it is possible to measure Q and W, and since the distance D from the explosion is known the magnitude of the product $f\tau$ can be determined from the equations in § 7.96. Hence, to obtain f and τ individually, one of these two quantities must be determined independently of the other. The method used is to obtain f for different conditions from calculations checked by observations, as stated in § 7.88. The values of τ are then derived from measurements of $f\tau$ made at a large number of weapons tests.

7.98 The transmittance τ for any given atmospheric condition depends on the solid angle over which scattered radiation can reach a particular exposed object. For the present purpose it will be assumed that the target is such, e.g., an appreciable flat area, that scattered radiation is received from all directions above, in addition to the direct thermal radiation from the source. Transmittance data for these conditions are presented in Fig. 7.98 in terms of burst altitude and distance of a surface target from ground zero for a cloudless atmosphere with a visibility of 12 miles. Since actual visibilities in cities are often less, the values in Fig. 7.98 are conservative.

7.99 The transmittance values in Fig. 7.98 were used, in conjunction with equation (7.96.4) and the thermal partitions from Table 7.88, to obtain the data from which the curves in Fig. 7.42 were constructed. If H is the height of burst and d is the distance from ground zero of a given point on the surface, the corresponding slant range for use in equation (7.96.4) is $D = (d^2 + H^2)^{1/2}$. A height of burst of 200 $W^{0.4}$ feet, with W in kilotons, was used for the calculations, but the results in Fig. 7.42 are reasonably accurate for air bursts at any altitude up to some 15,000 feet.

7.100 Under unusual conditions and especially for cities at high-altitude locations, the visibility might be greater than at sea level and the transmittance would be larger than the values given in Fig. 7.98. The curves show that most attenuation of radiation occurs within a few thousand feet of the surface; thus, the much clearer air at higher altitudes has less effect. For bursts above about 150,000 feet (28 miles), the transmittance changes slowly with the altitude. Experimental data indicate that multiplying the transmittance by 1.5 corrects approximately for the effect of reflection from a cloud layer over the burst. The same correction may be made for a snow-covered ground surface. If the burst and target are both between a

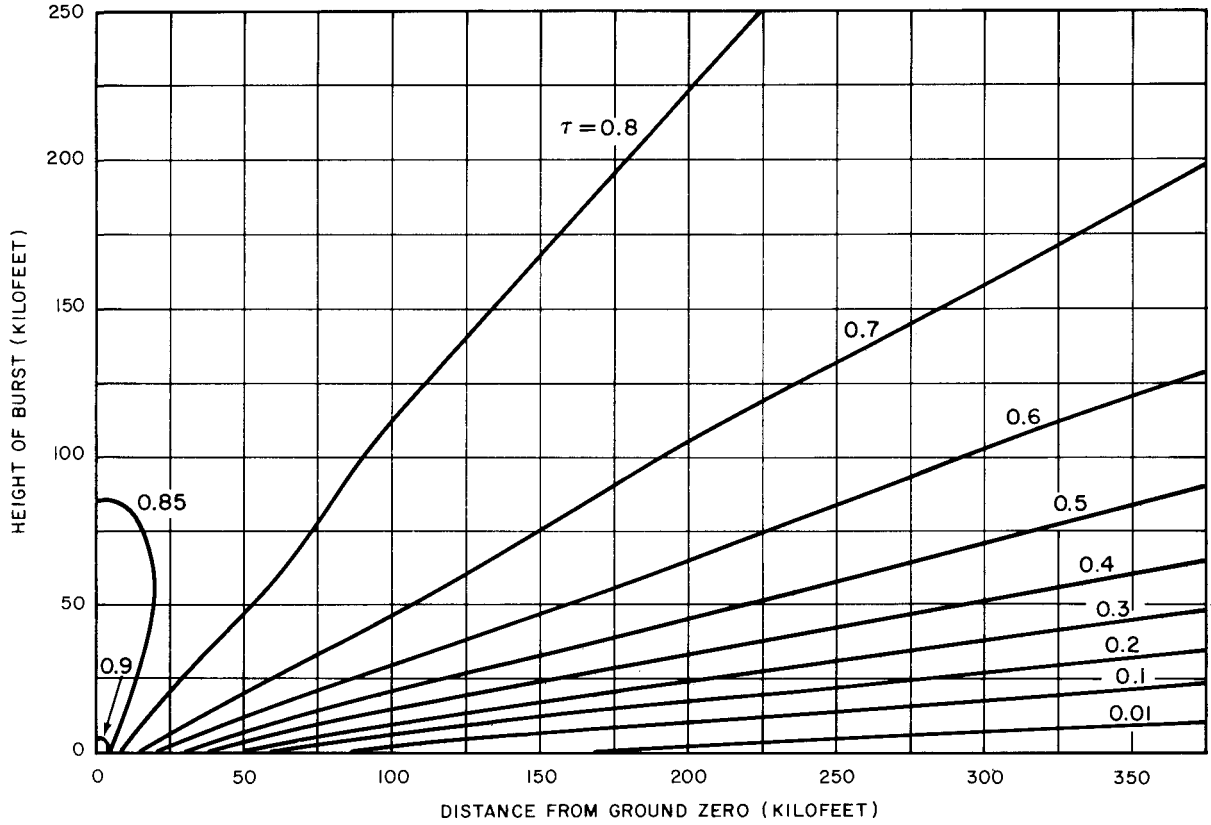

Figure 7.98. Transmittance, τ, to a target on the ground on a typical clear day (visibility = 12 miles).

cloud layer and a snow covered surface, the correction is $1.5 \times 1.5 = 2.25$.

SURFACE BURSTS

7.101 For a surface burst, the radiant exposures along the earth's surface will be less than for equal distances from an air burst of the same total yield. This difference arises partly, as indicated in § 7.20, from the decreased transmittance of the intervening low air layer due to dust and water vapor produced by the explosion. Furthermore, the normal atmosphere close to the earth's surface transmits less than at higher altitudes. In order to utilize the equations in § 7.96 to determine radiant exposure for surface bursts, the concept of an "effective thermal partition" is used, together with the normal transmittance, such as given in Fig. 7.98, for the existing atmospheric conditions. Based upon experimental data, contact surface bursts can be represented fairly well by an effective thermal partition of 0.18. Values of the thermal partition for other surface bursts are shown in Table 7.101; they have been derived by assigning a thermal partition of 0.18 to a contact surface burst and interpolating between that value and the air burst thermal partition values in Table 7.88.

VERY-HIGH-ALTITUDE BURSTS

7.102 In the calculation of the thermal radiation exposure at the surface of the earth from very-high-altitude nuclear explosions, two altitude regions must be considered because of the change in the fireball behavior that occurs at altitudes in the vicinity of about 270,000 feet (§ 7.91). At burst heights from roughly 160,000 to 200,000 feet (30 to 38 miles), the ther-

Table 7.101

EFFECTIVE THERMAL PARTITION FOR SURFACE BURSTS

Height of Burst (feet)	Thermal Partition — Total Yield (kilotons)				
	1	10	100	1,000	10,000
20	0.19	*	*	*	*
40	0.21	0.19	*	*	*
70	0.23	0.21	0.19	*	*
100	0.26	0.22	0.20	*	*
200	0.35	0.25	0.21	0.19	*
400	**	0.33	0.25	0.21	0.19
700	**	**	0.28	0.24	0.21
1,000	**	**	0.34	0.26	0.22
2,000	**	**	**	0.34	0.26
4,000	**	**	**	**	0.33
7,000	**	**	**	**	0.35

*These may be treated as contact surface bursts, with $f = 0.18$.
**Air bursts; for values of f see Table 7.88.

mal energy capable of causing damage at the surface of the earth drops sharply from about 60 percent to about 25 percent, i.e., from $f = 0.60$ to $f = 0.25$. As the height of burst is increased above 200,000 feet, the thermal partition remains about 0.25 up to a height of burst of approximately 260,000 feet (49 miles). Since a nearly spherical fireball forms within this latter altitude region, equation (7.93.3) becomes

$$Q \text{ (cal/cm}^2) = \frac{21.4\ W\tau}{D^2}, \quad (7.102.1)$$

where D is the slant range in kilofeet, and W is the yield in kilotons. A linear interpolation of the variation of thermal partition with burst altitude may be performed for bursts between 160,000 feet and 200,000 feet; however, in view of the uncertainties in high-altitude burst phenomenology, it may be desirable to use the high (0.60) or the low (0.25) value throughout this burst altitude region, depending on the degree of conservatism desired.

7.103 At burst altitudes of roughly 270,000 feet and above, the thermal radiation is emitted from the thick X-ray pancake at a mean altitude of about 270,000 feet, essentially independent of the actual height of burst (§ 7.91). In order to use the equations in § 7.96 to calculate radiant exposures at various distances from the burst, the approximation is made of replacing the disklike radiating region by an equivalent source point defined in the following manner. If the distance d from ground zero to the target position where Q is to be calculated is less than the height of burst, H, the source may be regarded as being located at the closest point on a circle with the median radius at an altitude of 270,000 feet; this is indicated by the point S in Fig. 7.103. Hence, for the target point X, the appropriate slant range is given approximately by

$$D \text{ (kilofeet)} \approx \{(270)^2 + [\tfrac{1}{2}(H - 270) - d]^2\}^{1/2}, \quad (7.103.1)$$

with d and H in kilofeet. This expression holds even when d is greater than $\frac{1}{2}(H - 270)$; although the quantity in the square brackets is then negative, the square is positive. The slant range, D_0, for ground zero is obtained by setting d in equation (7.103.1) equal to zero; thus,

$$D_0 \text{ (kilofeet)} \approx [(270)^2 + \tfrac{1}{2}(H - 270)^2]^{1/2}.$$

If the distance d is greater than the height of burst, the equivalent point source may be taken to be approximately at the center of the radiating disk at 270,00 feet altitude; then

$$D \text{ (kilofeet)} \approx [(270)^2 + d^2]^{1/2}.$$

7.104 For the heights of burst under consideration, it is assumed that the fraction 0.8 of the total yield is emitted as X-ray energy and that 0.25 of this energy is absorbed in the radiating disk region. Hence, $0.8 \times 0.25 = 0.2$ of the total yield is absorbed. For calculating the radiant exposure, the total yield W in the equations in § 7.96 is consequently replaced by $0.2W$. Furthermore, the equivalent of the thermal partition is called the "thermal efficiency," ε, defined as the effective fraction of the absorbed energy that is

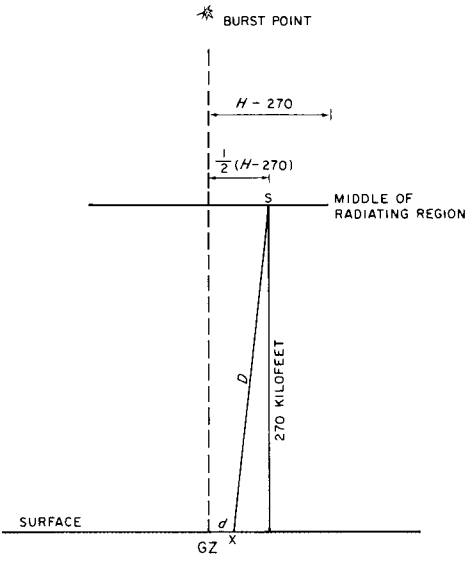

Figure 7.103. Equivalent point source at median radius when height of burst exceeds distance of the target, X, from ground zero.

reradiated. Hence equation (7.96.3), for example, becomes

$$Q \text{ (cal/cm}^2) = \frac{17.1\ \varepsilon\ W\tau}{D^2},$$

where D in kilofeet is determined in accordance with the conditions described in the preceding paragraph. The values of ε given in Fig. 7.104 as a function of height of burst and yield were obtained by theoretical calculations.[6] The transmittance may be estimated from Fig. 7.98 but no serious error would be involved by setting it equal to unity for the large burst heights involved.

7.105 With the information given above, it is possible to utilize the equations in § 7.96 to calculate the approximate radiant exposure, Q, for points on the earth's surface at a given distance, d, from ground zero, for a prescribed height of burst, H, for explosions of essentially all burst altitudes. If d and H are specified, the appropriate slant range can be determined. Tables 7.88 and 7.101 and Fig. 7.104 are used to obtain the required thermal partition or thermal efficiency, and the transmittance can be estimated from Fig. 7.98 for the known d and H. Suppose, however, it is required to reverse the calculations and to find the slant range to a surface target (or the corresponding distance from ground zero for a specified height of burst) at which a particular value of Q will be attained. The situation is then much more difficult because τ can be estimated only when the slant range or distance from ground zero is known. One approach would be to prepare figures like Fig. 7.42 for several heights of burst and to interpolate among them for any other burst height. Another possibility is to make use of an interation procedure by guessing a value of τ, e.g., $\tau = 1$, to determine a first approximation to D. With this value of D and the known height of burst, an improved estimate of τ can be obtained from Fig. 7.98. This is then utilized to derive a better approximation to D, and so on until convergence is attained.

[6] The calculations are actually for the fraction of the absorbed X-ray energy reradiated within 10 seconds; for estimating effects on the ground, the subsequent reradiation can be neglected.

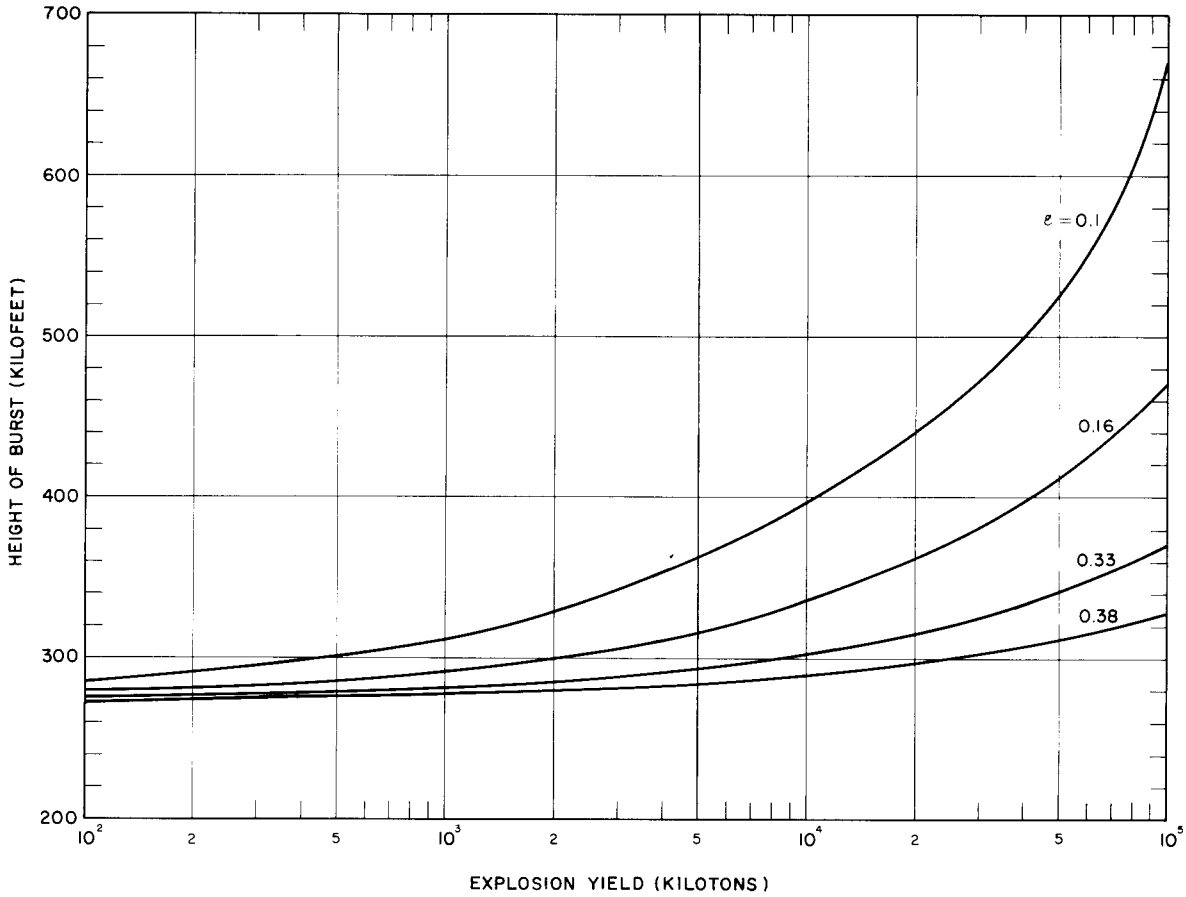

Figure 7.104 Fraction of absorbed X-ray energy reradiated from high-altitude bursts

BIBLIOGRAPHY

*BETHE, H. A., *et al.*, "Blast Wave," University of California, Los Alamos Scientific Laboratory, March 1958, LA–2000.

BRODE, H. L., "Review of Nuclear Weapons Effects," *Ann. Rev. Nuclear Sci.*, **18**, 153(1968).

CHANDLER, C. C., *et al.*, "Prediction of Fire Spread Following Nuclear Explosions," Pacific Southwest Forest and Range Experiment Station, Berkeley, California, 1963, U.S. Forest Service Paper PSW–5.

GIBBONS, M. G., "Transmissivity of the Atmosphere for Thermal Radiation from Nuclear Weapons," U.S. Naval Radiological Laboratory, August 1966, USNRDL–TR–1060.

GOODALE, T., "Effects of Air Blast on Urban Fires," URS Research Co., Burlingame, California, December 1970, OCD Work Unit 2534I.

**GUESS, A. W., and R. M. CHAPMAN, "Reflection of Point Source Radiation from a Lambert Plane onto a Plane Receiver," Air Force Cambridge Research Center, TR–57–253, Library of Congress, Washington, D.C., 1957.

**HARDY, J. D., "Studies on Thermal Radiation," Cornell University Medical College, PB 154–803, Library of Congress, Washington, D.C., 1952.

*LAUGHLIN, K. P., "Thermal Ignition and Response of Materials," Office of Civil Defense and Mobilization, 1957, WT–1198.

MARTIN, S. B., "The Role of Fire in Nuclear Warfare: An Interpretative Review of the Current Technology for Evaluating the Incendiary Consequences of the Strategic and Tactical Uses of Nuclear Weapons," URS Research Co., San Mateo, California, August 1974, DNA 2692F.

MIDDLETON, W. E., "Vision Through the Atmosphere," University of Toronto Press, 1958.

PASSELL, T. O., and R. I. MILLER, "Radiative Transfer from Nuclear Detonations Above 50–Km Altitude," *Fire Research Abstracts and Reviews*, **6**, 99 (1964), National Academy of Sciences—National Research Council.

*RANDALL, P. A., "Damage to Conventional and Special Types of Residences Exposed to Nuclear Effects," Office of Civil Defense and Mobilization, March 1961, WT–1194.

*VISHKANTA, R., "Heat Transfer in Thermal Radiation Absorbing and Scattering Material," Argonne National Laboratory, May 1960, ANL 6170.

WIERSMA, S. J., and S. B. MARTIN, "Evaluation of the Nuclear Fire Threat to Urban Areas," Stanford Research Institute, Menlo Park, California, September 1973, SRI PYU–8150.

*These documents may be purchased from the National Technical Information Service, Department of Commerce, Springfield, Virginia, 22161.

**These documents may be obtained from the Library of Congress, Washington, D.C. 20402.

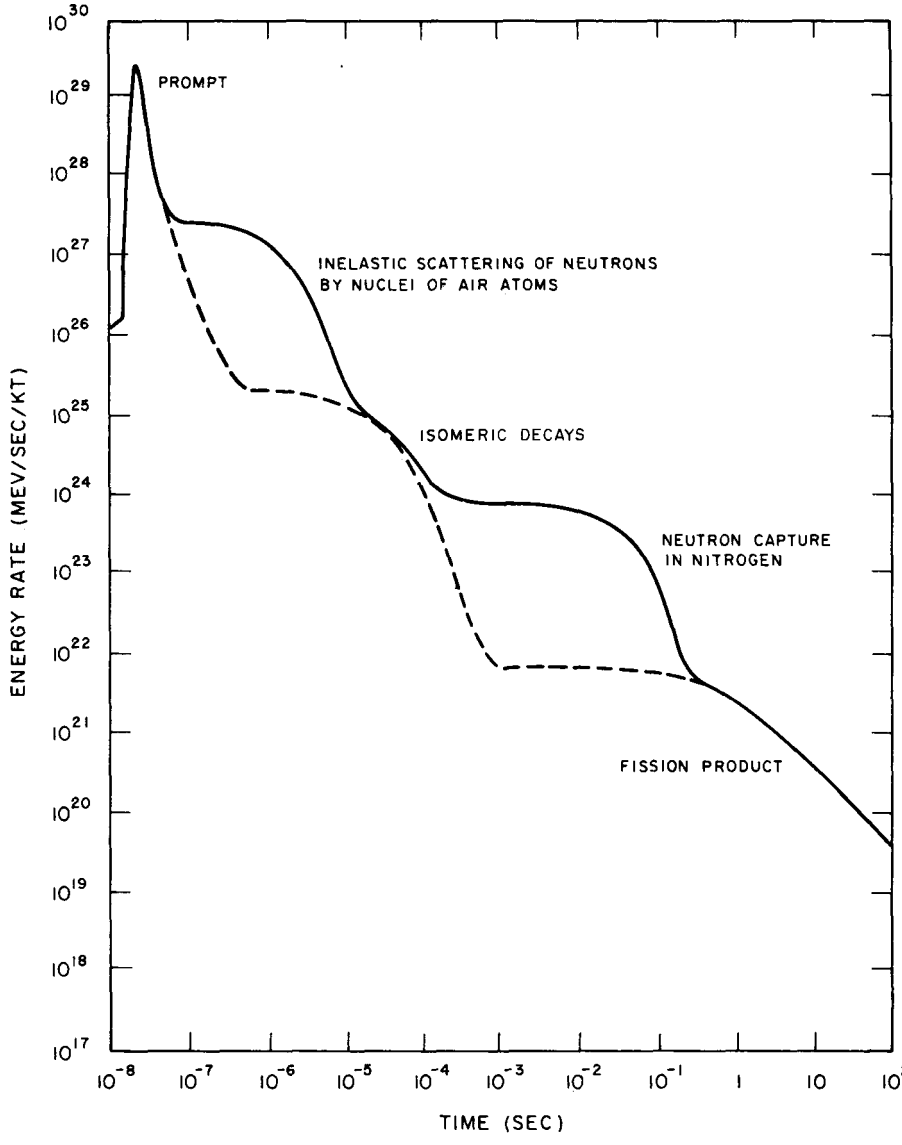

Figure 8.14. Calculated time dependence of the gamma-ray energy output per kiloton energy yield from a hypothetical nuclear explosion. The dashed line refers to an explosion at very high altitude.

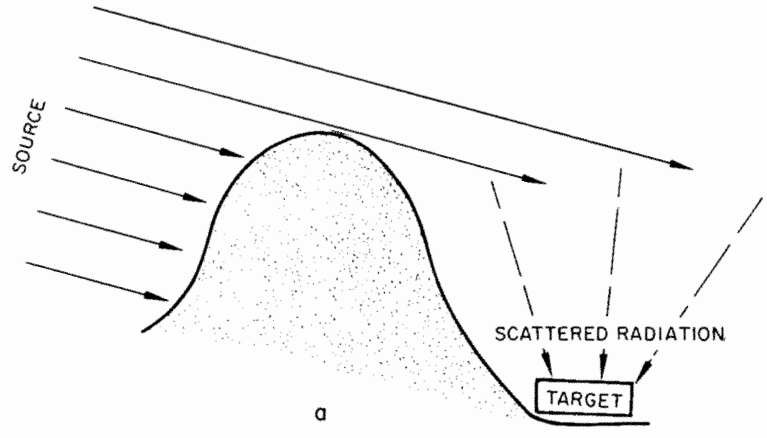

Figure 8.45a. Target exposed to scattered gamma radiation.

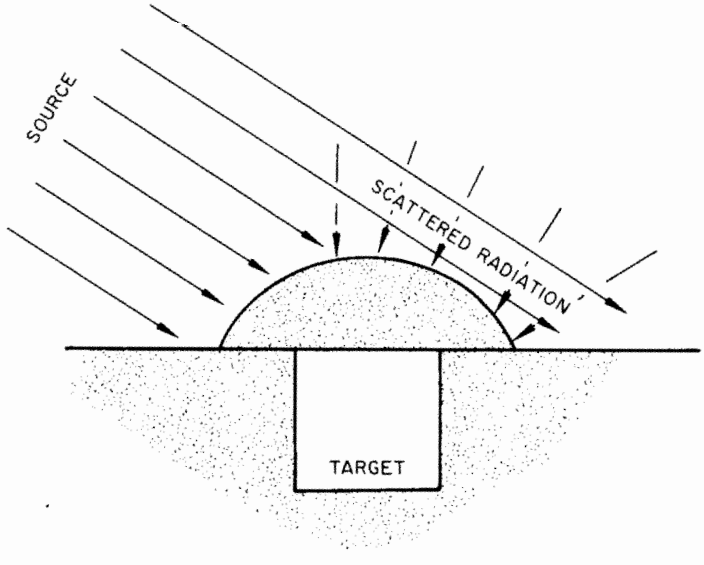

Figure 8.45b. Target shielded from scattered gamma radiation.

tors; the most significant are the energy yield of the explosion and the distance from the burst point. These two quantities affect the relative importance of the several components of the initial gamma radiation. The larger the yield and the greater the distance, the greater will be the hydrodynamic enhancement of the fission product gamma rays (§ 8.36). As this enhancement is increased, the relative importance of the fission product gamma rays is increased. Thus, for larger yields and greater distances, the fission product gamma rays, which are important at late times relative to the other components of the initial gamma radiation, provide a larger percentage of the total dose. The percentage of the total dose received up to various times for two different cases is shown in Fig. 8.47. One curve refers to a distance of 1,000 yards from a 20-kiloton air burst and the other to 2,500 yards from a 5-megaton explosion. It is seen that in the former case about 65 percent and in the latter case about 5 percent of the total initial gamma radiation dose is received during the first second after the detonation.

8.48 If some shelter could be obtained, e.g., by falling prone behind a substantial object, within a second of seeing the explosion flash, in certain circumstances it might make the difference between life and death. The curves in Fig. 8.47 show that avoidance of part of the initial gamma-ray dose would be more practicable for explosions of higher energy yields.

NEUTRONS

SOURCES OF NEUTRONS

8.49 Although neutrons are nuclear particles of appreciable mass, whereas gamma rays are electromagnetic waves (§ 8.17), their harmful effects on the body and their ability to damage certain materials are similar in character. Like gamma rays, only very large doses of neutrons may possibly be detected by the human senses. Neutrons can penetrate a considerable distance through the air and constitute a hazard that is greater than might be expected from the small fraction (about 1 percent) of the explosion energy which they carry.

8.50 Essentially all the neutrons accompanying a nuclear explosion are released either in the fission or fusion process (§§ 1.42, 1.69). All of the neutrons from the latter source and over 99 percent of the fission neutrons are produced almost immediately, within less than a millionth of a second of the initiation of the explosion. These are referred to as the "prompt" neutrons. In addition, somewhat less than 1 percent of the fission neutrons, called the "delayed" neutrons, are emitted subsequently. The majority of these delayed neutrons are released within the first minute, and so constitute part of the initial nuclear radiation. At distances greater than about 2,000 yards from a multimegaton explosion, the dose from delayed neutrons can exceed that from

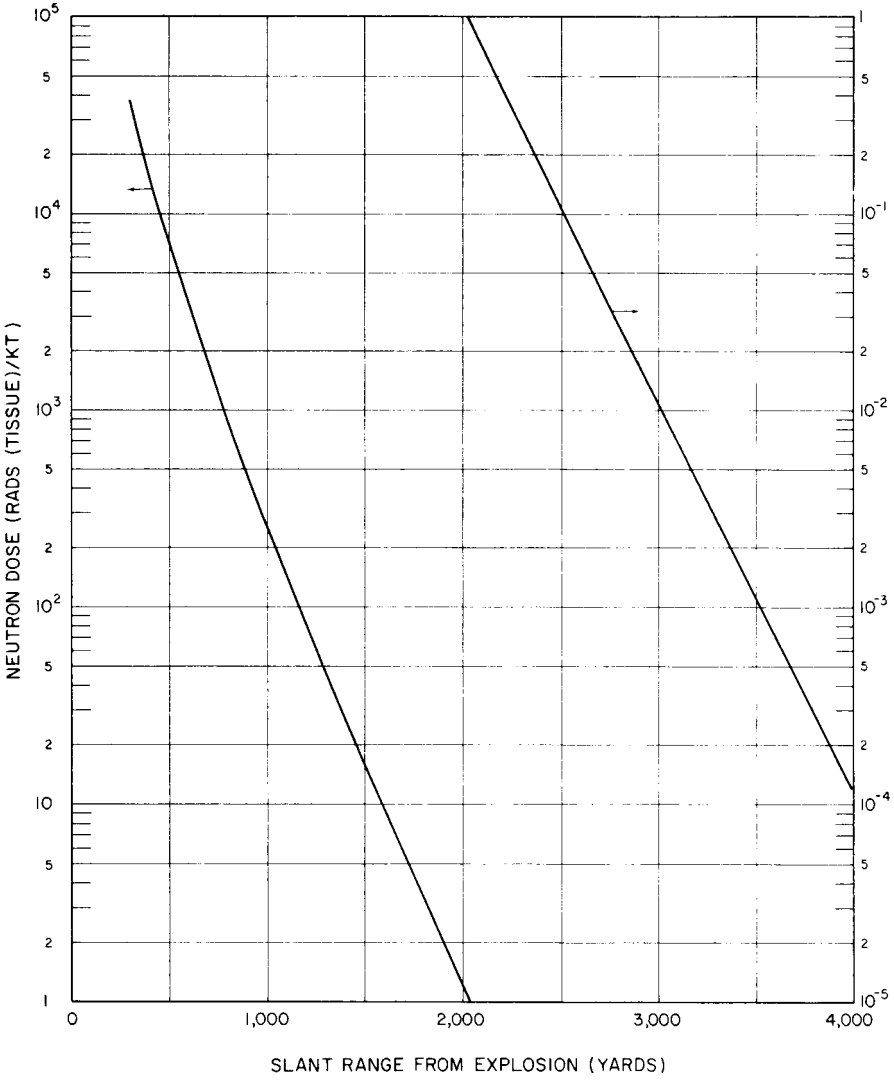

Figure 8.123b. Initial neutron dose per kiloton total yield as a function of slant range from thermonuclear weapon air bursts, based on 0.9 normal sea-level air density.

BIBLIOGRAPHY

ABBOTT, L. S., "Shielding Against Initial Radiations from Nuclear Explosions," Oak Ridge National Laboratory, July 1973, ORNL-RSIC-36.

*AUXIER, J. A., *et al.*, "Nuclear Weapons Free-Field Environment Recommended for Initial Radiation Shielding Calculations," Oak Ridge National Laboratory, February 1972, ORNL-TM-3396.

"Basic Radiation Protection Criteria," NCRP Report No. 39, National Council on Radiation Protection, Washington, D.C., 1971.

ETHERINGTON, H. (Ed.), "Nuclear Engineering Handbook," McGraw-Hill Book Co., Inc., 1958.

FRENCH, R. L., "A First-Last Collision Model of the Air/Ground Interface Effects on Fast-Neutron Distributions," *Nuclear Sci. and Eng.*, **19**, 151 (1964).

FRENCH, R. L., and L. G. MOONEY, "Initial Radiation Exposure from Nuclear Weapons," Radiation Research Associates, Fort Worth, Texas, July 1972, RRA-T7201.

*FRITZSCHE, A. E., N. E. LORIMIER, and Z. G. BURSON, "Measured Low-Altitude Neutron and Gamma Dose Distributions Due to a 14-MeV Neutron Source," E. G., and G., Inc., Las Vegas, Nevada, 1969, EGG 1183-1449.

*FRITZSCHE, A. E., N. E. LORIMIER, and Z. G. BURSON, "Measured High-Altitude Neutron and Gamma Dose Distributions Due to a 14-MeV Neutron Source," E. G., and G., Inc., Las Vegas, Nevada, 1969, EGG 1183-1438.

GWYN, C. W., D. L. SCHARFETTER, and J. L. WIRTH, "The Analysis of Radiation Effects in Semiconductor Junction Devices," Sandia Corporation, Albuquerque, New Mexico, July 1967, SC-R-67-1158.

JONES, T. D., and F. F. HAYWOOD, "Transmission of Photons Through Common Shielding Media," Oak Ridge National Laboratory, October 1974, ORNL-TM-4728.

*KEITH, J. R., and F. H. SHELTON, "Neutron Transport in Non-Uniform Air by Monte Carlo Calculations, Volume I," Kaman Nuclear, Colorado Springs, Colorado, January 1969, DASA 2236-I, KN-774-69-1.

*KUKHTEVICH, V. I., *et al.*, "Protection from Penetrating Radiation of Nuclear Explosions," English translation, Joint Publications Research Service, U.S. Department of Commerce, July 1971, JPRS 53498.

LARIN, F., "Radiation Effects in Semiconductor Devices," John Wiley and Sons, Inc., 1968.

MARSHALL, J. D., and M. B. WELLS, "The Effects of Cut-Off Energy on Monte Carlo Calculated Gamma-Ray Dose Rates in Air," Radiation Research Associates, Fort Worth, Texas, 1966, RRA-M67.

MOONEY, L. G., "Calculations of Weapon Radiation Doses in Single-Compartment Above-Ground Concrete Structures," Radiation Research Associates, Fort Worth, Texas, November 1969, RRA-M93.

National Bureau of Standards, "Measurement of Absorbed Dose of Neutrons and Mixtures of Neutrons and Gamma Rays," NCRP Report No. 25, U.S. Government Printing Office, 1961, National Bureau of Standards Handbook 75.

"Protection Against Neutron Radiation," NCRP Report No. 38, National Council on Radiation Protection, Washington, D. C., 1971.

"Radiation Damage and Defects in Semiconductors," Conference Series, No. 16, July 1972. The Institute of Physics (London), 1973.

"Recommended Techniques for the Measurement of Selected Nuclear Radiation Effects on Electronic Components," IBM Electronics Systems Center, Owego, New York, August 1967, DASA 627, Vol. II.

*SCHAEFER, N. M. (Editor), "Reactor Shielding for Nuclear Engineers," U.S. AEC Report TID-25951, 1973.

*STRAKER, E. A., "Time-Dependent Neutron and Secondary Gamma-Ray Transport in an Air-Over-Ground Geometry, Volume II. Tabulated Data," Oak Ridge National Laboratory, September 1968, ORNL 4289.

*STRAKER, E. A., "Status of Neutron Transport in the Atmosphere," Oak Ridge National Laboratory, July 1970, ORNL-TM-3065.

VOOK, F. L. (Editor), "Radiation Effects in Semiconductors," Proceedings of the Santa Fe Conference on Radiation Effects in Semiconductors, Plenum Press, 1968.

*These publications may be purchased from the National Technical Information Service, Department of Commerce, Springfield, Virginia, 22161.

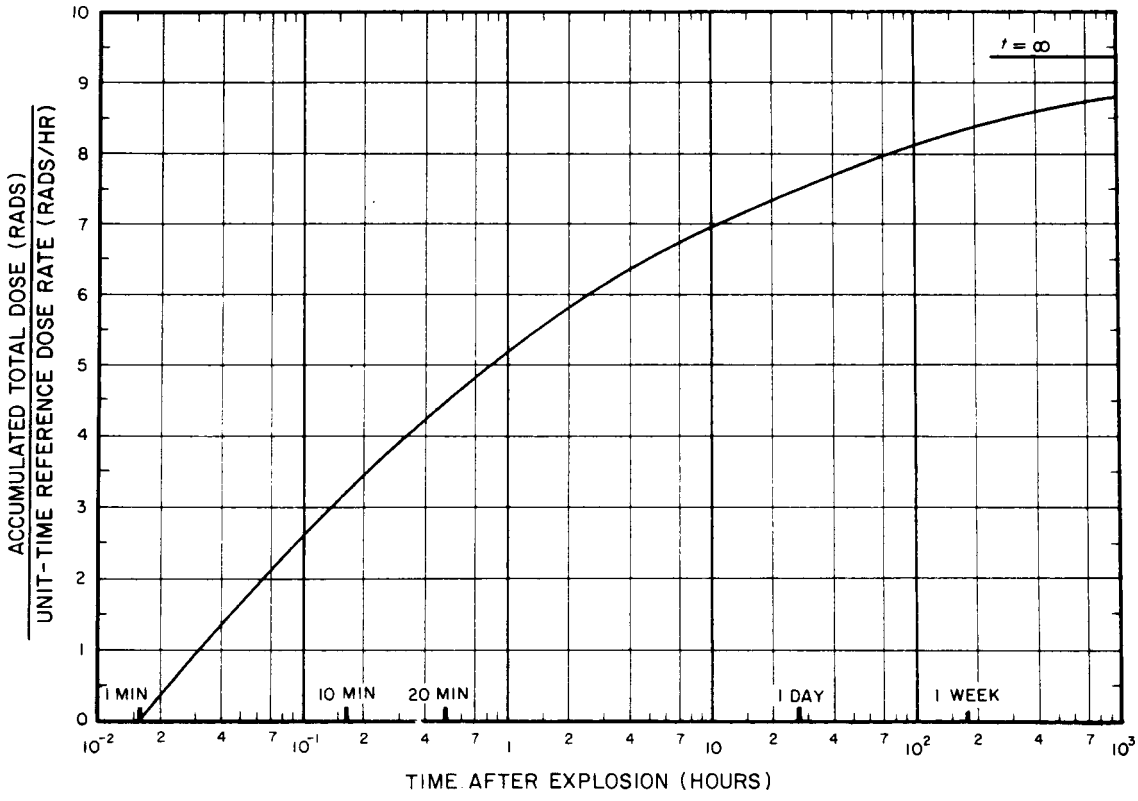

Figure 9.20. Curve for calculating accumulated total dose from early fallout at various times after explosion.

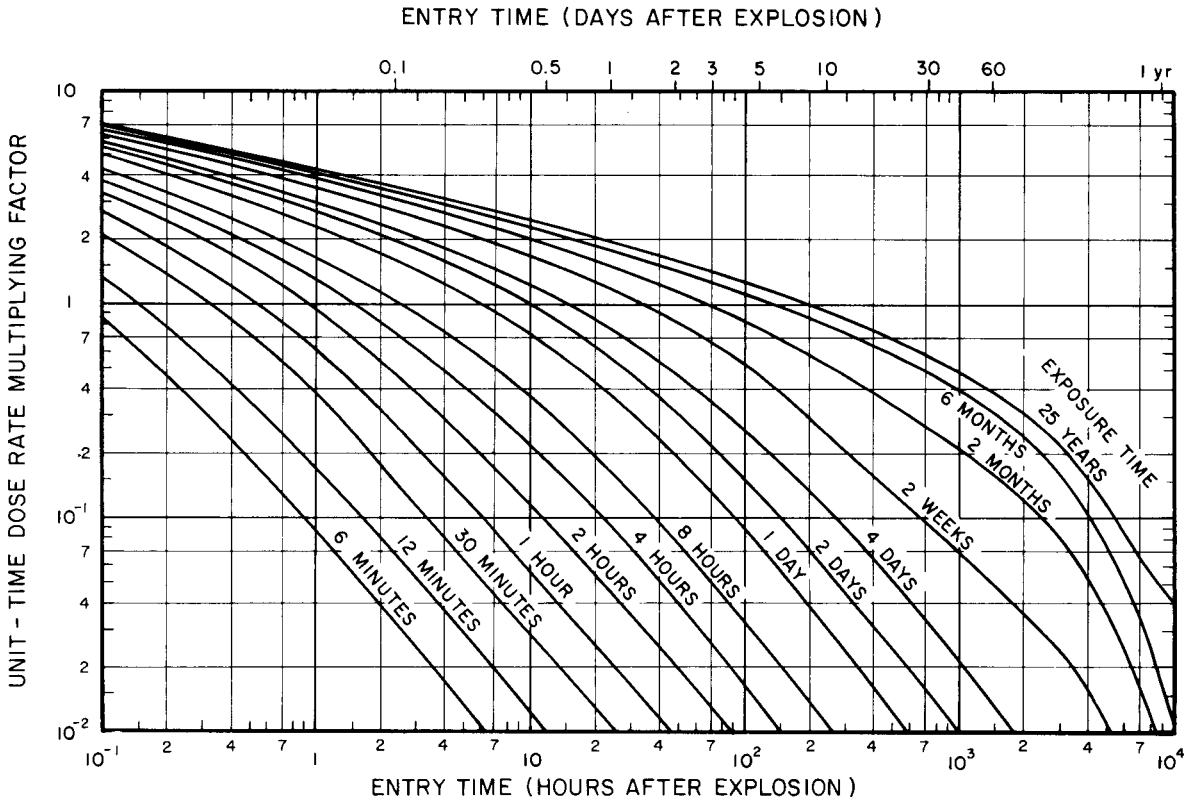

Figure 9.26. Curves for calculating accumulated radiation dose from early fallout based on unit-time reference dose rate.

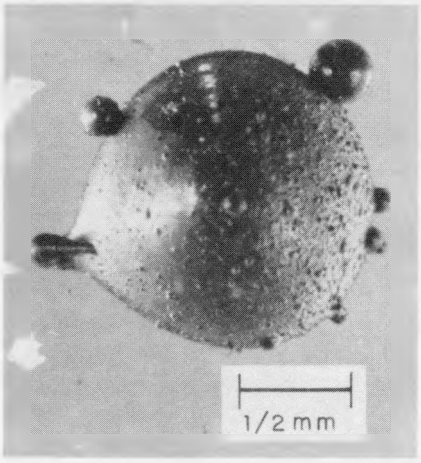

Figure 9.50a. A typical fallout particle from a tower shot in Nevada. The particle has a dull, metallic luster and shows numerous adhering small particles.

Figure 9.50b. A fallout particle from a tower shot in Nevada. The particle is spherical with a brilliant, glossy surface.

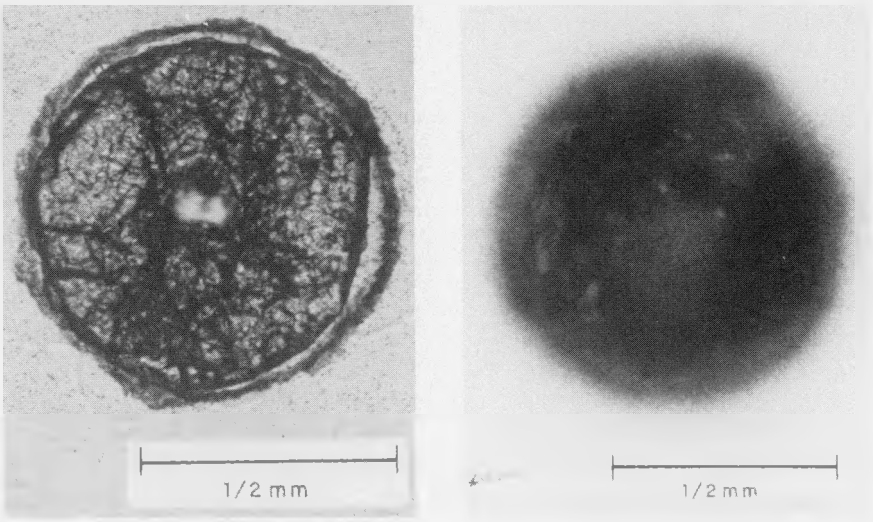

Figure 9.50c. Photograph (left) and autoradiograph (right) of a thin section of a spherical particle from a ground-surface shot at Eniwetok. The radioactivity is uniformly distributed throughout the particle.

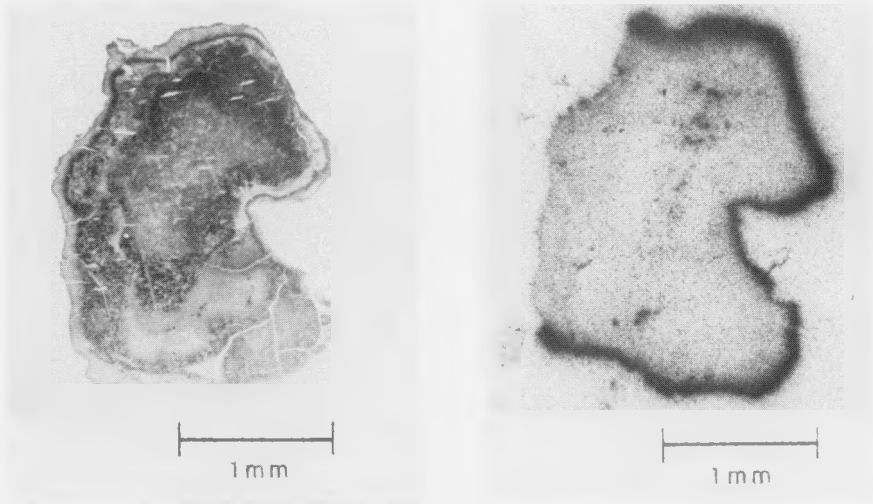

Figure 9.50d. Photograph (left) and autoradiograph (right) of a thin section of an irregular particle from a ground-surface shot at Bikini. The radioactivity is concentrated on the surface of the particle.

The base surge is influenced strongly by the wind, moving as an entity at the existing wind speed and direction. Initially, the base surge is highly radioactive, but as it expands and becomes diluted the concentration of fission products, etc., decreases. This dispersion, coupled with radioactive decay, results in comparatively low dose rates from the base surge by about 30 minutes after the burst (§ 2.77 *et seq.*).

9.55 The radioactivity in the water is initially present in a disk-like "pool," usually not more than 300 feet deep, near the ocean surface which is moved by the local currents. The pool gradually expands into a roughly annular form, but it reverts to an irregular disk shape at later times. Eventually, downward mixing and horizontal turbulent diffusion result in a rapid dilution of the radioactivity, thus reducing the hazard with time.

9.56 In the Bikini BAKER test (§ 2.63), the contaminated fallout (or rainout) consisted of both solid particles and a slurry of sea salt crystals in drops of water. This contamination was difficult to dislodge and had there been personnel on board the ships used in the test, they would have been subjected to considerable doses of radiation if the fallout were not removed immediately.[6] Since the BAKER shot was fired in shallow water, the bottom material may have helped in the scavenging of the radioactive cloud, thus adding to the contamination. It is expected that for shallow bursts in very deep water the fallout from the cloud will be less than observed at the test in Bikini lagoon.

9.57 An indication of the rate of spread of the active material and the decrease in the dose rate following a shallow underwater burst is provided by the data in Table 9.57, obtained after the Bikini BAKER test. Although the dose rate in the water was still fairly high after 4 hours, there would be considerable attenuation in the interior of a ship, so that during the time required to cross the contaminated area the total dose received would be small. Within 2 or 3 days after the BAKER test the radioactivity had spread over an area of about 50 square miles, but the radiation dose rate in the water was so low that the region could be traversed in safety.

Table 9.57

DIMENSIONS AND DOSE RATE IN CONTAMINATED WATER AFTER THE 20-KILOTON UNDERWATER EXPLOSION AT BIKINI

Time after explosion (hours)	Contaminated area (square miles)	Mean diameter (miles)	Maximum dose rate (rads/hr)
4	16.6	4.6	3.1
38	18.4	4.8	0.42
62	48.6	7.9	0.21
86	61.8	8.9	0.042
100	70.6	9.5	0.025
130	107	11.7	0.008
200	160	14.3	0.0004

[6]The technique of washdown of ships, by continuous flow of water over exposed surfaces to remove fallout as it settles, was developed as a result of the Bikini BAKER observations.

Table 9.74a

ESTIMATED RAINFALL DURATION FOR RAINOUT

Percent of Cloud Scavenged	Duration of Rainfall (hours)
25	0.07
50	0.16
75	0.32
90	0.53
99	1.1

Table 9.74b

ESTIMATED RAINFALL DURATION FOR WASHOUT

Percent of Cloud Scavenged	Duration of Rainfall (hours)		
	Light	Moderate	Heavy
25	8	1.6	0.8
50	19	3.8	1.9
75	38	7.7	3.6
90	64	13	6.4
99	128	26	13

FALLOUT PATTERNS

9.75 Information concerning fallout distribution has been obtained from observations made during nuclear weapons tests at the Nevada Test Site and the Eniwetok Proving Grounds.[7] However, there are many difficulties in the analysis and interpretation of the results, and in their use to predict the situation that might arise from a land surface burst over a large city. This is particularly the case for the megaton-range detonations at the Eniwetok Proving Grounds. Since the fallout descended over vast areas of the Pacific Ocean, the contamination pattern of a large area had to be inferred from a relatively few radiation dose measurements (§ 9.105). Furthermore, the presence of sea water affected the results, as will be seen below.

9.76 Nuclear tests in the atmosphere in Nevada have been confined to weapons having yields below 100 kilotons and most of the detonations were from the tops of steel towers 100 to 700

[7]The Eniwetok Proving Grounds, called the Pacific Proving Ground before 1955, included test sites on Bikini and Eniwetok Atolls and on Johnston and Christmas Islands in the Pacific Ocean.

feet high or from balloons at levels of 400 to 1,500 feet. None of these could be described as a true surface burst and, in any event, in the tower shots there is evidence that the fallout was affected by the tower. There have been a few surface bursts, but the energy yields were about 1 kiloton or less, so that they provided relatively little useful information concerning the effects to be expected from weapons of higher energy. Tests of fusion weapons with yields up to 15 megatons TNT equivalent have been made at the Pacific Ocean test sites. A very few were detonated on atoll islands, but most of the shots in the Bikini and Eniwetok Atolls in 1958 were fired on barges in the lagoons or on coral reefs. In all cases, however, considerable quantities of sea water were drawn into the radioactive cloud, so that the fallout was probably quite different from what would have been associated with a true land surface burst.

9.77 The irregular nature of the fallout distribution from two tests in Nevada is shown by the patterns in Figs. 9.77a and b; the contour lines are drawn through points having the indicated dose rates at 12 hours after the detonation time. Figure 9.77a refers to the BOLTZMANN shot (12 kilotons, 500-foot tower) of May 28, 1957 and Fig. 9.77b to the TURK shot (43 kilotons, 500-foot tower) of March 7, 1955. Because of the difference in wind conditions, the fallout patterns are quite different. Furthermore, attention should be drawn to the hot spot, some 60 miles NNW of the northern boundary of the Nevada Test Site, that was observed in connection with the BOLTZMANN test. This area was found to be seven times more radioactive than its immediate surroundings. The location was directly downwind of a mountain range and rain was reported in the general vicinity at the time the fallout occurred. Either or both of these factors may have been responsible for the increased radioactivity.

9.78 Measurement of fallout activity from megaton-yield weapons in the Pacific Ocean area has indicated the presence of marked irregularities in the overall pattern. Some of these may have been due to the difficulties involved in collecting and processing the limited data. Nevertheless, there is evidence to indicate that a hot spot some distance (50 to 75 miles) downwind of the burst point may be typical of the detonations at the Eniwetok Proving Grounds and, in fact, some fallout prediction methods have been designed to reproduce this feature. The occurrence of these hot spots may have been a consequence of the particular wind structure (§ 9.66). The times for most explosions at the Eniwetok Proving Grounds coincided with complex wind structures from the altitude of the stabilized cloud to the surface. The large directional changes in the wind served to contain the fallout more locally than if the wind were blowing in one direction.

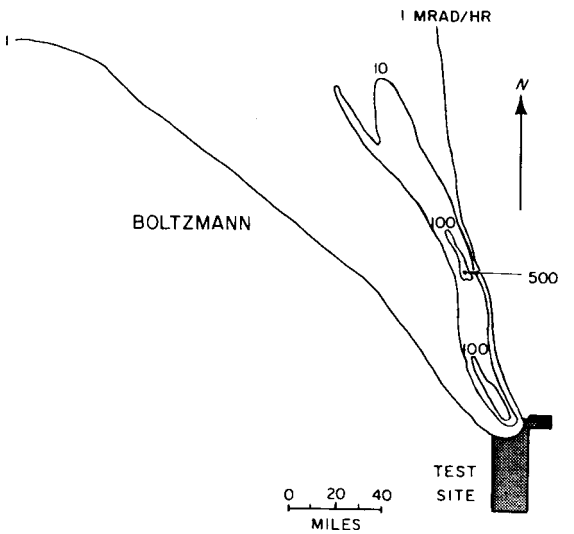

Figure 9.77a. Early fallout dose-rate contours from the BOLTZMANN shot at the Nevada Test Site.

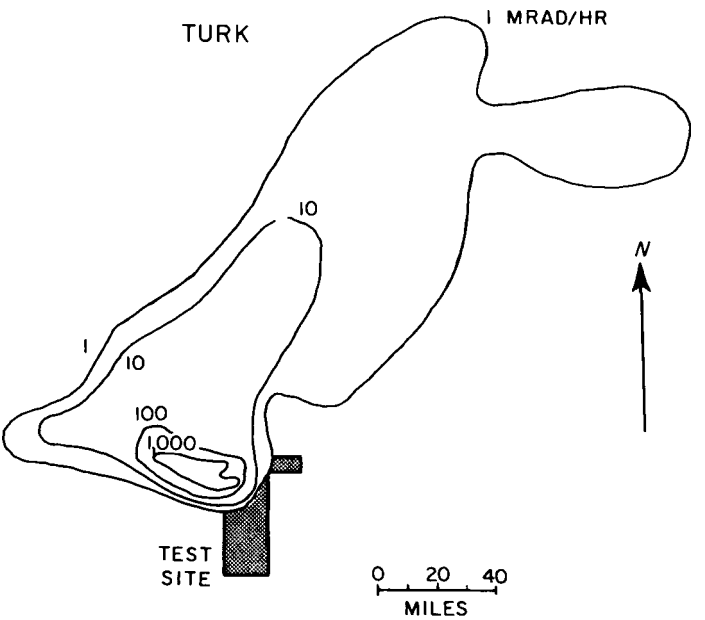

Figure 9.77b. Early fallout dose-rate contours from the TURK shot at Nevada Test Site.

FALLOUT PREDICTIONS FOR LAND SURFACE BURSTS

PREDICTION OF FALLOUT PATTERNS

9.79 Several methods, of varying degree of complexity, have been developed for predicting dose rates and integrated (total) doses resulting from fallout at various distances from ground (or surface) zero. These methods fall into four general categories; they are, in decreasing order of complexity, and hence detail, the mathematical fallout model, the analog method, the danger sector forecast, and the idealized fallout pattern. Each of these techniques requires, of course, a knowledge of the total and fission yields of the explosion, the burst height, and the wind structure to the top of the radioactive cloud in the vicinity of the burst. The more complex procedures require a forecast of the winds and weather in the locality over a period of several hours to a few days after the explosion. In making these forecasts, the considerable seasonable variations in wind patterns must be kept in mind.

9.80 In the fallout model method, an attempt is made to describe fallout mathematically and, with various inherent assumptions, to predict the dose-rate distribution contours resulting from a particular situation. The most reliable procedures are very complex and require use of a large digital computer in their application to a variety of circumstances. They are, consequently, employed primarily in theoretical studies of the fallout process, in making planning estimates, and in the preparation of templates for use with analog prediction methods. Apart from a few instances, less detailed mathematical models, which do not require digital computers, have been used to predict fallout distribution patterns during nuclear tests.

9.81 The analog technique, which is essentially a comparison process, utilizes a pattern chosen from a catalog of fallout contour patterns covering a wide range of yields and wind conditions. The choice is determined by the similarity between the yield and wind in the given situation and those in the catalog pattern. The catalog can consist of actual fallout patterns and others interpolated and extrapolated from these, or of patterns obtained by calculation from a mathematical fallout model.

9.82 The danger sector forecast requires a minimum of detailed information in order to give a qualitative picture of the general fallout area and an idea of the arrival times. Although it provides a rough indication of the relative degree of hazard, there is little or no information concerning the actual dose rates to be expected at various locations. The method yields a prediction quickly and simply and is probably as accurate as the explosion yield and meteorological information will justify in an operational (field) situation. The fourth prediction method, based on the use of idealized fallout distribution patterns, is described in some detail below. Such idealized patterns are derived from a detailed mathematical model, as described in § 9.80, based on average or most probable conditions.

IDEALIZED FALLOUT PATTERNS

9.83 Idealized fallout contour patterns have been developed which represent the average fallout field for a given yield and wind condition. No attempt is made to indicate irregularities which will undoubtedly occur in a real fallout pattern, because the conditions determining such irregularities are highly variable and uncertain. Nevertheless, in spite of their limitations, idealized patterns are useful for planning purposes, for example in estimating the overall effect of fallout from a large-scale nuclear attack. Although they will undoubtedly underestimate the fallout in some locations and overestimate it in others, the evaluation of the gross fallout problem over the whole area affected should not be greatly in error.

9.84 For a detailed fallout distribution prediction, the winds from the surface to all levels in the radioactive cloud must be considered. However, for the idealized patterns, the actual complex wind system is replaced by an approximately equivalent "effective wind." Various methods have been used to define the effective wind, i.e., speed and direction, for the generation of idealized patterns. The effective wind that is appropriate for use with the idealized patterns described below should be obtained by first determining the average wind from the ground to the base and to the top of the stabilized cloud (§ 2.15). The effective wind is then the mean of these two average winds.

9.85 By assuming little or no wind shear, that is, essentially no change in wind direction at different altitudes, the idealized fallout contour patterns have a regular cigar-like shape, as will be seen shortly. But if the wind direction changes with altitude, the fallout will spread over a wider angle, as in Fig. 9.77a, and the activity, i.e., the radiation dose rate, at a given distance from ground (or surface) zero will be decreased because the same amout of radioactive contamination will cover a larger area. Lower wind speeds will make the pattern shorter in the downwind direction because the particles will not travel so far before descending to earth; the activity at some distance from the burst point will be lower and the high dose rates immediately downwind of ground zero will be increased. If the wind speed is higher, the contaminated area will be greater, and the radioactivity will be higher at large distances from surface zero and lower immediately downwind of ground zero.

DEVELOPMENT OF FALLOUT PATTERN

9.86 Before showing an idealized fallout distribution pattern it is important to understand how such a pattern develops over a large area during a period of several hours following a surface burst. The situation will be illustrated by the diagrams in Figs. 9.86a and b, which apply to a 2-megaton explosion with 50 percent fission yield. The effective wind speed was taken as 15 miles per hour. Fig. 9.86a shows a number of contour lines for certain (arbitrary) round-number values of the dose rate, as would be observed on the ground, at 1, 6, and 18 hours, respectively, after the explosion. A series of total (or accumulated) dose contour lines for the same times are given in Fig. 9.86b. It will be understood, of course,

that the various dose rates and doses change gradually from one contour line to the next. Similarly, the last contour line shown does not represent the limit of the contamination, since the dose rate (and dose) will continue to fall off over a greater distance.

9.87 Consider, first, a location about 20 miles directly downwind from ground zero. At 1 hour after the detonation, the observed dose rate is seen to be roughly 3 rads/hr but it will rise rapidly and will reach a value over 500 rads/hr sometime between 1 and 2 hours. The dose rate will then decrease to about 200 rads/hr at 6 hours; at 18 hours it is down to roughly 50 rads/hr. The increase in dose rate after 1 hour means that at the specified location the fallout was not complete at that time. The subsequent decrease after about 2 hours is then due to the natural decay of the fission products. Turning to Fig. 9.86b, it is seen that the total radiation dose received at the given location by 1 hour after the explosion is small, because the fallout has only just started to arrive. By 6 hours, the total dose has reached more than 1,000 rads and by 18 hours a total dose of some 2,000 rads will have been accumulated. Subsequently, the total dose will continue to increase, toward the infinite time value, but at a slow rate (see Table 9.22).

9.88 Next, consider a point 100 miles downwind from ground zero. At 1 hour after the explosion the dose rate, as indicated in Fig. 9.86a, is zero, since the fallout will not have reached the specified location. At 6 hours, the dose rate is about 1 rad per hour and at 18 hours about 5 rads per hour. The fallout commences at somewhat more than 6 hours after the detonation and it is essentially complete at 9 hours, although this cannot be determined directly from the contours given. The total accumulated dose, from Fig. 9.86b, is seen to be zero at 1 hour after the explosion, less than 1 rad at 6 hours, and about 80 rads at 18 hours. The total (infinite time) dose will not be as great as at locations closer to ground zero, because the quantity of fission products reaching the ground decreases at increasing distances from the explosion.

9.89 In general, therefore, at any given location at a distance from a surface burst, some time will elapse between the explosion and the arrival of the fallout. This time will depend on the distance from ground zero and the effective wind velocity. When the fallout first arrives, the dose rate is small, but it increases as more and more fallout descends. After the fallout is complete, the radioactive decay of the fission products will cause the dose rate to decrease. Until the fallout commences, the accumulated dose will, of course, be small, but after its arrival the total accumulated radiation dose will increase continuously, at first rapidly and then somewhat more slowly, over a long period of time, extending for many months and even years.

9.90 The curves in Figs. 9.90a and b illustrate this behavior qualitatively; they show the variation with time of the dose rate and the accumulated dose from fallout at points near and far, respectively, in the downwind direction from a

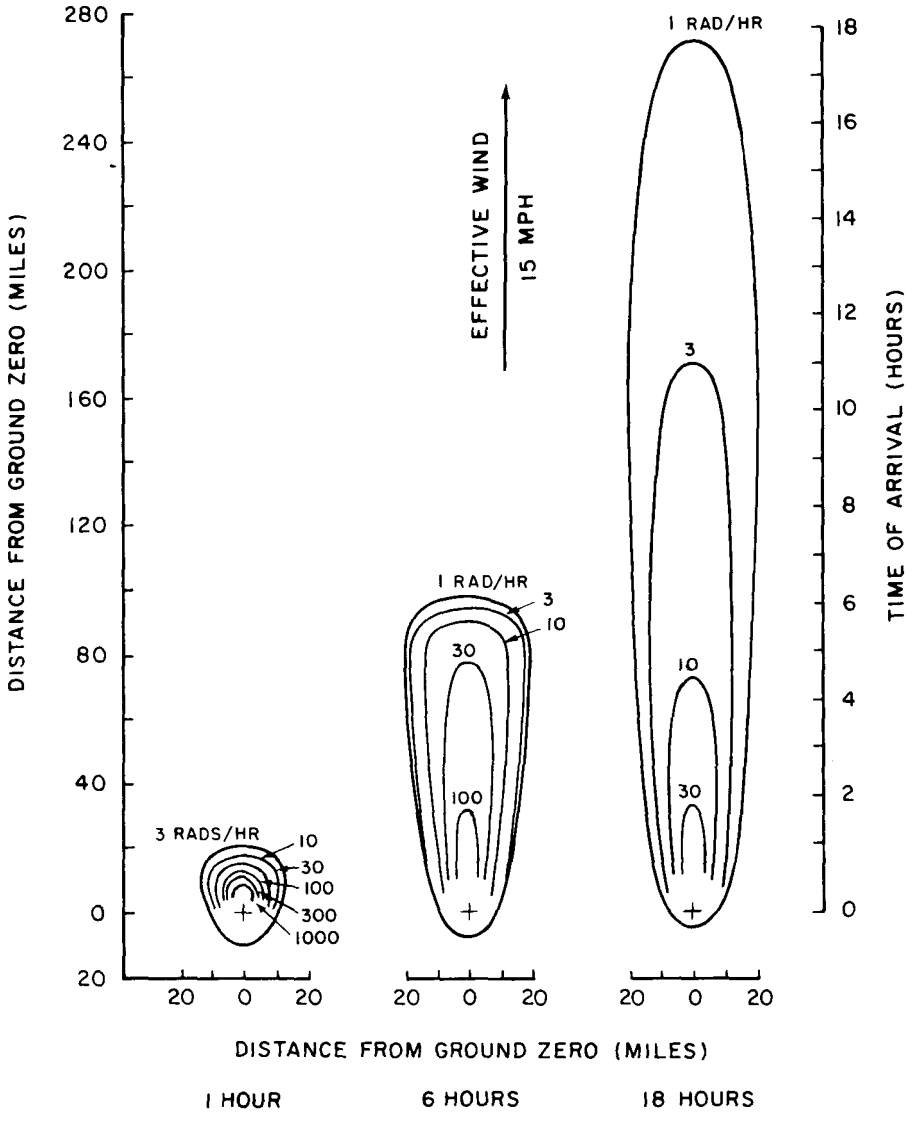

Figure 9.86a. Dose-rate contours from early fallout at 1, 6, and 18 hours after a surface burst with a total yield of 2 megatons and 1 megaton fission yield (15 mph effective wind speed).

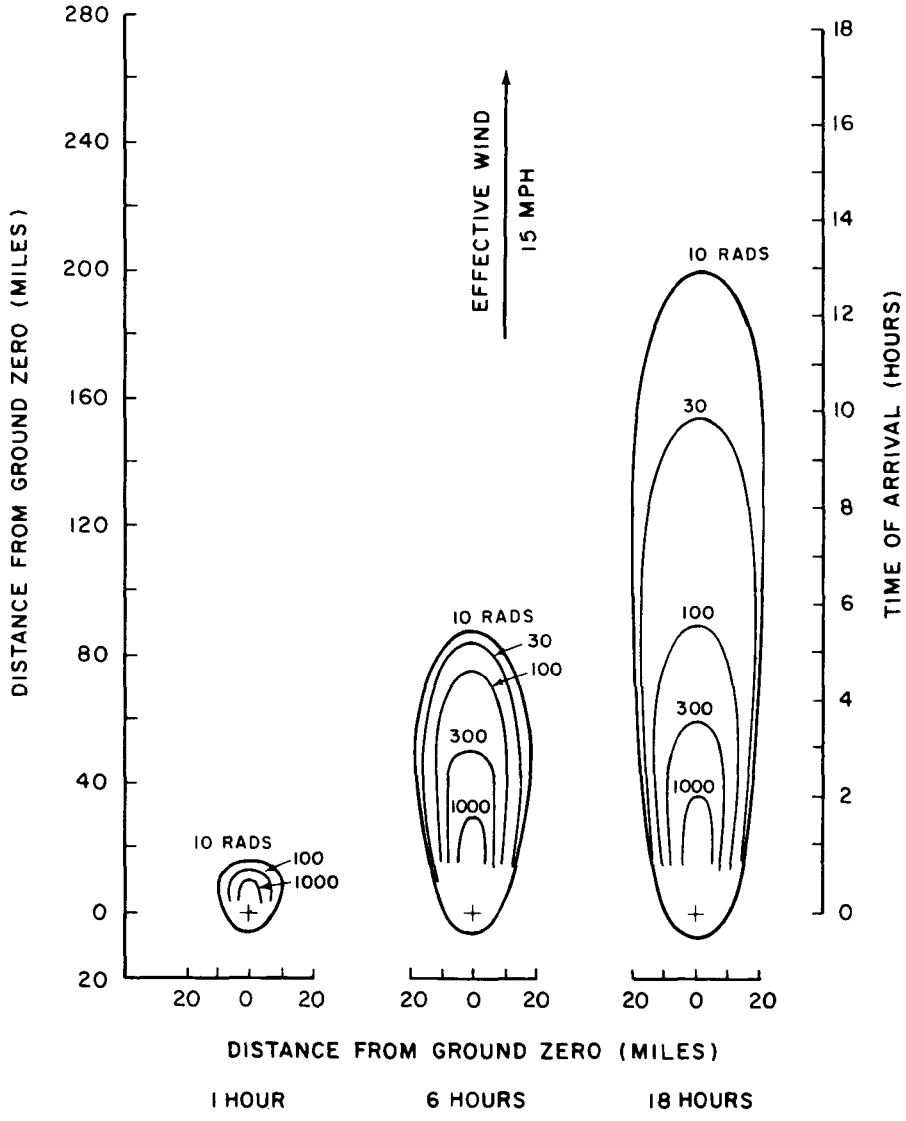

Figure 9.86b. Total-dose contours from early fallout at 1, 6, and 18 hours after a surface burst with a total yield of 2 megatons and 1-megaton fission yield (15 mph effective wind speed).

surface burst. Both the dose rate and the dose are zero until the fallout particles reach the given locations. At these times the dose rate commences to increase, reaches a maximum, and subsequently decreases, rapidly at first as the radioisotopes of short half-life decay, and then more slowly. The total accumulated dose increases continuously from the time of arrival of the fallout toward the limiting (infinite time) value.

9.91 Since the mushroom cloud grows rapidly in radius and reaches its stabilized altitude before the winds can act on it significantly, the time of arrival of the fallout at a particular location is measured by the distance from the portion of the cloud nearest to that location and the speed of the effective wind. The time of arrival is equal to the distance from ground zero to the point of interest minus the radius of the cloud, divided by the effective wind speed. For the present purpose the radius of the stabilized cloud as a function of yield may be obtained from Fig. 2.16. The radius is affected to some extent by the properties of the atmosphere, in particular by the height of the tropopause. The curve in Fig. 2.16 represents a reasonable average for mid-latitudes. The radius of the stabilized cloud is only important in calculating the time of arrival for locations relatively close to ground zero and for large-yield weapons. If the cloud radius is small in comparison with the distance from ground zero to the point of interest, e.g., for low yields or large distances, the cloud radius may be neglected in calculating fallout arrival times.

UNIT-TIME REFERENCE DOSE RATE

9.92 The representation of dose rate and accumulated dose curves, of the form of Figs. 9.86a and b, for all times following a nuclear detonation would obviously be a highly complicated matter. Fortunately, the situation can be simplified by utilizing an idealized fallout pattern in terms of the unit-time reference dose rate, mentioned in § 9.16 *et seq.* By means of the curves given earlier in the chapter (Figs. 9.16a and b and Fig. 9.20) it is then possible to estimate dose rates and total doses from fallout at any given time for a specified distance downwind from the burst point. The calculations are valid only if all the early fallout has descended at that time.

9.93 The general form of the idealized unit-time reference dose-rate contours for land surface bursts is shown in Fig. 9.93. The dimensions that define the various contours are indicated for the 1-rad per hour contour. In a real situation all contour lines would be closed in the upwind direction as shown for the 1-rad per hour contour. The scaling relationships, for calculating the downwind distance, the maximum width, the ground-zero width of the idealized unit-time dose-rate contours, for contact surface bursts (§ 2.127 footnote) of W kilotons yield are summarized in Table 9.93. The effective wind is 15 miles per hour in each case with wind shear of 15°. The upwind distance depends on the cloud radius; it is estimated to be approximately one-half the ground-zero width, i.e., the upwind contours may be represented roughly by semicircles centered at ground zero. The contour scaling relationships are dependent upon the nature of the surface; the values in Table 9.93 are applicable to most surface materials in the continental United States (cf. § 9.63).

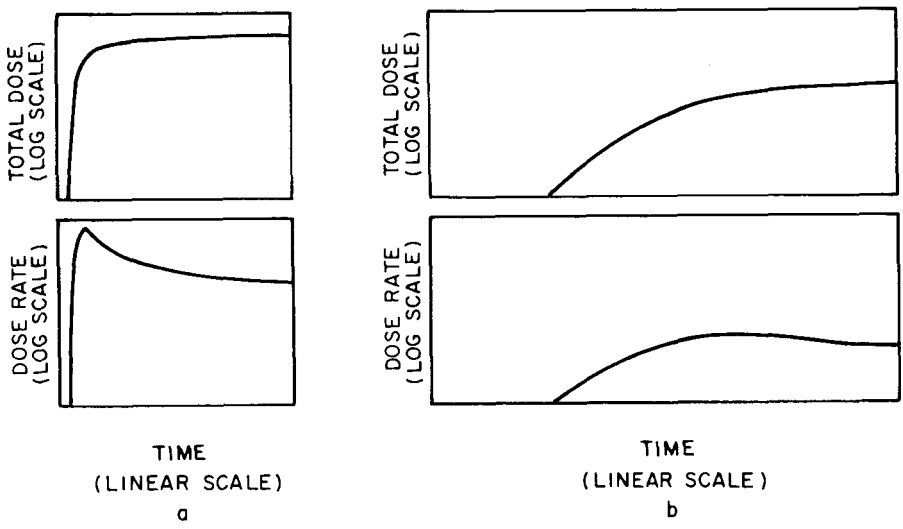

Figure 9.90a. Qualitative representation of dose rate and accumulated dose from fallout as a function of time after explosion at a point not far downwind from ground zero.

Figure 9.90b. Qualitative representation of dose rate and accumulated dose from fallout as a function of time after explosion at a point far downwind from ground zero.

9.94 Idealized contour shapes and sizes are a function of the total yield of the weapon, whereas the dose-rate contour values are determined by the fission yield. Thus, in order to obtain idealized fallout patterns for a weapon that does not derive all of its yield from fission, the dose-rate values of the contour lines for a weapon of the same total yield should be multiplied by the ratio of the fission yield to the total yield. For example, for a weapon having a total yield of W kilotons with 50 percent of the energy derived from fission, the contour dimensions are first determined from Table 9.93 for a yield of W kilotons. The unit-time reference dose rates are then multiplied by 0.5. Except for isolated points in the immediate vicinity of ground zero, observations indicate that unit-time reference dose rates greater than about 5,000 rads/hr are unlikely. In any event, the locations of such high reference values will be within the areas of complete devastation from other effects.

9.95 The idealized reference dose rates obtained by the methods described above apply to doses that would be received in the open over a completely smooth surface. Such surfaces provide a convenient reference for calculations, but they do not occur to any great extent in nature. Even the surface roughness in relatively level terrain will make the actual values smaller than the idealized values. A reduction (or terrain shielding) factor of about 0.7 is appropriate under such circumstances. A reduction factor of 0.5 to 0.6 would be more suitable for rough, hilly terrain. Any shelter would decrease the dose received from early fallout (§ 9.120).

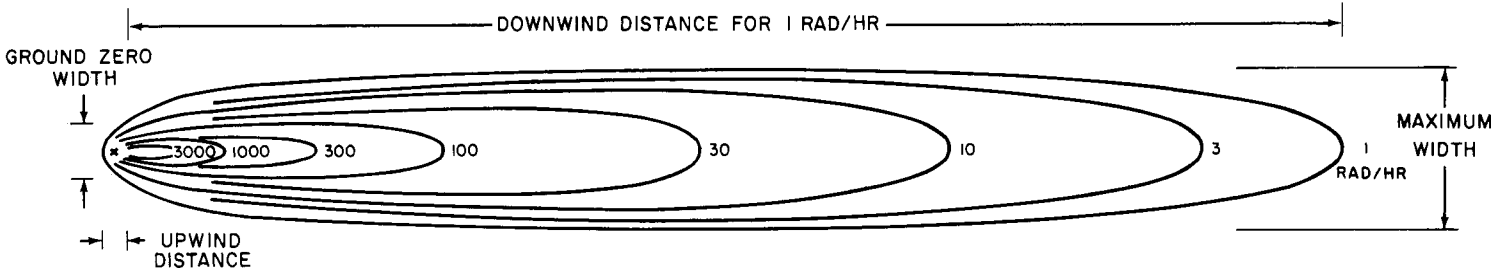

Figure 9.93. Illustration of idealized unit-time dose-rate pattern for early fallout from a surface burst. (The contour dimensions are indicated for a dose rate of 1 rad/hr.)

Table 9.93

SCALING RELATIONSHIPS FOR UNIT-TIME REFERENCE DOSE-RATE CONTOURS FOR A CONTACT SURFACE BURST WITH A YIELD OF W KILOTONS AND A 15 MPH WIND

Reference dose rate (rads/hr)	Downwind distance (statute miles)	Maximum width (statute miles)	Ground zero width (statute miles)
3,000	$0.95\ W^{0.45}$	$0.0076\ W^{0.86}$	$0.026\ W^{0.58}$
1,000	$1.8\ W^{0.45}$	$0.036\ W^{0.76}$	$0.060\ W^{0.57}$
300	$4.5\ W^{0.45}$	$0.13\ W^{0.66}$	$0.20\ W^{0.48}$
100	$8.9\ W^{0.45}$	$0.38\ W^{0.60}$	$0.39\ W^{0.42}$
30	$16\ W^{0.45}$	$0.76\ W^{0.56}$	$0.53\ W^{0.41}$
10	$24\ W^{0.45}$	$1.4\ W^{0.53}$	$0.68\ W^{0.41}$
3	$30\ W^{0.45}$	$2.2\ W^{0.50}$	$0.89\ W^{0.41}$
1	$40\ W^{0.45}$	$3.3\ W^{0.48}$	$1.5\ W^{0.41}$

SCALING FOR EFFECTIVE WIND

9.96 The effective wind speed and direction vary with the heights of the top and bottom of the stabilized cloud (§ 9.84). For a weapon of given yield, these heights will depend upon many factors, including the density and relative humidity of the atmosphere and the altitude of the tropopause. Nevertheless, within the accuracy of the idealized unit-time reference dose-rate contours, approximate values of the cloud heights may be used. The curves in Fig. 9.96 are based on the same model as was used in deriving the dose-rate contours and scaling relationships in § 9.93. They may be taken to be representative of the average altitudes to which nuclear clouds from surface (or low air) bursts of various yields might be expected to rise in the mid-latitudes, e.g., over the United States.

9.97 If there is no directional shear, then doubling the effective wind speed would cause the particles of a given size that originate at a particular location within the cloud to reach the ground at twice the distance from ground zero, so that they are spread over roughly twice the area. However, particles of many different sizes will arrive at any given point on the ground as a result of the different travel times from different points of origin in the large nuclear cloud. Consequently, simple scaling relationships for wind speed are not possible. Examination of test data and the results of calculations with computer codes suggest the following approximate scaling procedure: for effective wind speeds of v miles per hour, the downwind distances derived from Table 9.93 are multiplied by the factor F, where

$$F = 1 + \frac{v - 15}{60}$$

for effective wind speeds greater than 15 miles per hour, and

$$F = 1 + \frac{v - 15}{30}$$

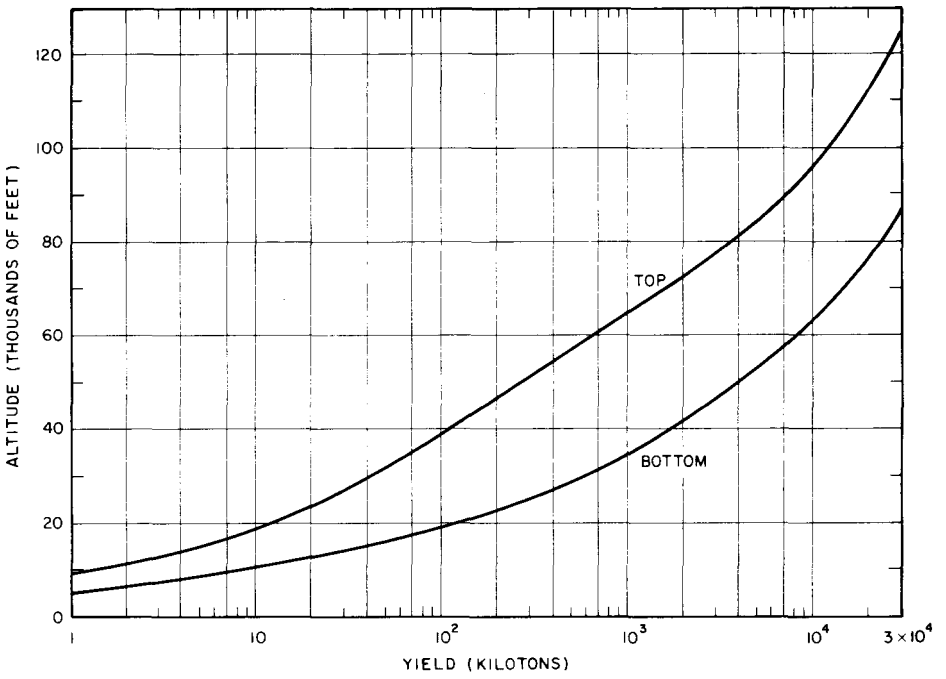

Figure 9.96. Altitudes of the stabilized cloud top and cloud bottom as a function of total energy yield for surface or low air bursts.

for wind speeds less than 15 miles per hour. These relations hold reasonably well for simple wind structures, i.e., for winds with very little directional shear, and for effective wind speeds between about 8 and 45 miles per hour. As defined in § 9.84, effective winds with speeds greater than 45 miles per hour are not common, and speeds less than 8 miles per hour generally result from large changes in directional wind shear with increasing altitude. The fallout patterns would then be too complex to be represented by idealized dose-rate contours.

9.98 As the downwind distance for a given unit-time reference dose-rate contour increases with increasing wind speed, the maximum width of that contour will decrease somewhat. Conversely, a decrease in downwind distance of a given contour with decreasing wind speed will be accompanied by an increase in maximum width of that contour. For an increase in wind speed, within the limits of the simple wind structures and wind speeds for which the idealized contours apply, the changes in maximum width of a given contour will be small, and wind scaling may be ig-

nored. This may also be done for the upwind distances and hence for the ground-zero widths. An increase in the wind speed will tend to decrease upwind distances by causing the particles to drift toward ground zero as they fall. At the lower 1-hour reference dose rates, e.g., 100 rads/hr or less, the upwind distances will in fact decrease with increasing wind speed. However, the larger particles, which are mainly responsible for the close-in high dose rates, descend very quickly and the high dose-rate contours will not be greatly affected by the wind speed. Consequently, since simple wind scaling is not possible and the upwind distances are relatively short, a conservative approach is to assume that wind speed has no effect on upwind distances (and ground-zero widths).

FALLOUT EXAMPLE

Given: A 10-megaton surface burst, 50-percent fission yield, with an effective wind speed of 30 miles per hour.

Find: The idealized unit-time reference dose rate, the fallout arrival time, and the dose accumulated by an exposed person during the first week following fallout arrival at points 100, 200, and 300 miles directly downwind from ground zero.

Solution: Preliminary estimates, based on Table 9.93, indicate that the idealized unit-time reference dose rates are in the range of 300 to 3,000 rads/hr. For a total yield of 10 MT, i.e., $W = 10^4$ KT, and an effective wind of 30 mph ($F = 1.25$ from § 9.97), the following downwind distances are obtained from Table 9.93.

Dose rate	3,000	1,000	300 rads/hr
Distance	75	142	355 miles.

Interpolation indicates that the unit-time reference dose rates are 1,800 rads/hr at 100 miles, 620 rads/hr at 200 miles, and 360 rads/hr at 300 miles. (The best method of interpolation is to plot the known points on logarithmic paper and to read the desired values from a smooth curve connecting the points.) The corresponding idealized reference dose rates for 50 percent fission yield would then be 900, 310, and 180 rads/hr at 100, 200, and 300 miles, respectively. *Answer.*

From Fig. 2.16, the cloud radius for a 10 MT explosion is about 21 miles; this should be subtracted from the distances from ground zero in order to determine the fallout arrival (or entry) times. For a 30-mph wind, these are (100–21)/30 = 2.6 hours at 100 miles, (200–21)/30 = 6 hours at 200 miles, and (300–21)/30 = 9.3 hours at 300 miles. *Answer*

Within the accuracy of the idealized unit-time dose-rate contours, the entry times for Fig. 9.26 may be rounded off

to 3, 6, and 10 hours, respectively. The multiplying factors for an exposure 1 week after arrival of the fallout are then found to be about 2.3 at 100 miles, 1.6 at 200 miles, and 1.4 at 300 miles. The approximate total accumulated doses at the required distances would then be as follows:

Distance (miles)	Dose (rads)
100	$900 \times 2.3 = 2{,}070$
200	$310 \times 1.6 = 496$
300	$180 \times 1.4 = 252$

Answer

These doses would be reduced by the appropriate surface roughness (or terrain shielding) factor (§ 9.95).

LIMITATIONS OF IDEALIZED CONTOURS

9.99 Both the idealized 15-mile per hour pattern dimensions and the wind scaling procedure tend to maximize the downwind extent of the dose-rate contours since they involve the postulate that there is little wind shear. This is not an unreasonable assumption for the continental United States, since the wind shear is generally small at altitudes of interest from the standpoint of fallout. If there is a greater wind shear, e.g., 20° or more between the top and bottom of the mushroom head, the fallout pattern would be wider and shorter than that based on Table 9.93. The actual unit-time reference dose rate at a specified downwind distance from ground zero for a given effective wind speed would then be smaller than predicted. The crosswind values at certain distances would, however, be increased. In some cases of extreme shear the pattern will extend from ground zero in two or more directions. In these cases, it is impossible to define a downwind direction, and idealized contours are of little value in describing the shape of the pattern (cf. Fig. 9.77b).

9.100 In order to emphasize the limitations of the idealized fallout patterns, Figs. 9.100a and b are presented here. The former shows the idealized unit-time reference dose-rate contours for a 10-megaton, 50-percent fission surface burst and an effective wind speed of 30 miles per hour. In Fig. 9.100b an attempt is made to indicate what the actual situation might be like as a result of variations in local meteorological and surface conditions. Near ground zero the wind is from the southwest but the mean wind gradually changes to a westerly and then a northwesterly direction over a distance of a few hundred miles. These changes in the mean wind are reflected in Fig. 9.100b, but, since the idealized pattern is based on a single effective wind, the changes in the mean wind do not affect Fig. 9.100a. The total contamination of the area is about the same in both cases, but the details of the distribution, e.g., the occurrence of hot spots, which are shown shaded in Fig. 9.100b, is quite

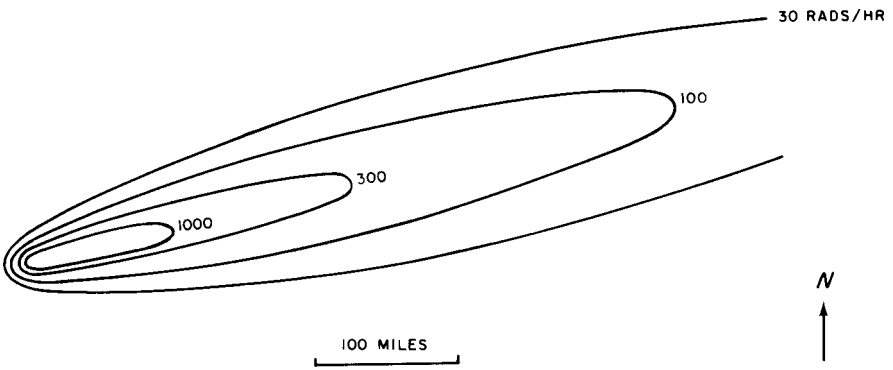

Figure 9.100a. Idealized unit-time reference dose-rate contours for a 10-megaton, 50-percent fission, surface burst (30 mph effective wind speed).

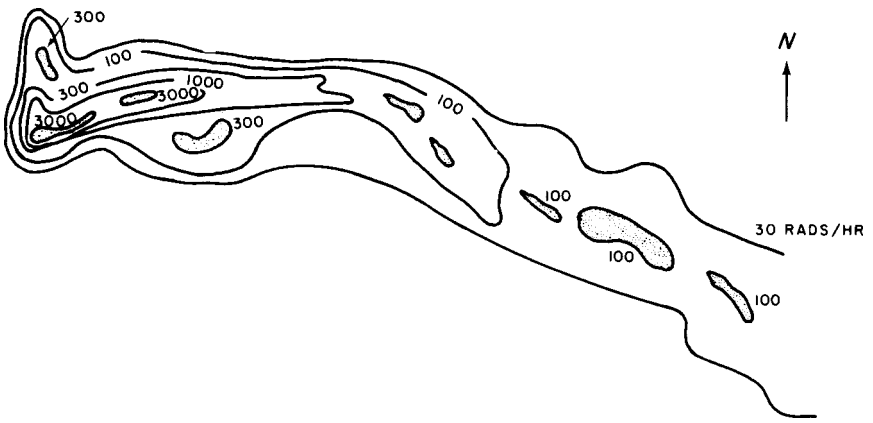

Figure 9.100b. Corresponding actual dose-rate contours (hypothetical).

different. The pattern in Fig. 9.100b is hypothetical and not based on actual observations; its purpose is to call attention to the defects of the idealized fallout pattern. But since the factors causing deviations from the ideal vary from place to place and even from day to day, it is impossible to know them in advance. Consequently, the best that can be done here is to give an idealized pattern and show how it may be used to provide an overall picture of the contamination while, at the same time, indicating that in an actual situation there may be marked differences in the details of the distribution.

FACTORS AFFECTING FALLOUT PATTERNS

9.101 It must be emphasized that the procedures described above for developing idealized fallout patterns are intended only for overall planning. There are several factors which will affect the details of the distribution of the early fallout and also the rate of decrease of the radioactivity. Near ground zero, activity induced by neutrons in the soil may be significant, apart from that due to the fallout. However, the extent of the induced activity is very variable and difficult to estimate (§ 9.49). The existence of unpredictable hot spots will also affect the local radiation intensity. Furthermore, precipitation scavenging will have an important effect on the fallout pattern (§ 9.67 *et seq.*). The data presented in the preceding paragraphs are applicable to very smooth surfaces of large size. As mentioned in § 9.95, even ground roughness in what would normally be considered flat countryside might reduce the dose rates to about 70 percent of those predicted for a smooth surface. In a city, buildings, trees, etc., will reduce the average intensity still further.

9.102 The rate of decay of the early fallout radioactivity, and hence the total dose accumulated over a period of time, will be affected by weathering. Wind may transfer the fallout from one location to another, thus causing local variations. Rain, after the fallout has descended, may wash the particles into the soil and this will tend to decrease the dose rate observed above the ground. The extent of the decrease will, of course, depend on the climatic and surface conditions. In temperate regions in the absence of rain, the weathering effect will probably be small during the first month after the explosion, but over a period of years the fallout dose rate would decrease to about half that which would otherwise be expected.

9.103 In attempting to predict the time that must elapse, after a nuclear explosion, for the radiation dose rate to decrease to a level that will permit reentry of a city or the resumption of agricultural operations, use may be made of the (continuous) decay curves in Figs. 9.16a and b or of equivalent data. It is inadvisable, however, to depend entirely on these estimates because of the uncertainties mentioned above. Moreover, even if the decay curve could be relied upon completely, which is by no means certain, the actual composition of the fallout is known to vary with distance from ground zero (§ 9.08) and the decay rate will vary accordingly. At 3 months after a nuclear explosion, the dose rate will have fallen to about 0.01 percent, i.e., one ten-thousandth part, of its value at 1 hour, so that almost any

contaminated area will be safe enough to enter for the purposes of taking a measurement with a dose-rate meter, provided there has been no additional contamination in the interim.

THE HIGH-YIELD EXPLOSION OF MARCH 1, 1954

9.104 The foregoing discussion of the distribution of the early fallout may be supplemented by a description of the observations made of the contamination of the Marshall Islands area following the high-yield test explosion (BRAVO) at Bikini Atoll on March 1, 1954. The total yield of this explosion was approximately 15-megatons TNT equivalent. The device was detonated about 7 feet above the surface of a coral reef and the resulting fallout, consisting of radioactive particles ranging from about one-thousandth to one-fiftieth of an inch in diameter, contaminated an elongated area extending over 330 (statute) miles downwind and varying in width up to over 60 miles. In addition, there was a severely contaminated region upwind extending some 20 miles from the point of detonation. A total area of over 7,000 square miles was contaminated to such an extent that avoidance of death or radiation injury would have depended upon evacuation of the area or taking protective measures.

9.105 The available data, for the estimated total doses accumulated at various locations by 96 hours after the BRAVO explosion, are shown by the points in Fig. 9.105. Through these points there have been drawn a series of contour lines which appear to be in moderately good agreement with the data. However, other patterns are possible; one, for example, ascribes the large radiation doses on the northern islands of Rongelap Atoll to a hot spot and brings the 3,000-rad contour line in much closer to Bikini Atoll. Because of the absence of observations from large areas of ocean, the choice of the fallout pattern, such as the one in Fig. 9.105, is largely a matter of guesswork. Nevertheless, one fact is certain: there was appreciable radioactive contamination at distances downwind of 300 miles or more from the explosion.

9.106 The doses to which the contours in Fig. 9.105 refer were calculated from instrument records. They represent the maximum possible exposures that would be received only by individuals who remained in the open, with no protection against the radiation, for the whole time. Any kind of shelter, e.g., within a building, or evacuation of the area would have reduced the dose received. On the other hand, persons remaining in the area for a period longer than 96 hours after the explosion would have received larger doses of the residual radiation.

9.107 A radiation dose of 700 rads over a period of 96 hours would probably prove fatal in the great majority of cases. It would appear, therefore, that following the test explosion of March 1, 1954, there was sufficient radioactivity from the fallout in a downwind belt about 170 miles long and up to 35 miles wide to have seriously threatened the lives of nearly all persons who remained in the area for at least 96 hours following the detonation without taking protective measures of any kind. At distances of 300 miles or more downwind, the number of deaths due to short-term radiation effects would have been negli-

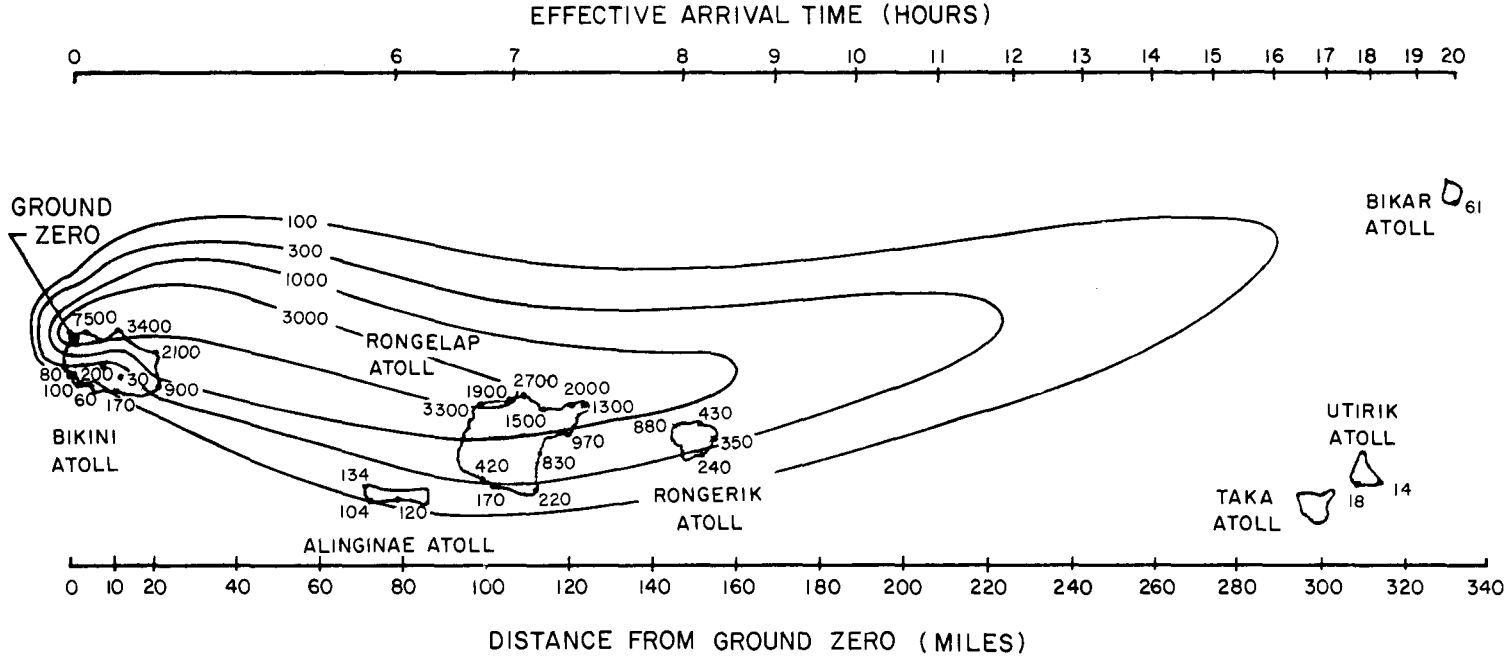

Figure 9.105. Estimated total (accumulated) dose contours in rads at 96 hours after the BRAVO test explosion.

gible, although there would probably have been many cases of sickness resulting in temporary incapacity.

9.108 The period of 96 hours after the explosion, for which Fig. 9.105 gives the accumulated radiation doses, was chosen somewhat arbitrarily. It should be understood, however, as has been frequently stated earlier in this chapter, that the radiations from the fallout will continue to be emitted for a long time, although at a gradually decreasing rate. The persistence of the external gamma radiation may be illustrated in connection with the BRAVO test by considering the situation at two different locations in Rongelap Atoll. Fallout began about 4 to 6 hours after the explosion and continued for several hours at both places.

9.109 The northwestern tip of the atoll, 100 miles from the point of detonation, received 3,300 rads during the first 96 hours after the fallout started. This was the heaviest fallout recorded at the same distance from the explosion and may possibly have represented a hot spot, as mentioned above. About 25 miles south, and 115 miles from ground zero, the dose over the same period was only 220 rads. The inhabitants of Rongelap Atoll were in this area, and were exposed to radiation dosages up to 175 rads before they were evacuated some 44 hours after the fallout began (§§ 12.124, 12.156). The maximum theoretical exposures in these two areas of the atoll for various time intervals after the explosion, calculated from the decay curves given earlier in this chapter, are recorded in Table 9.109.

9.110 It must be emphasized that the calculated values in Table 9.109 represent the maximum doses at the given locations, since they are based on the assumption that exposed persons remain out-of-doors for 24 hours each day and that no measures are taken to remove radioactive contamination. Furthermore, no allowance is made for weathering or the possible dispersal of the particles by winds. For example, the dose rates measured on parts of the Marshall Islands on the 25th day following the explosion were found to be about 40 percent of the expected values. Rains were known to have occurred during the second week, and these were probably responsible for the major decrease in the contamination.

Table 9.109

CALCULATED RADIATION DOSES AT TWO LOCATIONS IN RONGELAP ATOLL FROM FALLOUT FOLLOWING THE MARCH 1, 1954 TEST AT BIKINI

Exposure period after the explosion	Accumulated dose in this period (rads)	
	Inhabited location	Uninhabited location
First 96 hours	220	3,300
96 hours to 1 week	35	530
1 week to 1 month	75	1,080
1 month to 1 year	75	1,100
Total to 1 year	405	6,010
1 year to infinity	About 8	About 115

9.111 In concluding this section, it may be noted that the 96-hour dose contours shown in Fig. 9.105, representing the fallout pattern in the vicinity of Bikini Atoll after the high-yield explosion of March 1, 1954, as well as the idealized unit-time reference dose-rate contours from Table 9.93, can be regarded as more-or-less typical, so that they may be used for planning purposes. Nevertheless, it should be realized that they cannot be taken as an absolute guide. The particular situation which developed in the Marshall Islands was the result of a combination of circumstances involving the energy yield of the explosion, the very low burst height (§ 9.104), the nature of the surface below the point of burst, the wind system over a large area and to a great height, and other meteorological conditions. A change in any one of these factors could have affected considerably the details of the fallout pattern.

9.112 In other words, it should be understood that the fallout situation described above is one that can happen, but is not necessarily one that will happen, following the surface burst of a high fission-yield weapon. The general direction in which the fallout will move can be estimated fairly well if the wind pattern is known. But the total and fission yields of the explosion and the height of burst, in the event of a nuclear attack, are unpredictable. Consequently, it is impossible to determine in advance how far the seriously contaminated area will extend, although the time at which the fallout will commence at any point could be calculated if the effective wind speed and direction were known.

9.113 In spite of the uncertainties concerning the exact fallout pattern, there are highly important conclusions to be drawn from the results described above. One is that the residual nuclear radiation from a surface burst can, under some conditions, represent a serious hazard at great distances from the explosion, well beyond the range of blast, shock, thermal radiation, and the initial nuclear radiation. Another is that plans can be made to minimize the hazard, but such plans must be flexible, so that they can be adapted to the particular situation which develops after the attack.

ATTENUATION OF RESIDUAL NUCLEAR RADIATION

ALPHA AND BETA PARTICLES

9.114 In their passage through matter, alpha particles produce considerable direct ionization and thereby rapidly lose their energy. After traveling a certain distance, called the "range," an alpha particles ceases to exist as such.[8] The range of an alpha particle depends upon its initial energy, but even those from plutonium, which have a moderately high energy, have an average range of only just over 1½ inches in air. In more dense media, such as water or body tissue, the range is less, being about one-thousandth part of the range

[8] An alpha particle is identical with a nucleus of the element helium (§ 1.65). When it has lost most of its (kinetic) energy, it captures two electrons and becomes a harmless (neutral) helium atom.

in air. Consequently, alpha particles from radioactive sources cannot penetrate even the outer layer of the unbroken skin (epidermis). It is seen, therefore, that as far as alpha particles arising from sources outside the body are concerned, attenuation is no problem.

9.115 Beta particles, like alpha particles, are able to cause direct ionization in their passage through matter. But the beta particles dissipate their energy less rapidly and so have a greater range in air and in other materials. Many of the beta particles emitted by the fission products traverse a total distance of 10 feet (or more) in the air before they are absorbed. However, because the particles are continually deflected by electrons and nuclei of the medium, they follow a tortuous path, and so their effective (or net) range is somewhat less.

9.116 The range of a beta particle is shorter in more dense media, and the average net distance a particle of given energy can travel in water, wood, or body tissue is roughly one-thousandth of that in air. Persons in the interior of a house would thus be protected from beta radiation arising from fission products on the outside. It appears that even moderate clothing provides substantial attenuation of beta radiation, the exact amount varying, for example, with the weight and number of layers. Only beta radiation from material ingested or in contact with the body poses a hazard.

GAMMA RADIATION

9.117 The residual gamma radiations present a different situation. These gamma rays, like those which form part of the initial nuclear radiation, can penetrate considerable distances through air and into the body. Shielding will be required in most fallout situations to reduce the radiation dose to an acceptable level. Incidentally, any method used to decrease the gamma radiation will also result in a much greater attenuation of both alpha and beta particles.

9.118 The absorption (or attenuation) by shielding materials of the residual gamma radiation from fission products and from radioisotopes produced by neutron capture, e.g., in sodium, manganese, and in the weapon residues, is based upon exactly the same principles as were described in Chapter VIII in connection with the initial gamma radiation. Except for the earliest stages of decay, however, the gamma rays from fallout have much less energy, on the average, than do those emitted in the first minute after a nuclear explosion. This means that the residual gamma rays are more easily attenuated; in other words, compared with the initial gamma radiation, a smaller thickness of a given material will produce the same degree of attenuation.

9.119 Calculation of the attenuation of the gamma radiation from fallout is different and in some ways more complicated than for the initial radiations. The latter come from the explosion point, but the residual radiations arise from fallout particles that are widely distributed on the ground, on roofs, trees, etc. The complication stems from the fact that the effectiveness of a given thickness of material is influenced by the fallout distribution (or geometry) and hence depends on the degree of contamination and its location relative to the position where protection is desired. Estimates of the attenuation of residual

radiation in various structures have been made, based partly on calculations and partly on measurements with simulated fallout.

9.120 Some of the results of these estimates are given in Table 9.120 in terms of a dose-transmission factor (§ 8.72). Ranges of values are given in view of the uncertainties in the estimates themselves and the variations in the degree of shielding that may be obtained at different locations within a structure. (Shielding data for the same structures for initial nuclear radiation are given in Table 8.72.) All of the structures are assumed to be isolated, so that possible effects of adjacent buildings have been neglected. For vehicles, such as automobiles, buses, trucks, etc., the transmission factor is about 0.5 to 0.7. Rough estimates can thus be made of the shielding from fallout radiation that might be expected in various situations. Depending upon his location, a person in the open in a built-up city area would receive from about 20 to 70 percent of the dose that would be delivered by the same quantity of fallout in the absence of the buildings. An individual standing against a building in the middle of a block would receive a much smaller dose than one standing at the intersection of two streets. In contaminated agricultural areas, the gamma-ray dose above the surface can be reduced by turning over the soil so as to bury the fallout particles.

Table 9.120

FALLOUT GAMMA-RAY DOSE TRANSMISSION FACTORS FOR VARIOUS STRUCTURES

Structure	Dose transmission factor
Three feet underground	0.0002
Frame house	0.3–0.6
Basement	0.05–0.1
Multistory building (apartment type):	
Upper stories	0.01
Lower stories	0.1
Concrete blockhouse shelter:	
9-in. walls	0.007–0.09
12-in. walls	0.001–0.03
24-in. walls	0.0001–0.002
Shelter, partly above grade:	
With 2 ft earth cover	0.005–0.02
With 3 ft earth cover	0.001–0.005

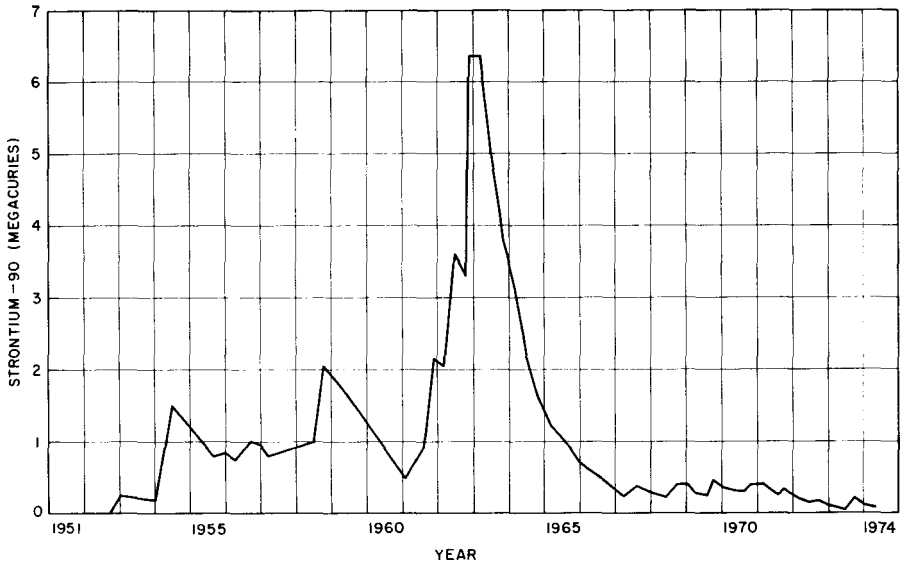

Figure 9.143a. Stratospheric burden (or inventory) of strontium-90.

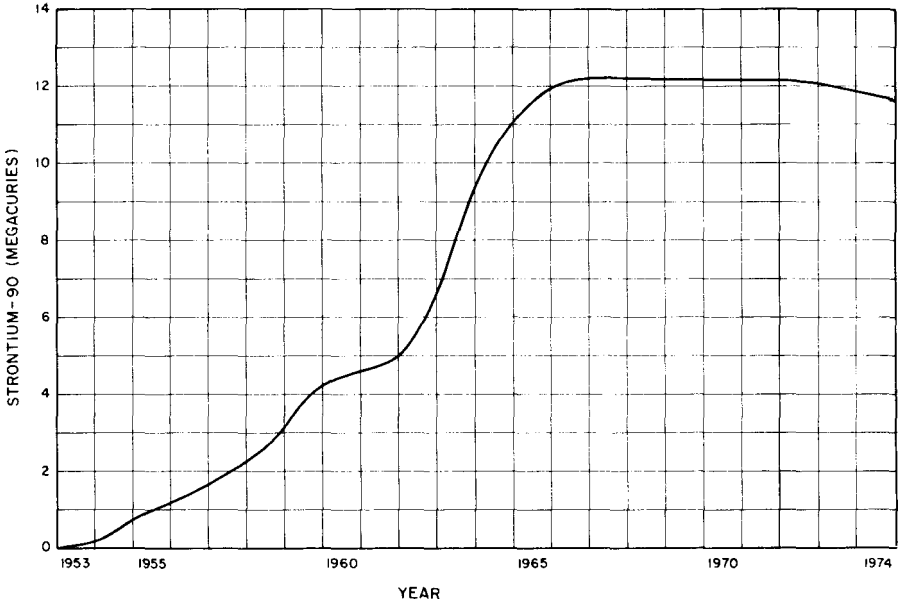

Figure 9.143b. Surface burden (or inventory) of strontium-90.

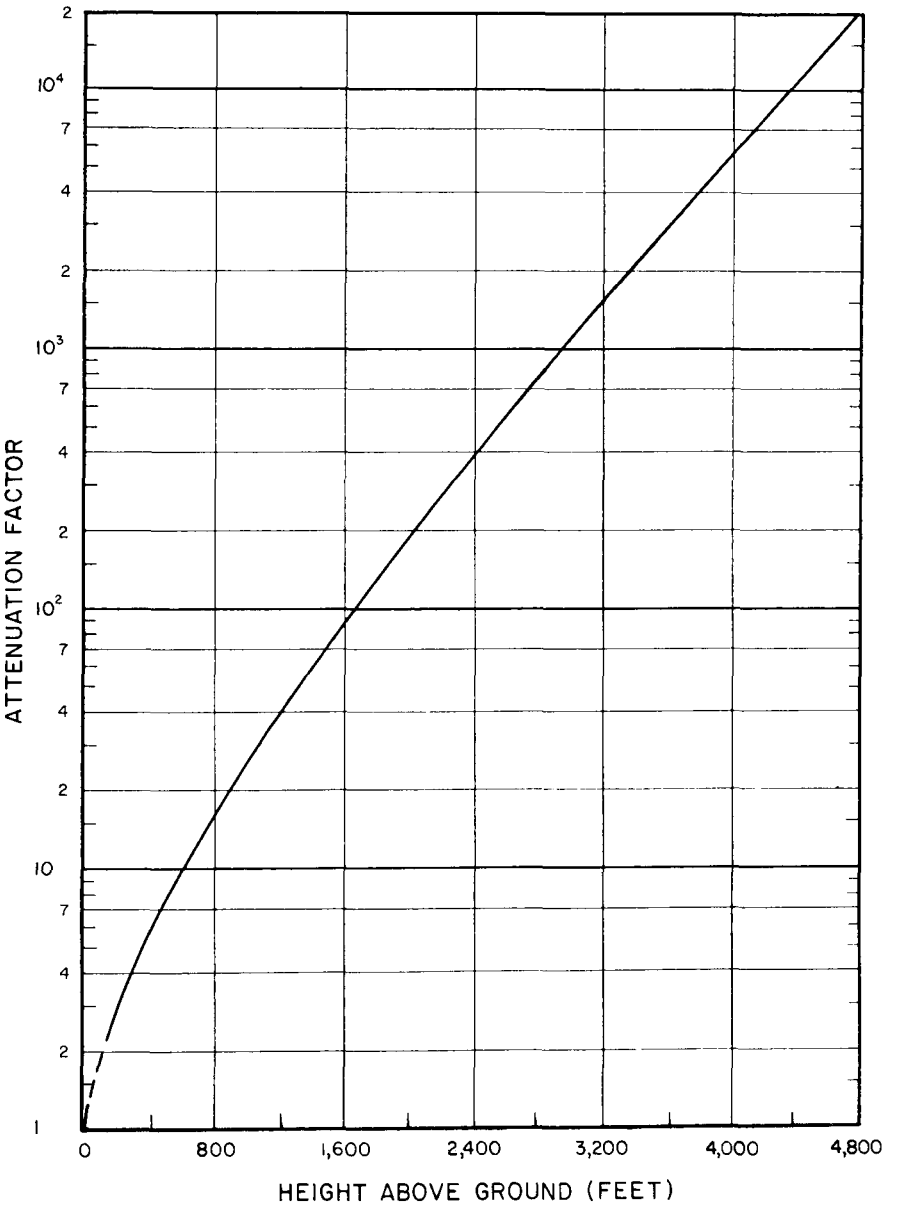

Figure 9.157. Altitude attenuation factor for early fallout radiation dose rate relative to the dose rate 3 feet above the ground.

BIBLIOGRAPHY

BUNNEY, L. R., and D. SAM, "Gamma-Ray Spectra of Fractionated Fission Products," Naval Ordnance Laboratory, June 1971, NOLTR 71–103.

BURSON, Z. G., "Fallout Radiation Protection Provided by Transportation Vehicles," EG & G, Inc., Las Vegas, Nevada, October 1972, EGG–1183–1566.

CRAWFORD, T. V., "Precipitation Scavenging and 2BPUFF," University of California, Lawrence Livermore Laboratory, December 1971, UOPKA 71–14.

CROCKER, G. R., "Fission Product Decay Chains: Schematics with Branching Fractions, Half-Lives, and Literature References," U.S. Naval Radiological Defense Laboratory, June 1967, USNRDL–TR–67–111.

CROCKER, G. R., and T. TURNER, "Calculated Activities, Exposure Rates, and Gamma Spectra for Unfractionated Fission Products," U.S. Naval Radiological Defense Laboratory, December 1965, USNRDL–TR–1009.

CROCKER, G. R., and M. A. CONNORS, "Gamma-Emission Data for the Calculation of Exposure Rates from Nuclear Debris, Volume I, Fission Products," U.S. Naval Radiological Defense Laboratory, June 1965, USNRDL–TR–876.

CROCKER, G. R., J. D. O'CONNOR, and E. C. FREILING, "Physical and Radiochemical Properties and Fallout Particles," U.S. Naval Radiological Defense Laboratory, June 1965, USNRDL–TR–899.

"Department of Defense Land Fallout Prediction System," Defense Atomic Support Agency, Washington, D.C.; U.S. Army Nuclear Defense Laboratory; U.S. Naval Radiological Defense Laboratory; Technical Operations Research, Burlington, Massachusetts, 1966, DASA 1800–I through 1800–VII.

DOLAN, P. J., "Gamma Spectra of Uranium-235 Fission Products at Various Times After Fission," Armed Forces Special Weapons Project, Washington, D.C., March 1959, AFSWP 524.

DOLAN, P. J., "Calculation of Abundances and Activities of the Products of High-Energy Neutron Fission of Uranium-238," Defense Atomic Support Agency, Washington, D.C., May 1959, DASA 525.

DOLAN, P. J., "Gamma Spectra of Uranium-238 Fission Products at Various Times After Fission," Defense Atomic Support Agency, Washington, D.C., May 1959, DASA 526.

*ENGLEMANN, R. J., and W. G. N. SLINN, Coordinators, "Precipitation Scavenging (1970)," AEC Symposium Series No. 22, U.S. Atomic Energy Commission, December 1970.

FEELY, H. W., *et al.*, "Final Report on Project Stardust, Volumes I through III," Isotopes, A Teledyne Company, Westwood, New Jersey, October 1967, DASA 2166–1 through 2166–3.

FERBER, G. J., "Distribution of Radioactivity with Height in Nuclear Clouds," Proceedings of the Second Conference sponsored by the Fallout Studies Branch, U.S. Atomic Energy Commission, November 1965.

FREILING, E. C., and N. E. BALLOU, "Nature of Nuclear Debris in Sea Water," *Nature*, **195**, 1283 (1962).

KNOX, J. B., T. V. CRAWFORD, and W. K. CRANDALL, "Potential Exposures from Low-Yield Free Air Bursts," University of California, Lawrence Livermore Laboratory, December 1971, UCRL–51164.

*KREY, P. W., and B. KRAJEWSKI, "HASL Model of Atmospheric Transport," Health and Safety Laboratory, U.S. Atomic Energy Commission, New York, N.Y., September 1969, HASL–215.

KREY, P. W., and B. KRAJEWSKI, "Comparison of Atmospheric Transport Model Calculations with Observations of Radioactive Debris," *J. Geophys. Res.*, **75**, 2901 (1970).

*KREY, P. W., M. SCHONBERG, and L. TOONKEL, "Updating Stratospheric Inventories to April 1974," Fallout Program Quarterly Summary Report, Health and Safety Laboratory, U.S. Energy Research and Development Administration, New York, N.Y., July 1975, HASL–294.

LEE, H., P. W. WONG, and S. L. BROWN, "SEER II: A New Damage Assessment Fallout Model," Stanford Research Institute, Menlo Park, California, May 1972, DNA 3008F.

MARTIN, J. R., and J. J. KORANDA, "The Importance of Tritium in the Civil Defense Context," University of California, Lawrence Livermore Laboratory, March 1971, UCRL–73085.

National Academy of Sciences, Advisory Committee on Civil Defense, Subcommittee on Fallout, "Response to DCPA Questions on Fallout," Defense Civil Preparedness Agency, Research Report No. 19, May 1973.

PETERSON, "An Empirical Model for Estimating World-Wide Deposition from Atmospheric Nuclear Detonations," *Health Physics*, **18**, 357 (1970).

Table 10.122

EFFECTS OF NUCLEAR DETONATIONS ON RADIO AND RADAR SYSTEMS

Frequency Band	Degradation Mechanism	Spatial Extent and Duration of Effects*	Comments
VLF	Phase changes, amplitude changes	Hundreds to thousands of miles; minutes to hours	Ground wave not affected, lowering of sky wave reflection height causes rapid phase change with slow recovery. Significant amplitude degradation of sky wave modes possible
LF	Absorption of sky waves, defocusing	Hundreds to thousands of miles; minutes to hours	Ground wave not affected, effects sensitive to relative geometry of burst and propagation path
MF	Absorption of sky waves, defocusing	Hundreds to thousands of miles; minutes to hours	Ground wave not affected
HF	Absorption of sky waves, loss of support for F-region reflection, multipath interference	Hundreds to thousands of miles, burst region and conjugate; minutes to hours	Daytime absorption larger than nighttime, F-region disturbances may result in new modes, multipath interference
VHF	Absorption, multipath interference, or false targets resulting from resolved multipath radar signals	Few miles to hundreds of miles; minutes to tens of minutes	Fireball and D-region absorption, FPIS circuits may experience attenuation or multipath interference
UHF	Absorption	Few miles to tens of miles; seconds to few minutes	Only important for line-of-sight propagation through highly ionized regions

*The magnitudes of spatial extent and duration are sensitive functions of detonation altitude and weapon yield.

in Table 11.32. However, the amount of energy collected is not always a sufficient criterion for damage. For example, an EMP surge can sometimes serve as a trigger mechanism by producing arcing or a change of state which, in turn, allows the normal operating voltage to cause damage to a piece of equipment. Thus, analysis of sensitivity to EMP may require consideration of operational upset and damage mechanisms in addition to the energy collected.

PROTECTIVE MEASURES

11.33 A general approach to the examination of a system with regard to its EMP vulnerability might include the

Table 11.32

DEGREES OF SUSCEPTIBILITY TO THE EMP

Most Susceptible

Low-power, high-speed digital computer, either transistorized or vacuum tube (operational upset)

Systems employing transistors or semiconductor rectifiers (either silicon or selenium):
- Computers and power supplies
- Semiconductor components terminating long cable runs, especially between sites
- Alarm systems
- Intercom system
- Life-support system controls
- Some telephone equipment which is partially transistorized
- Transistorized receivers and transmitters
- Transistorized 60 to 400 cps converters
- Transistorized process control systems
- Power system controls and communication links

Less Susceptible

Vacuum-tube equipment that does not include semiconductor rectifiers:
- Transmitters
- Receivers
- Alarm systems
- Intercom systems
- Teletype–telephone
- Power Supplies

Equipment employing low-current switches, relays, meters:
- Alarms
- Life-support systems
- Power system control panels
- Panel indicators and status boards
- Process controls

Hazardous equipment containing:
- Detonators
- Squibs
- Pyrotechnical devices
- Explosive mixtures
- Rocket fuels

Other:
- Long power cable runs employing dielectric insulation
- Equipment associated with high-energy storage capacitors
- Inductors

Least Susceptible

High-voltage 60 cps equipment:
- Transformers, motors
- Lamps (filament)
- Heaters
- Rotary converters
- Heavy-duty relays, circuit breakers
- Air-insultated power cable runs

following steps. First, information concerning the system components and devices is collected. The information is categorized into physical zones based on susceptibility and worst-case exposure for these items. It must be borne in mind in this connection that energy collected in one part of a system may be coupled directly or indirectly (by induction) to other parts. By using objective criteria, problem areas are identified, analyzed, and tested. Suitable changes are made as necessary to correct deficiencies, and the modified system is examined and tested. The approach may be followed on proposed systems or on those already existing, but experience indicates that the cost of retrofitting EMP protection may often be prohibitive. Consequently, it is desirable to consider the vulnerability of the system early during the design stage.

11.34 A few of the practices that may be employed to harden a system against EMP damage are described below. The discussion is intended to provide a general indication of the techniques rather than a comprehensive treatment of what is a highly technical and specialized area. Some of the methods of hardening against the EMP threat are shielding, proper circuit layout, satisfactory grounding, and various protective devices. If these measures do not appear to be adequate, it may be advisable to design equipment with vacuum tubes rather than solid-state components, if this is compatible with the intended use of the equipment.

11.35 A so-called "electromagnetic" shield consists of a continuous metal, e.g., steel, soft iron, or copper, sheet surrounding the system to be protected. Shielding of individual components or small subsystems is generally not practical because of the complexity of the task. Good shielding practice may include independent zone shields, several thin shields rather than one thick one, and continuous joints. The shield should not be used as a ground or return conductor, and sensitive equipment should be kept away from shield corners. Apertures in shields should be avoided as far as possible; doors should be covered with metal sheet so that when closed they form a continuous part of the whole shield, and ventilation openings, which cannot be closed, should be protected by special types of screens or waveguides. In order not to jeopardize the effectiveness of the shielding, precautions must be taken in connection with penetrations of the housing by conductors, such as pipes, conduits, and metal-sheathed cables (§ 11.59).

11.36 Recommendations for circuit layout include the use of common ground points, twisted cable pairs, system and intrasystem wiring in "tree" format (radial spikes), avoiding loop layouts and coupling to other circuits, use of conduit or cope trays, and shielded isolated transformers. The avoidance of ground return in cable shields is also recommended. Some procedures carry over from communications and power engineering whereas others do not.

11.37 From the viewpoint of EMP protection, cable design represents an extension of both shielding and circuit practices. Deeply buried (more than 3 feet underground) cables, shield layer continuity at splices, and good junction box contacts are desirable. Ordinary braid shielding should be avoided.

Compromises are often made in this area in the interest of economy, but they may prove to be unsatisfactory.

11.38 Good grounding practices will aid in decreasing the susceptibility of a system to damage by the EMP. A "ground" is commonly thought of as a part of a circuit that has a relatively low impedance to the local earth surface. A particular ground arrangement that satisfies this definition may, however, not be optimum and may be worse than no ground for EMP protection. In general, a ground can be identified as the chassis of an electronic circuit, the "low" side of an antenna system, a common bus, or a metal rod driven into the earth. The last depends critically on local soil conditions (conductivity), and it may result in resistively coupled currents in the ground circuit. A good starting point for EMP protection is to provide a single point ground for a circuit cluster, usually at the lowest impedance element — the biggest piece of the system that is electrically immersed in the earth, e.g., the water supply system.

11.39 Various protective devices may be used to supplement the measures described above. These are related to the means commonly employed to protect radio and TV transmission antennas from lightning strokes and power lines from current surges. Examples are arresters, spark gaps, band-pass filters, amplitude limiters, circuit breakers, and fuses. Typically, the protective device would be found in the "EMP room" at the cable entrance to an underground installation, in aircraft antenna feeds, in telephone lines, and at power entry panels for shielded rooms. On a smaller scale, diodes, nonlinear resistors, silicon-controlled rectifier clamps, and other such items are built into circuit boards or cabinet entry panels.

11.40 Few of the devices mentioned above are by themselves sufficient as a complete solution to a specific problem because each has some limitation in speed of response, voltage rating, power dissipation capacity, or reset time. Hence, most satisfactory protective devices are hybrids. For example, a band-pass filter may be used preceding a lightning arrester. The filter tends to stretch out the rise time of the EMP, thus providing sufficient time for the arrester to become operative. In general, a hybrid protection device must be designed specially for each application.

TESTING

11.41 Because of the complexities of the EMP response, sole reliance cannot be placed on predictions based on analysis. Testing is essential to verify analysis of devices, components, and complete systems early in the design stage. Testing also is the only known method that can be used to reveal unexpected effects. These may include coupling or interaction modes or weaknesses that were overlooked during the design. In some simple systems, nonlinear interaction effects can be analyzed numerically, but as a general rule testing is necessary to reveal them. As a result of the test, many of the original approximations can be refined for future analysis, and the data can improve the analytic capability for more complex problems. Testing also locates weak or susceptible points in components or systems early enough for economic improvement. After the improvements,

testing confirms that the performance is brought up to standard. A complete system should be tested to verify that it has been hardened to the desired level; subsequent periodic testing will indicate if any degradation has resulted from environmental or human factors.

11.42 Since the cessation of atmospheric weapons tests, heavy reliance has been placed on simulation to test the EMP hardness of systems. The classes of EMP tests include: (1) low-level current mapping; (2) high-level current injection; (3) high-level electromagnetic fields. Low-level current mapping should be used at the beginning of any test program. With the system power turned off, the magnitudes and signatures on internal cables are determined in a low-level field. This provides an insight into the work that must follow. After indicated improvements are made, a high-level current can be injected directly into the system with the system power on to explore for nonlinearities, and to uncover initial indications of system effects. If subsystems malfunction, it may be desirable to conduct extensive subsystem tests in the laboratory. Finally, test in a high-level electromagnetic field is essential.

11.43 The type of excitation must be defined in any type of test. The two principal choices are: (1) waveform simulations, which provide time-domain data, and (2) continuous wave (CW) signals, which provide frequency-domain data. If the intent is to match a system analysis in the frequency domain to measured system response, CW signals may be the more suitable. If the test results were being compared to known electronic thresholds, it is frequently necessary to test in the time domain. Both types of tests should be considered for a complete analysis.

11.44 Large-scale simulators are required for the final test of large systems. The two principal kinds of large simulators are metallic structures that guide an electromagnetic wave past a test object, and antennas that radiate an electromagnetic field to the object. Each type of simulator may use either pulse generators (time domain) or CW signal generators (frequency domain). Pulse generators themselves can be either high-level single shot or low-level repetitive.

11.45 The essential elements of a guided-wave or transmission-line simulator include a pulser, a transition section, working volume, and a termination. An electromagnetic wave of suitable amplitude and wave shape is generated by the pulser. This wave is guided by a tapered section of transmission line (the transition section) from the small cross-sectional dimension of the pulser output to the working volume. The working volume, where the test object is located, should be large enough to provide a certain degree of field uniformity over the object. This condition is satisfied if the volume of the test object is about one-third (or less) that of the working volume, depending on the degree of field perturbation that is acceptable. The termination region prevents the reflection of the guided wave back into the test volume; it consists of a transition section that guides the incident wave to a geometrically small resistive load whose impedance is equal to the characteristic impedance of the transmission line structure.

11.46 The basic types of radiating

simulators are long wire, biconical dipole, or conical monopole. The long wire is usually a long dipole oriented parallel to the earth's surface. It is supported above the ground by nonconducting poles with high-voltage insulators. The two arms of the dipole are symmetric about the center and constructed from sections of lightweight cylindrical conductor, such as irrigation pipe. Pipe sections decrease in diameter with increasing distance from the center, and resistors are placed between the pipe sections to shape the current wave and to reduce resonances. The two arms of the dipole are oppositely charged, and when the voltage across the spark gap at the dipole center reaches the breakdown voltage, the gap begins conducting and a wave front propagates away from the gap.

11.47 Conical and biconical antennas use pulsers, such as Marx generators or CW transmitters, instead of relying on the discharge of static surface charges. The antennas consist of lightweight conducting surfaces or wire grids.

11.48 Electromagnetic scale modeling may sometimes be an important alternative to full-scale testing of a system. Because of the difficulty in introducing minute openings or poor bonds into models, and since these often control interior fields, the usefulness of modeling ordinarily is limited to the measurement of external fields, voltages, and currents. Once these parameters are known for a complex structure, perhaps having cable runs, analysis can often provide internal field quantities of interest.

EMP AND ELECTRIC POWER SYSTEMS

11.49 Some indication of the possible threat of the EMP to commercial electric power system may be obtained by considering the effects of lightning strokes and switching surges. In power systems, protection against lightning is achieved by means of overhead "ground" wires and lightning arresters of various types. By providing an effective shunt, an overhead ground can divert most of the lightning surge from the phase conductors. Such grounding, however, would afford only partial protection from the EMP. Furthermore, although there are some similarities between the consequences of lightning and those of the EMP, there are differences in the nature of the current (or voltage) pulse which make the lightning arresters in common use largely ineffective for the EMP.

11.50 The general manner of the growth and decay of the current induced by the EMP from a high-altitude burst in an overhead transmission line is indicated by the calculated curve in Fig. 11.50. The details of the curve will vary with the conditions, but the typical features of the current pulse are as shown: a very rapid rise to a peak current of several thousand amperes in a fraction of a microsecond followed by a decay lasting up to a millisecond for a long transmission line. The current surge in an overhead power line caused by a lightning stroke increases to a maximum more slowly and persists for a longer time than for the EMP. As a result, older conventional lightning arresters are less effective for the EMP from

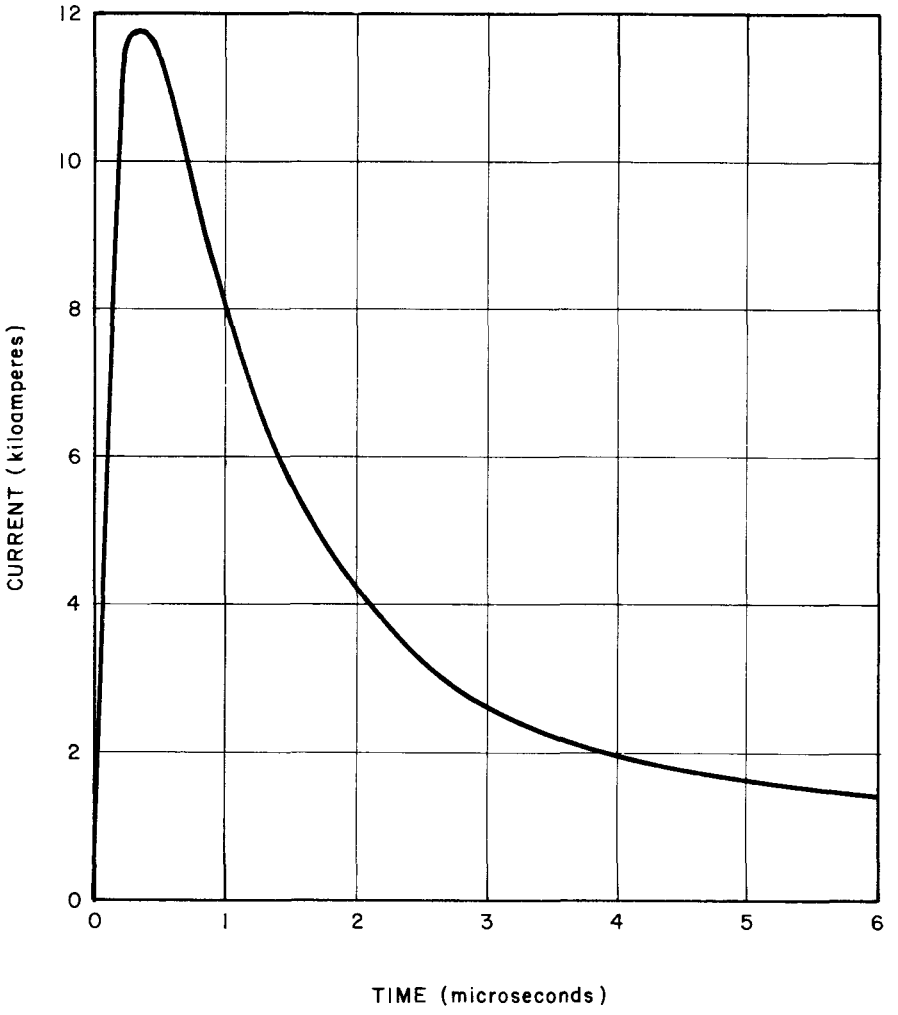

Figure 11.50. Typical form of the current pulse induced by the EMP from a high-altitude nuclear explosion in a long overhead power line. (The actual currents and times will depend to some extent on the conditions.)

high-altitude explosions than for lightning. Modern lightning arresters, however, can provide protection against EMP in many applications and hybrid arresters (§ 11.40) are expected to be even better.

11.51 In the absence of adequate protection, the surge voltages on overhead power lines produced by the EMP could cause insulator flashover, particularly on circuits of medium and low voltage. (The components of high-voltage transmission systems should be able to withstand the EMP surge voltages.) If

flashovers occur in the event of a high-altitude burst many would be experienced over a large area. Such simultaneous multiple flashovers could lead to system instability.

11.52 Switching surges occur when power lines are energized or de-energized. In systems of moderate and low voltage such surges can cause breakers in the switching circuit to operate erroneously, but the effect of the EMP is uncertain because the current rise in a switching surge is even slower than for lightning. In extra-high-voltage (EHV) lines, i.e., 500 kilovolts or more, switching surges are accompanied by a rapidly increasing radiated electromagnetic field similar to that of the EMP. The currents induced in control and communications cables are sufficient to cause damage or malfunction in associated equipment. The information obtained in connection with the development of protective measures required for EHV switching stations should be applicable to EMP protection.

11.53 There is a growing movement in the electric power industry to substitute semiconductor devices for vacuum tubes in control and communications circuits. Solid-state components are, however, particularly sensitive to the EMP. Even a small amount of energy received from the pulse could result in erroneous operation or temporary failure. Computers used for automatic load control would be particularly sensitive and a small amount of EMP energy, insufficient to cause permanent damage, could result in faulty operation or temporary failure. Special attention is thus required in the protection of such equipment.

EMP AND RADIO STATIONS

11.54 Unless brought in underground and properly protected, power and telephone lines could introduce substantial amounts of energy into radio (and TV) stations. A major collector of this energy, however, would be the transmitting (or receiving) antennas since they are specially designed for the transmission and reception of electromagnetic energy in the radiofrequency region. The energy collected from the EMP would be mainly at the frequencies in the vicinity of the antenna design frequency.

11.55 Antenna masts (or towers) are frequently struck by lightning and spark gaps are installed at the base of the tower to protect the station equipment. But the gaps in common use, like those in power lines, are not very effective against the EMP. Actually, when an antenna is struck by lightning, the supporting guy wires, rather than the spark gaps, serve to carry most of the lightning current to the ground. Although the guy wires have insulators along their length, arcing occurs across them thereby providing continuity for the current. This flashover of the insulators would not, however, provide protection against the EMP. In fact, the guy wires would then serve as additional collectors of the EMP energy by induction.

11.56 In spite of protective devices, both direct and indirect, damage to radio stations by lightning is not rare. The most commonly damaged component is the capacitor in the matching network at the base of the antenna; it generally suffers dielectric failure. Capacitors and inductors in the phasor circuit are also subject to damage. It is expected that

high-voltage capacitors would be sensitive to damage by the EMP. Such damage could result in shorting of the antenna feed line to the ground across the capacitor, thus precluding transmission until the capacitor is replaced. Experience with lightning suggests that there may also be damage to coaxial transmission lines from dielectric flashover. Solid-state components, which are now in common use in radio stations, would, of course, be susceptible to damage by the EMP and would need to be protected.

11.57 Radio transmitting stations employ various means to prevent interference from their own signals. These include shielding of audio wiring and components with low-level signals, single-point grounding, and the avoidance of loops. Such practices would be useful in decreasing the EMP threat.

EMP AND TELEPHONE SYSTEMS

11.58 Some of the equipment in telephone systems may be susceptible to damage from the EMP energy collected by power supply lines and by the subscriber and trunk lines that carry the signals. Various lightning arresting devices are commonly used for overhead telephone lines, but they may provide limited protection against the EMP unless suitably modified. Steps are being taken to improve the ability of the long-distance telephone network in the United States to withstand the EMP as well as the other effects of a nuclear explosion.

11.59 In a properly "hardened" system, coaxial cables are buried underground and so also are the main and auxiliary repeater or switching centers. In the main (repeater and switching) stations, the building is completely enclosed in a metal EMP shield. Metal flashing surrounds each metallic line, e.g., pipe, conduit, or sheathed cable, entering or leaving the building, and the flashing is bonded to the line and to the shield. Where this is not possible, protectors or filters are used to minimize the damage potential of the EMP surge. Inside the building, connecting cables are kept short and are generally in straight runs. An emergency source of power is available to permit operation to continue in the event of a failure (or disconnection) of the commercial power supply. The auxiliary (repeater) stations, which are also underground, do not have exterior shielding but the electronic equipment is protected by steel cases.

THEORY OF THE EMP[2]

DEVELOPMENT OF THE RADIAL ELECTRIC FIELD

11.60 The energies of the prompt gamma rays accompanying a nuclear explosion are such that, in air, Compton scattering is the dominant photon interaction (see Fig. 8.97b). The scattered photon frequently retains sufficient en-

[2]The remainder of this chapter may be omitted without loss of continuity.

ergy to permit it to repeat the Compton process. Although scattering is somewhat random, the free electrons produced (and the scattered photons) tend, on the average, to travel in the radial direction away from the burst point. The net movement of the electrons constitutes an electron current, referred to as the Compton current. The prompt gamma-ray pulse increases rapidly to a peak value in about 10^{-8} second or so, and the Compton current varies with time in a similar manner.

11.61 When the electrons are driven radially outward by the flux of gamma rays, the atoms and molecules from which they have been removed, i.e., the positive ions, travel outward more slowly. This results in a partial separation of charges and a radial electric field. The lower energy (secondary) electrons generated by collisions of the Compton electrons are then driven back by the field toward the positive charges. Consequently, a reverse electron current is produced and it increases as the field strength increases. This is called the "conduction current" because, for a given field strength, its magnitude is determined by the electrical conductivity of the ionized medium. The conductivity depends on the extent of ionization which itself results from the Compton effect; hence the conductivity of the medium will increase as the Compton current increases. Thus, as the radial field grows in strength so also does the conduction current. The conduction current flows in such a direction as to oppose this electric field; hence at a certain time, the field will cease to increase. The electric field is then said to be "saturated." At points near the burst, the radial electric field reaches saturation sooner and is somewhat stronger than at points farther away.

11.62 In a perfectly homogeneous medium, with uniform emission of gamma rays in all directions, the radial electric field would be spherically symmetrical. The electric field will be confined to the region of charge separation and no energy will be radiated away. In a short time, recombination of charges in the ionized medium occurs and the electric field strength in all radial directions decreases within a few microseconds. The energy of the gamma rays deposited in the ionized sphere is then degraded into thermal radiation (heat). If the symmetry of the ionized sphere is disturbed, however, nonradial oscillations will be initiated and energy will be emitted as a pulse of electromagnetic radiation much of which is in the radiofrequency region of the spectrum. Since, in practice, there is inevitably some disturbance of the spherical symmetry in a nuclear explosion, all such explosions are accompanied by a radiated EMP, the strength of which depends on the circumstances.

GENERAL CHARACTERISTICS OF THE EMP

11.63 The radiation in the EMP covers a wide range of frequencies with the maximum determined by the rise time of the Compton current. This is typically of the order of 10^{-8} second and the maximum frequency for the mechanism described above is then roughly 10^8 cycles per second, i.e., 10^8 hertz or 100 megahertz. Most of the radiation will, however, be emitted at lower frequencies in the radiofrequency range. The rise time is generally somewhat

shorter for high-altitude bursts than for surface and medium-altitude bursts; hence, the EMP spectrum in high-altitude bursts tends toward higher frequencies than in bursts of the other types.

11.64 The prompt gamma rays from a nuclear explosion carry, on the average, about 0.3 percent of the explosion energy (Table 10.138) and only a fraction of this, on the order of approximately 10^{-2} for a high-altitude burst and 10^{-7} for a surface burst, is radiated in the EMP. For a 1-megaton explosion at high altitude, the total energy release is 4.2×10^{22} ergs and the amount that is radiated as the EMP is roughly 10^{18} ergs or 10^{11} joules. Although this energy is distributed over a very large area, it is possible for a collector to pick up something on the order of 1 joule (or so) of EMP energy. The fact that a small fraction of a joule, received as an extremely short pulse, could produce either permanent or temporary degradation of electronic devices, shows that the EMP threat is a serious one.

11.65 Although all nuclear bursts are probably associated with the EMP to some degree, it is convenient to consider three more-or-less distinct (or extreme) types of explosions from the EMP standpoint. These are air bursts at medium altitudes, surface bursts, and bursts at high altitudes. Medium-altitude bursts are those below about 19 miles in which the deposition region does not touch the earth's surface. The radius of the sphere ranges roughly from 3 to 9 miles, increasing with the burst altitude. The EMP characteristics of air bursts at lower altitudes, in which the deposition region does touch the earth, are intermediate between medium-altitude and surface bursts. At burst altitudes below about 1.2 miles, the radiated pulse has the general characteristics of that from a surface burst.

MEDIUM-ALTITUDE AIR BURSTS

11.66 In an air burst at medium altitude, the density of the air is somewhat greater in the downward than in the upward direction. The difference in density is not large, although it increases with the radius of the deposition (or source) region, i.e., with increasing altitude. The frequency of Compton collisions and the ionization of the air will vary in the same manner as the air density. As a result of the asymmetry, an electron current is produced with a net component in the upward direction, since the symmetry is not affected in the azimuthal (radial horizontal) direction. The electron current pulse initiates oscillations in the ionized air and energy is emitted as a short pulse of electromagnetic radiation. The EMP covers a wide range of frequencies and wave amplitudes, but much of the energy is in the low-frequency radio range. In addition, a high-frequency pulse of short duration is radiated as a result of the turning of the Compton electrons by the earth's magnetic field (§ 11.71).

11.67 The magnitude of the EMP field radiated from an air burst will depend upon the weapon yield, the height of burst (which influences the asymmetry due to the atmospheric density gradient), and asymmetries introduced by the weapon (including auxiliary equipment, the case, or the carrying vehicle). At points outside the deposit-

ion region, for the lower-frequency EMP arising from differences in air density, the radiated electric field $E(t)$ at any specified time t as observed at a distance R from the burst point is given by

$$E(t) = \frac{R_0}{R} E_0(t) \sin \theta, \qquad (11.67.1)$$

where R_0 is the radius of the deposition region, $E_0(t)$ is the radiated field strength at the distance R_0, i.e., at the beginning of the radiating region, at the time t, and θ is the angle between the vertical and a line joining the observation point to the burst point. It follows from equation (11.67.1) that, as stated in § 11.06, the EMP field strength is greatest in directions perpendicular to the (vertical) electron current. Values of $E_0(t)$ and R_0 are determined by computer calculations for specific situations; $E_0(t)$ is commonly from a few tens to a few hundred volts per meter and R_0 is from about 3 to 9 miles (§ 11.09). The interaction of the gamma rays with air falls off roughly exponentially with distance; hence, the deposition region does not have a precise boundary, but R_0 is taken as the distance that encloses a volume in which the conductivity is 10^{-7} mho per meter or greater.

SURFACE BURSTS

11.68 In a contact surface burst, the presence of the ground introduces a strong additional asymmetry. Compared with air, the ground is a very good absorber of neutrons and gamma rays and a good conductor of electricity. Therefore, the deposition region consists approximately of a hemisphere in the air and there is a net electron current with a strong component in the upward direction. Further, the conducting ground provides an effective return path for the electrons with the result that current loops are formed. That is, electrons travel outward from the burst in the air, then return toward the burst point through the higher conductivity ground. These current loops generate very large azimuthal magnetic fields that run clockwise around the burst point (looking down on the ground) in the deposition region, especially close to the ground (Fig. 11.10). At points very near the burst, the air is highly ionized and its conductivity exceeds the ground conductivity. The tendency for the conduction current to shift to the ground is therefore reduced, and the magnetic fields in the ground and in the air are decreased correspondingly.

11.69 Large electric and magnetic fields are developed in the ground which contribute to the EMP, in addition to the fields arising from the deposition region. As a result of the number of variables that can affect the magnitude and shape of the fields, it is not possible to describe them in a simple manner. The peak radiated fields at the boundary of the deposition region are ten to a hundred times stronger in a direction along the earth than for a similar air burst. The variation with distance of the *peak* radiated electric field along the earth's surface is given by

$$E = \frac{R_0}{R} E_0 , \qquad (11.69.1)$$

where E_0 is the peak radiated field at the radius R_0 of the deposition region and E is the peak field at the surface distance R from the burst point. For observation

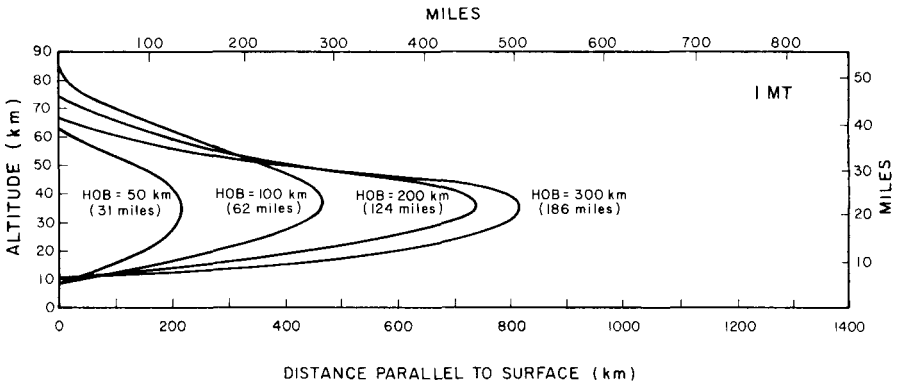

Figure 11.70a. Deposition regions for 1-MT explosions at altitudes of 31, 62, 124, and 186 miles.

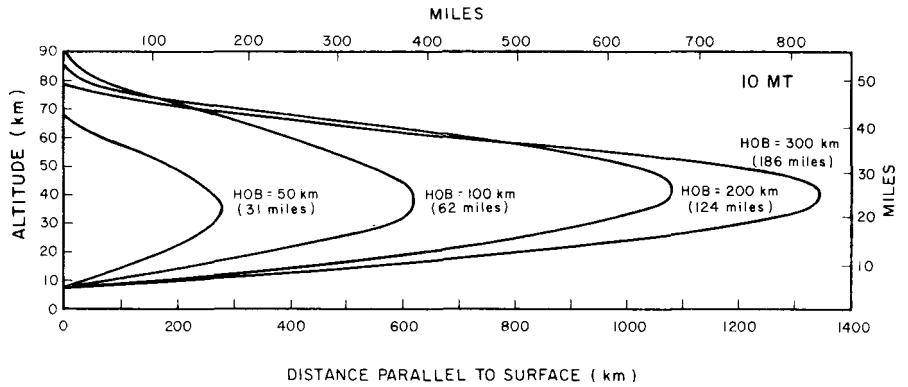

Figure 11.70b. Deposition regions for 10-MT explosions at altitudes of 31, 62, 124, 186 miles.

points above the surface the peak radiated field falls off rapidly with increasing distance. As stated in § 11.12, R_0 is roughly 2 to 5 miles, depending on the explosion yield; E_0 may be several kilovolts per meter.

HIGH-ALTITUDE BURSTS

11.70 The thickness and extent of half of the deposition region for bursts of 1 and 10 megatons yield, respectively, for various heights of burst (HOB) are shown in Figs. 11.70a and b. The abscissas are distances in the atmosphere measured parallel to the earth's surface from ground zero. The curves were computed from the estimated gamma-ray emissions from the explosions and the known absorption coefficients of the air at various densities (or altitudes). At small ground distances, i.e., immediately below the burst, the deposition region is thicker than at larger distances because the gamma-ray intensity decreases with distance from the burst point. Since the gamma rays pass through air of increasing density as they travel toward the ground, most are absorbed in a layer between altitudes of roughly 40 and 10 miles.

11.71 Unless they happen to be ejected along the lines of the geomagnetic field, the Compton electrons resulting from the interaction of the gamma-ray photons with the air molecules and atoms in the deposition region will be forced to follow curved paths along the field lines.[3] In doing so they are subjected to a radial acceleration and the ensemble of turning electrons, whose density varies with time, emits electromagnetic radiations which add coherently. The EMP produced in this manner from a high-altitude burst—and also to some extent from an air burst—is in a higher frequency range than the EMP arising from local asymmetries in moderate-altitude and surface bursts (§ 11.63).

11.72 The curves in Figs. 11.70a and b indicate the dimensions of the deposition (source) region, but they do not show the extent of coverage on (or near) the earth's surface. The EMP does not radiate solely in a direction down from the source region; it also radiates from the edges and at angles other than vertical beneath this region. Thus, the effect at the earth's surface of the higher-frequency EMP extends to the horizon (or tangent point on the surface as viewed from the burst). The lower frequencies, however, will extend even beyond the horizon because these electromagnetic waves can follow the earth's curvature (cf. § 10.92). Table 11.72 gives the distances along the surface from ground zero to the tangent point for several burst heights.

Table 11.72

GROUND DISTANCE TO TANGENT POINT FOR VARIOUS BURST ALTITUDES

Burst Altitude (miles	Tangent Distance (miles)
62	695
93	850
124	980
186	1,195
249	1,370
311	1,520

11.73 The peak electric field (and its amplitude) at the earth's surface from a high-altitude burst will depend upon the explosion yield, the height of burst, the location of the observer, and the orientation with respect to the geomagnetic field. As a general rule, however, the field strength may be expected to be tens of kilovolts per meter over most of the area receiving the EMP radiation. Figure 11.73 shows computed contours for E_{max}, the maximum peak electric field, and various fractions of E_{max} for burst altitudes between roughly 60 and 320 miles, assuming a yield of a few hundred kilotons or more. The distances, measured along the earth's surface, are shown in terms of the height of burst. The spatial distribution of the EMP electric field depends on the geomagnetic field and so varies with the latitude; the results in the figures apply generally for ground zero between about 30° and 60° north latitude. South of the geomagnetic equator the directions indicating magnetic north and east in the figure would become south and west, respectively. It is evident from Fig.

[3] At higher altitudes, when the atmospheric density is much less and collisions with air atoms and molecules are less frequent, continued turning of the electrons (beta particles) about the field lines leads to the helical motion referred to in §§ 2.143, 10.27.

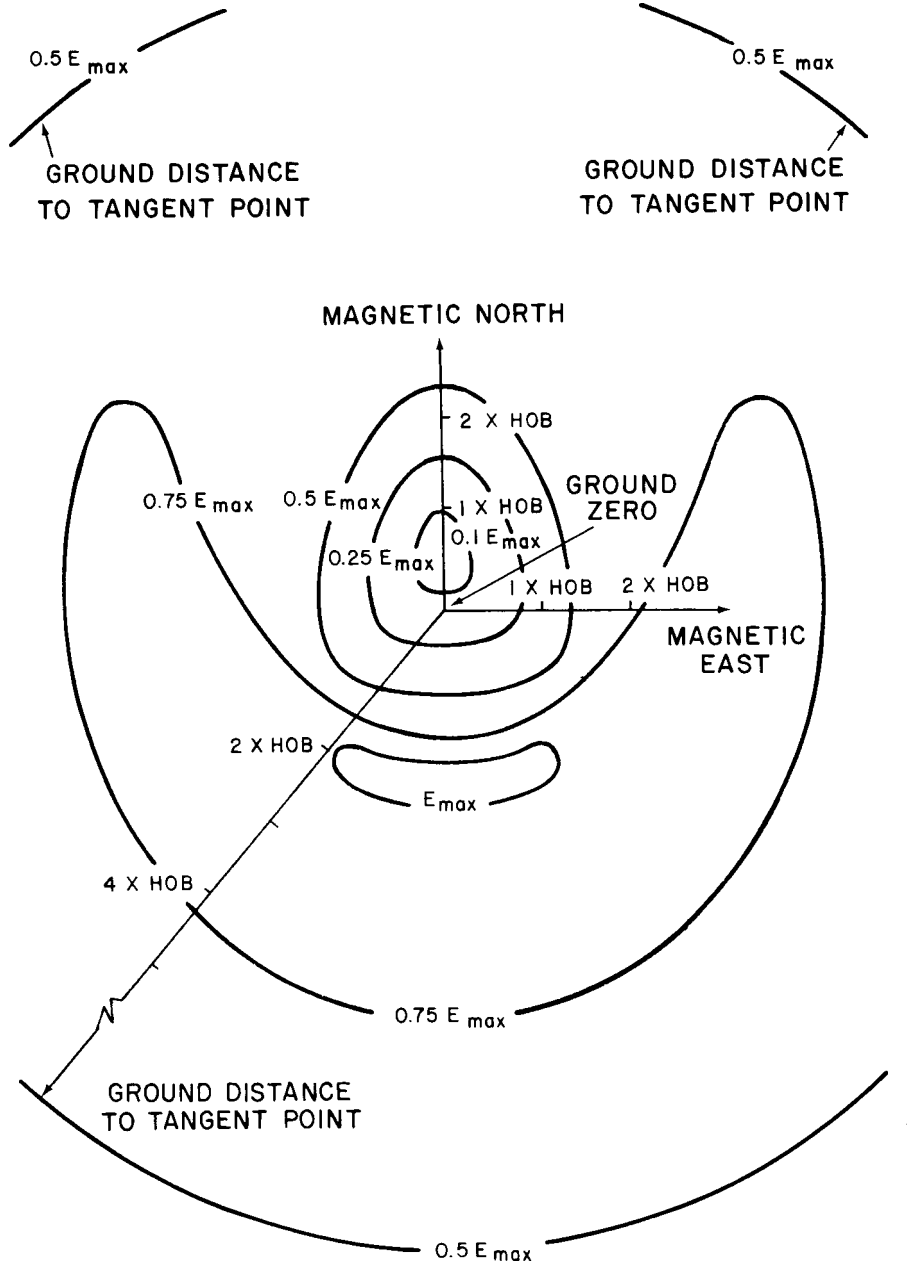

Figure 11.73. Variations in peak electric fields for locations on the earth's surface for burst altitudes between 60 and 320 miles and for ground zero between 30° and 60° north latitude. The data are applicable for yields of a few hundred kilotons or more.

11.73 that over most of the area affected by the EMP the electric field strength on the ground would exceed $0.5E_{max}$. For yields of less than a few hundred kilotons, this would not necessarily be true because the field strength at the earth's tangent could be substantially less than $0.5\ E_{max}$.

11.74 The reason why Fig. 11.73 does not apply at altitudes above about 320 miles is that at such altitudes the tangent range rapidly becomes less than four times the height of burst. The distance scale in the figure, in terms of the HOB, then ceases to have any meaning. For heights of burst above 320 miles, a set of contours similar to those in Fig. 11.73 can be plotted in terms of fractions of the tangent distance.

11.75 The spatial variations of EMP field strength arise primarily from the orientation and dip angle of the geomagnetic field, and geometric factors related to the distance from the explosion to the observation point. The area of low field strength slightly to the north of ground zero in Fig. 11.73 is caused by the dip in the geomagnetic field lines with reference to the horizontal direction. Theoretically, there should be a point of zero field strength in the center of this region where the Compton electrons would move directly along the field lines without turning about them, but other mechanisms, such as oscillations within the deposition region, will produce a weak EMP at the earth's surface. The other variations in the field strength at larger ground ranges are due to differences in the slant range from the explosion.

11.76 The contours in Fig. 11.73 apply to geomagnetic dip angles of roughly 50° to 70°. Although E_{max} would probably not vary greatly with the burst latitude, the spatial distribution of the peak field strength would change with the dip angle. At larger dip angles, i.e., at higher latitudes than about 60°, the contours for E_{max} and $0.75\ E_{max}$ would tend more and more to encircle ground zero. Over the magnetic pole (dip angle 90°), the contours would be expected theoretically to consist of a series of circles surrounding ground zero, with the field having a value of zero at ground zero. At lower dip angles, i.e., at latitudes less than about 30°, the tendency for the contours to become less circular and to spread out, as in Fig. 11.73, would be expected to increase.

BIBLIOGRAPHY

BLOCK, R., *et al.*, "EMP Seal Evaluation," Physics International Co., San Leandro, California, January 1971.

BRIDGES, J. E., D. A. MILLER, and A. R. VALENTINO, "EMP Directory for Shelter Design," Illinois Institute of Technology Research Institute, Chicago, Illinois, April 1968.

*BRIDGES, J. E., and J. WEYER, "EMP Threat and Countermeasures for Civil Defense Systems," Illinois Institute of Technology Research Institute, Chicago, Illinois, November 1968.

*"Electromagnetic Pulse Problems in Civilian Power and Communications," Summary of a seminar held at Oak Ridge National Laboratory, August 1969, sponsored by the U.S. Atomic Energy Commission and the Department of Defense/Office of Civil Defense.

"Electromagnetic Pulse Sensor and Simulation Notes, Volumes 1–10," Air Force Weapons Laboratory, April 1967 through 1972, AFWL EMP 1–1 through 1–10.

"EMP Protection for Emergency Operating Centers," Department of Defense/Office of

Civil Defense, May 1971, TR-61-A.

"EMP Protective Systems," Department of Defense/Office of Civil Defense, November 1971, TR-61-B.

"EMP Protection for AM Radio Broadcast Stations," Department of Defense/Office of Civil Defense, May 1972, TR-61-C.

FOSS, J. W., and R. W. MAYO, "Operation Survival," *Bell Laboratories Record*, January 1969, page 11.

GILINSKY, V., and G. PEEBLES, "The Development of a Radio Signal from a Nuclear Explosion in the Atmosphere," *J. Geophys. Res.*, **73**, 405 (1968).

HIRSCH, F. G., and A. BRUNER, "Absence of Electromagnetic Pulse Effects on Monkeys and Dogs," *J. Occupational Medicine*, **14**, 380 (1972).

KARZAS, W. J. and R. LATTER, "Detection of Electromagnetic Radiation from Nuclear Explosions in Space," *Phys. Rev.* **137**, B1369 (1965).

LENNOX, C. R., "Experimental Results of Testing Resistors Under Pulse Conditions," Electrical Standards Division 2412, Sandia Laboratory, Albuquerque, New Mexico, November 1967.

MINDEL, I. N., Program Coordinator, "DNA EMP Awareness Course Notes," 2nd ed., Illinois Institute of Technology Research Institute, Chicago, Illinois, August 1973, DNA 2772T.

*NELSON, D. B., "Effects of Nuclear EMP on AM Broadcast Stations in the Emergency Broadcast System," Oak Ridge National Laboratory, July 1971, ORNL-TM-2830.

NELSON, D. B., "EMP Impact on U.S. Defenses," *Survive*, **2**, No. 6, 2 (1969).

NELSON, D. B., "A Program to Counter Effects of Nuclear EMP in Commercial Power Systems," Oak Ridge National Laboratory, October 1972, ORNL-TM-3552.

RICKETTS, L. W., *et al.*, "EMP Radiation and Protective Techniques," Wiley-Interscience, 1976.

*SARGIS, D. A., *et al.*, "Late Time Source for Close-In EMP," Science Applications, La Jolla, California, August 1972, DNA 3064F, SAI-72-556-L-J.

*These documents may be purchased from the National Technical Information Service, Department of Commerce, Springfield, Virginia 22161.

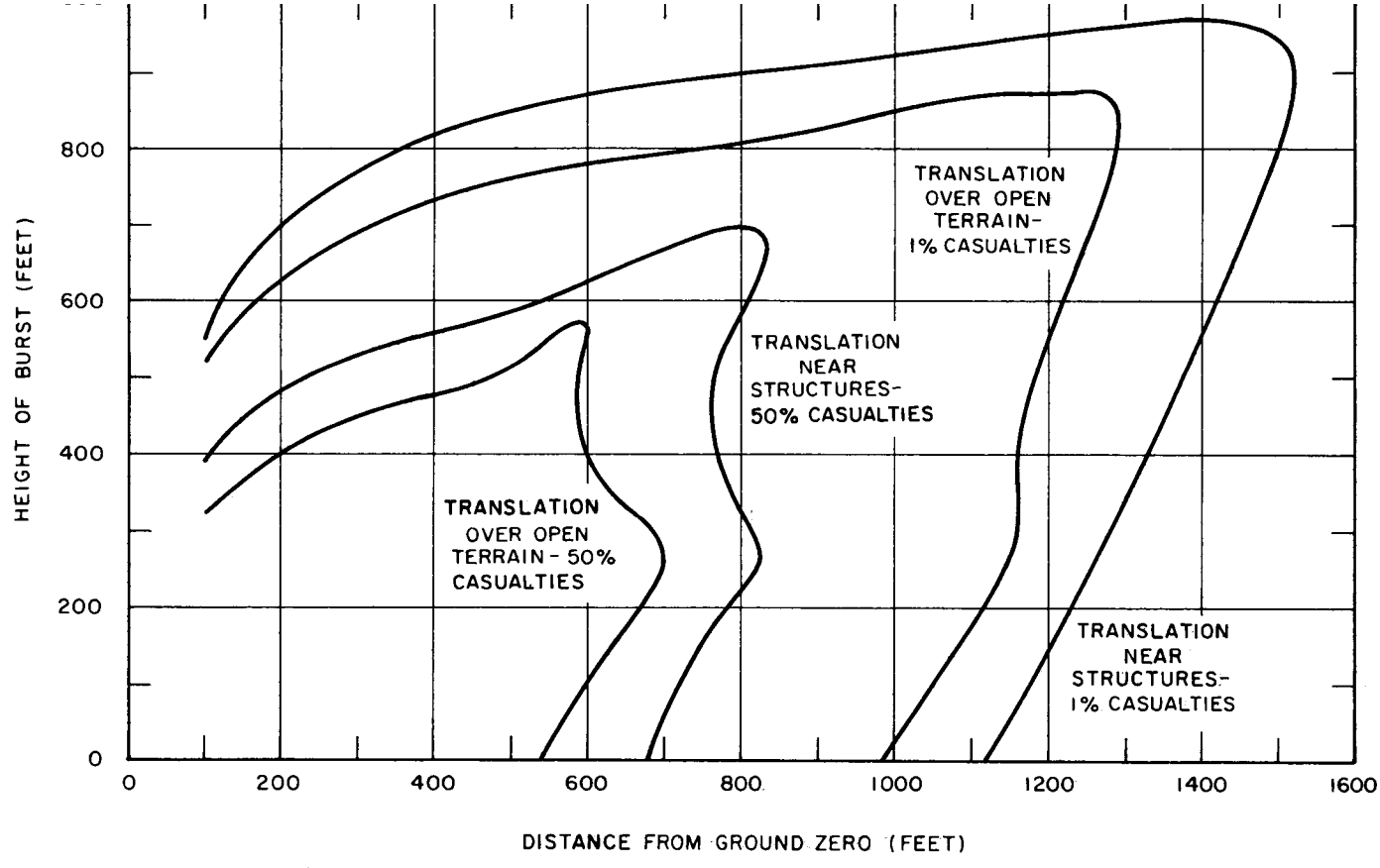

Figure 12.49. Casualties from translation near structures and over open terrain for a 1-kiloton explosion. (The curves for open terrain are more approximate than the others.)

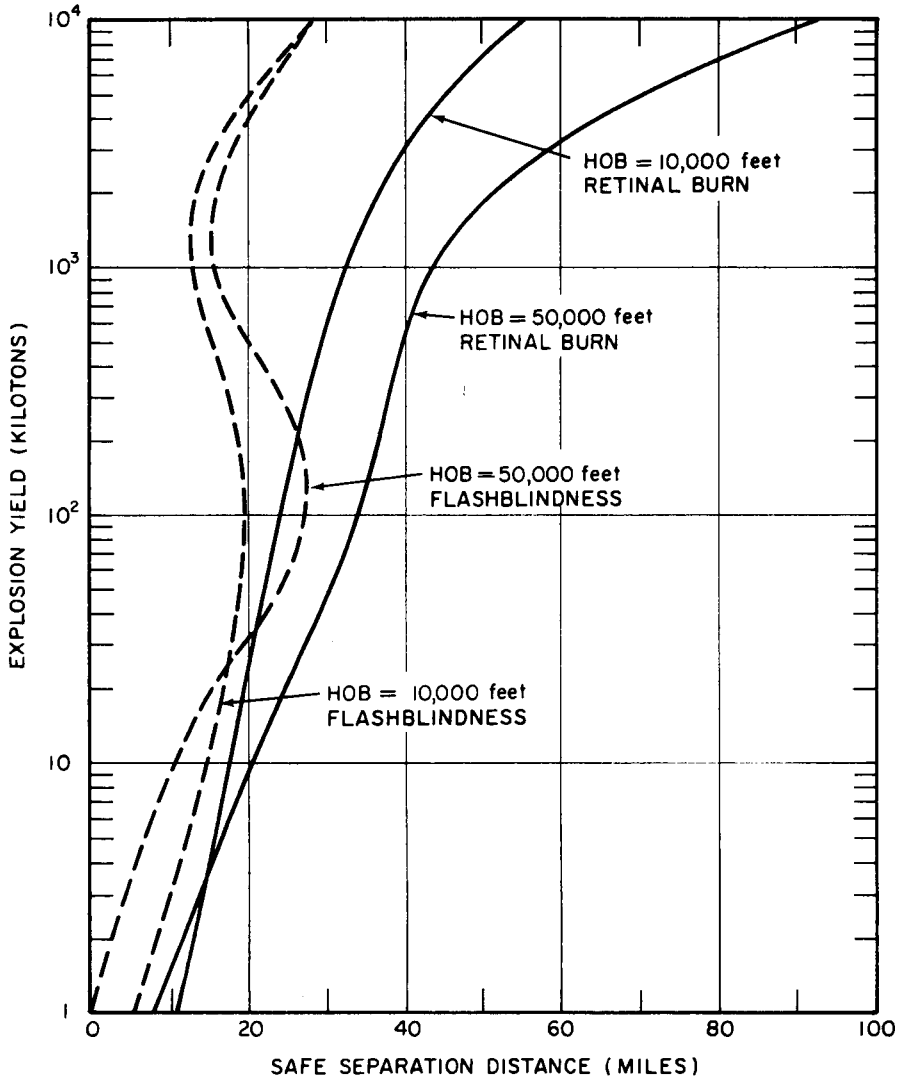

Figure 12.88a. Flashblindness and retinal burn safe separation distances for an observer on the ground, as a function of explosion yield, for burst heights of 10,000 feet and 50,000 feet on a clear day.

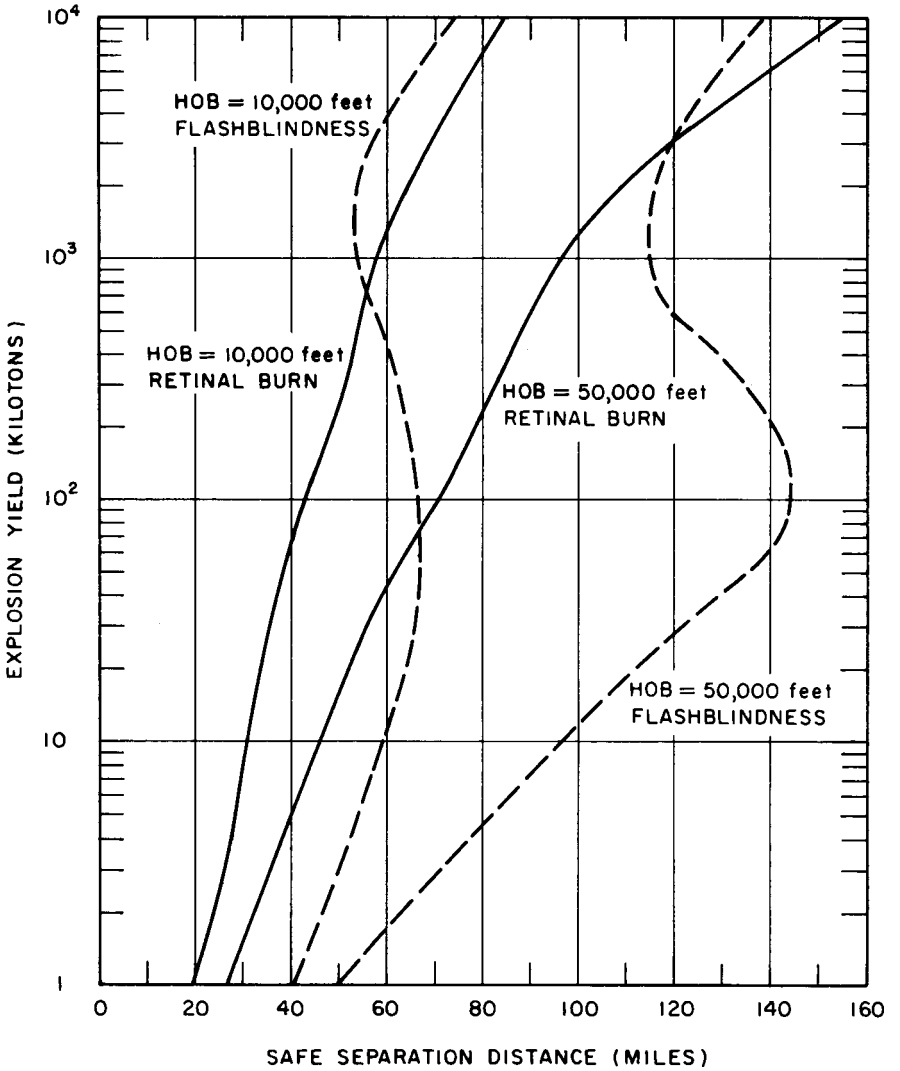

Figure 12.88b. Flashblindness and retinal burn safe separation distances for an observer on the ground, as a function of explosion yield, for burst heights of 10,000 feet and 50,000 feet at night.

Table 12.108

SUMMARY OF CLINICAL EFFECTS OF ACUTE IONIZING RADIATION DOSES

Range	0 to 100 rems Subclinical range	100 to 1,000 rems Therapeutic range			Over 1,000 rems Lethal range	
		100 to 200 rems	200 to 600 rems	600 to 1,000 rems	1,000 to 5,000 rems	Over 5,000 rems
		Clinical surveillance	Therapy effective	Therapy promising	Therapy palliative	
Incidence of vomiting	None	100 rems: infrequent 200 rems: common	300 rems: 100%	100%	100%	
Initial Phase						
Onset	—	3 to 6 hours	½ to 6 hours	¼ to ½ hour	5 to 30 minutes	Almost immediately**
Duration	—	≤ 1 day	1 to 2 days	≤ 2 days	≤ 1 day	
Latent Phase						
Onset	—	≤ 1 day	1 to 2 days	≤ 2 days	≤ 1 day*	Almost immediately**
Duration	—	≤ 2 weeks	1 to 4 weeks	5 to 10 days	0 th 7 days*	
Final Phase						
Onset	—	10 to 14 days	1 to 4 weeks	5 to 10 days	0 to 10 days	Almost immediately**
Duration	—	4 weeks	1 to 8 weeks	1 to 4 weeks	2 to 10 days	
Leading organ	Hematopoietic tissue				Gastrointestinal tract	Central nervous system
Characteristic signs	None below 50 rems	Moderate leukopenia	Severe leukopenia; purpura; hemorrhage; infection. Epilation above 300 rems.		Diarrhea; fever; disturbance of electrolyte balance.	Convulsions; tremor; ataxia; lethargy.
Critical period post-exposure	—	—	1 to 6 weeks		2 to 14 days	1 to 48 hours

Therapy	Reassurance	Reassurance; hematologic surveillance.	Blood transfusion; antibiotics.	Consider bone marrow transplantation.	Maintenance of electrolyte balance.	Sedatives
Prognosis	Excellent	Excellent	Guarded	Guarded	Hopeless	
Convalescent period Incidence of death	None None	Several weeks None	1 to 12 months 0 to 90%	Long 90 to 100%	— 100%	
Death occurs within	—	—	2 to 12 weeks	1 to 6 weeks	2 to 14 days	< 1 day to 2 days
Cause of death	—	—	Hemorrhage; infection		Circulatory collapse	Respiratory failure; brain edema.

*At the higher doses within this range there may be no latent phase.

**Initial phase merges into final phase, death usually occurring from a few hours to about 2 days; this chronology is possibly interrupted by a very short latent phase.